Basin Analysis

Short Course

given at

University of Potsdam and the GFZ

11-14 and 17 October 2016

Day 5 - Foreland Basins, Strike-slip Basins and Course Review

Professor Bernard Coakley

Geophysical Institute

University of Alaska - Fairbanks

continental lithospheric strength defines the extent of foreland basins

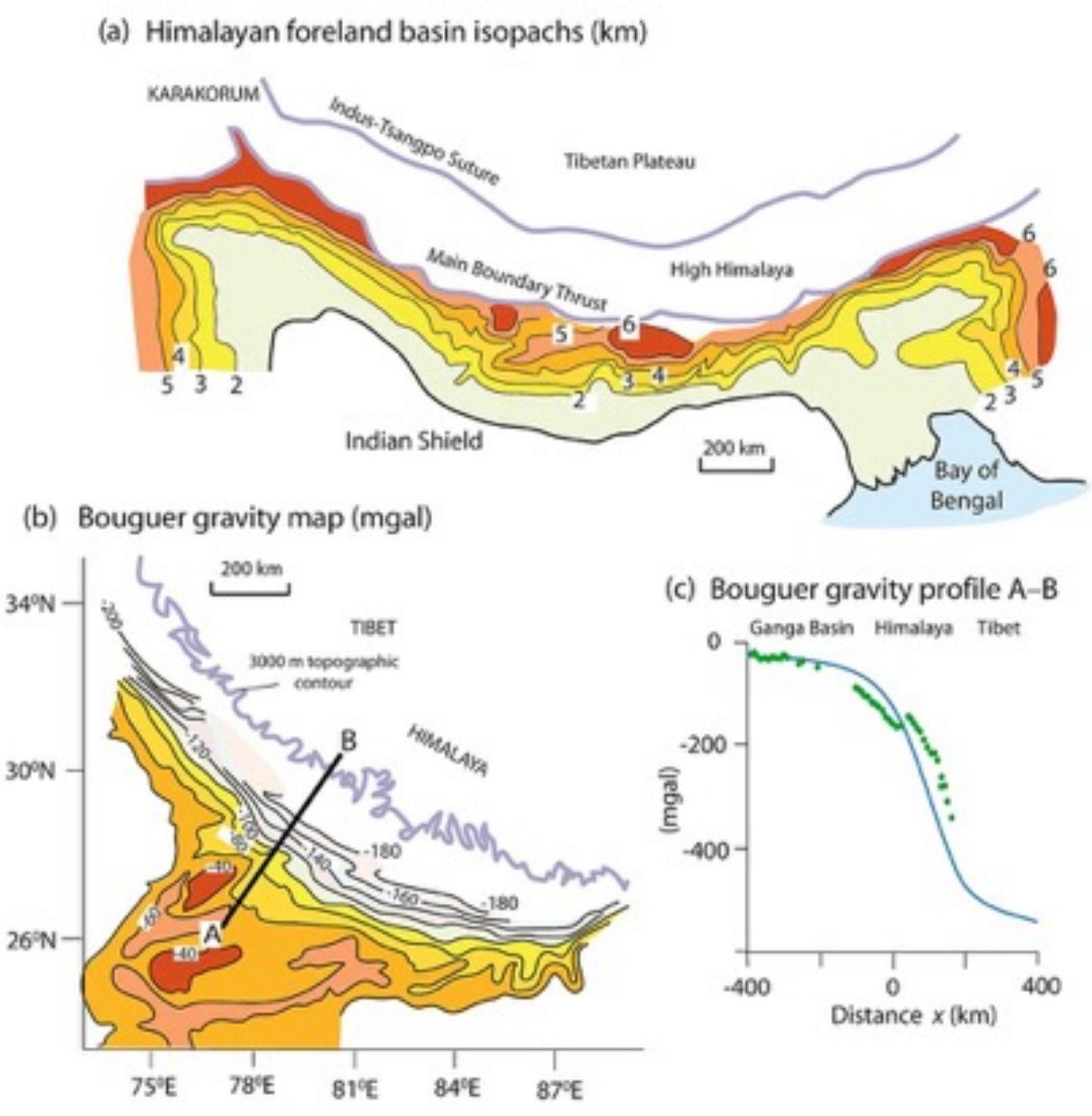

Fig. 4.6 The Himalaya and Ganga Basin. (a) Isopach map of sediment thicknesses in the Himalayan foreland basin, based on Raiverman *et al.* (1983). (b) Contours of Bouguer gravity anomaly over the Ganga Basin. (c) Observed Bouguer gravity anomalies along profile A–B, compared with the anomalies computed assuming the topography is locally compensated (Airy model) by thickening of the crust beneath central India. Note that there is an apparent mass excess in the Himalaya and a mass deficit over the Ganga Basin (after Lyon-Caen & Molnar 1985). (b) and (c) reproduced with permission of John Wiley & Sons, Inc.

gravity anomalies, T_e and the Ganges Basin

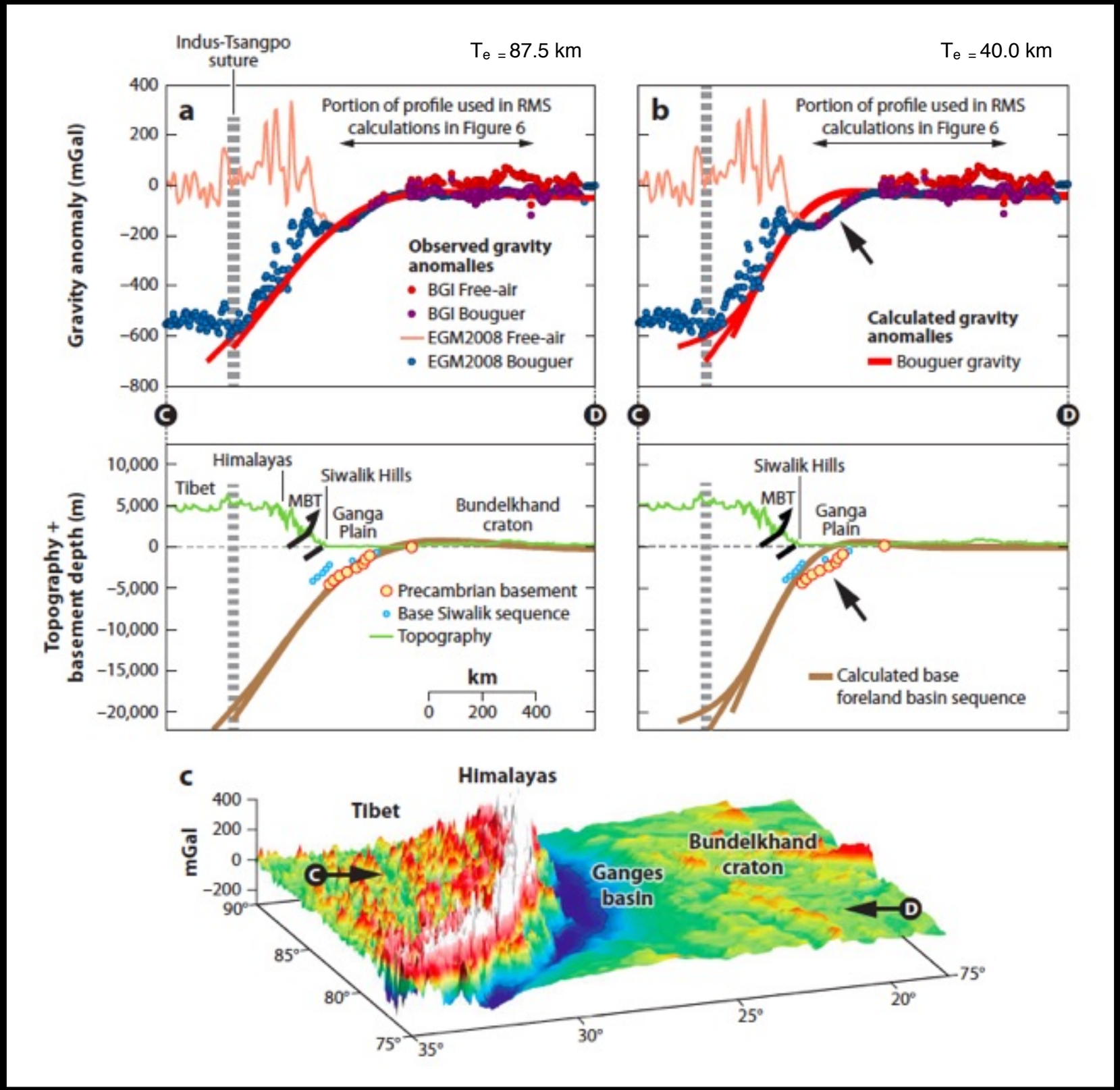

Te vs broken plate

minimize error in parameter space

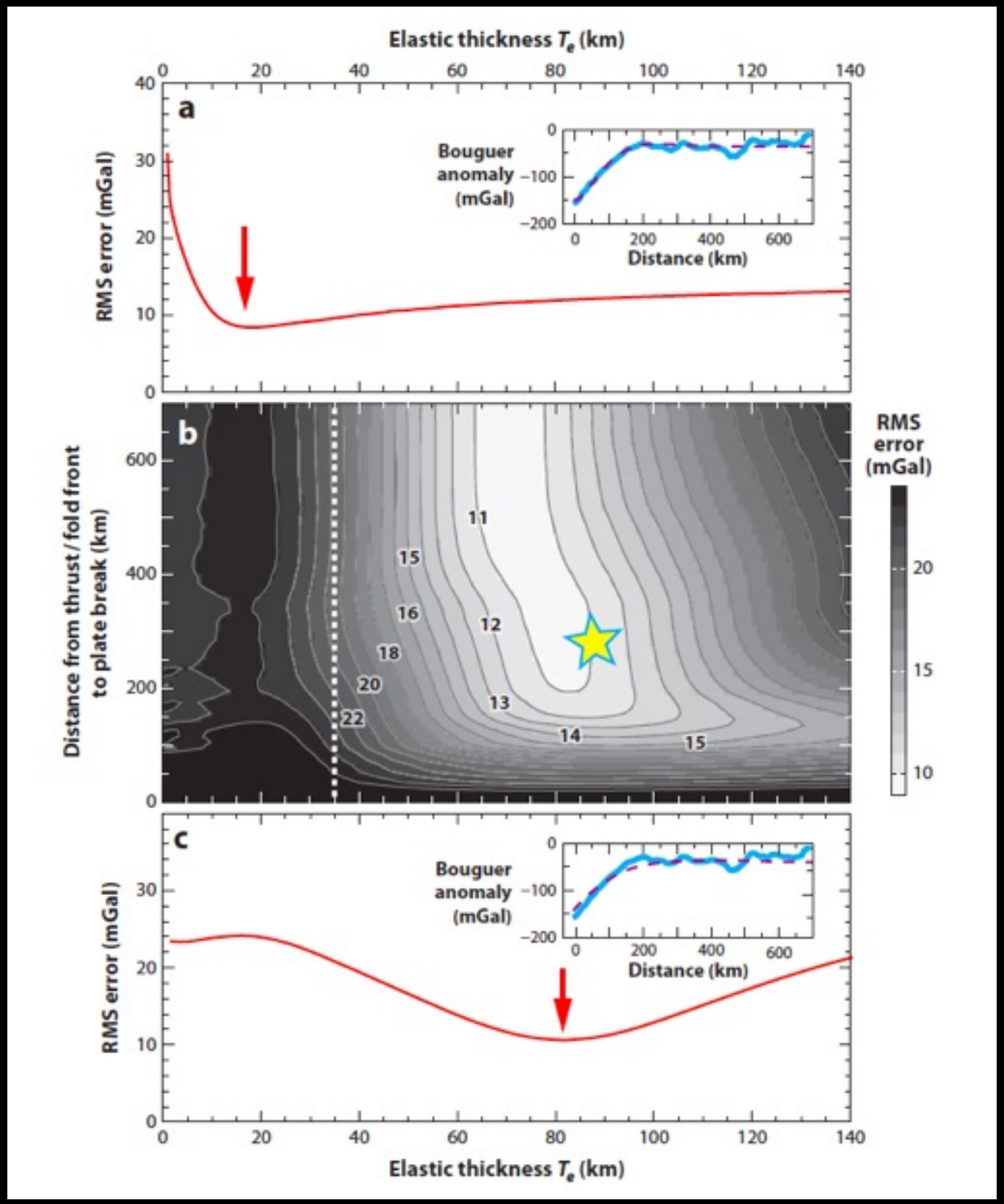

T_e estimates

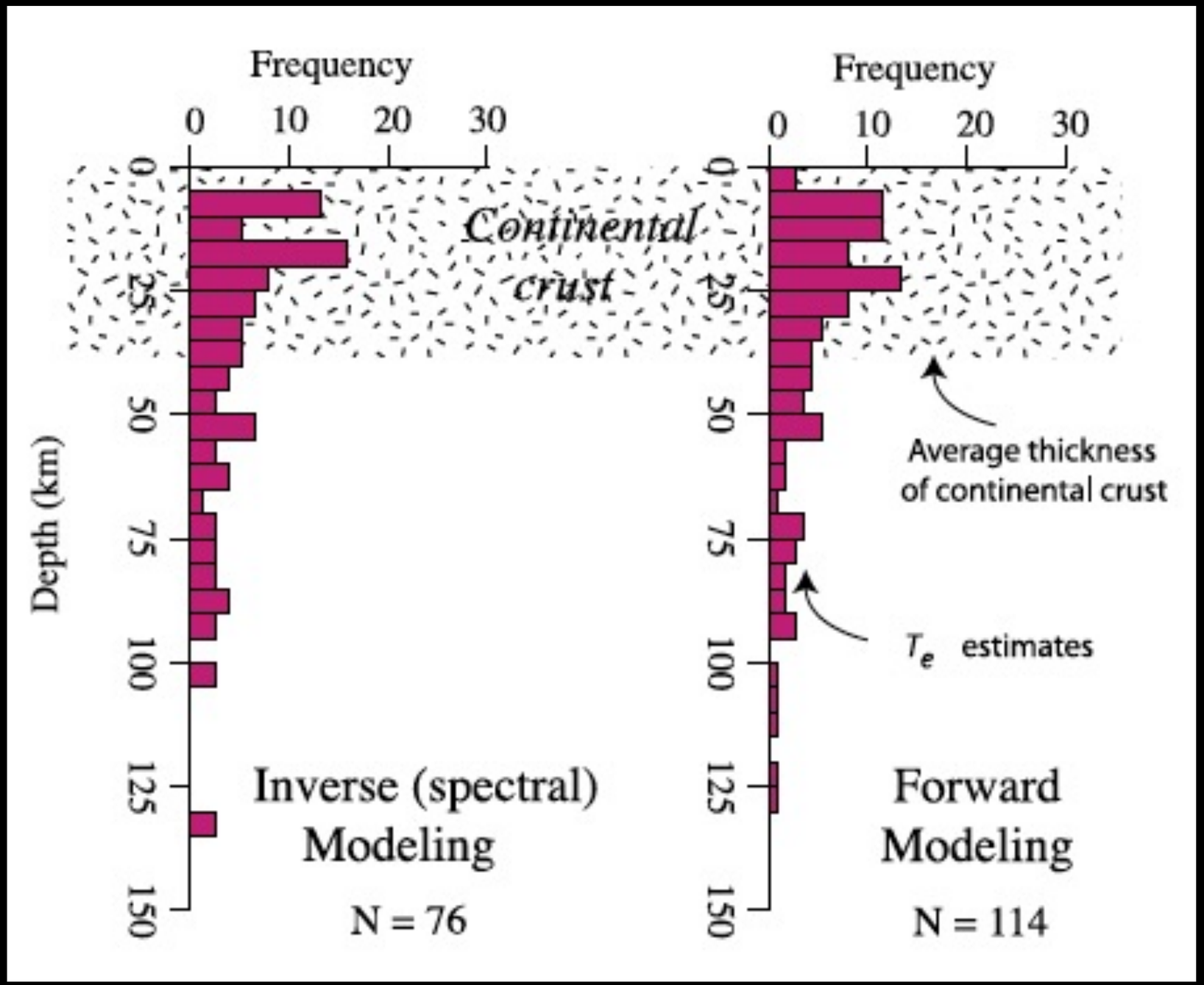

forebulge or outer rise map

gravity anomalies

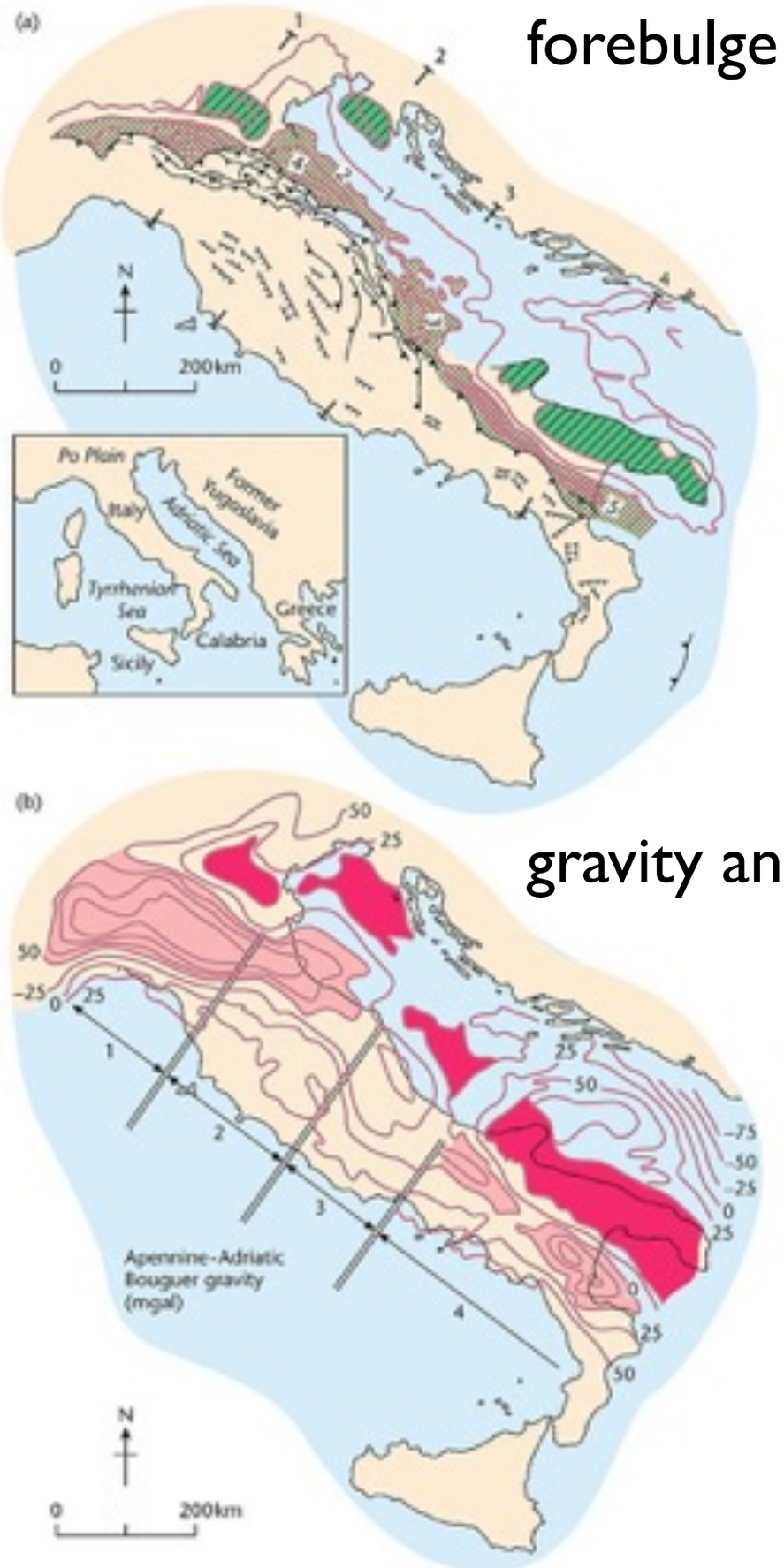

Fig. 4.18 (a) General map of the Apennine system showing depth to the base of the Pliocene in the Adriatic and Po basins at a 1 km contour interval. There are four distinct outer rise/forebulge segments recognised in the basal Pliocene surface (shown in wide diagonal hatch). The narrow diagonal hatch shows the Apennine foreland basin and parts of the basal Pliocene surface that is below 2 km in depth. (b) Simplified map of the Bouguer anomaly gravity field (milligals). Contour interval is 25 mgal. The four morphological outer rises correspond to Bouguer gravity highs, suggesting that they are maintained by regional flexure. The dark shaded areas represent anomalies of greater than 0 mgal in sectors 1 to 3 and 50 mgal in sector 4: light shading shows gravity anomalies less than −50 mgal in sectors 1 to 3 and 0 mgal in sector 4. These sectors are believed to be bounded by major tears in the subducted plate, segmenting it at depth. After Royden *et al.* (1987), compiled from Ogniben *et al.* (1975), Morelli *et al.* (1975) and Bertotti *et al.* (2001).

foreland basin heat flow

fluids in motion

competing models

tectonic squeegee or topographically driven flow?

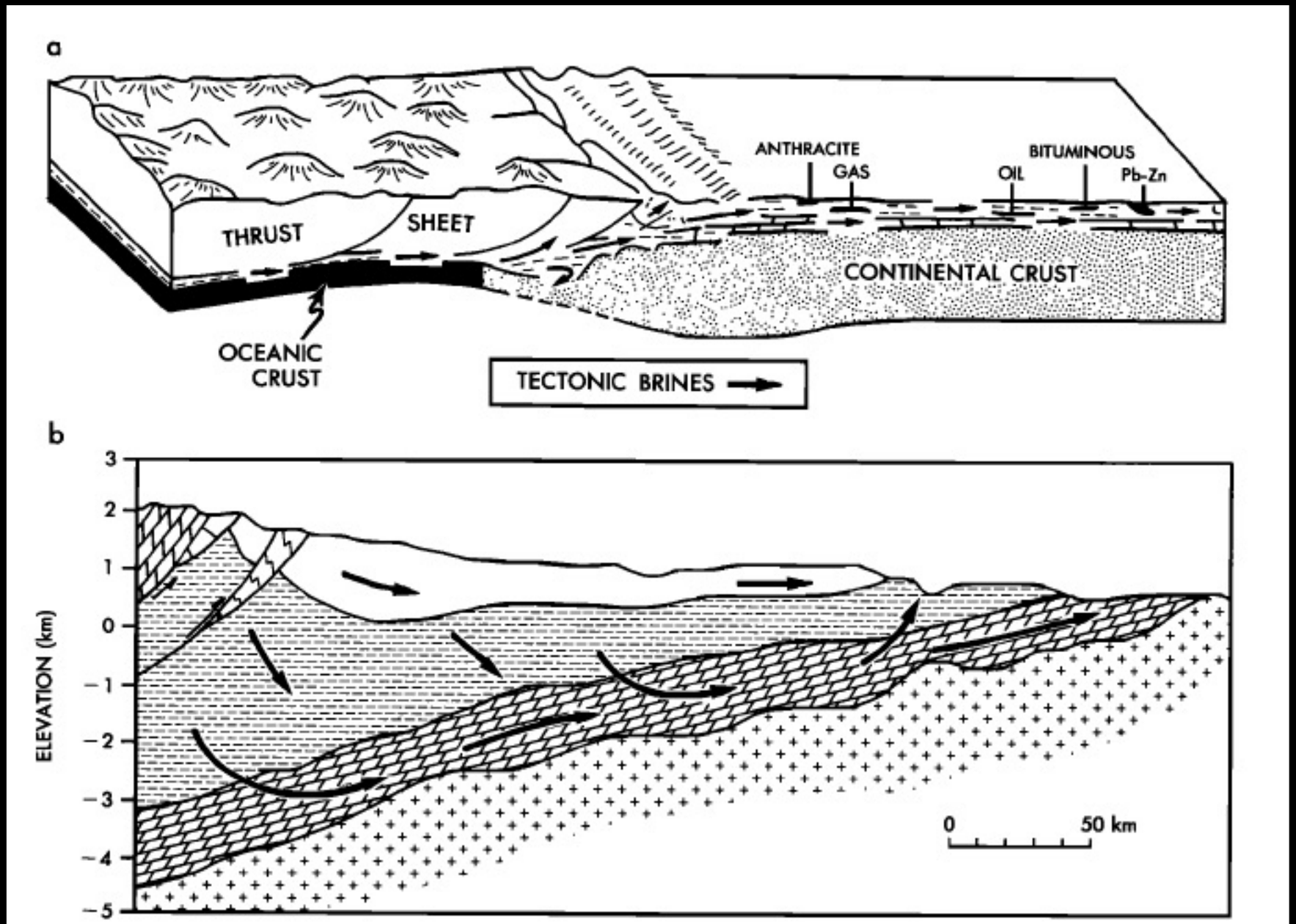

Fig. 2. Schematic illustration of hypotheses proposed as possible mechanisms of brine migration: (*a*) squeegee [after *Oliver*, 1986, p. 99]; and (*b*) topographically driven recharge [after *Garven and Freeze*, 1984*a*, p. 1091].

location of basins and MVT lead-zinc deposits

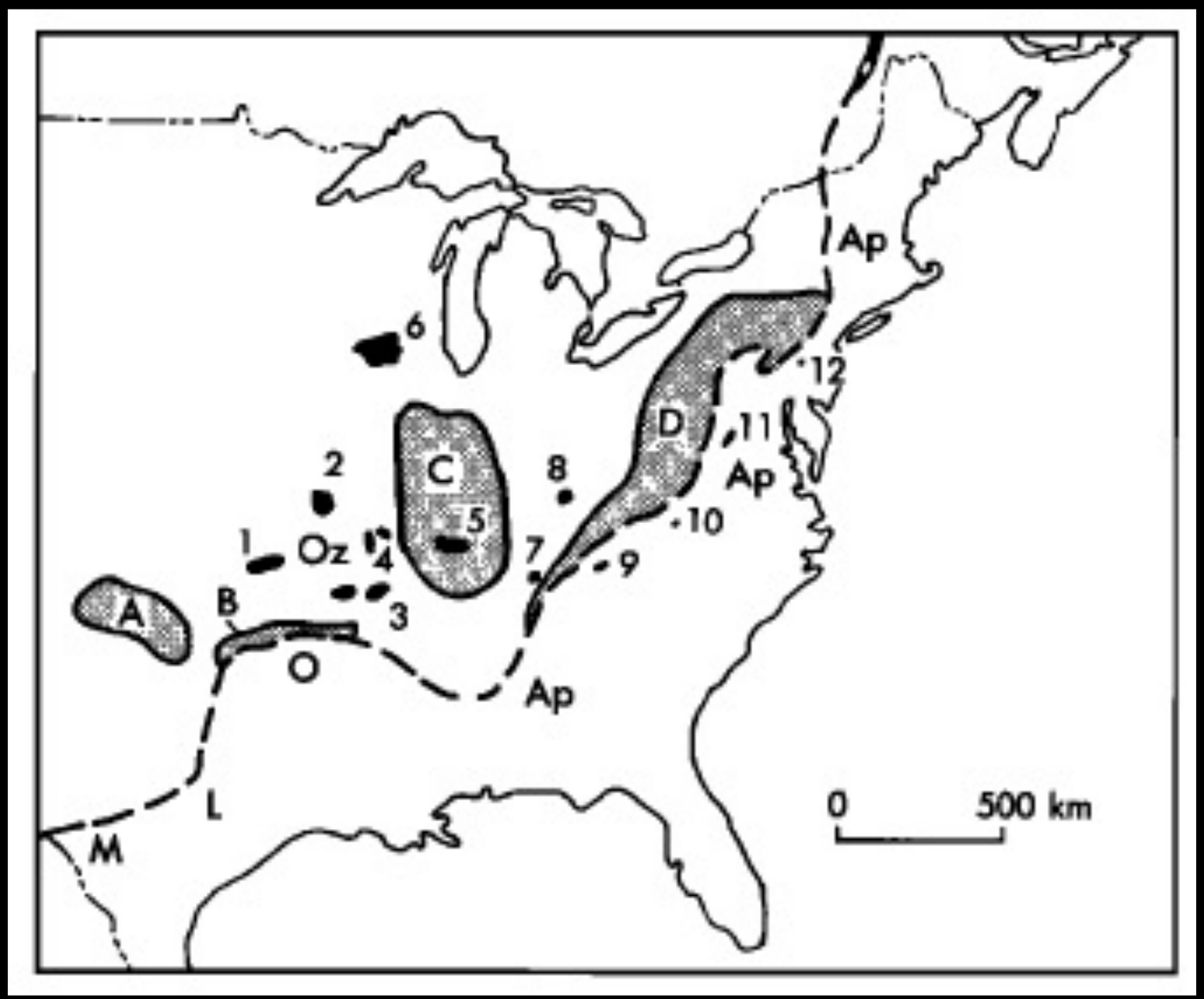

heat flow in northern Alaska

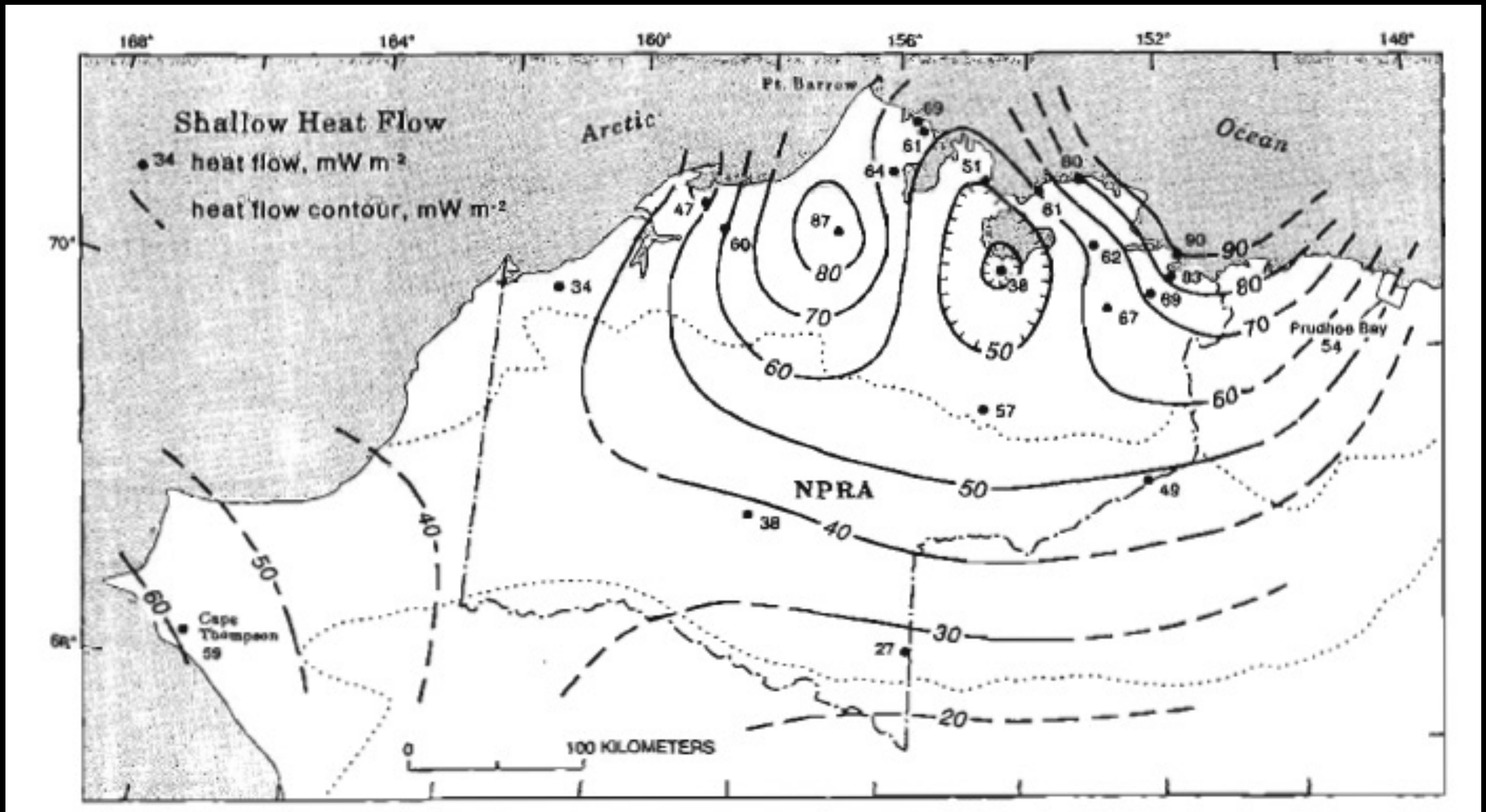

isotherms N-S section

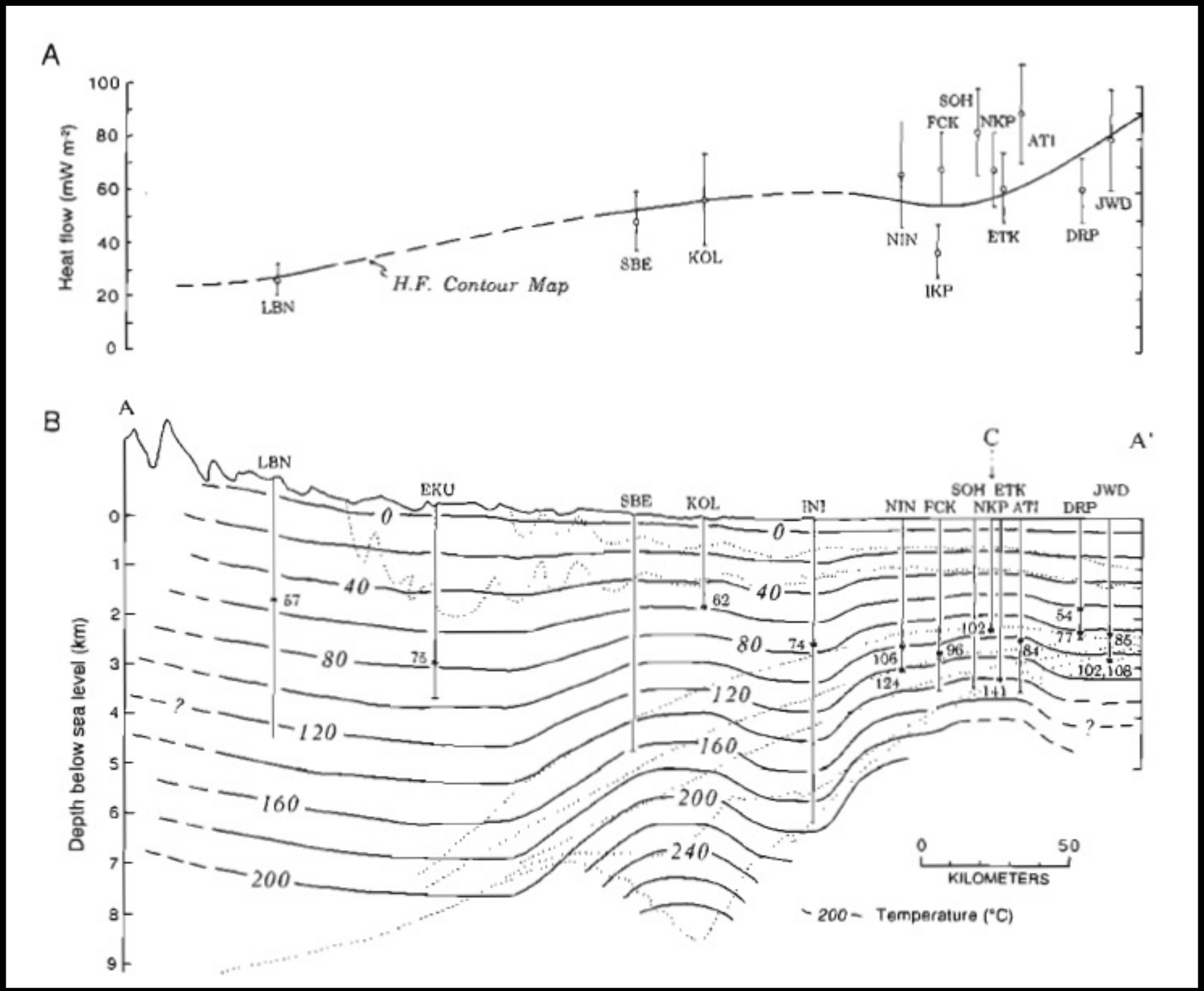

model set up

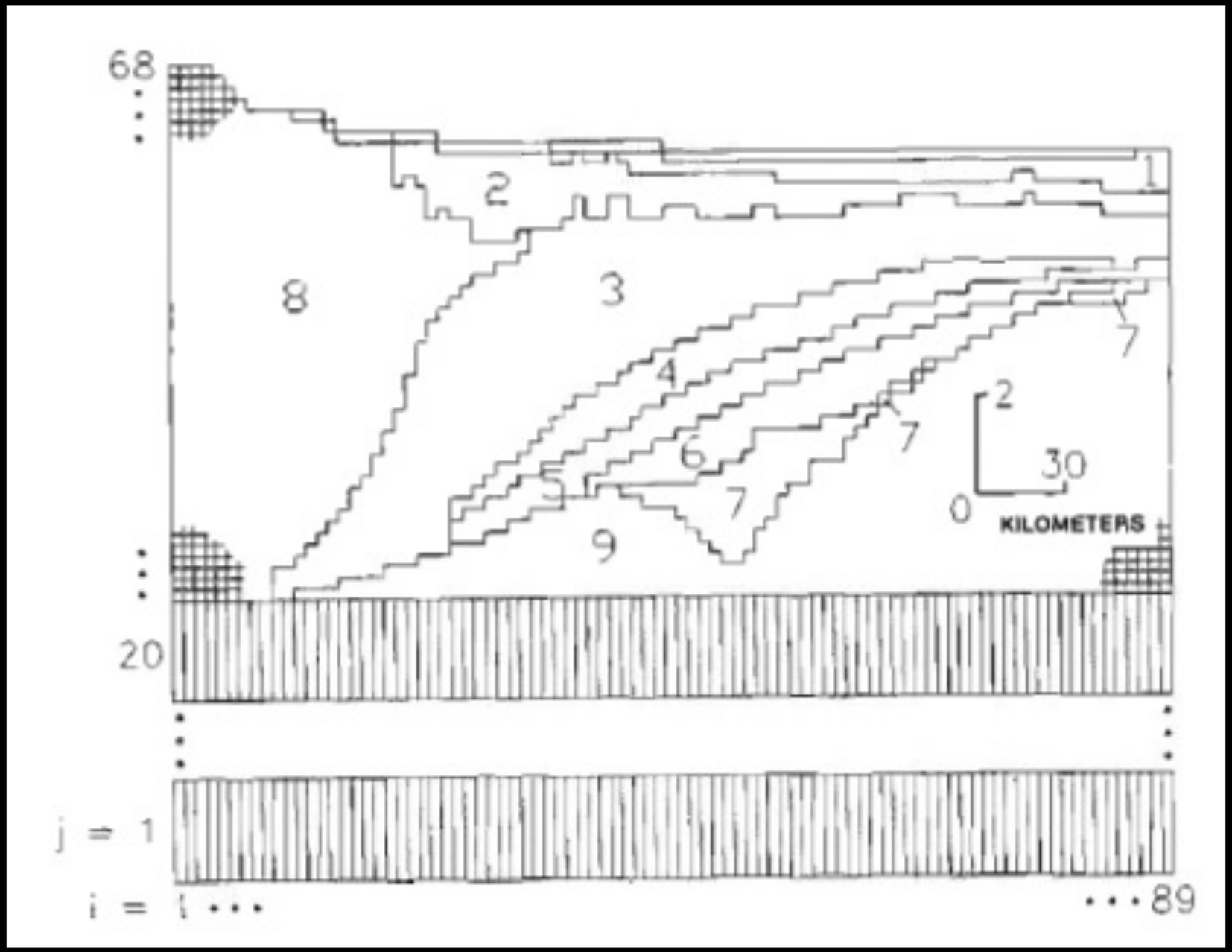

model estimates

water flow and heat flow

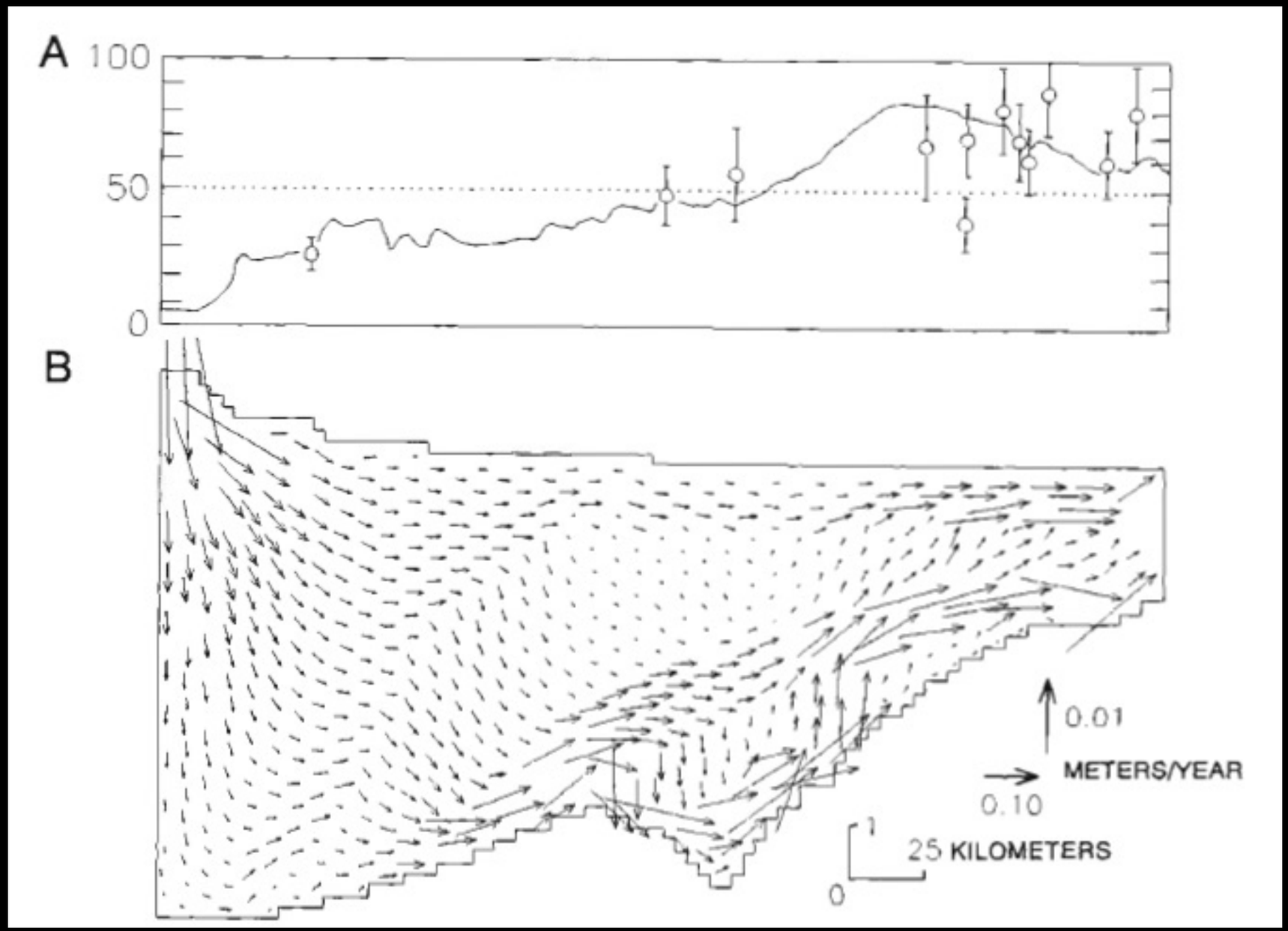

heat flow in forelands

- No crustal thinning
- A change in the concentration of radioactive elements?
- Likely basin fluid fluxes are the largest influence

constraints on wedge deformation

accretionary prisms and thrust wedges - the theory of critical taper

accretionary prism in 3-D

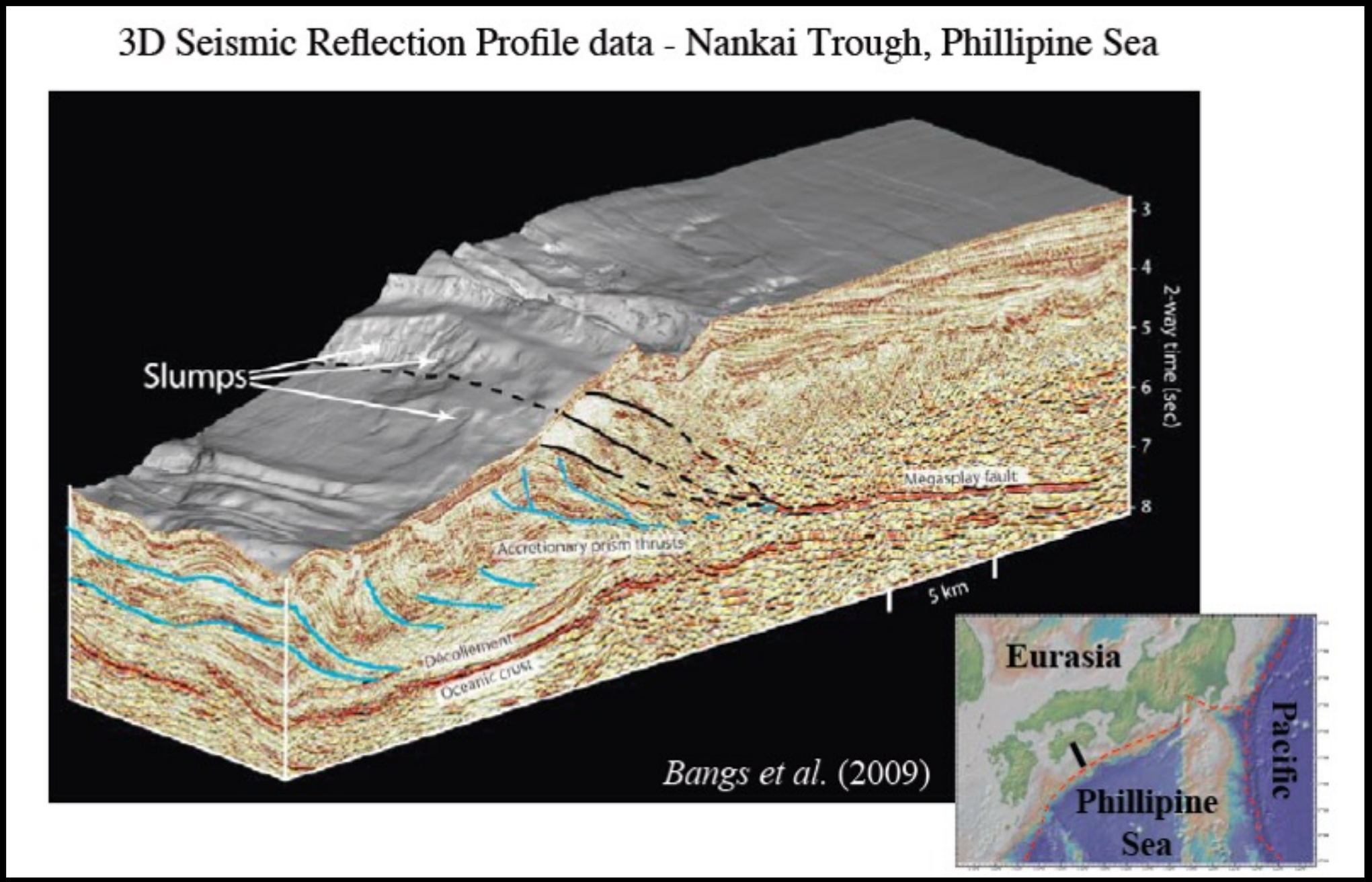

critical taper - a stressed wedge, everywhere on the verge of failure

an excellent model for accretionary prisms

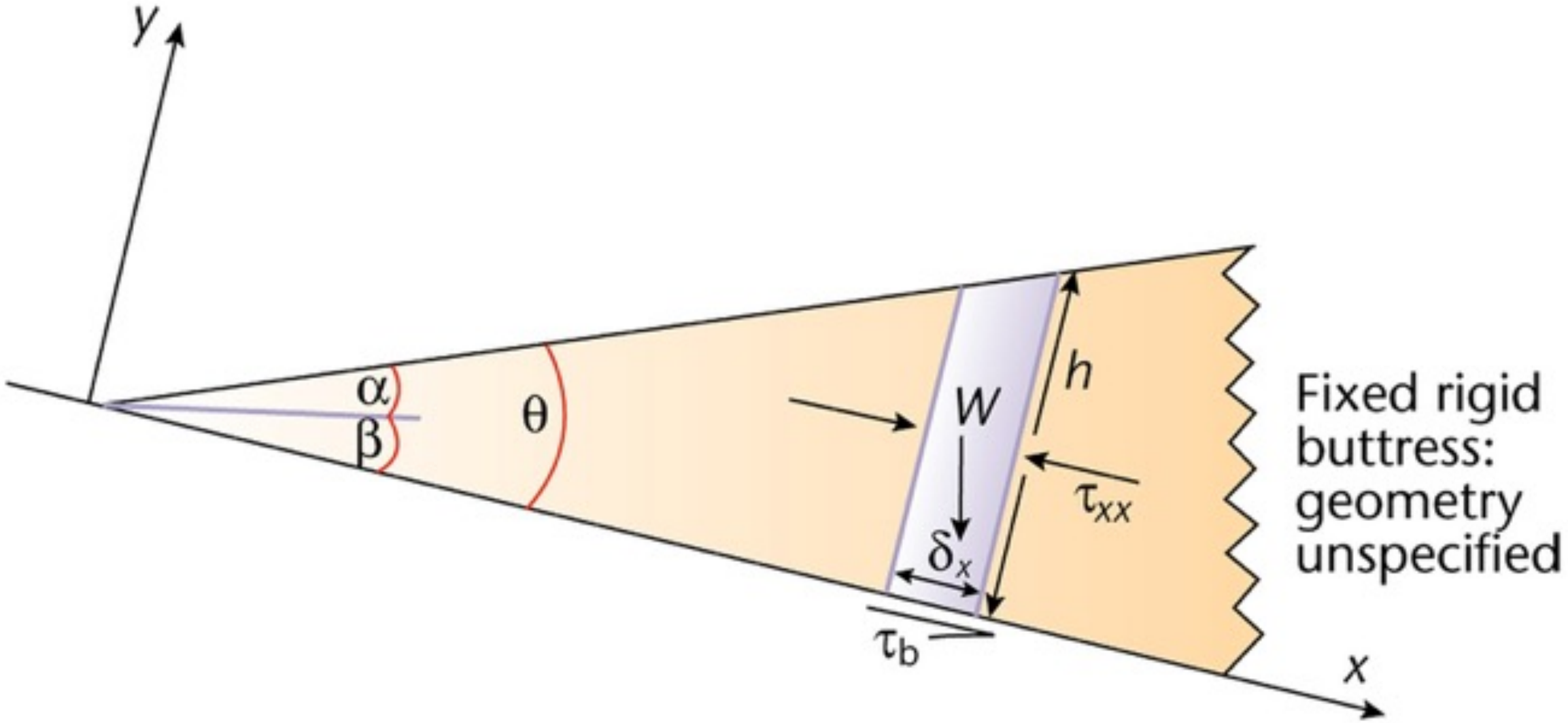

Fig. 4.23 Simplified model of an accretionary wedge (after Platt 1986). α is the surface slope, β is the basal slope and θ is the taper angle ($\alpha + \beta$). A small segment of the wedge of basal length δx and height h is subjected to a body force W, to a basal traction $\tau\delta x$, and to 'push' forces from the rear, produced by the longitudinal deviatoric stresses τ_{xx}. Frontal accretion, underplating, erosion and changes in basal shear stress (for example by changes in the rate of convergence/subduction) place the wedge out of equilibrium. The wedge responds by shortening and thickening or by collapsing by extension.

wedge structure
and evolution

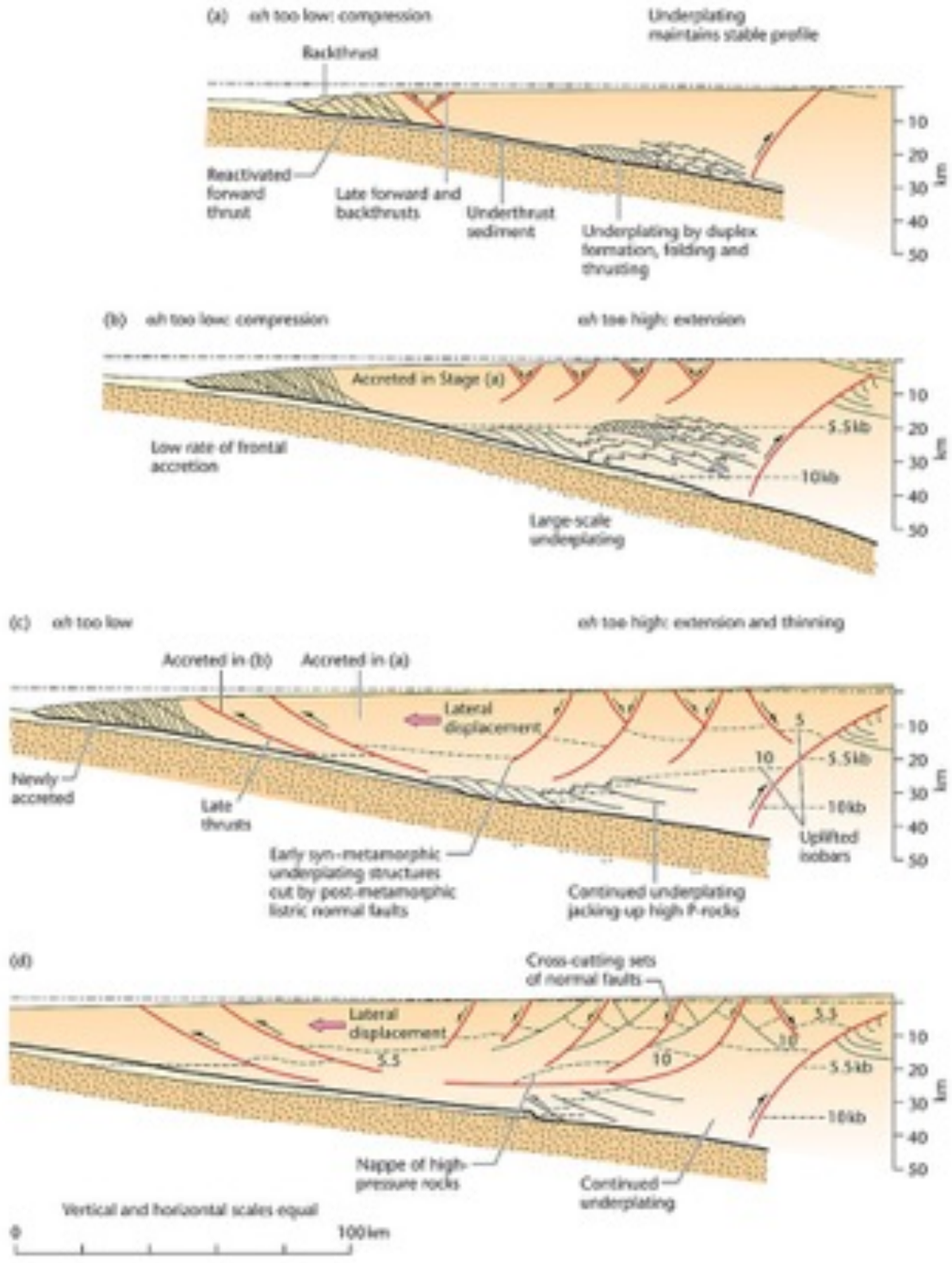

Fig. 4.24 Platt's (1986) evolutionary model of an accretionary wedge from youth to maturity. (a) Early stage with frontal accretion dominant. The gravitational effect of the surface slope (first term on right-hand side of eqn. [4.23]) is too low in the frontal region, which therefore shortens and thickens internally. (b) Large-scale underplating is the dominant mode of accretion, so that the rear of the wedge extends by extensional faulting and possibly by ductile flow near the base of the wedge. The deeper parts of the wedge may also undergo high-pressure metamorphism. (c) Continued underplating and resultant extension has lifted the high-pressure rocks towards the surface. Extension towards the rear of the wedge promotes some shortening (late thrusting) at the front. (d) In the mature stage, underplating and extension have brought the high-pressure rocks to levels accessible to erosion. The prism is now 300 km long, comparable to the Makran wedge of Pakistan. After Platt (1986).

the role of sedimentation and erosion

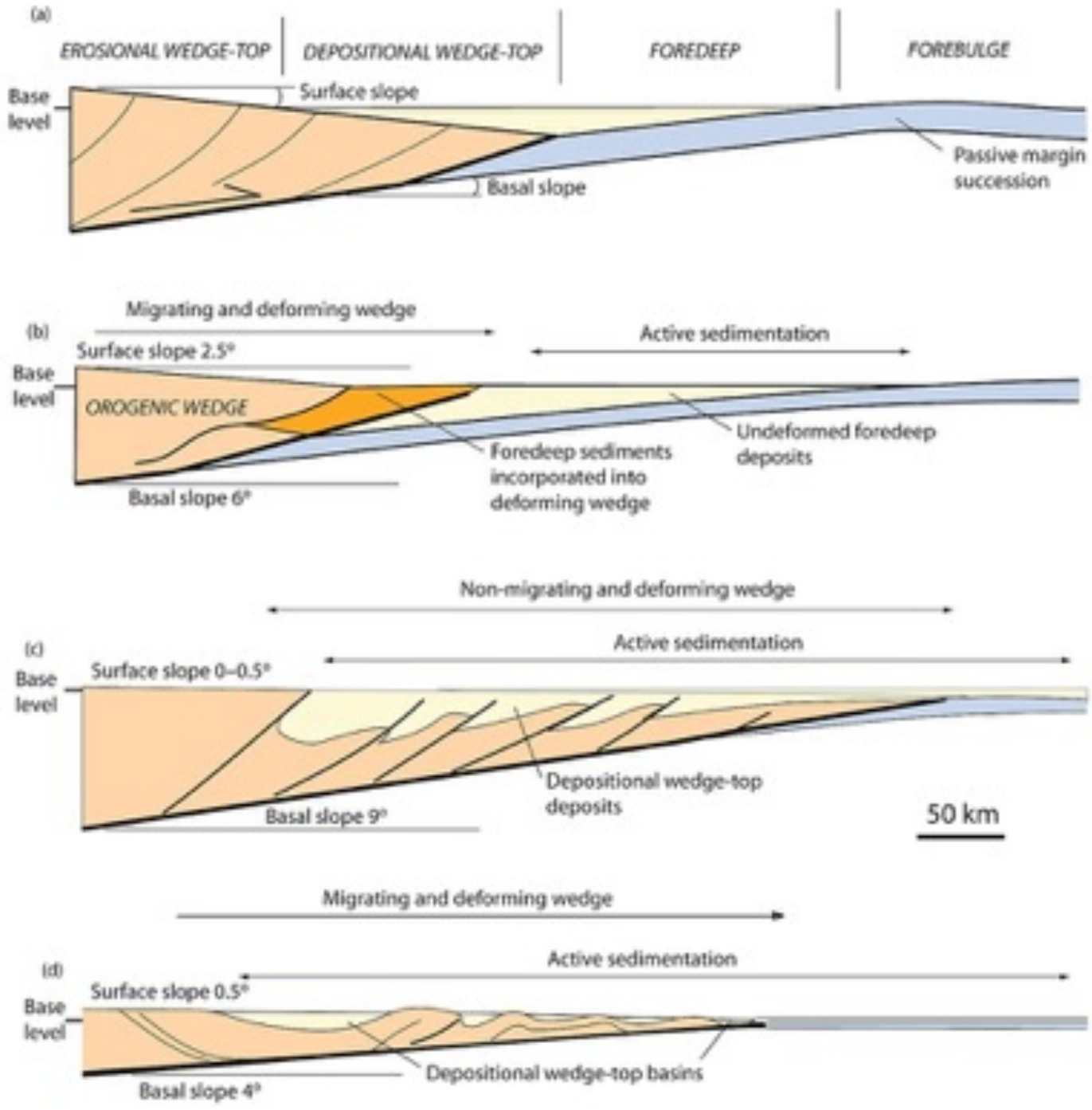

Fig. 4.25 Depositional versus erosional wedge tops, after Ford (2004). (a) The extent of the depositional and wedge-top zones depends on the geometry of the critically tapered wedge combined with the flexural response of the underlying lithosphere, resulting in a basal slope and a surface slope. (b) Basal slope of 6° and surface slope of 2.5°, showing an erosional wedge-top and depositional foredeep, with some foredeep sediment incorporated tectonically into the frontal part of the wedge. This situation may reflect a moderate basal strength of the wedge and a moderate flexural rigidity of the underlying plate. (c) Basal slope of 9° and surface slope of zero to 0.5°, with the wedge filling the deflection, and active sedimentation in wedge-top basins. This situation may reflect a weak underlying lithosphere. (d) Basal slope of 4° and surface slope of 0.5°, causing a narrow taper angle, with well-developed piggyback (wedge-top) basins within a deforming fold-thrust belt. The active sedimentation includes the deforming wedge and the foredeep. This situation characteristically results from the presence of a weak basal detachment comprising salt. Reproduced with permission of John Wiley & Sons, Ltd.

surface slope and decollement dip

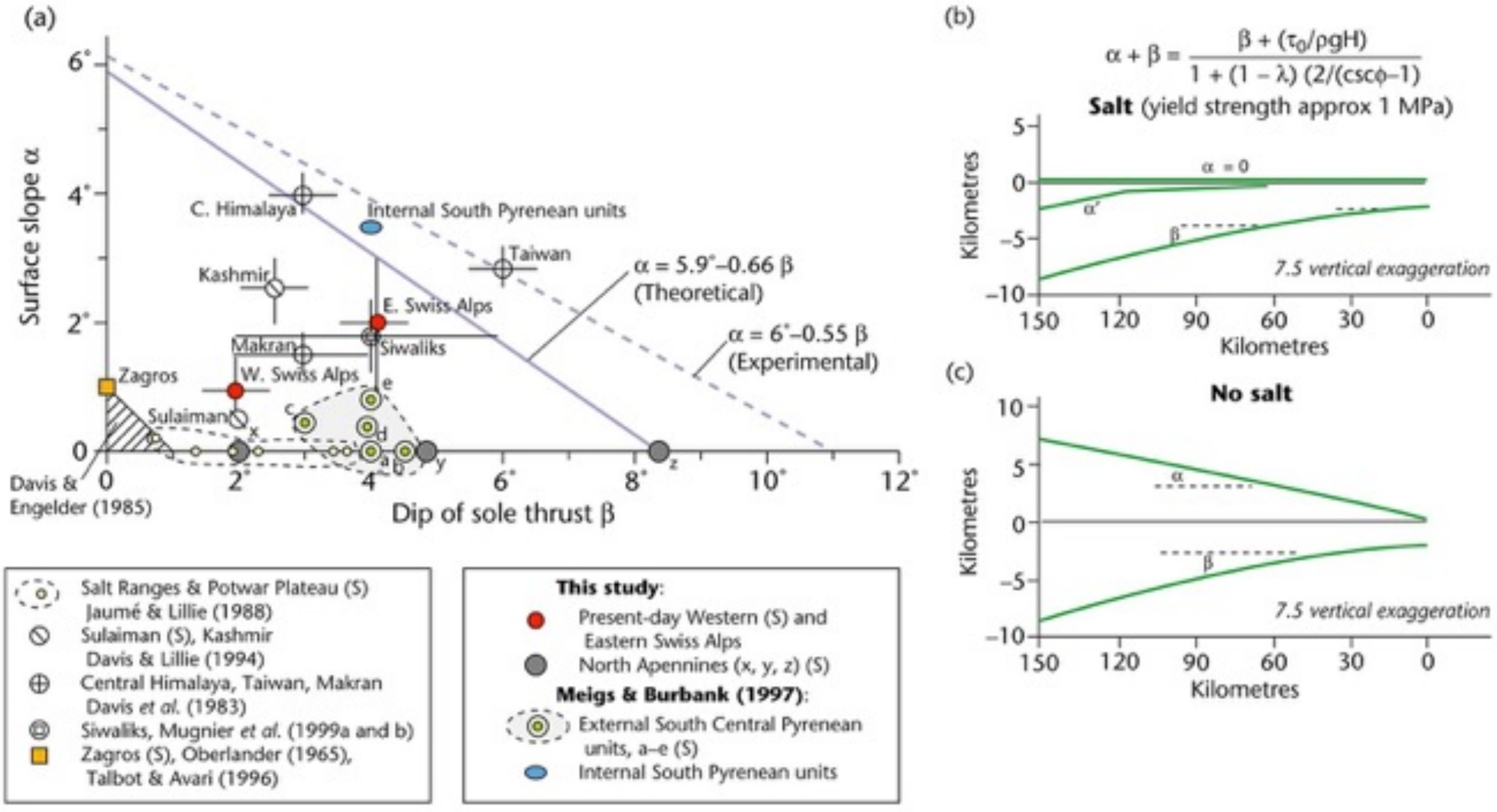

Fig. 4.26 Plot of orogenic wedges in terms of surface and basal slopes (a) with examples of theoretical and experimental curves for salt based (b) and non-salt based (c) orogenic wedges, from Ford (2004). Low surface slopes typify salt-based orogens. (S) in key to (a) indicates a salt basal detachment. Reproduced with permission of John Wiley & Sons, Ltd.

coupling
sedimentation
and deformation

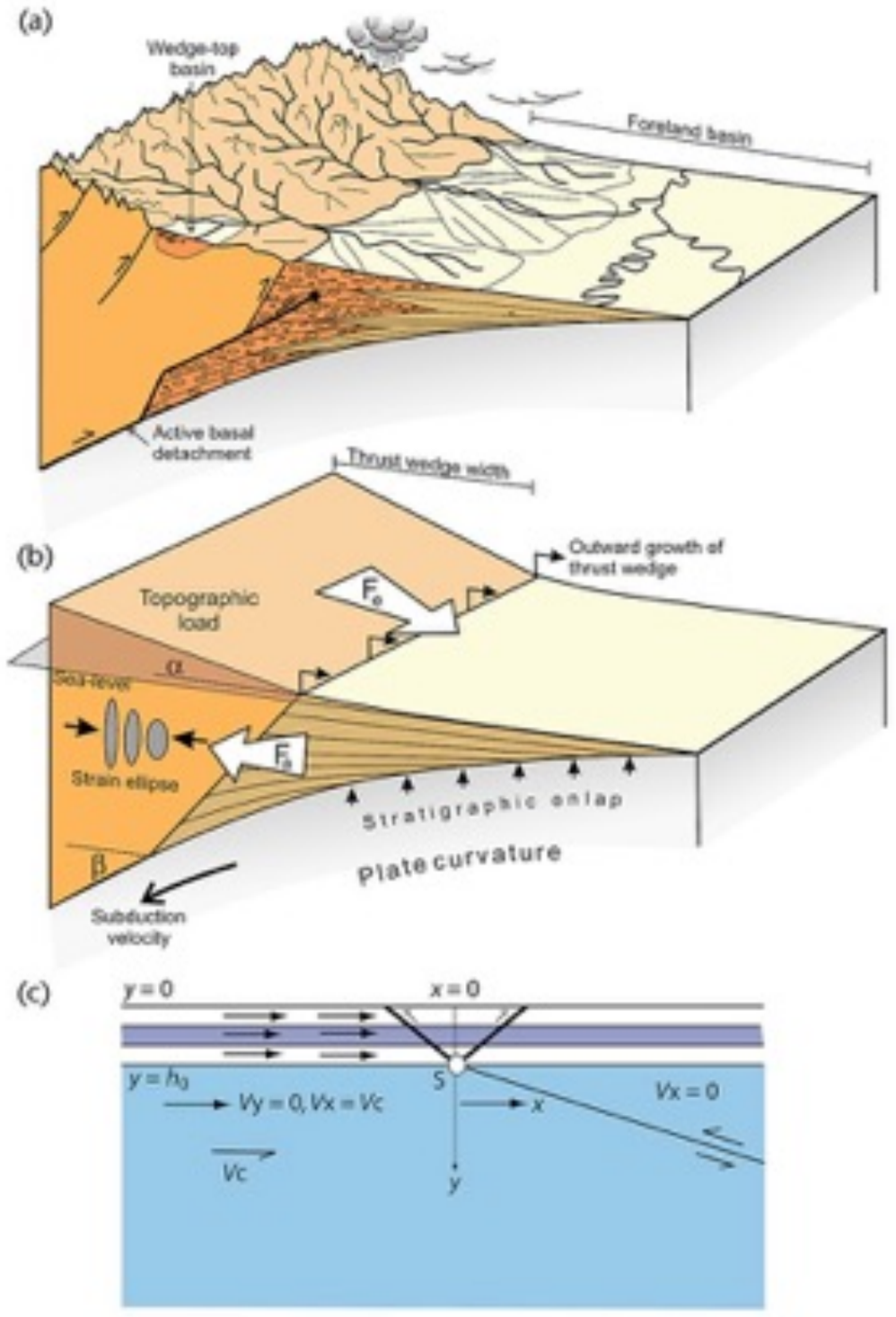

Fig. 4.27 Coupled thrust wedge/foreland basin systems, from Sinclair (2012) and reproduced with permission of John Wiley & Sons, Ltd. (a) Geological and topographic characteristics showing thrust wedge with ramp-flat staircase geometry of basal detachment. (b) Quantifiable parameters include the erosional (F_e) and tectonic (F_a) accretionary fluxes, the mean surface slope of the wedge α, and the mean slope of the basal detachment β. (c): geodynamic model, showing crustal deformation focused at a point S, where mantle of the plate on the left, moving with a constant tangential velocity of convergence V_c, detaches and is underthrusted. V_x and V_y are the horizontal and vertical velocities respectively. Overlying crust has initial thickness h_0 to the left of S. The tangential velocity to the right of S is zero. There is no stress on the upper surface. There is no requirement for a 'bulldozer' backstop in this geodynamic model. Inset modified from Willett *et al.* (1993).

Controls on accumulation in forelands

- Basin-forming mechanism
- Sediment transport/availability
- critical taper
- Isostasy and compaction

Accommodation Space

Space made available for sediment accumulation by basement subsidence

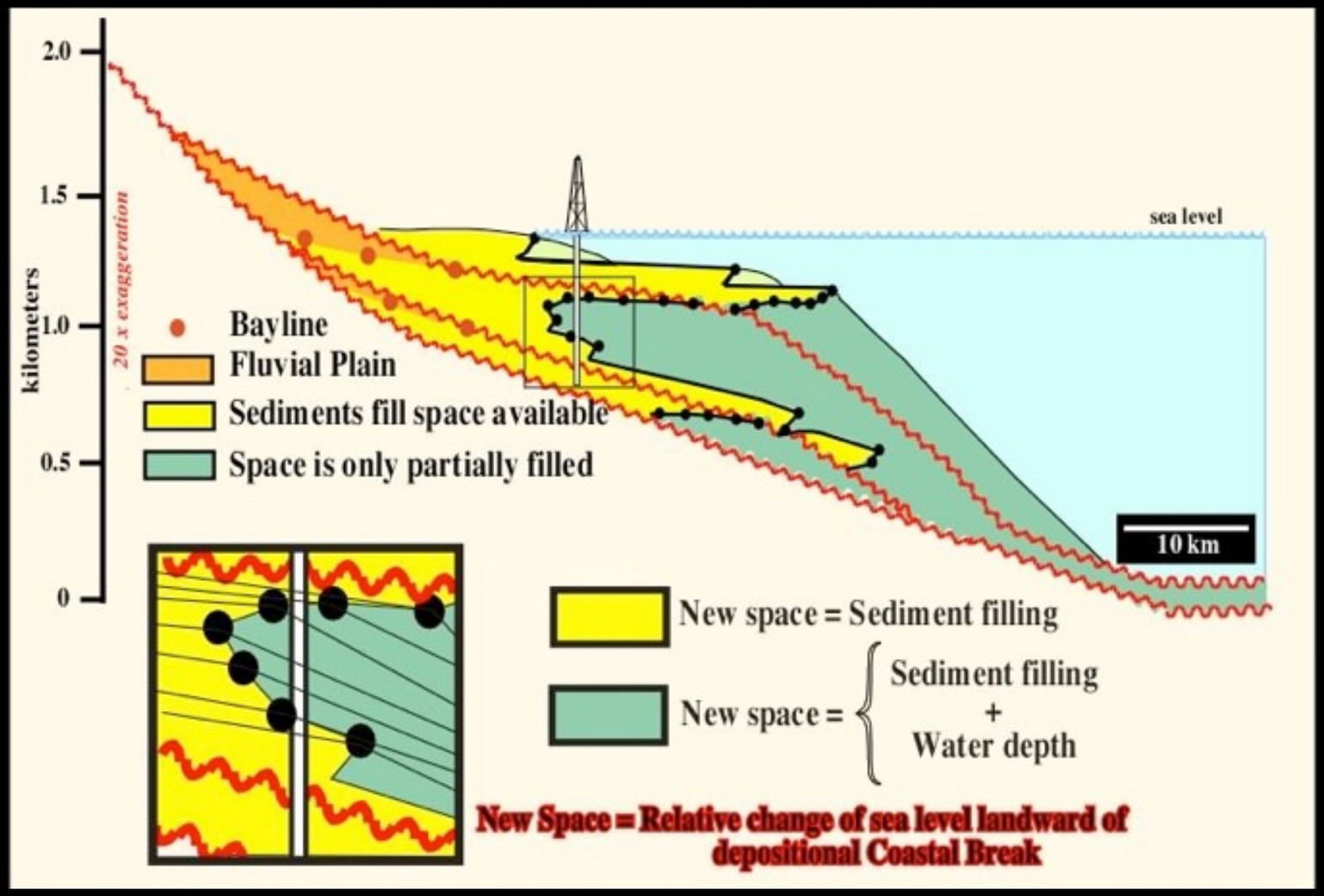

Tectonics act slowly over time, so each unconformity is, uniquely, a record of sea level change

What is the cause of unconformities?

- Sea level change
- Tectonic processes

Allocyclicity

- Sedimentary autocyclicity

In foreland basins, stratigraphy has been interpreted as being formed during alternating pulses of tectonic activity and “quiescence”

An assumption about tectonics

- Plate motions are the engine of earth deformation
- If plate motions are smooth and steady, then **local** tectonic reorganization is the only possible tectonic cause for basin-scale unconformities
- for a foreland basin, this requires changes in the distribution of the thrust load
- Given steady tectonics, how can you create distal unconformities in foreland basins?

Beaumont 1981

Geophys. J. R. astr. Soc. (1981) **65**, 291–329

Foreland basins

Christopher Beaumont *Oceanography Department, Dalhousie University, Halifax, Nova Scotia B3H 4J1, Canada*

Received 1980 April 18

Summary. The characteristic pattern of the subsidence, deformation, uplift and erosion of foreland basins, or exogeosynclines, has long been recognized by geologists as an integral part of the geosynclinal cycle yet only descriptive models have been proposed. This evolution is quantified in terms of a model of regional isostatic adjustment of the lithosphere under the mass load of the adjacent migrating fold-thrust mountain belt. It is shown that the foredeep, which received the clastic wedge of detritus from the core of the orogen and the fold-thrust belt, owes its existence to downward flexure of the litho-

Downloaded from http://gji.oxfordjournals.org/ at Universi

Rocky Mountains and the Alberta Foreland Basin

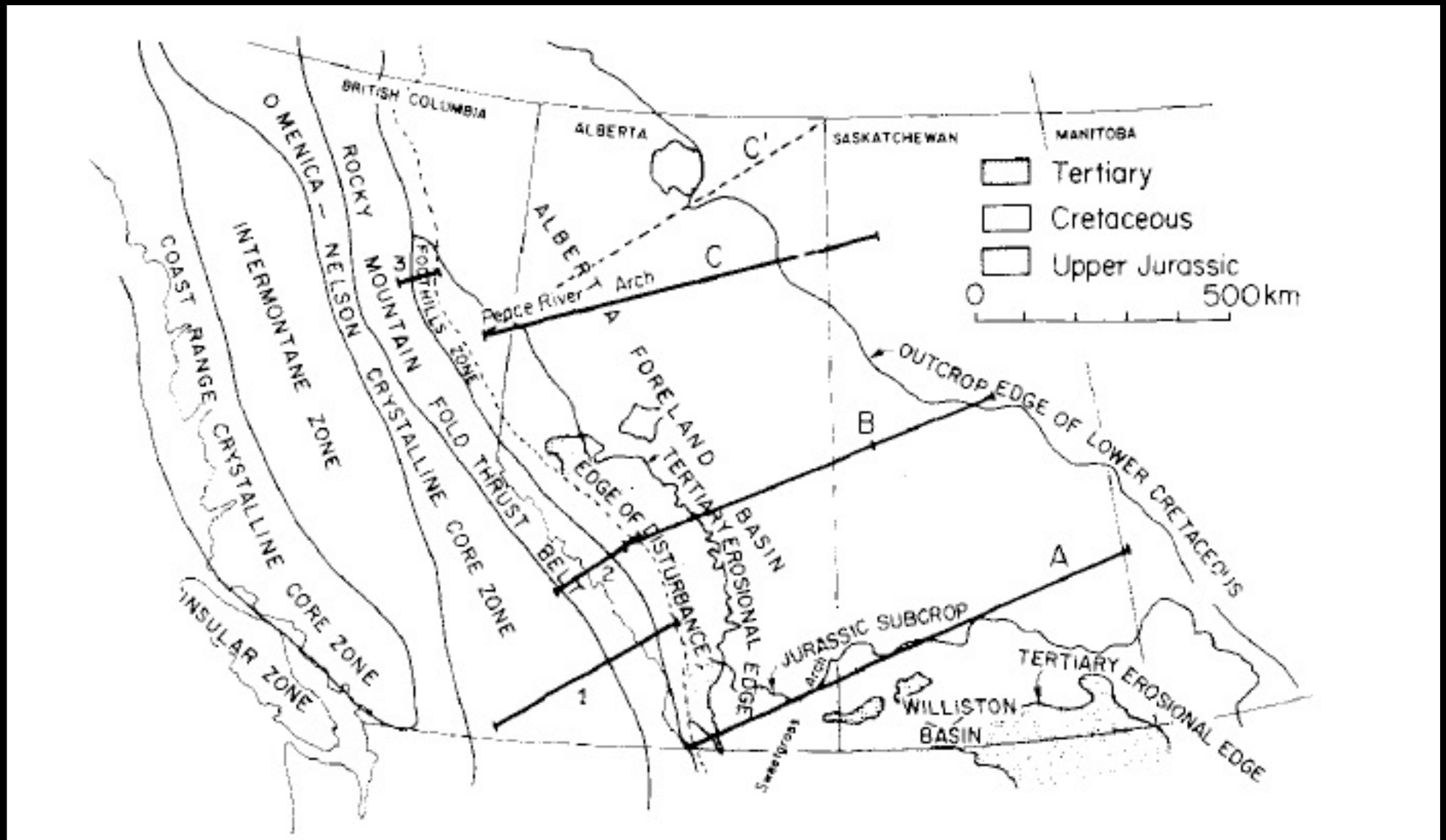

Model 1 - Section B

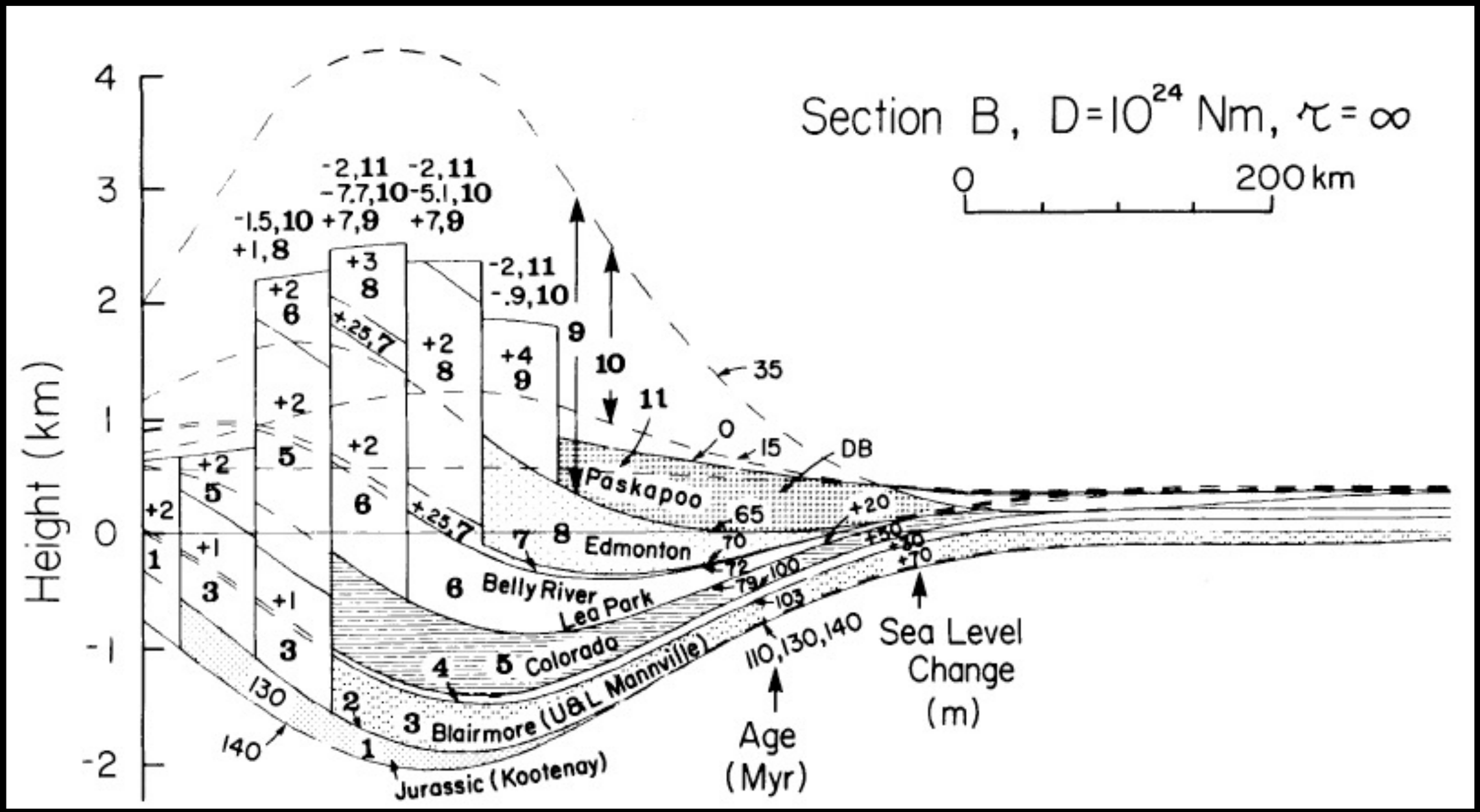

Model II - Section B

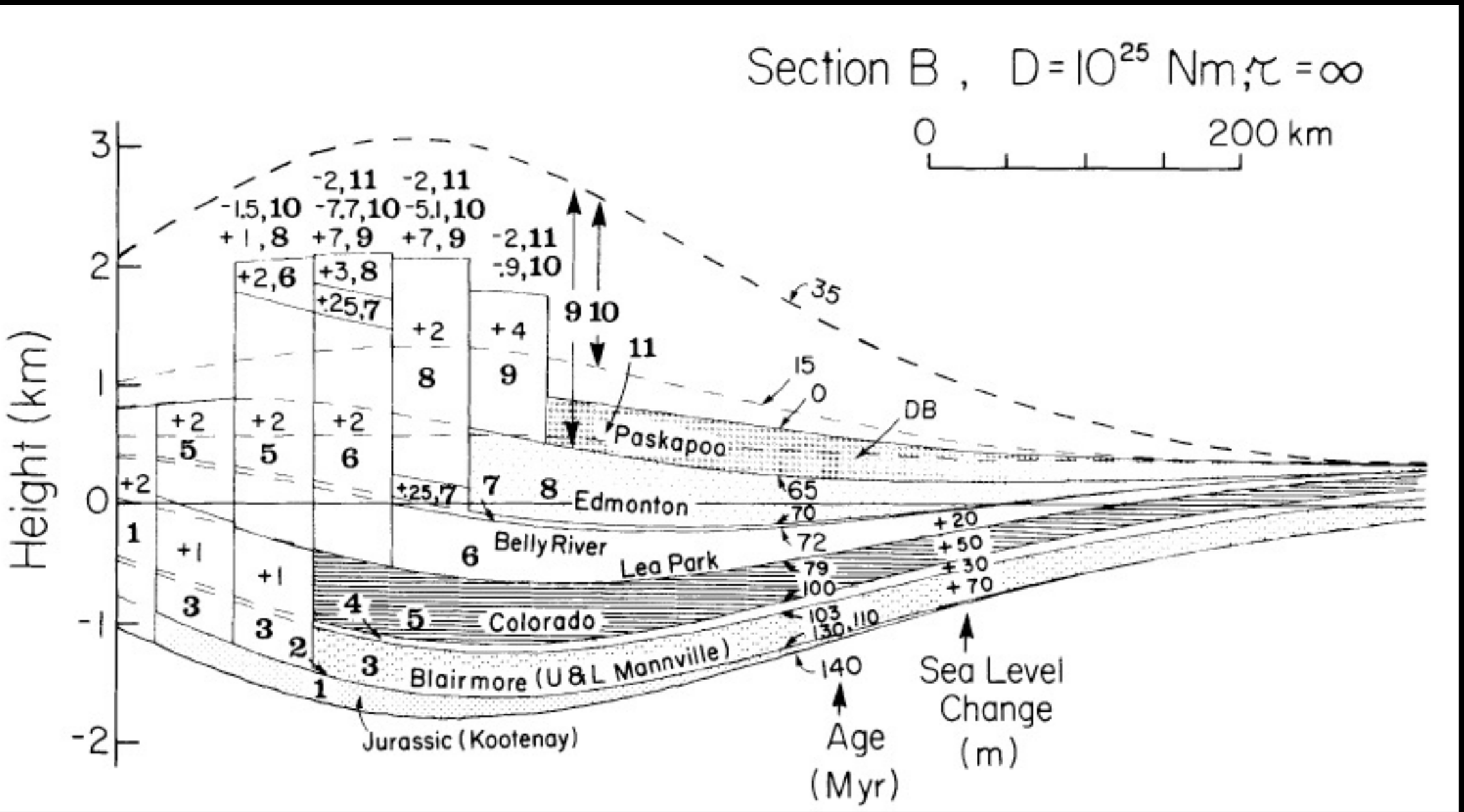

Model III - Section B

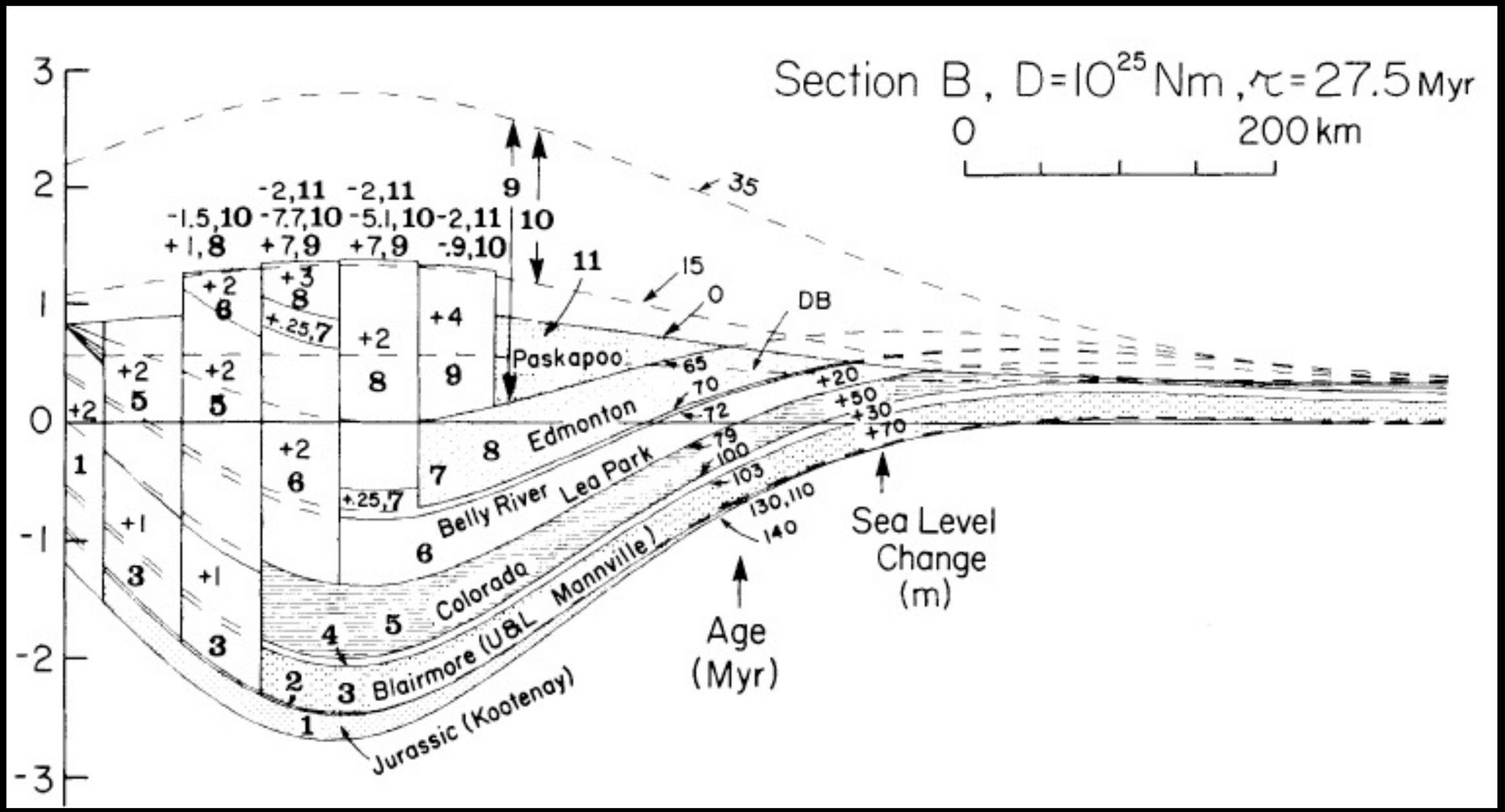

Problems

- assumes layer - cake stratigraphy
- each layer is associate with a new load
- assumes the basin is constantly full

Stratigraphy of Arctic Alaska

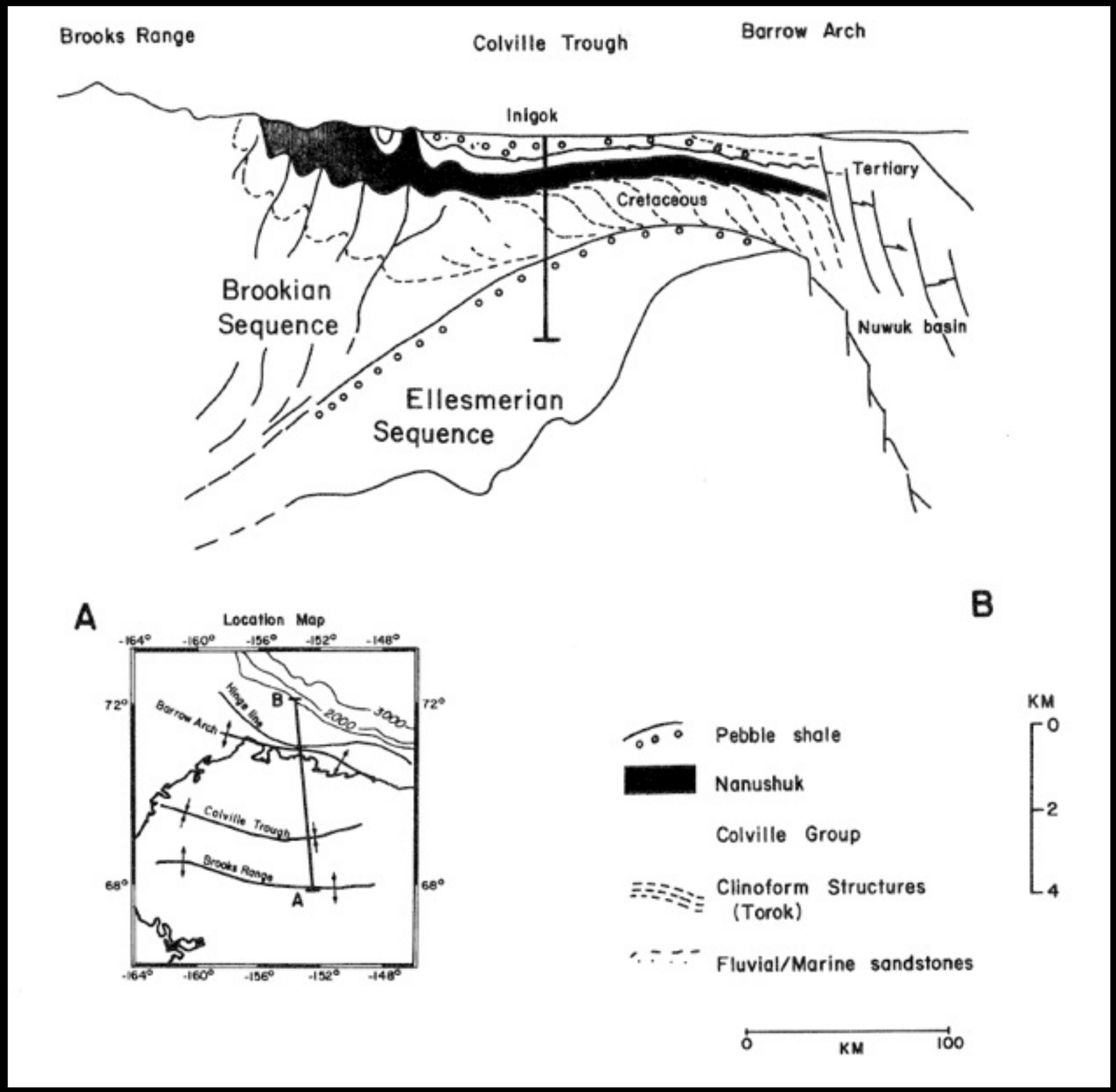

Sediment Sources

North and South

Colville Trough

Barrow Arch

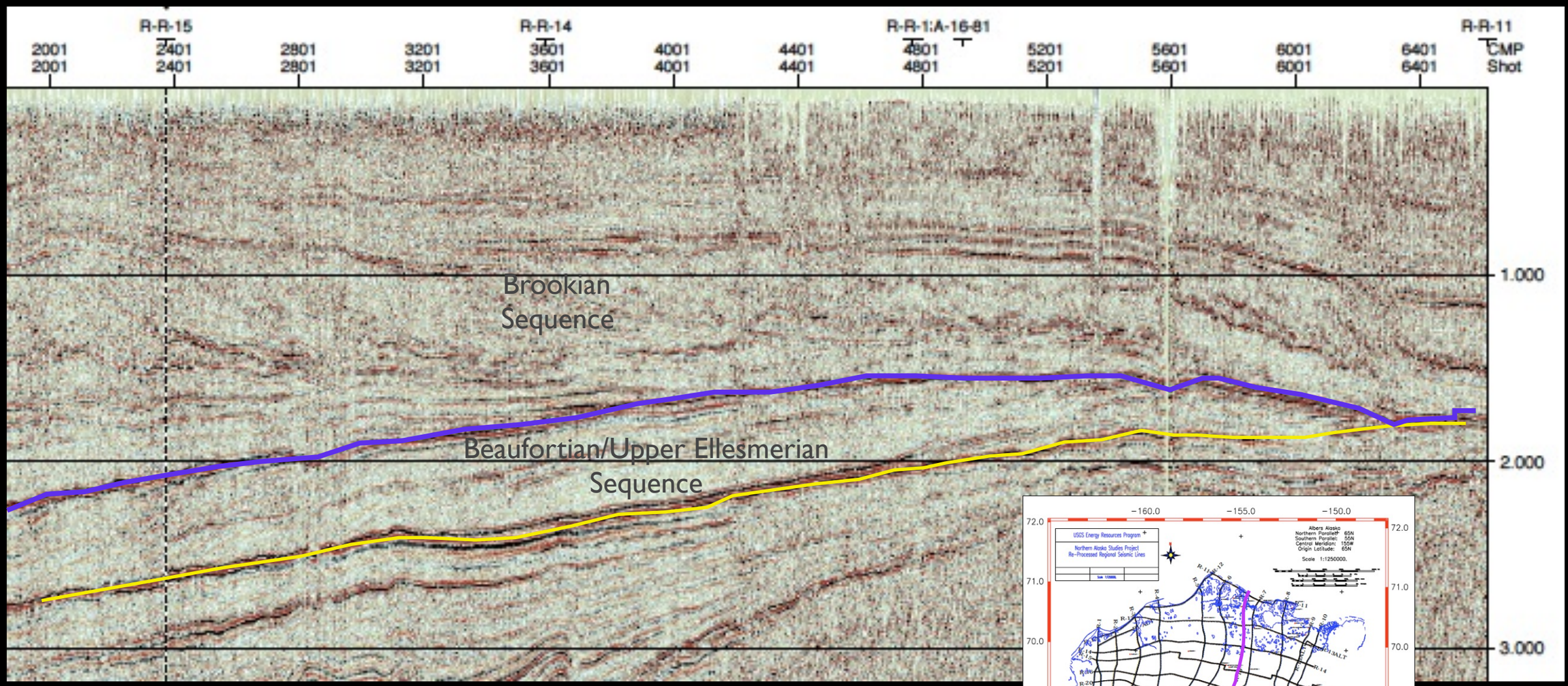

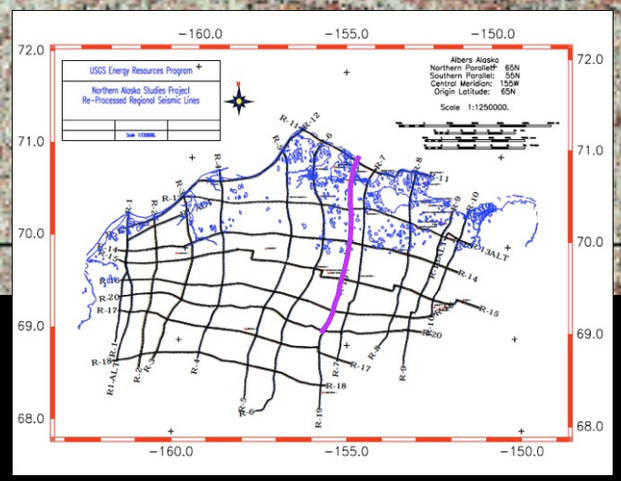

Gravity anomalies

10 mGal contour interval

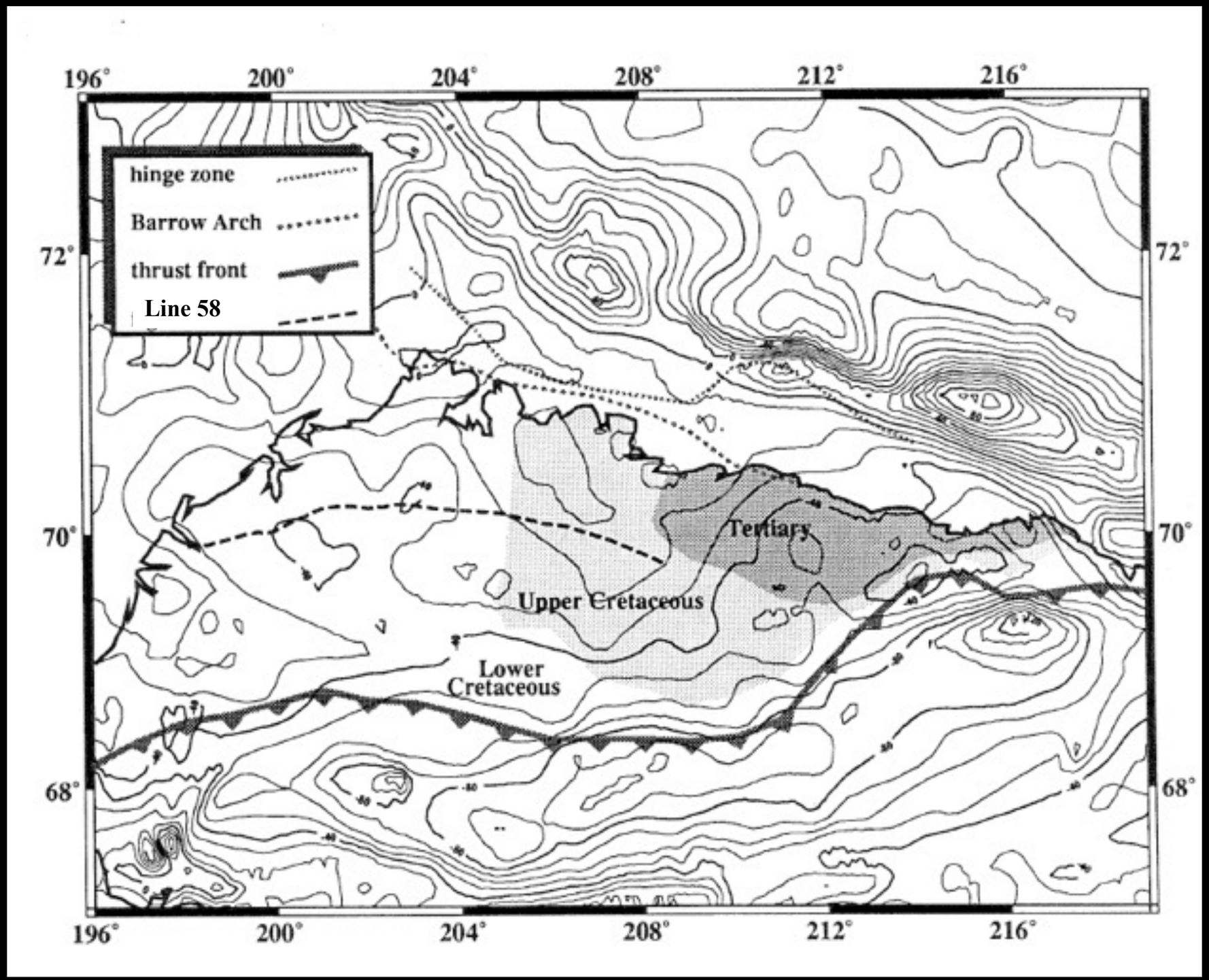

Line 58 Colville Trough

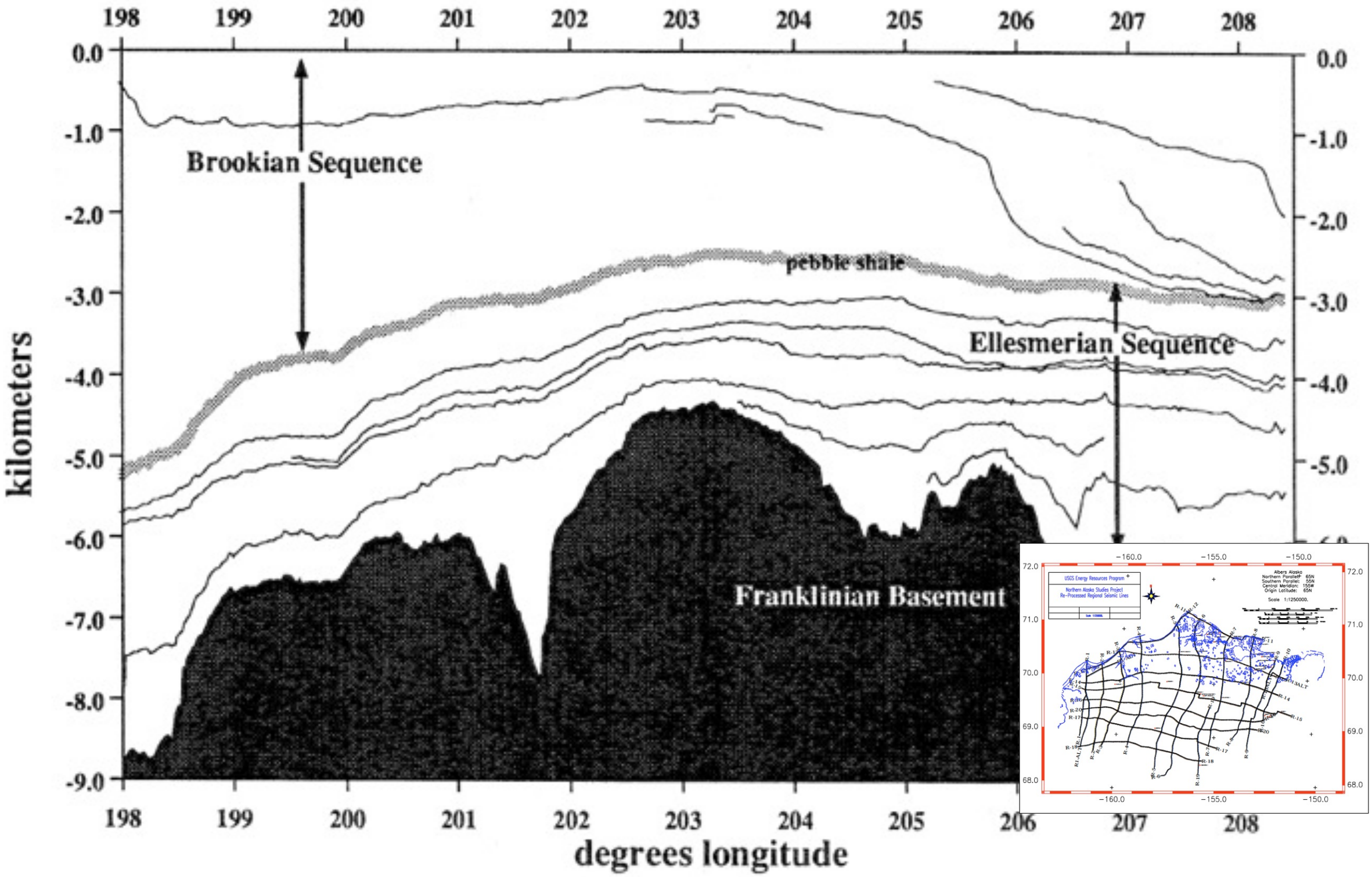

stratigraphy of Arctic Alaska

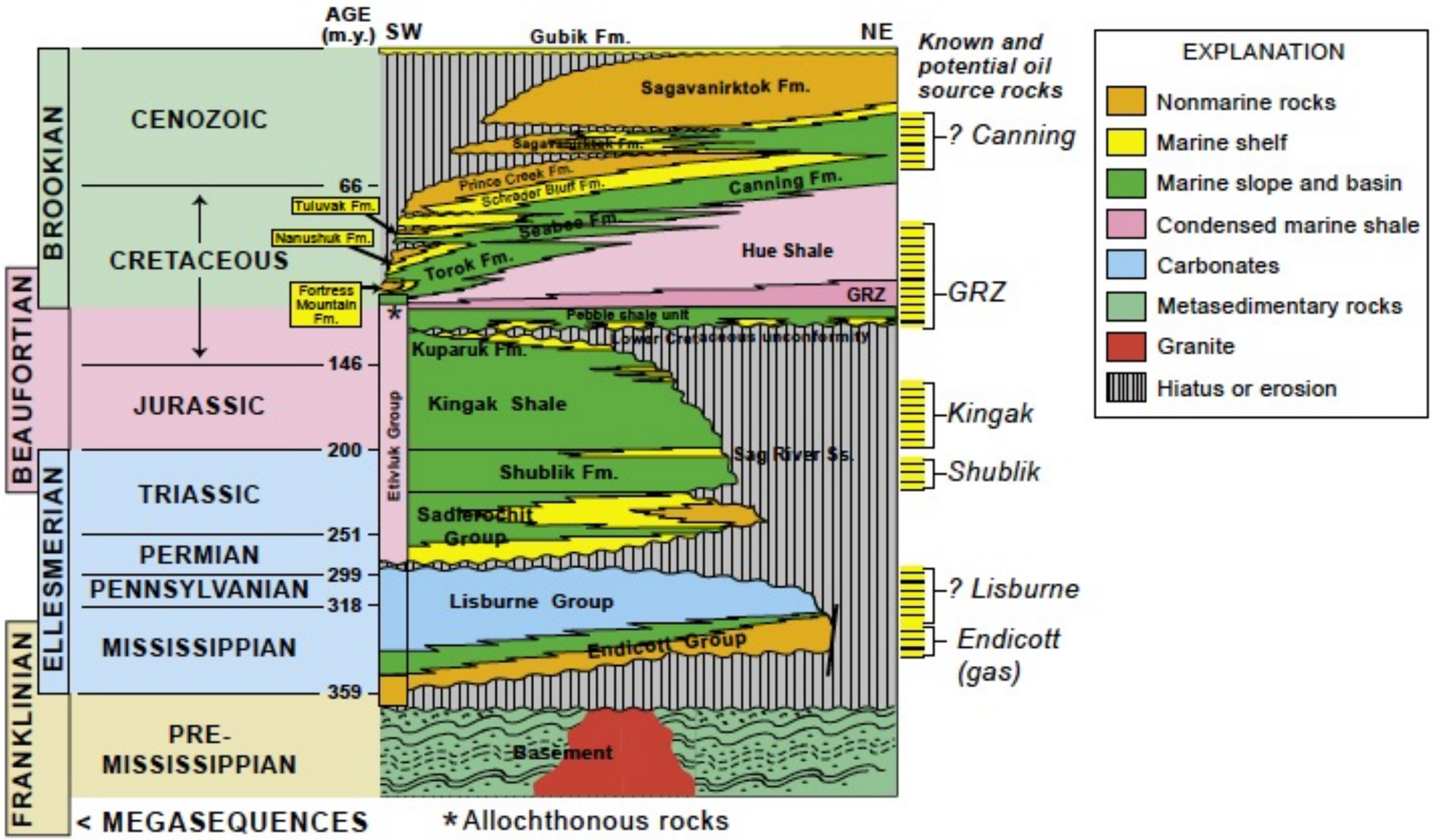

Transition from short, steep sediment transport systems to axial deltaic progradation

a simple basin model

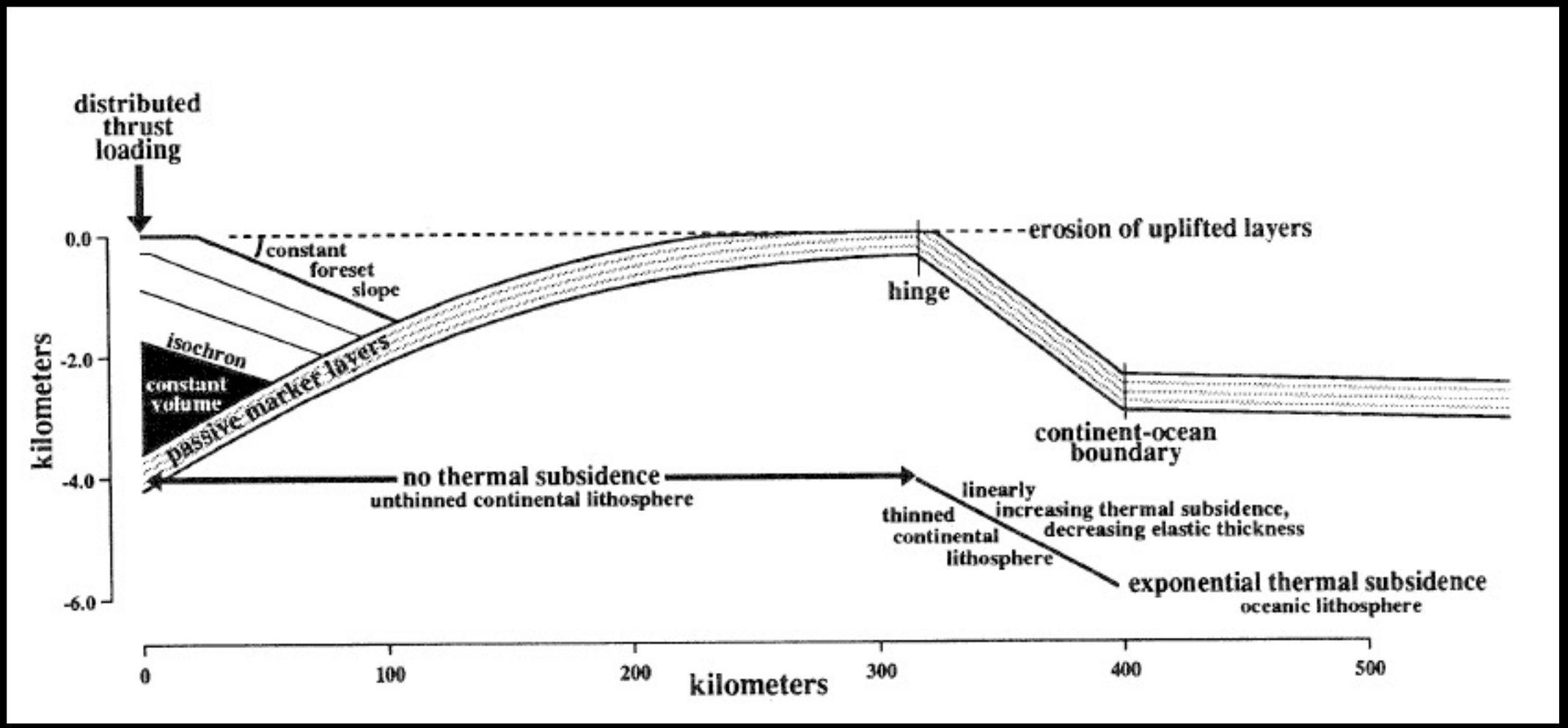

Basin partially full

increments of sediment re-shape accommodation space

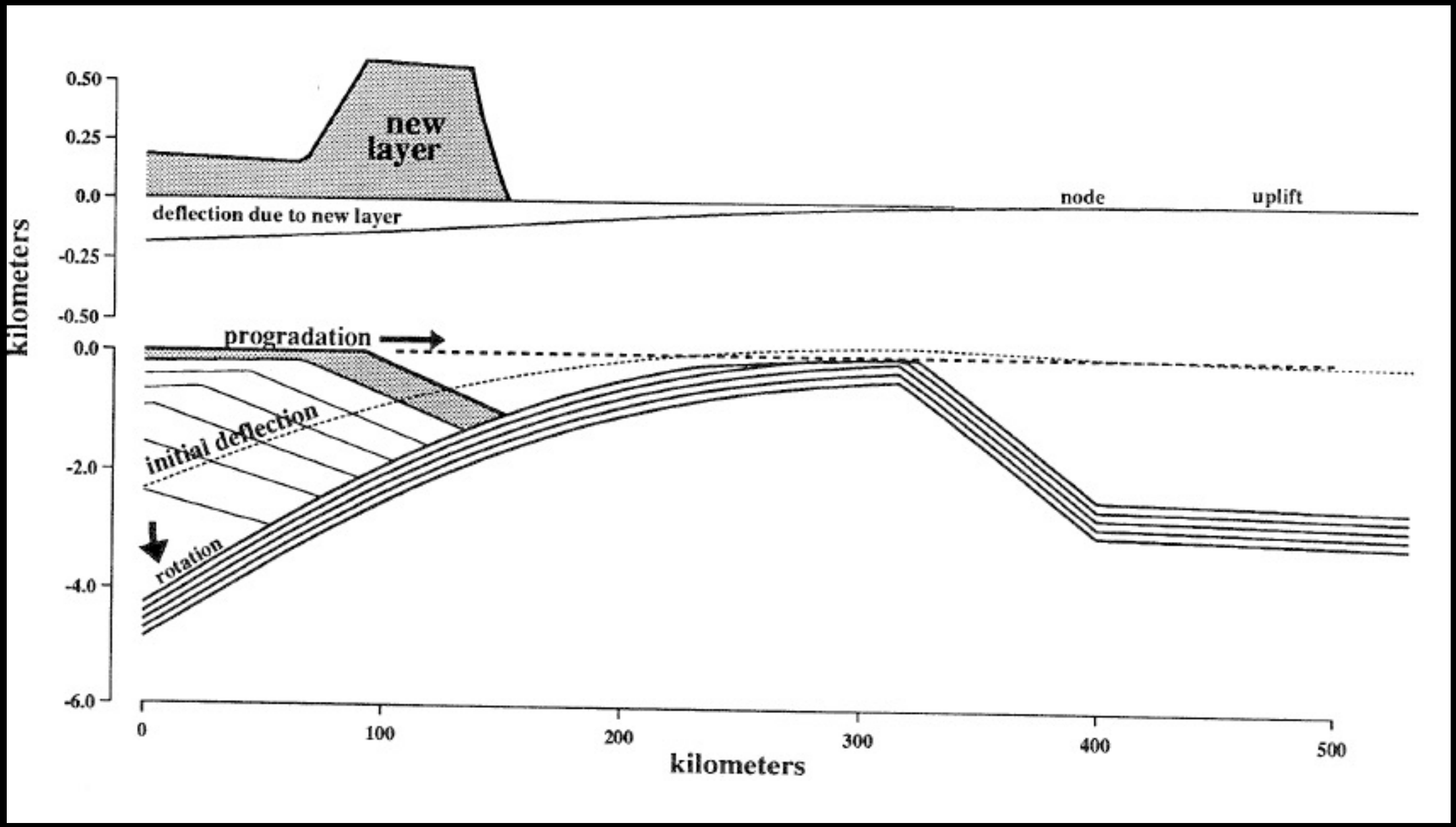

Full Basin - Cycle 1

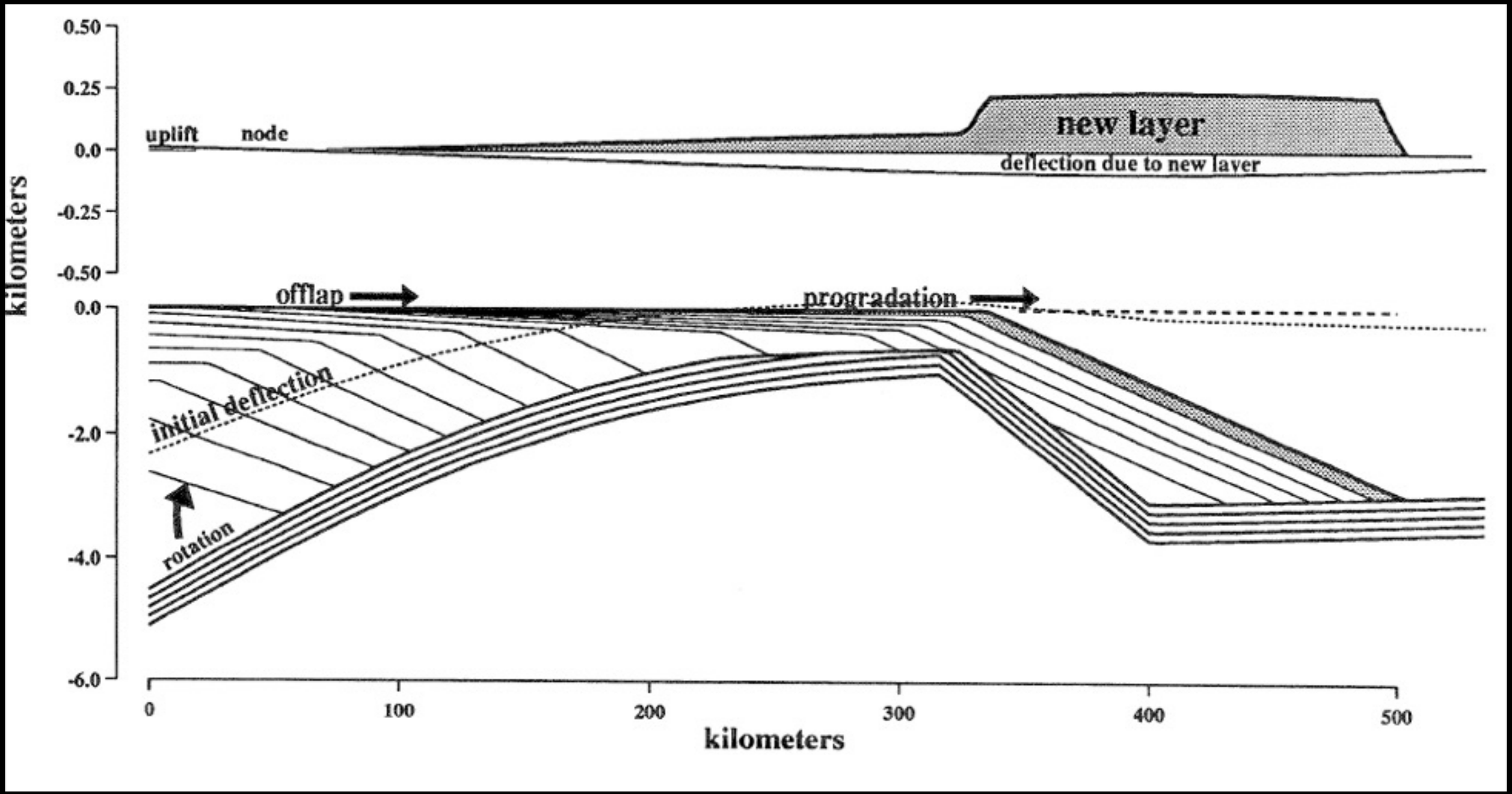

simple model parameters

TABLE 2.1. Parameters Used in Basin Model

Parameter	Value
Continental elastic thickness	65 km
Oceanic elastic thickness	15 km
Foreset slope	3°
Topset slope	0°
Time since rifting	20 m.y.
Sediment volume per layer	150 km^3
Load 1	1.0 x 10^{13} N
Load 2	0.15 x 10^{13} N
Load width*	140 km
Hinge zone*	360 km
Continent-Ocean boundary*	464 km

*Distance from left-hand (south) edge of the model.

constant thrust loads are not tectonic quiescence

Model Cycle-1

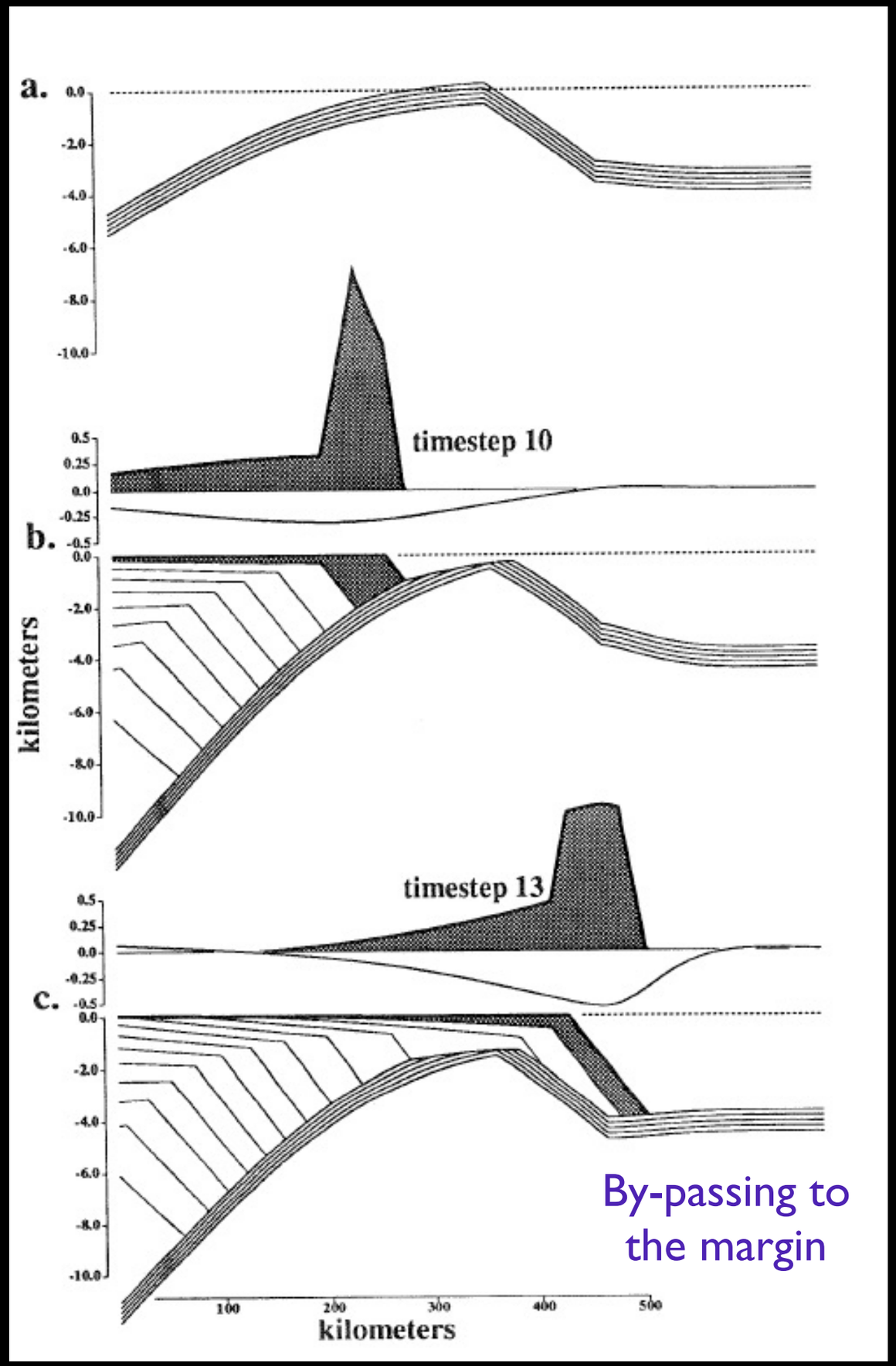

By-passing to the margin

Model
Cycle-11

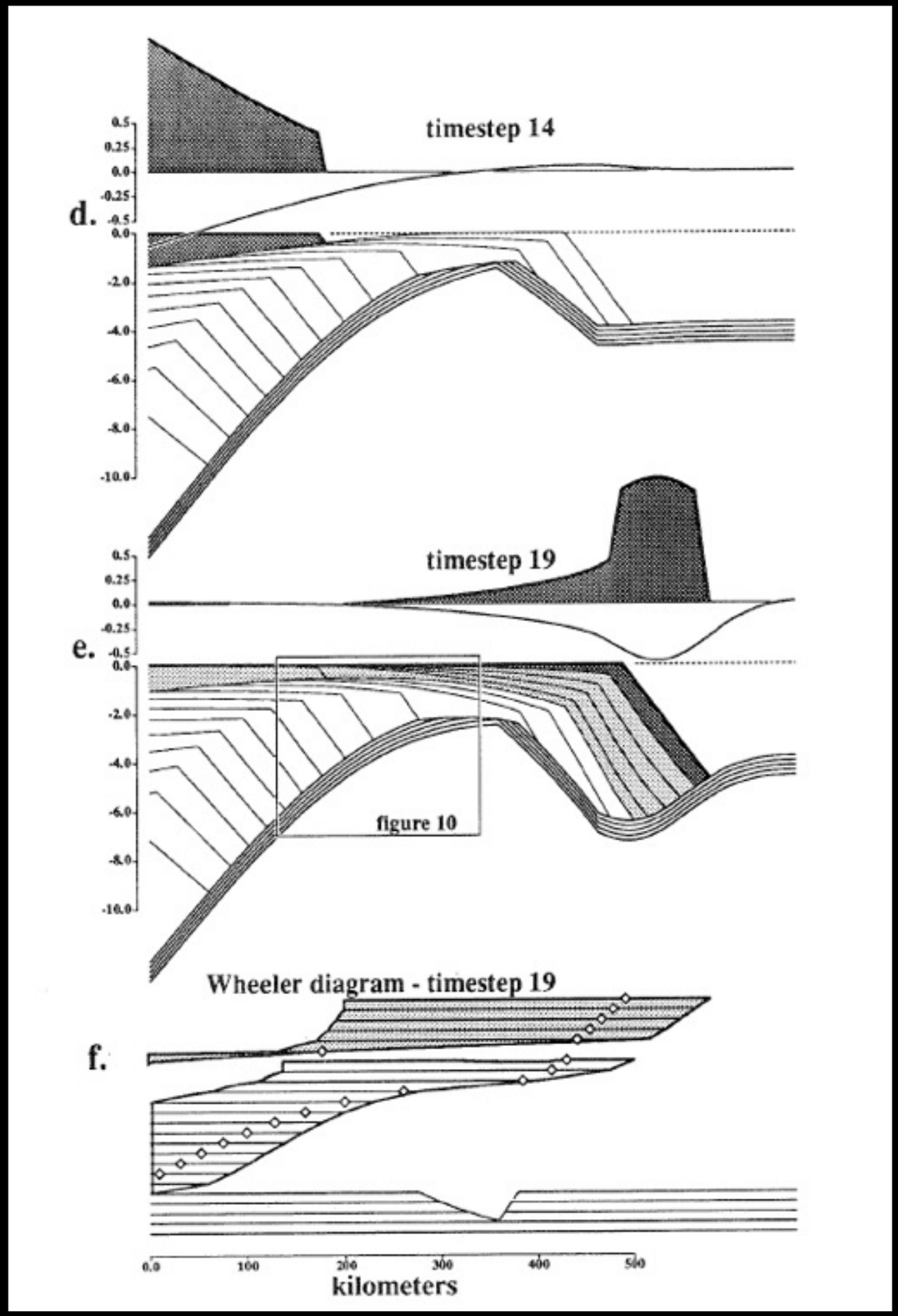

Model time horizons "fit" stratigraphy

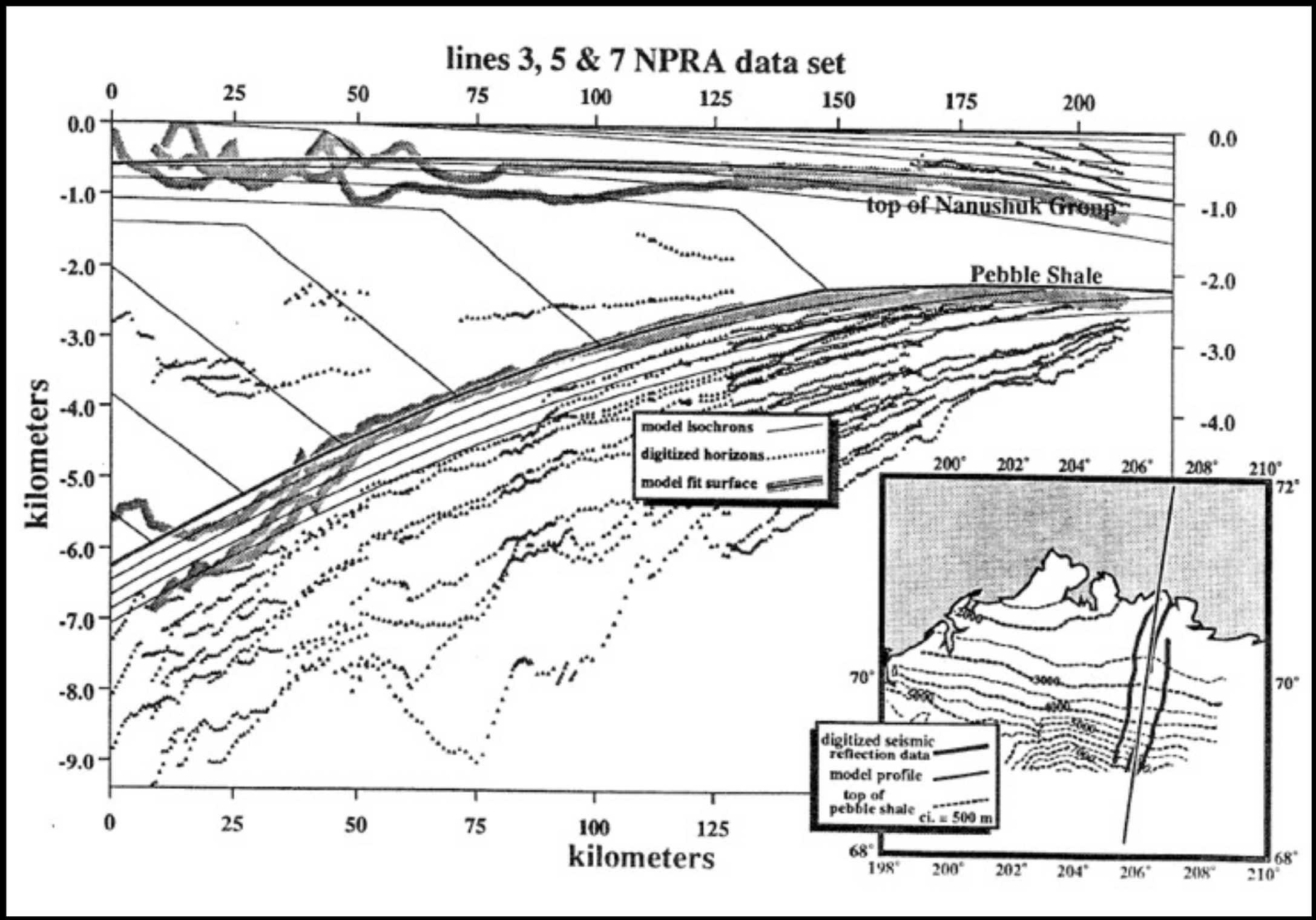

Historical Model Cycle 1

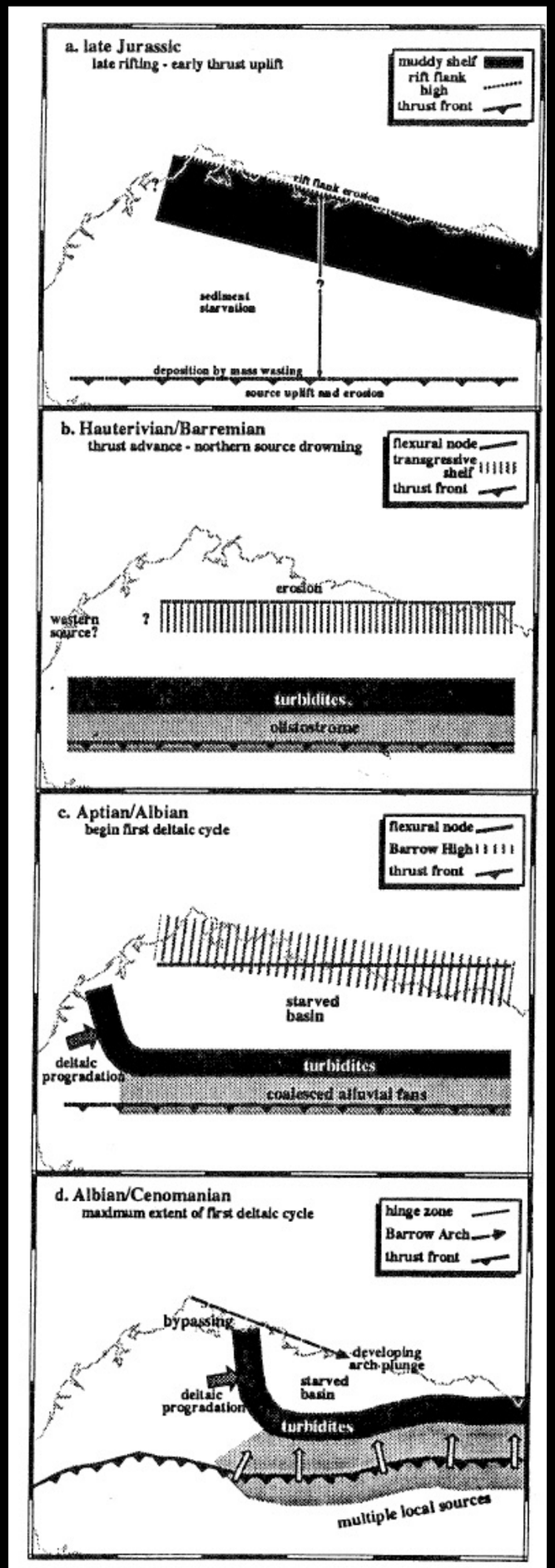

Historical Model Cycle 11

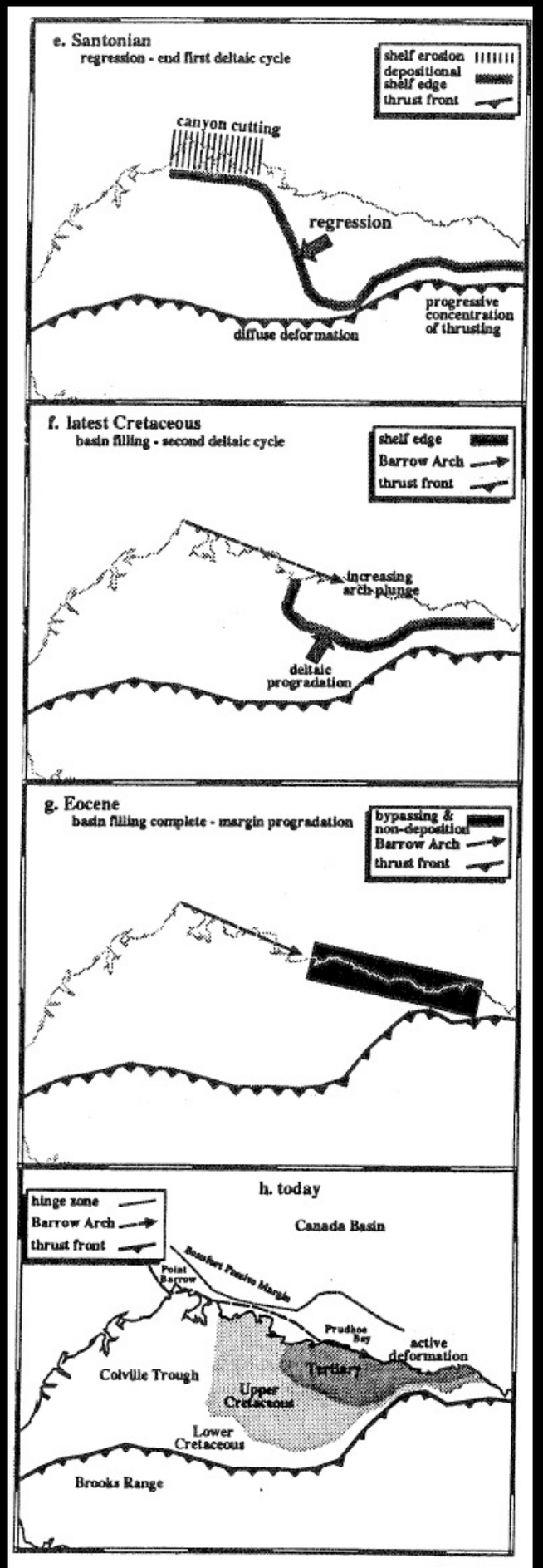

What about passive margins?

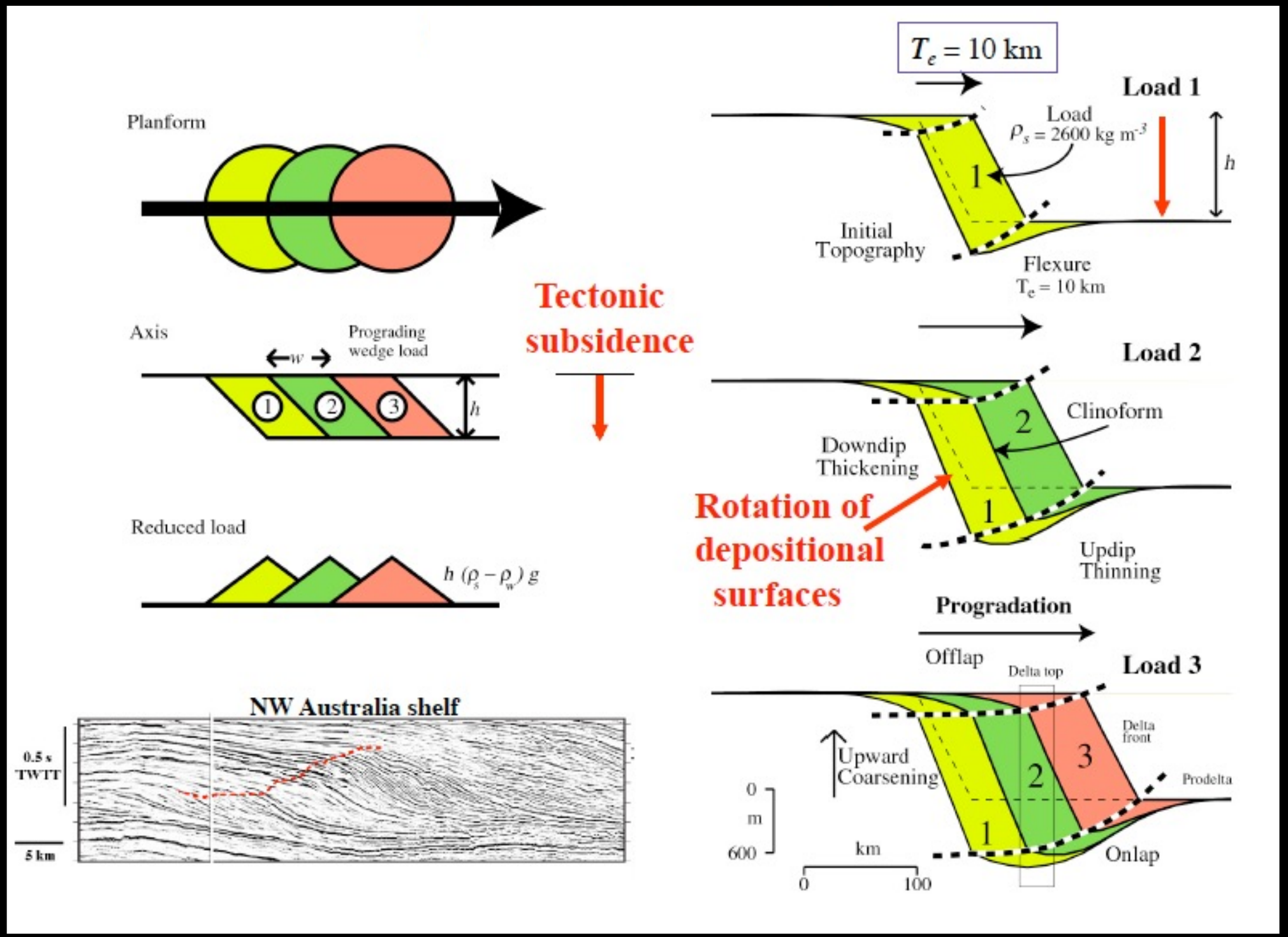

Watts 1989

US Gulf Coast

Watts 1989

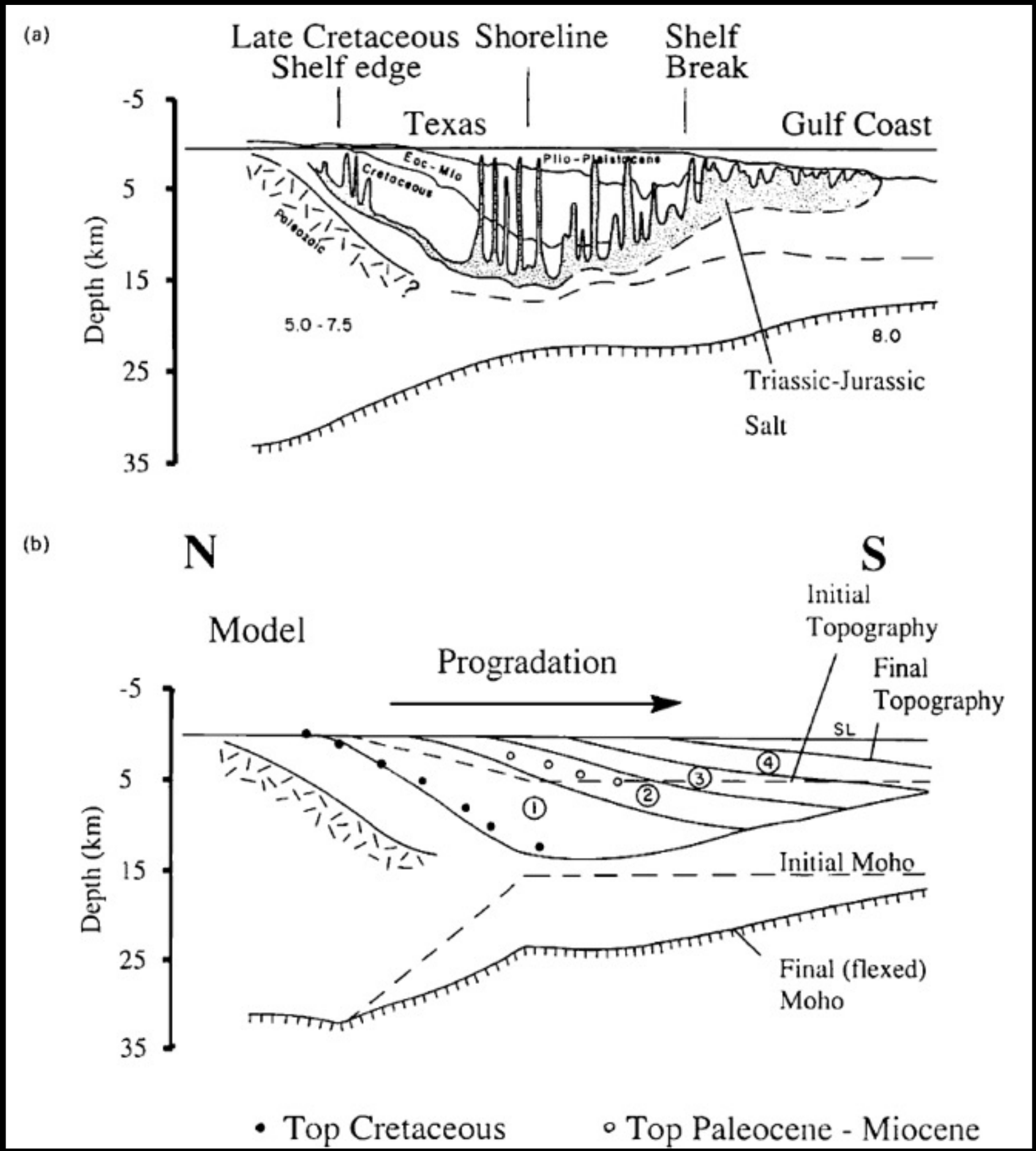

in map view

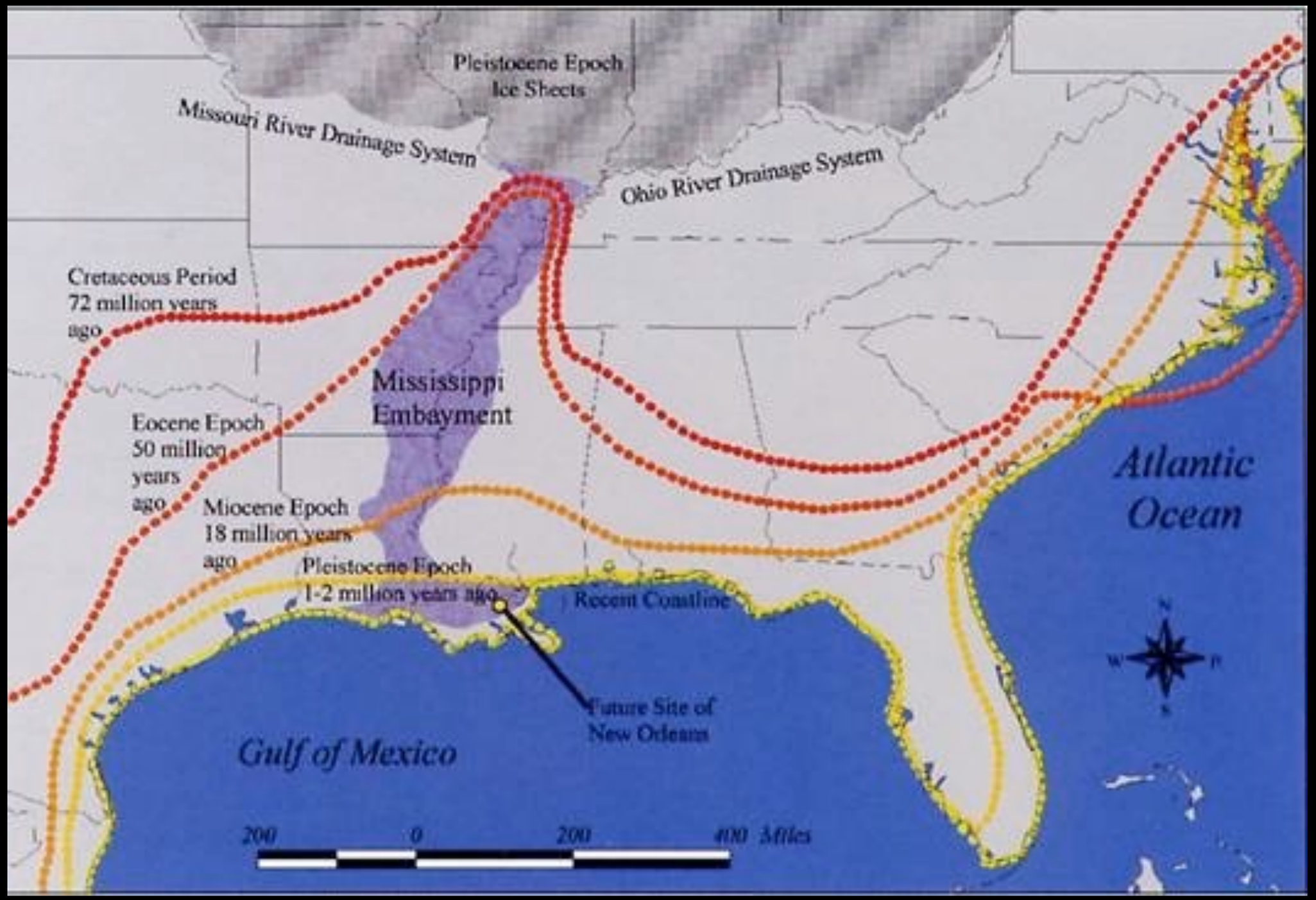
Pleistocene Epoch
Ice Sheets
Missouri River Drainage System
Ohio River Drainage System
Cretaceous Period
72 million years
ago
Mississippi
Embayment
Eocene Epoch
50 million
years
ago
Miocene Epoch
18 million years
ago
Pleistocene Epoch
1-2 million years ago
Recent Coastline
Future Site of
New Orleans
Gulf of Mexico
Atlantic
Ocean
200
0
200
400 Miles

- flexure and compaction amplify and redistribute accommodation space
- purely elastic flexure can explain gross sedimentary architecture
- where basin filling time is a significant fraction of relaxation time (assumed), we cannot expect to observe viscous effects in stratigraphy
- tectonic quiescence does not exist, we should look instead to coupling between sedimentation and deformation to explain apparently static basins
- given the stability of plate tectonic processes, we should look at local changes in the distribution of deformation to explain changes in the basin

modeling wedge dynamics

interaction between wedge dynamics and exhumation

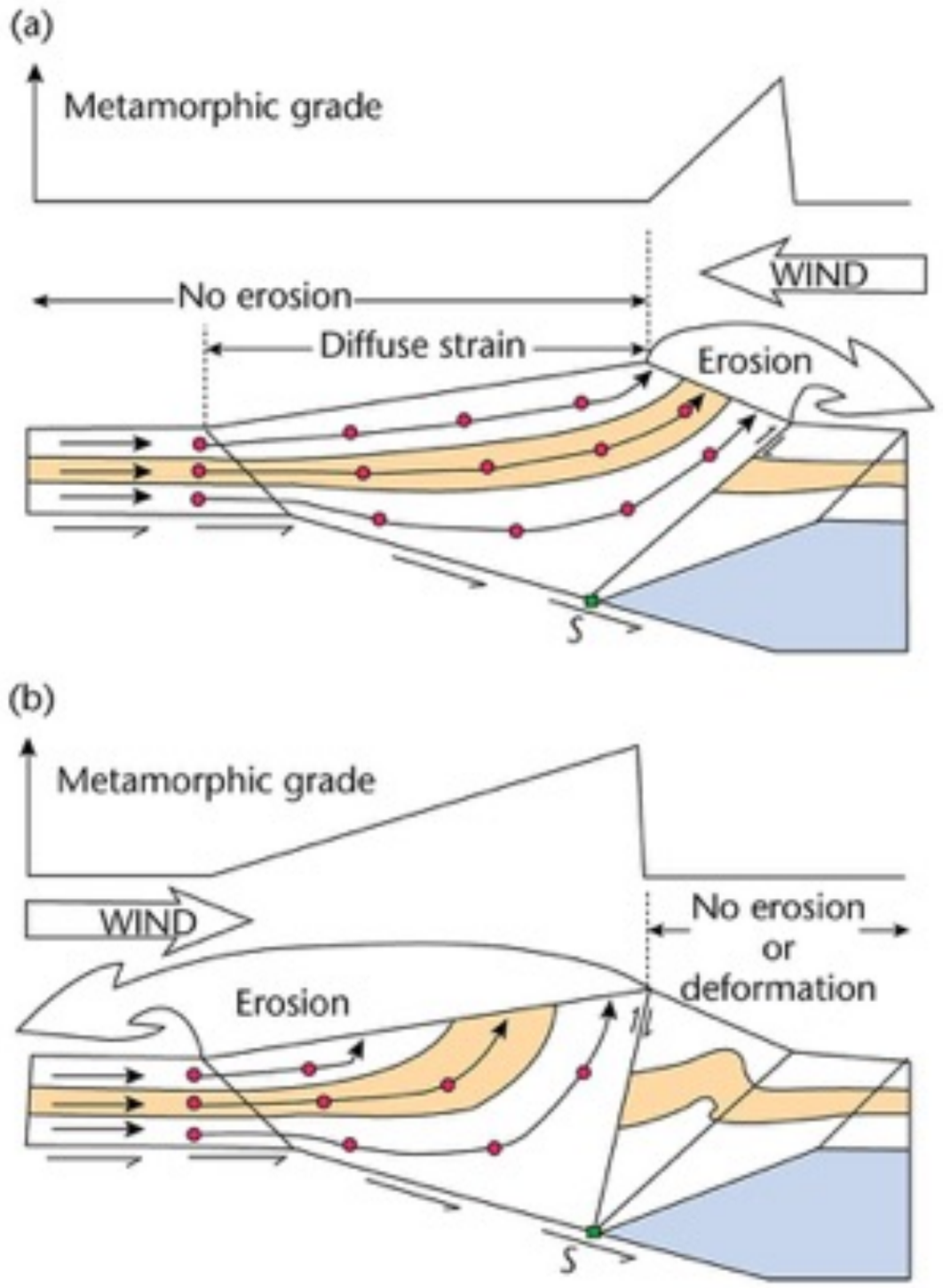

Fig. 4.28 Effects of erosion on a bivergent wedge (after Willett *et al*. 1993). Precipitation concentrated on the retro-wedge (a), and pro-wedge (b) increases erosion, causing an advection of high-grade metamorphic rocks from the middle and lower crust (and even mantle lithosphere) to the surface. Passive shaded layer shows middle crust. Lines are material trajectories, and dots show progressive equal-time positions of points originally aligned vertically.

erosion, deformation and exhumation

erosion distribution influences deformation

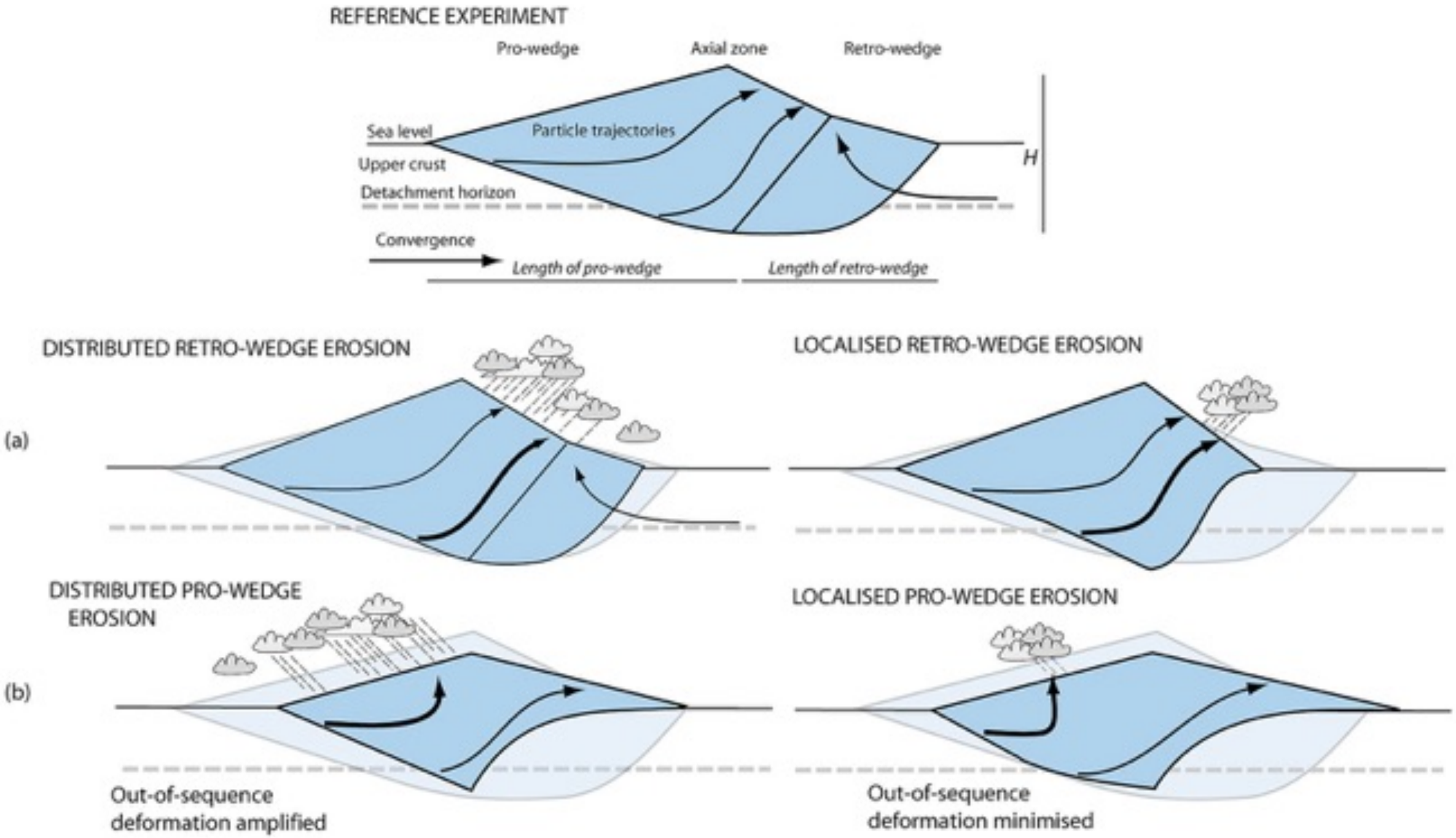

Fig. 4.29 Summary of results of analogue models investigating the effects of focused (localised) and distributed rainfall on the pro-wedge (b) and retro-wedge (a), after Hoth *et al*. (2006). Particle trajectories are shown in arrows. Thicker arrows indicate significant influence of erosion. Erosion drives larger fluxes towards surface and shortens length of retro- or pro-wedge compared to reference experiment.

analog models

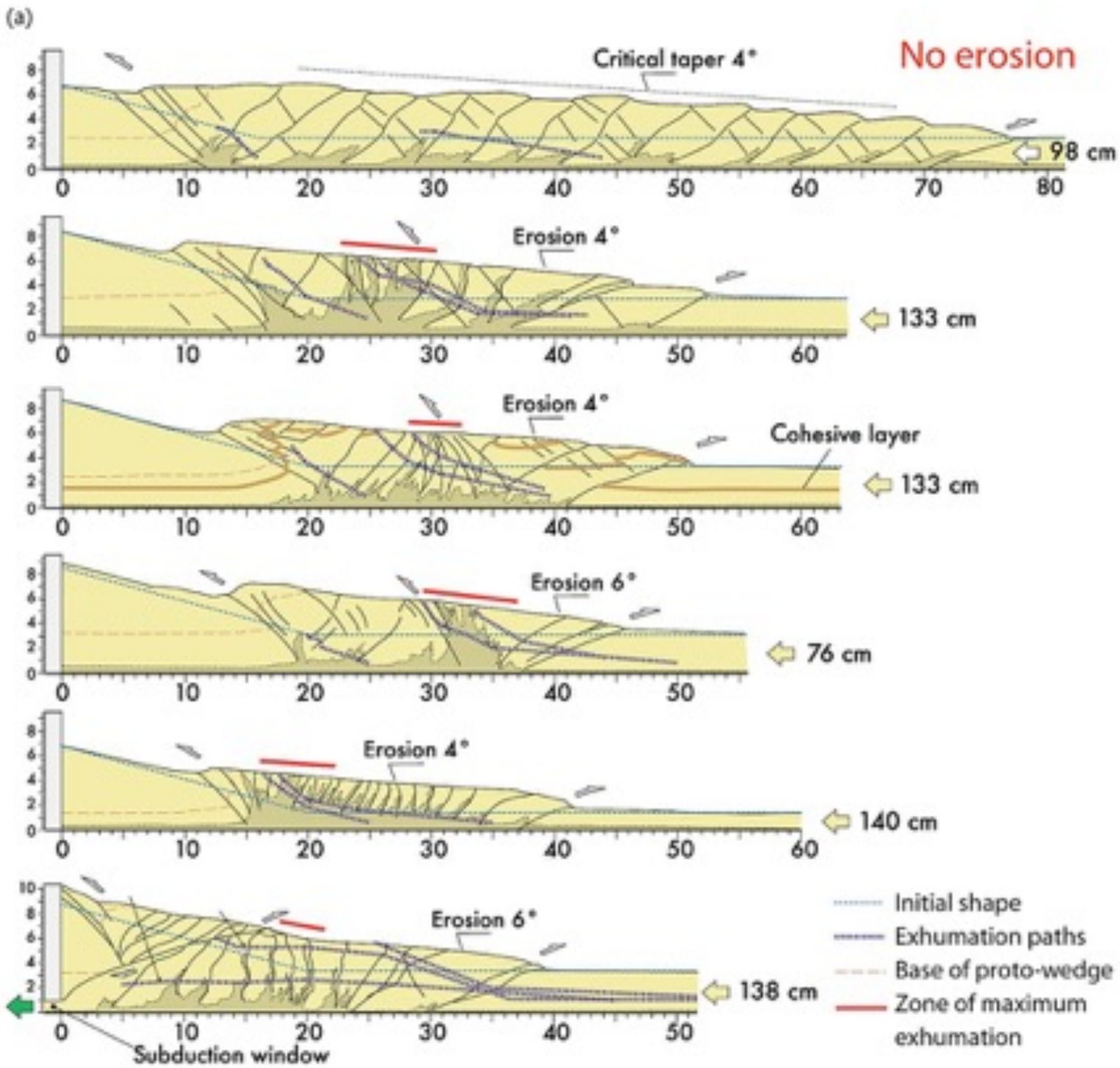

Fig. 4.43 Results of scaled sandbox analogue experiments to investigate the effect of erosion rate on the development of fold-thrust belts, from Konstantinovskaya & Malavieille (2005). Sequences begin with the no-erosion case, for low (a) and high (b) basal friction experiments. The no-erosion cases show an imbricated stack of uniformly spaced foreland-verging thrusts. The cases with erosion show the total amount of shortening on the right of each panel. In the low friction experiments, erosion causes exhumation to be concentrated at the mid-rear of the wedge, associated with clusters of closely spaced subvertical faults. In the high basal friction experiments, exhumation takes place along inclined thrusts in the middle part of the wedge. Erosion accounts for up to 50% of the total area of the initial model. Reproduced with permission of John Wiley & Sons, Inc.

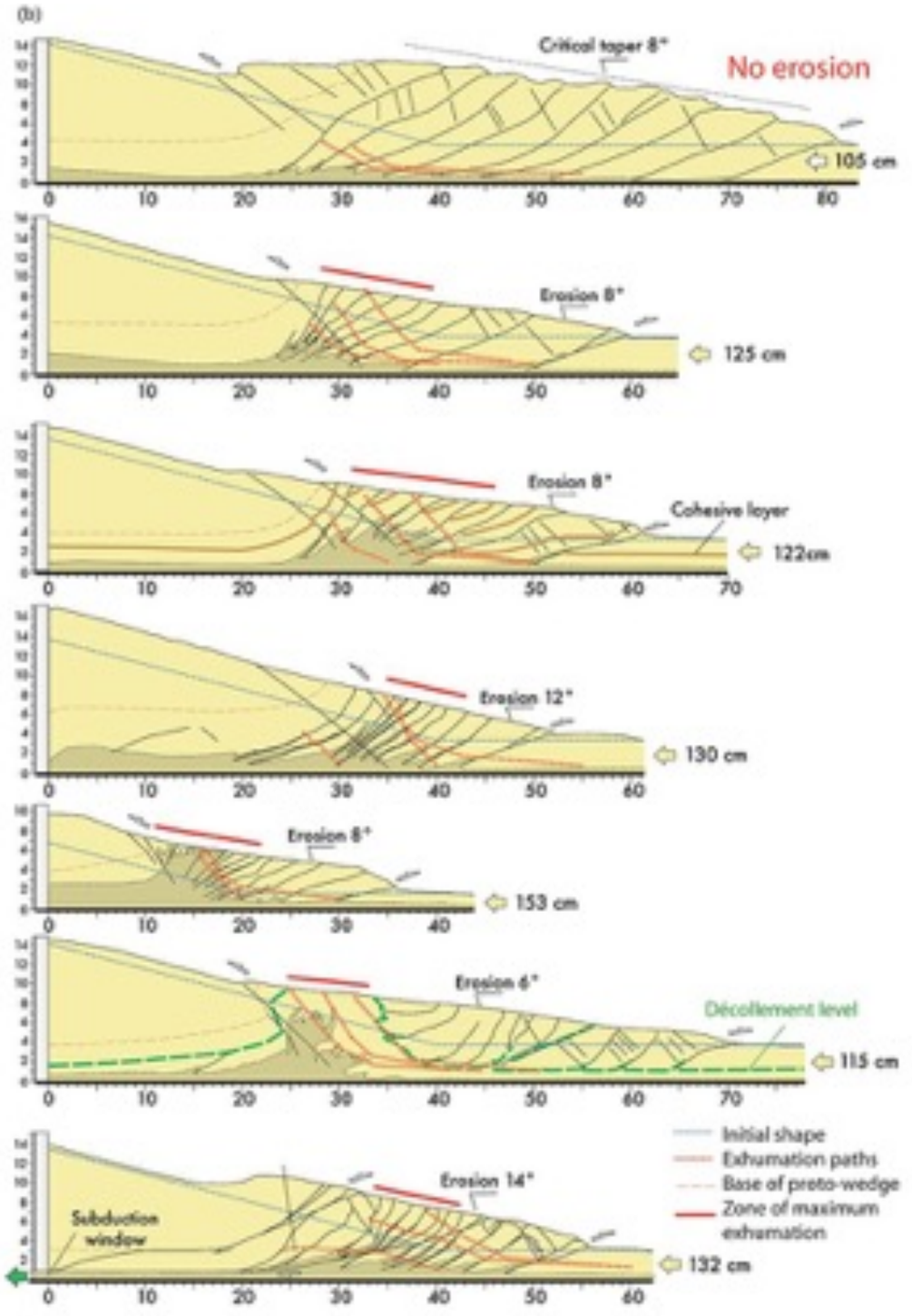

Fig. 4.43 *Continued*

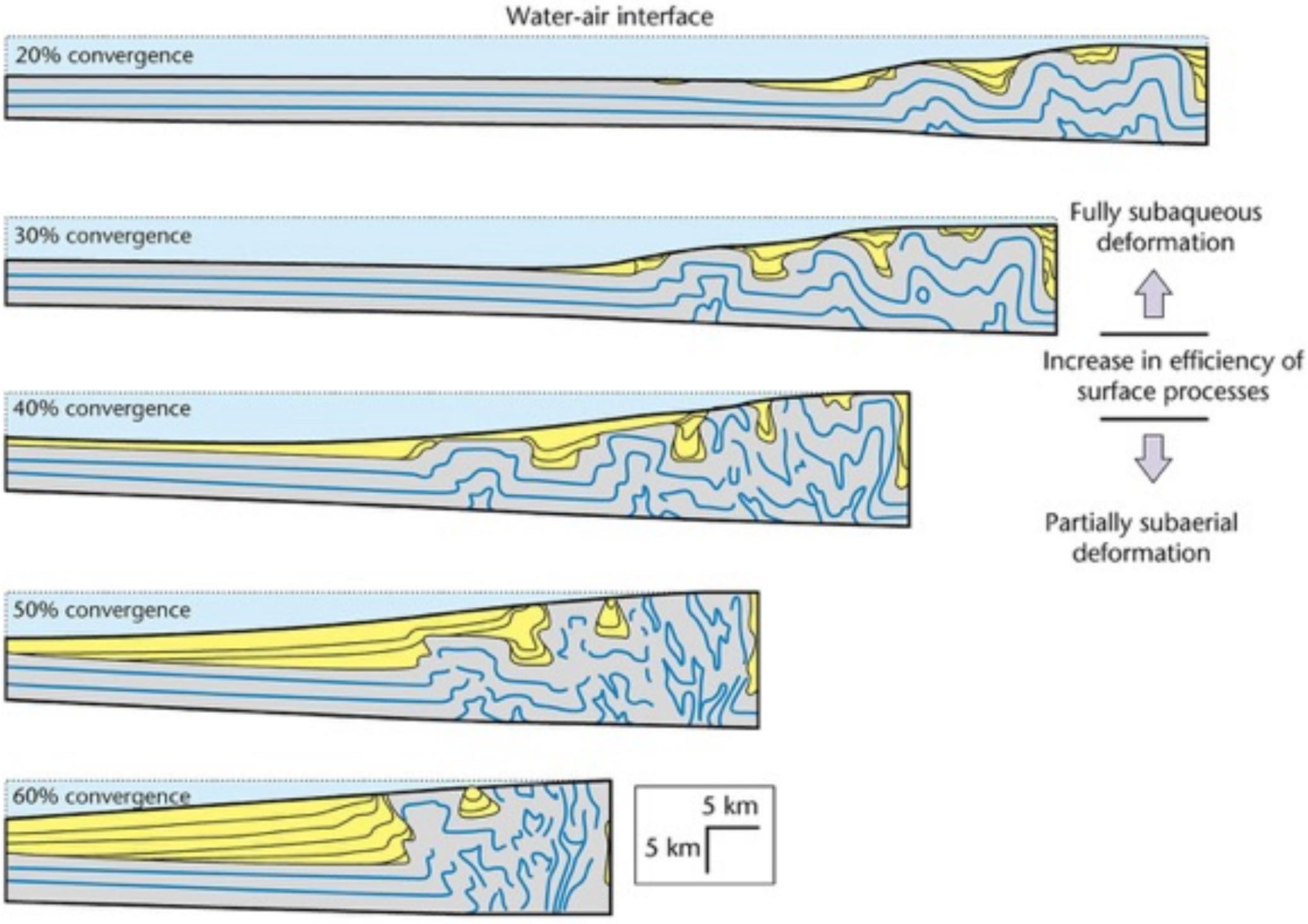

Fig. 4.44 Evolution of an orogenic wedge, from Simpson (2006b), using a thin layer of sediment on a flexing elastic lithosphere above a weak (inviscid) substrate, which undergoes progressive convergence and shortening. Erosion and deposition are governed by diffusion. The emergence of the wedge above sea level tends to reactivate tectonic deformation in the orogen, a reduction of orogen width and a stalling of frontal propagation. This leads to a cessation of wedge-top basin development and the promotion of thick foredeep deposition. Reproduced with permission of John Wiley & Sons, Ltd.

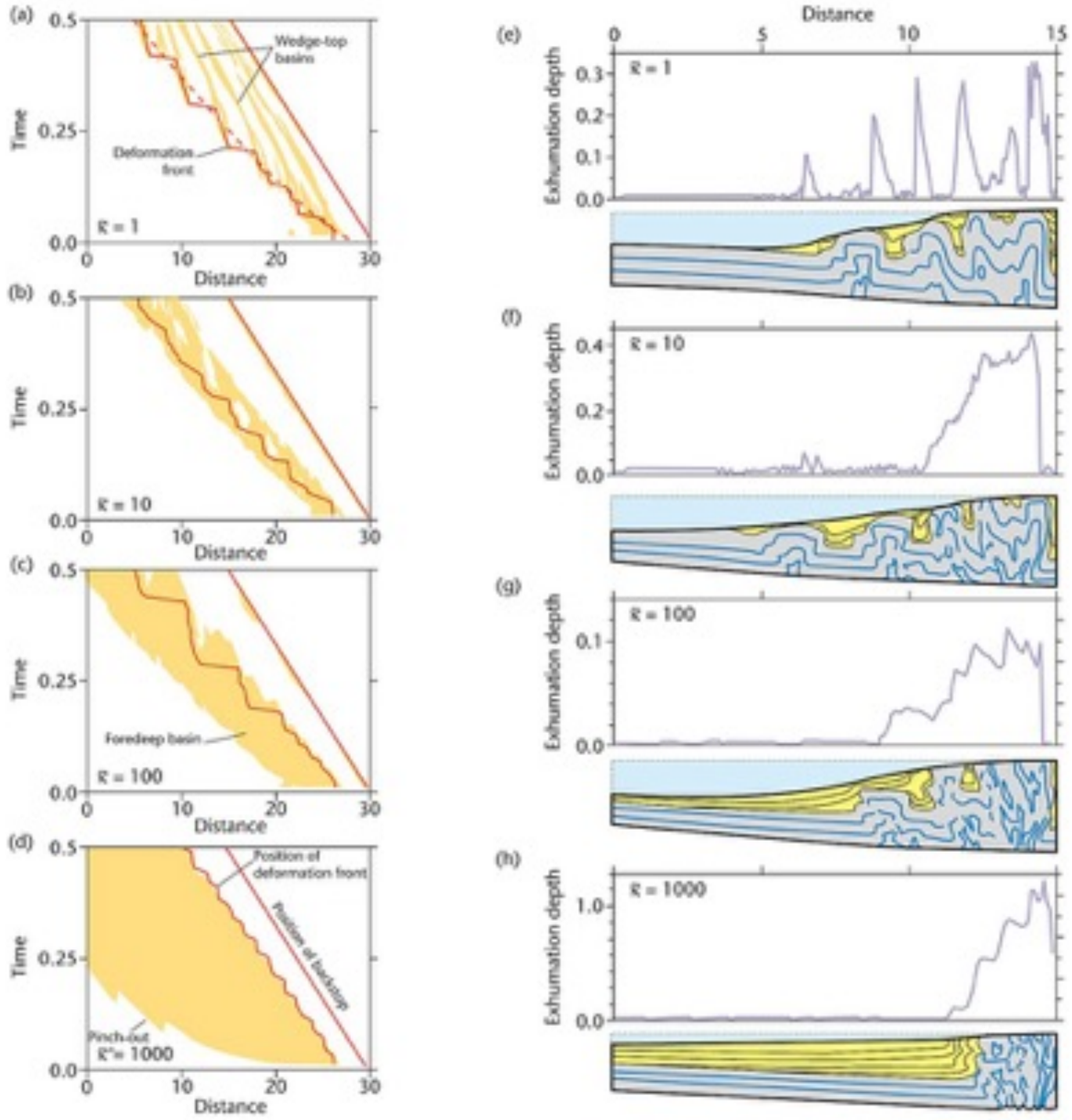

Fig. 4.45 Effect of surface processes on orogenic wedge and foreland basin evolution, after Simpson (2006c). Left: time-distance charts showing chronostratigraphy at different values of the dimensionless transport coefficient $\tilde{\kappa}$, from 1 to 1000. Wedge-top deposition at low values of $\tilde{\kappa}$ evolves into extensive foredeep deposition at high $\tilde{\kappa}$. The time scale is dimensionless, and the horizontal distance is scaled by the original thickness of the deforming layer. Right: shallow exhumation of arrays of folds at low values of $\tilde{\kappa}$ evolves to deep exhumation of wedge at high $\tilde{\kappa}$. The exhumation depth and the horizontal distance are both scaled by the original thickness of the deforming layer. Reproduced with permission of John Wiley & Sons, Ltd.

foreland basin stratigraphy in time

looking at the basin fill

sedimentation in a foreland basin system

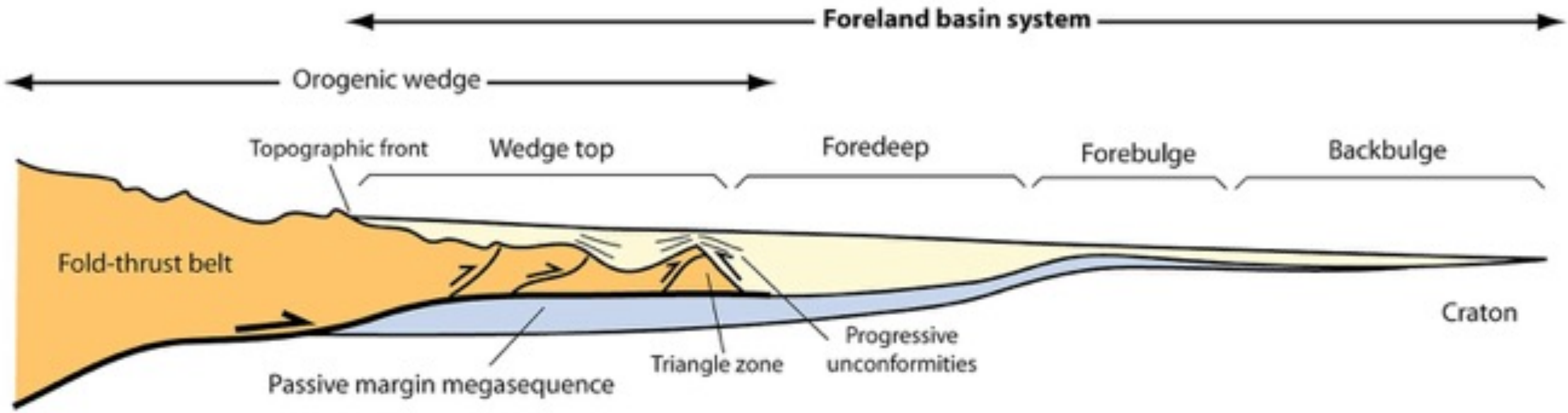

Fig. 4.35 The four depositional zones of a foreland basin system, as envisaged by DeCelles & Giles (1996). Reproduced with permission of John Wiley & Sons, Ltd.

interactions between sediments and deformation

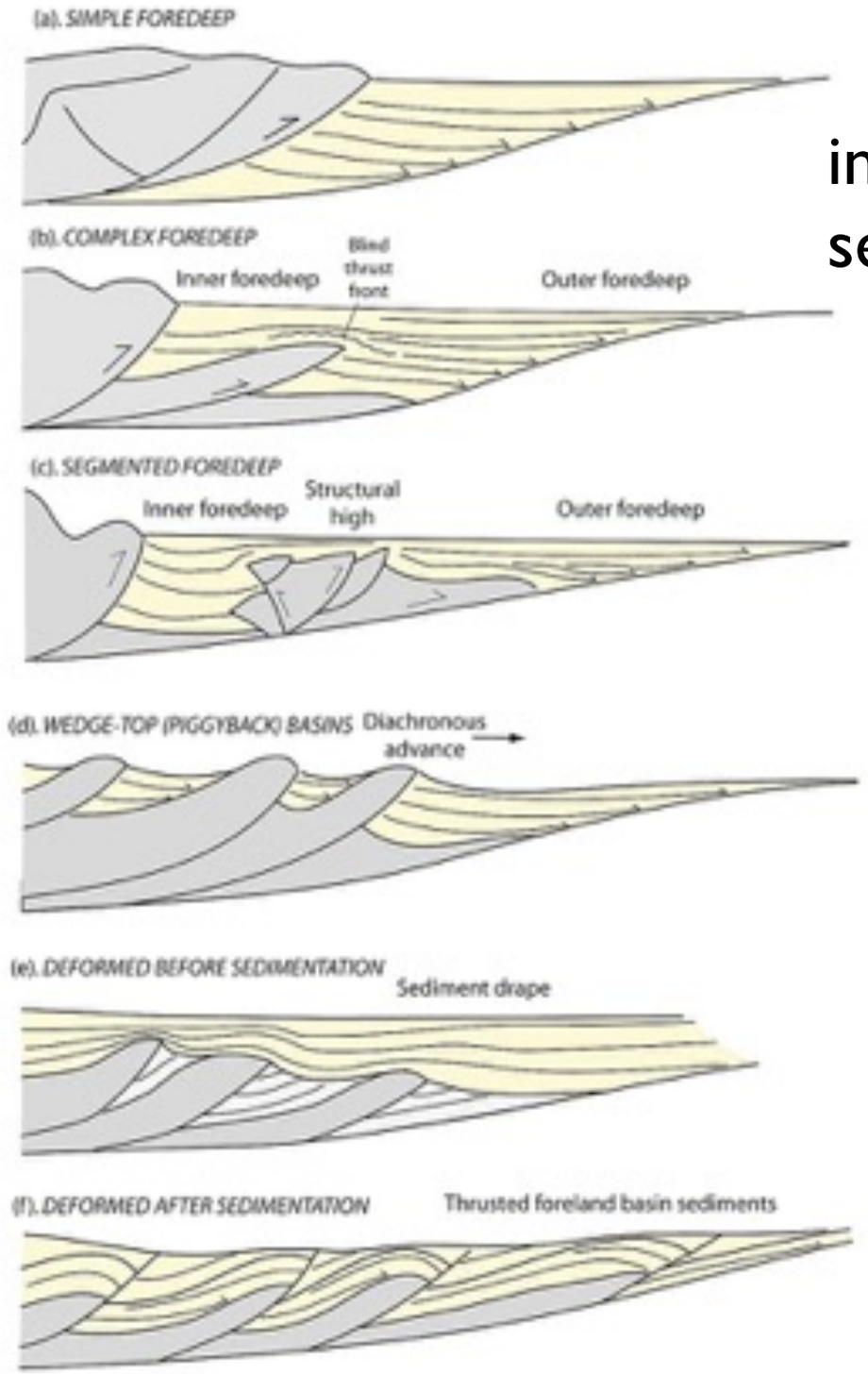

Fig. 4.36 Foreland basin/thrust belt interactions, based mainly on seismic records from the Apennines and foreland of Italy (modified from Ricci-Lucchi 1986). Basins may be simple, asymmetrical wedges with stratigraphic onlap onto the foreland plate, as in the North Alpine Foreland Basin of Switzerland (a). Basins may be complex as a result of tectonic advance into the basin, causing an inner foredeep separated from an outer foredeep by buried (blind) thrusts (b) or by more complex zones of faulting (c). The wedge-top may be disconnected from the foredeep, consisting of an array of piggyback basins separated by thrust culminations, as in the Eocene of the southern Pyrenees (d). Some basins are draped over a previously deformed substrate (e), whereas others are dissected and shortened after the period of foreland basin deposition (f). Reproduced with permission of John Wiley & Sons, Ltd.

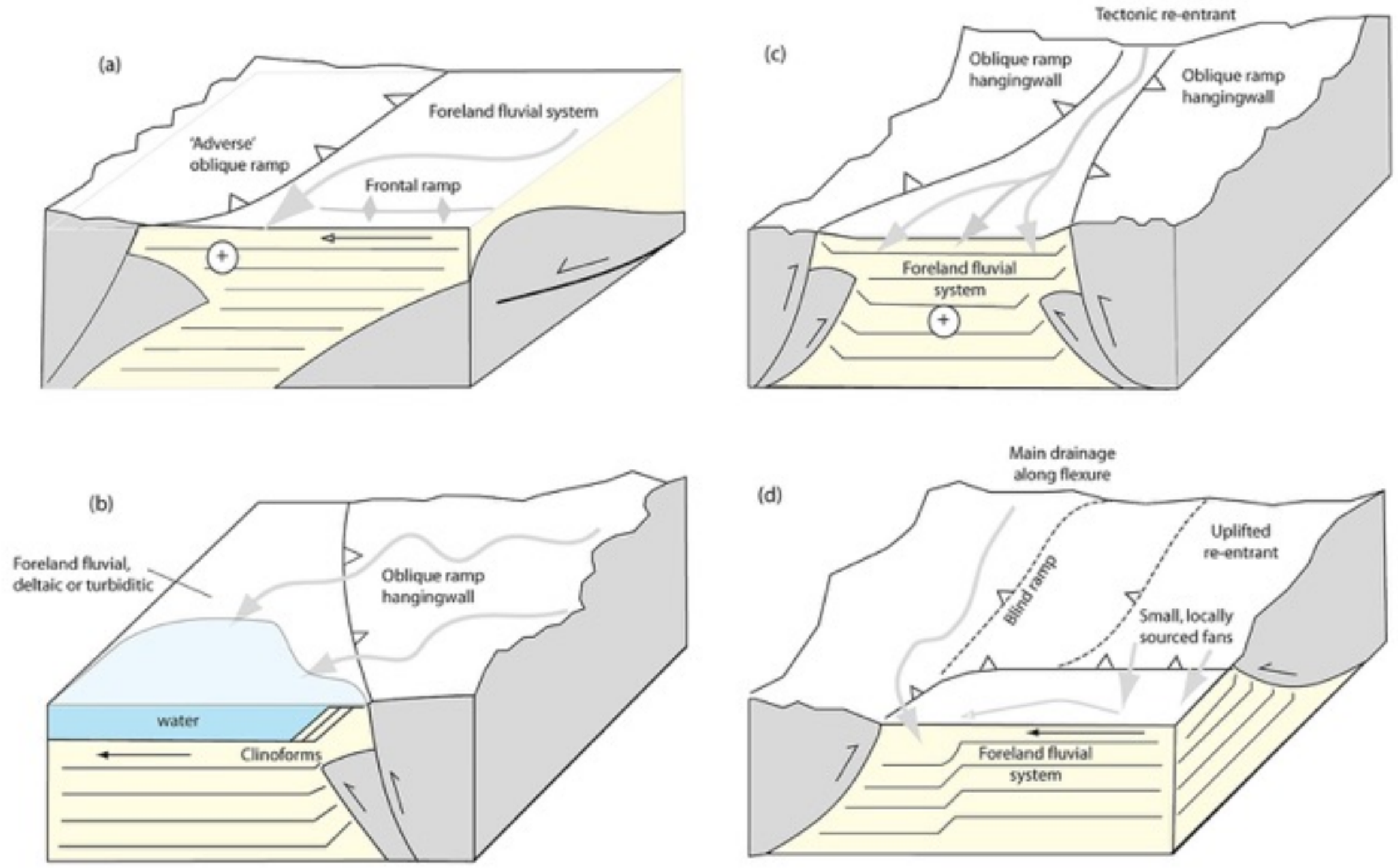

Fig. 4.37 Sediment dispersal patterns by rivers at mountain fronts, adapted from Vergés (2007), based on Pyrenean examples. (a) River guided by frontal ramp flows axially, and breaks through into outer foreland basin when faced with adverse topographic slope of oblique ramp hangingwall. (b) River originating on oblique ramp hangingwall flows down topography into fluvial system or marine embayment. (c) River system constrained by tectonic re-entrant between two oppositely verging oblique ramps, flows transversely into foreland fluvial system. (d) River flows down flexure associated with major oblique ramp, whereas smaller systems drain small catchments on thrust-related hangingwalls and flow longitudinally.

Molasse Basin stratigraphy

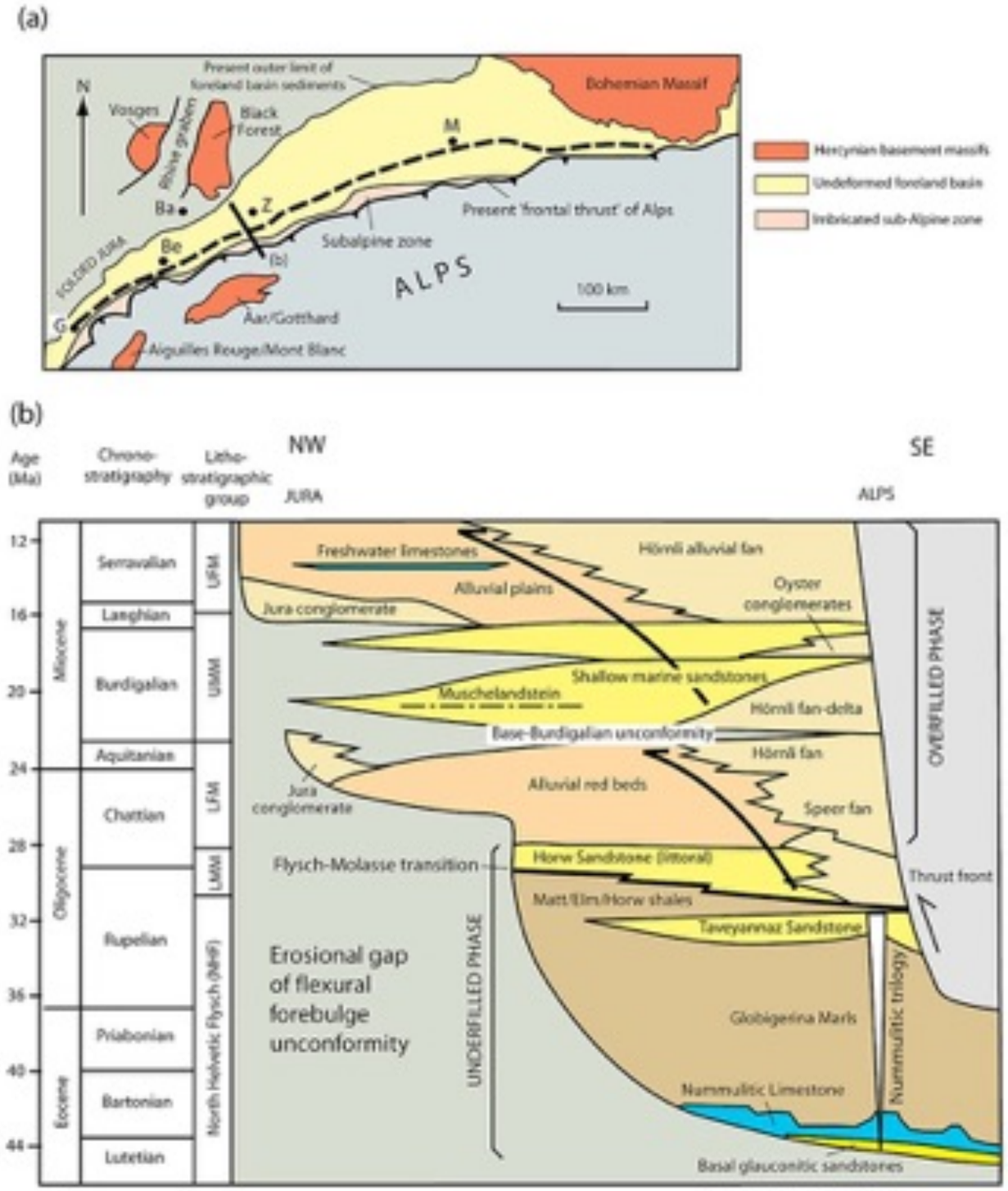

Fig. 4.38 The stratigraphy of the North Alpine Foreland Basin in the vicinity of Zürich, Switzerland (modified from Sinclair *et al.* 1991). (a) Map of North Alpine Foreland Basin: M, Munich; Z, Zürich; Be, Bern; B, Basel; G,Geneva. (b) The stratigraphy is made of a basal deepening-up sequence from shallow-water Nummulitic limestones to hemipelagic marls and turbidites derived from the Alpine orogen (the Nummulitic Trilogy), followed by two grand shallowing-up and coarsening-up cycles. Coarse clastic wedges fringe the Alpine thrust front, whereas the feather-edge of the basin along the Jura margin was relatively passive, with the exception of some local pockets of conglomerate. Reproduced with permission of John Wiley & Sons, Inc.

controlling parameters for sedimentation in a foreland basin

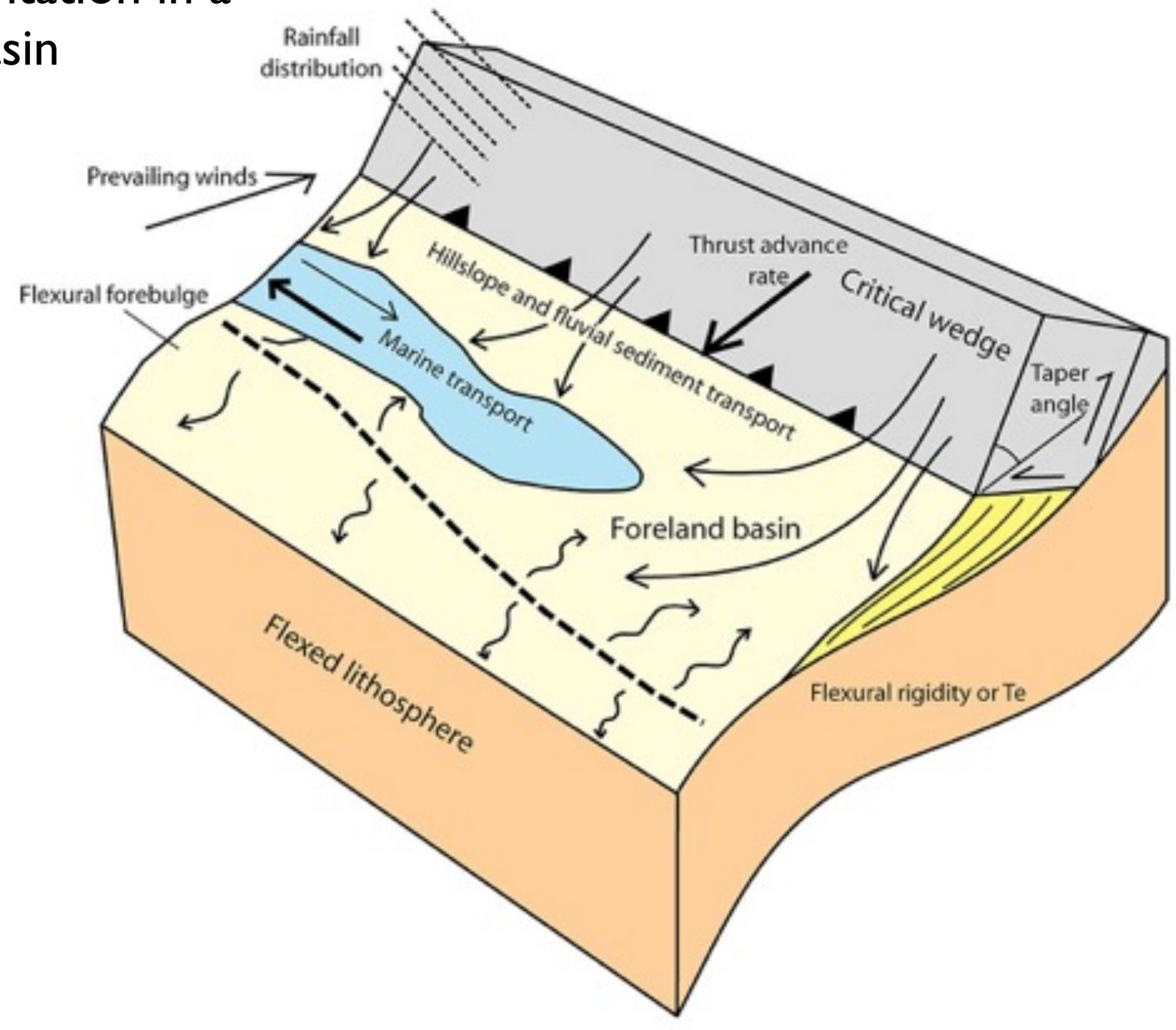

Fig. 4.39 Parameters necessary to describe a diffusive mountain belt system are the advance rate and surface taper of the orogenic wedge, flexural rigidity of the foreland plate, and sediment transport coefficients (Sinclair *et al.* 1991). The distinction between relatively local transport on hillslopes and far-field transport in river systems can either be tackled by attributing two different effective diffusivities to these geomorphic subsystems, or treating the fluvial transport as advective (Johnson & Beaumont 1995).

a simple, time dependent model of coupled deformation and sedimentation

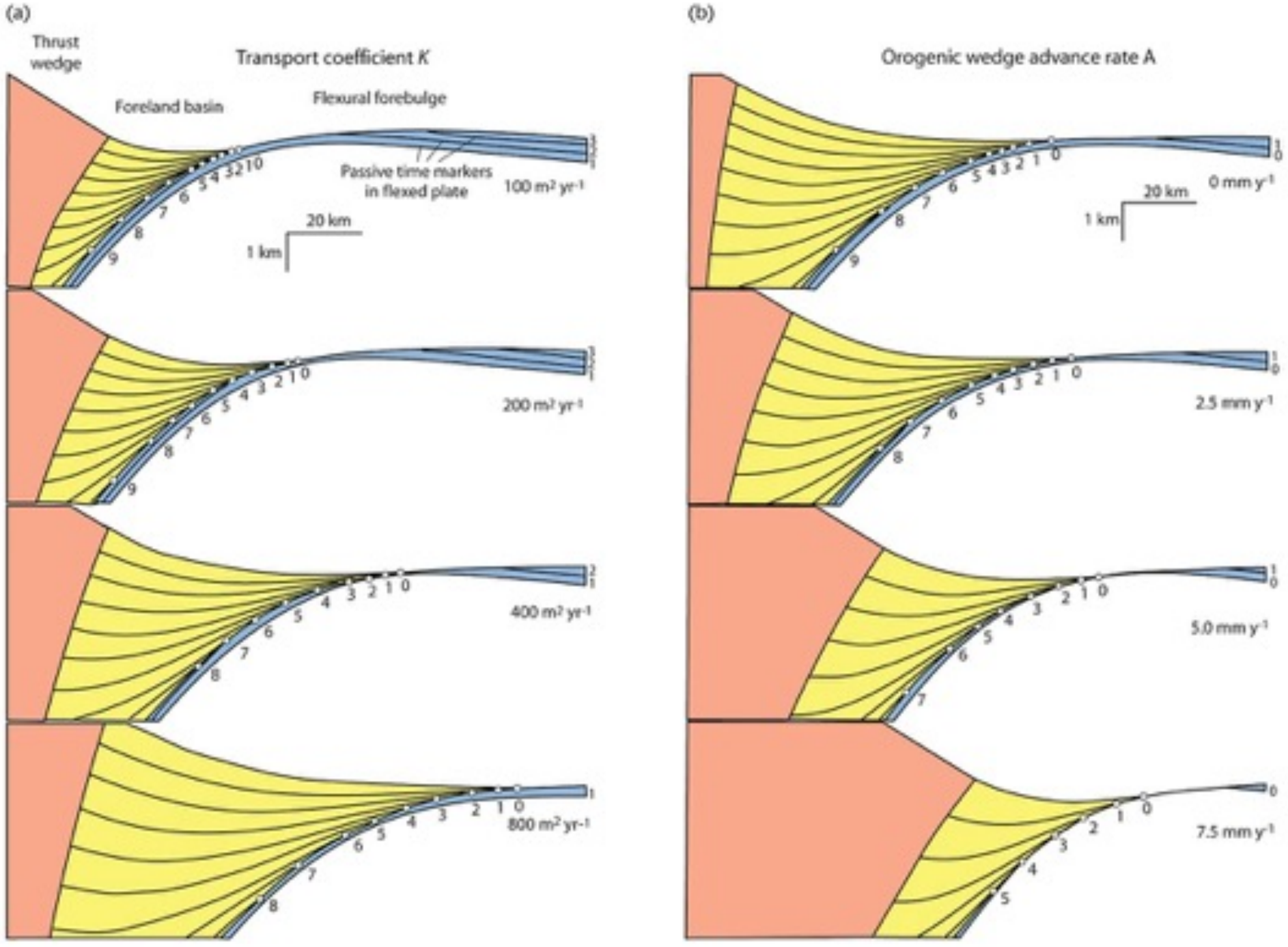

Fig. 4.40 Sensitivity tests of two of the parameters in Sinclair *et al.*'s (1991) diffusion model for mountain belt denudation and foreland basin evolution. The reference model involves a transport coefficient $K = 400\,m^2\,yr^{-1}$, slope angle = 1.5°, advance rate = $2.5\,mm\,yr^{-1}$, and equivalent elastic thickness of 20 km. In the sensitivity tests, one parameter is varied while the others are held constant at their reference values. Lines in basin are at equal-time steps (chrons). Numbered positions on top of foreland plate are pinch-out (stratigraphic onlap) positions. Lines within foreland plate are passive markers to show extent of erosion of foreland plate in flexural forebulge. (a) Effect of variations in transport coefficient K, showing major impact on basin depth, basin width and pinch-out migration rate. (b) Effect of variations in the orogenic advance rate, showing major impact on state of filling of the basin. Marine underfilled basins are favoured by low transport coefficients, low tapers and fast advance rates, whereas continental overfilled basins are favoured by high transport coefficients, high tapers and slow advance rates, irrespective of flexural rigidity. Reproduced with permission of John Wiley & Sons, Inc.

Geologic map of the Tien Shan

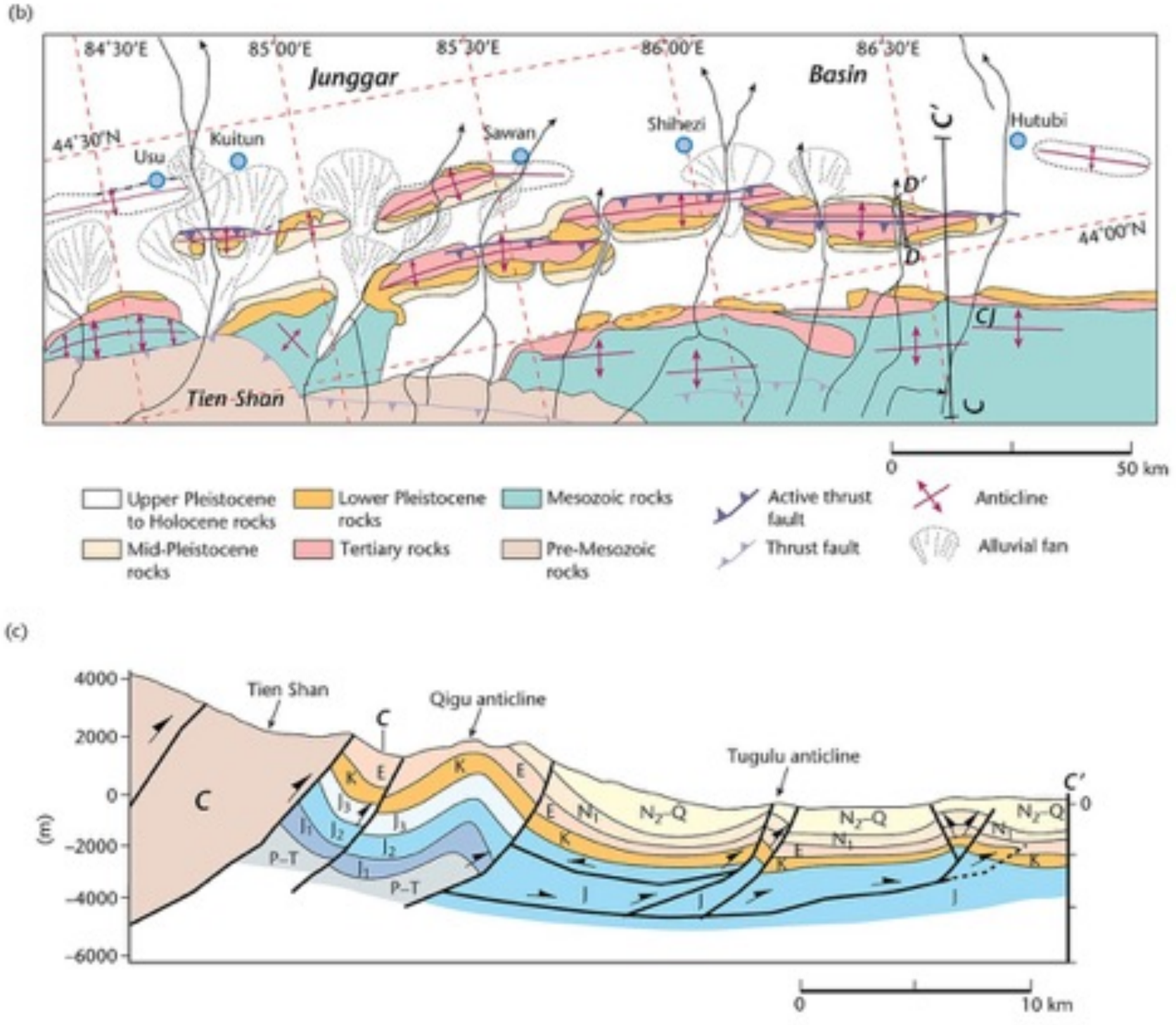

Fig. 4.47 *Continued*

Wilson cycle - foreland basin superimposed on a passive margin

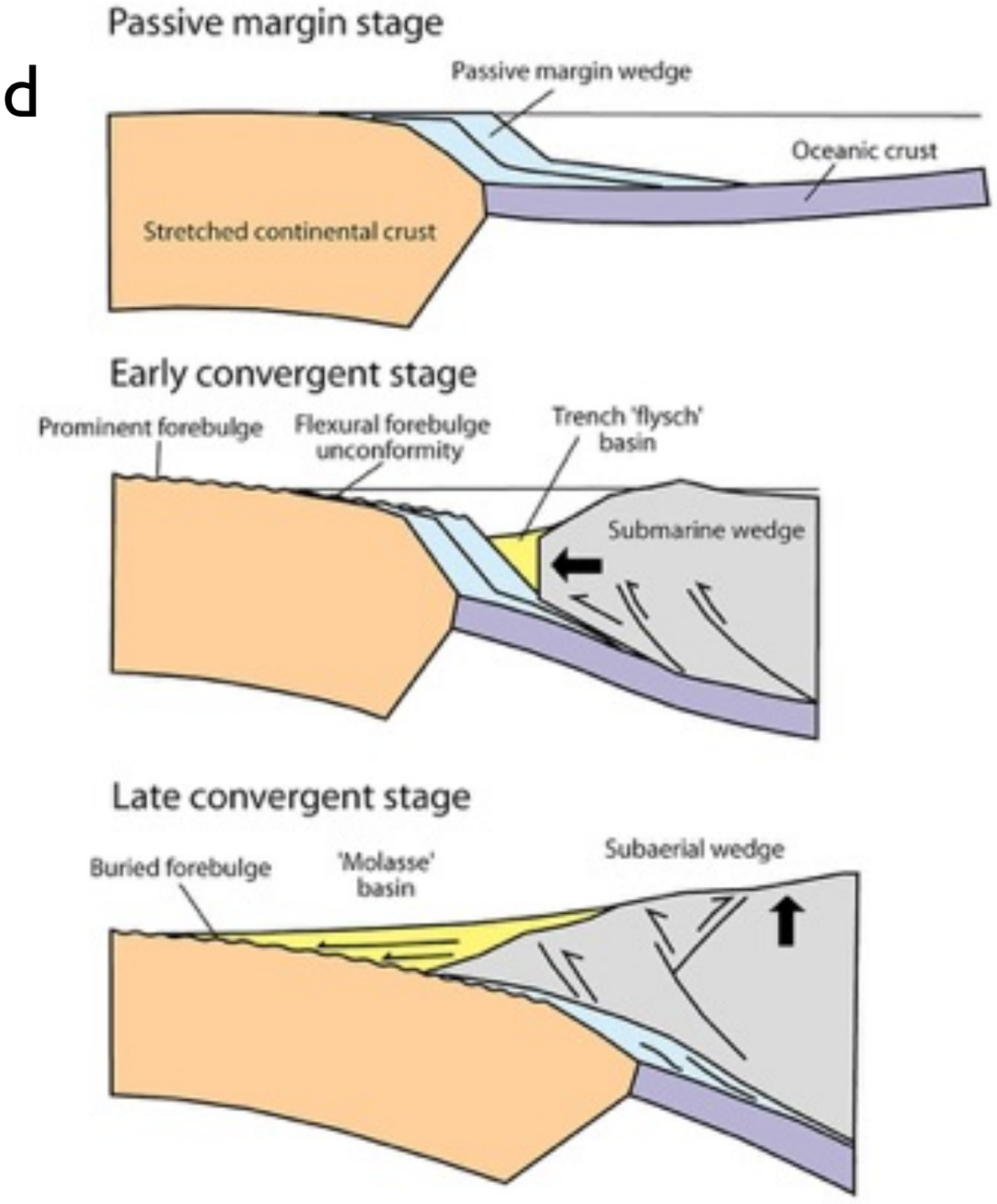

Fig. 4.49 Model involving orogenic loading of a previously stretched continental margin during the early stages of convergence (Stockmal *et al.* 1986 – AAPG © 1986 and reprinted by permission of the AAPG whose permission is required for further use; Watts 1992), modified by Allen *et al.* (1991). The first orogenic loads are emplaced on a weaker lithosphere at considerable water depths.

Wilson cycle - a simple flexural model of basin superimposition

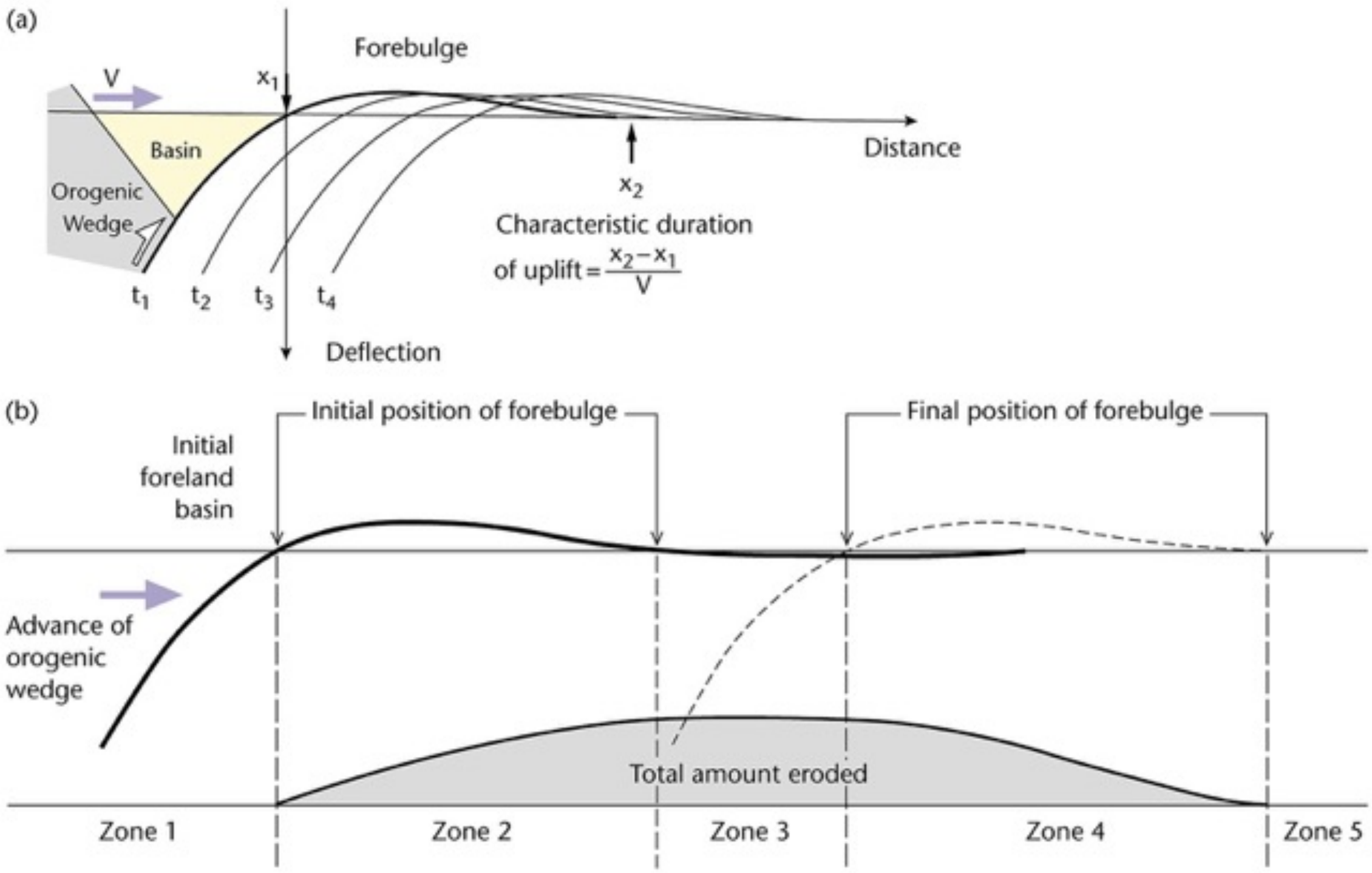

Fig. 4.50 (a) Flexural profiles at times t_1 to t_4, to show the duration of uplift in the flexural forebulge region, using a broken elastic plate. (b) Geometry of the flexural forebulge unconformity. The existence of inherited bathymetry causes zones 1 and 2 to be translated further onto the foreland plate, and zone 2 becomes narrower. After Crampton & Allen (1995).

wedge advance and onlap advance

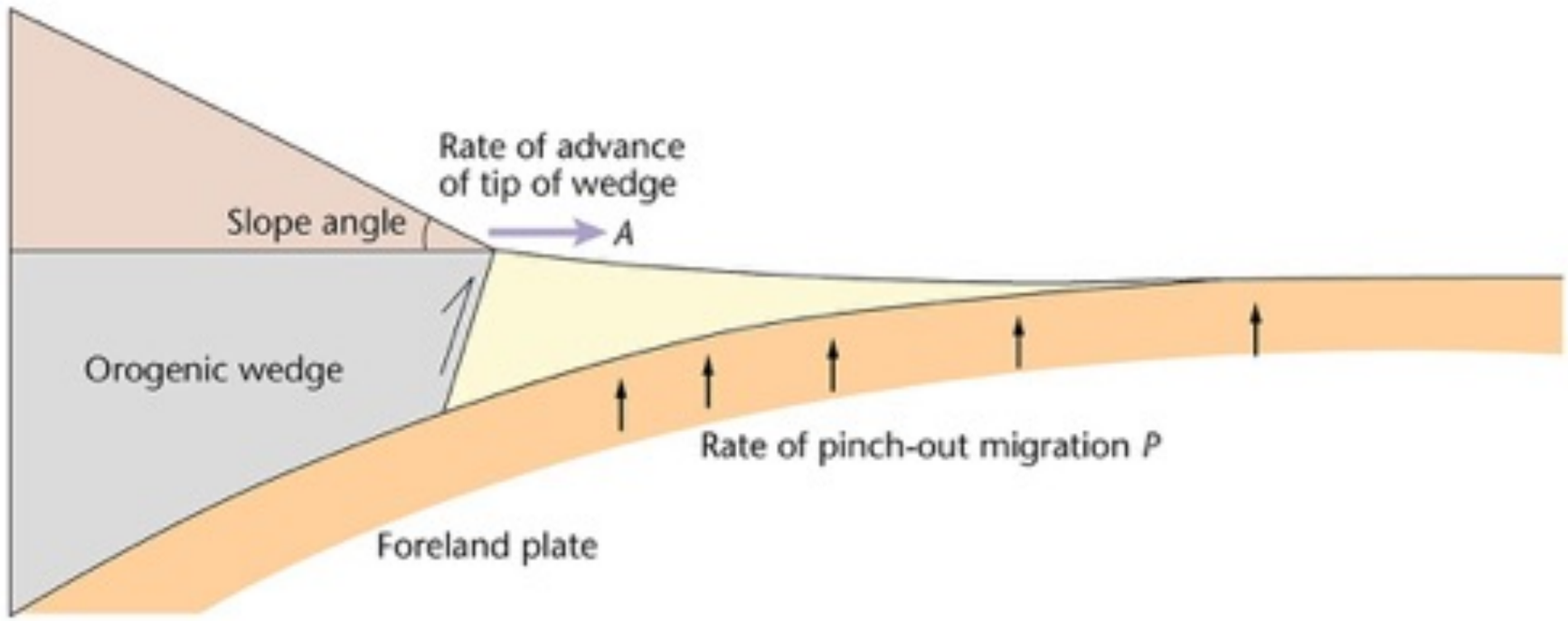

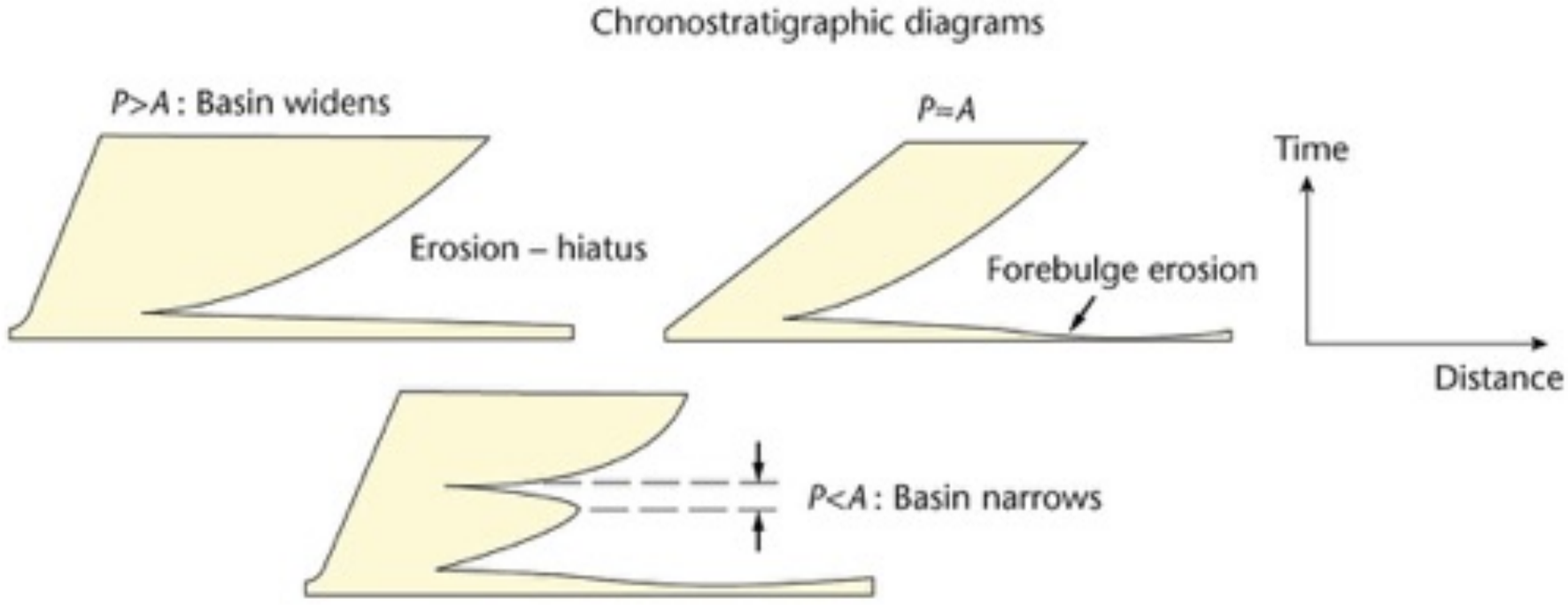

Fig. 4.52 Influence of the rates of advance of the tip of the orogenic wedge and of pinch-out migration on the foreland basin width. Note that onlap onto the foreland plate takes place even in the case of a time-constant basin width. A narrowing of the basin has been interpreted as due to viscoelastic relaxation, but can also result from reorganisation of the orogenic load on an elastic plate.

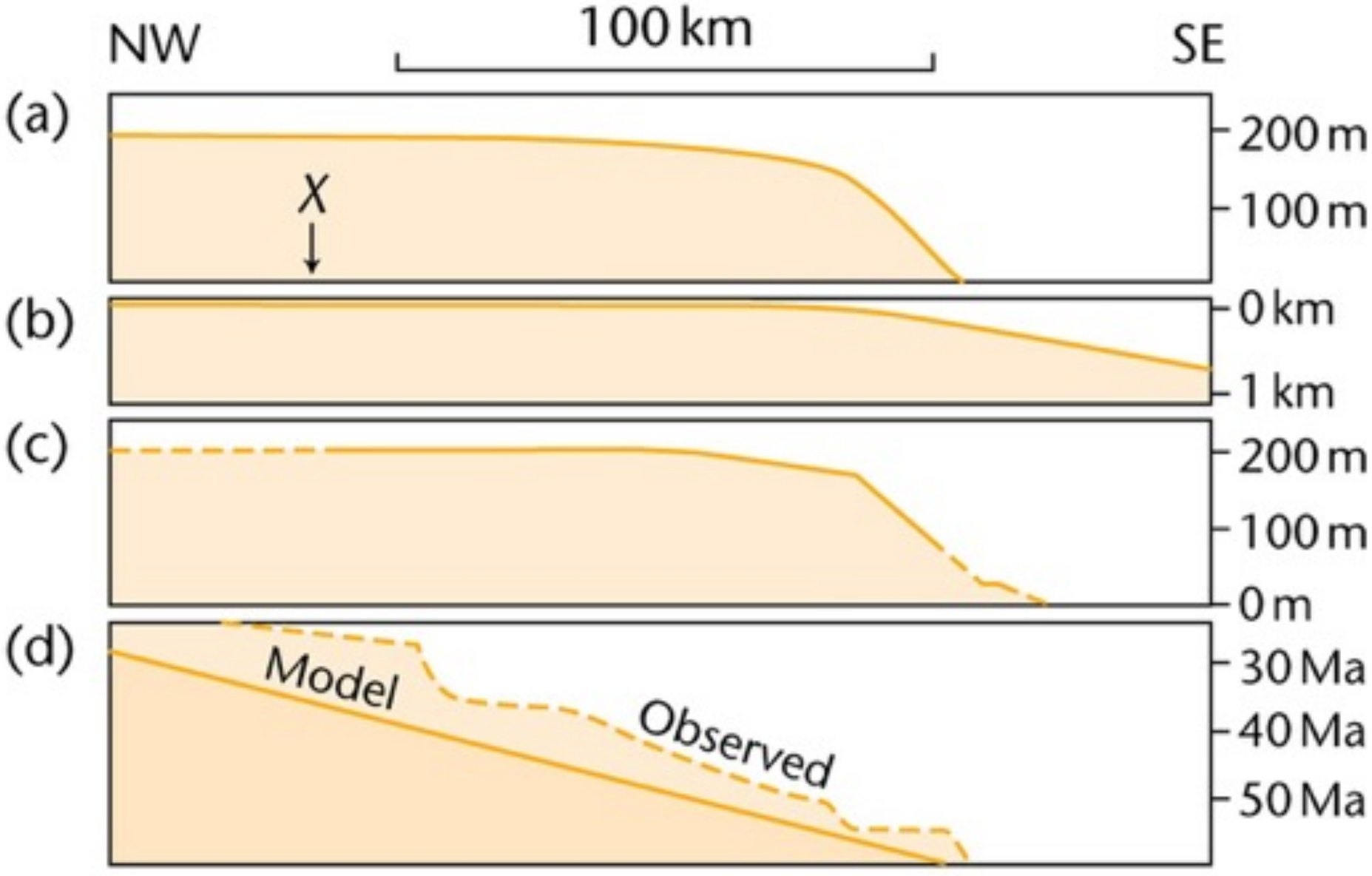

Fig. 4.51 Fit between model predictions for the forebulge unconformity and observations in eastern Switzerland, using the linear elastic model of Crampton & Allen (1995). (a) The modelled total erosion at the forebulge unconformity versus distance from the initial position of the orogenic wedge, with Te = 10 km, orogenic advance rate 8 mm yr^{-1} and erosion proportional to elevation with coefficient 0.02. Point *X* is initially 200 km from the orogenic front. Note the rapid increase in erosional gap from 0 to 200 m across the zone of inherited shelf bathymetry shown in (b). (c) The observed erosion versus approximate restored distance from the orogen (based on Herb 1988), showing close similarity to the modelled erosion. (d) As a test, the modelled onlap of sedimentary rocks overlying the unconformity are compared with the observed onlap along a restored section (based on Herb 1988, Sinclair *et al.* 1991 and Crampton & Allen 1995).

under-filled forelands vs over-filled forelands

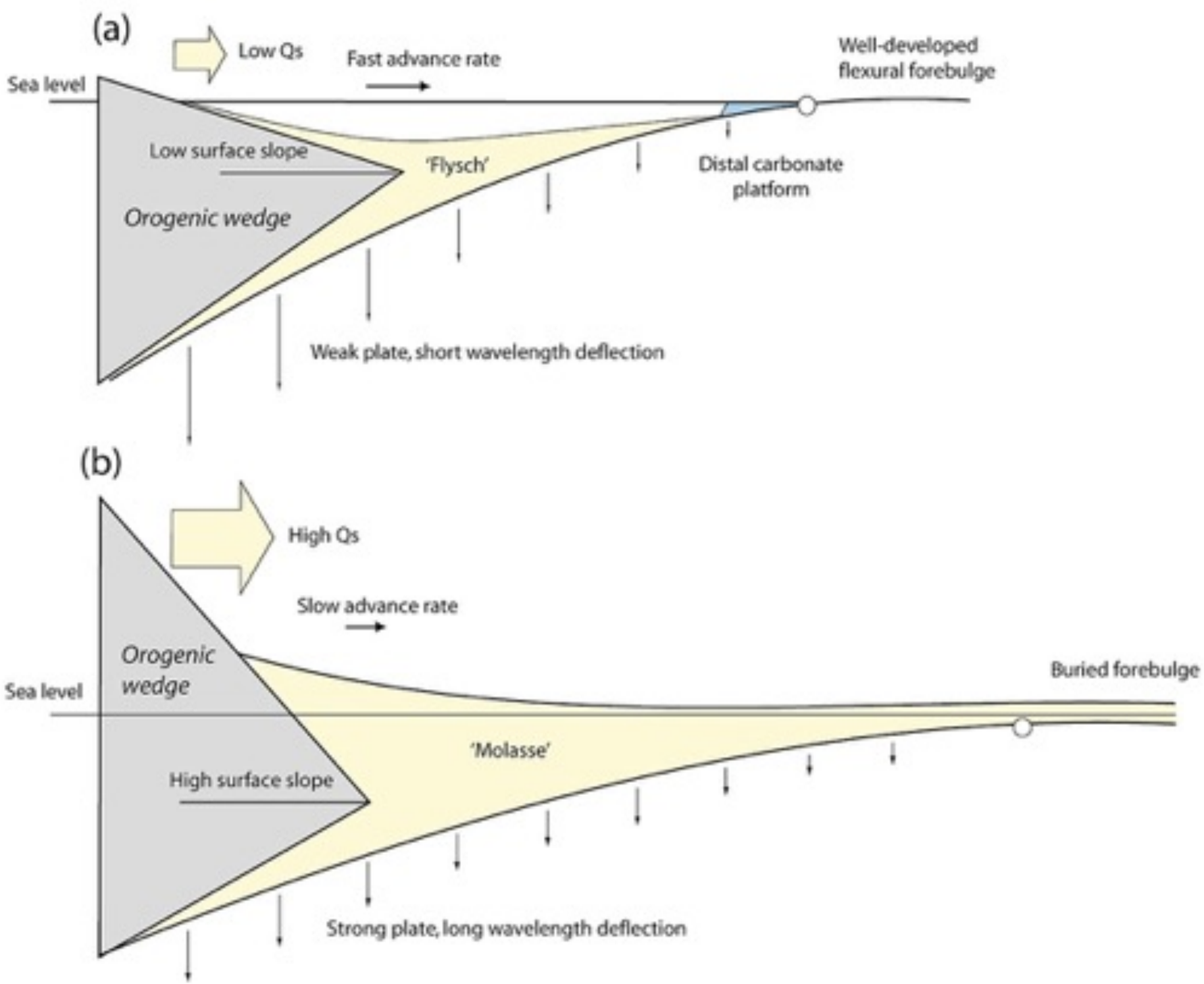

Fig. 4.53 Highly schematic illustration of the factors favouring underfilled 'flysch' basins (a) compared to overfilled 'Molasse' basins (b). Pro-foreland basin systems commonly evolve from flysch to Molasse stages.

analysis of intra-cratonic basin subsidence

Michigan Basin

intra-cratonic basins

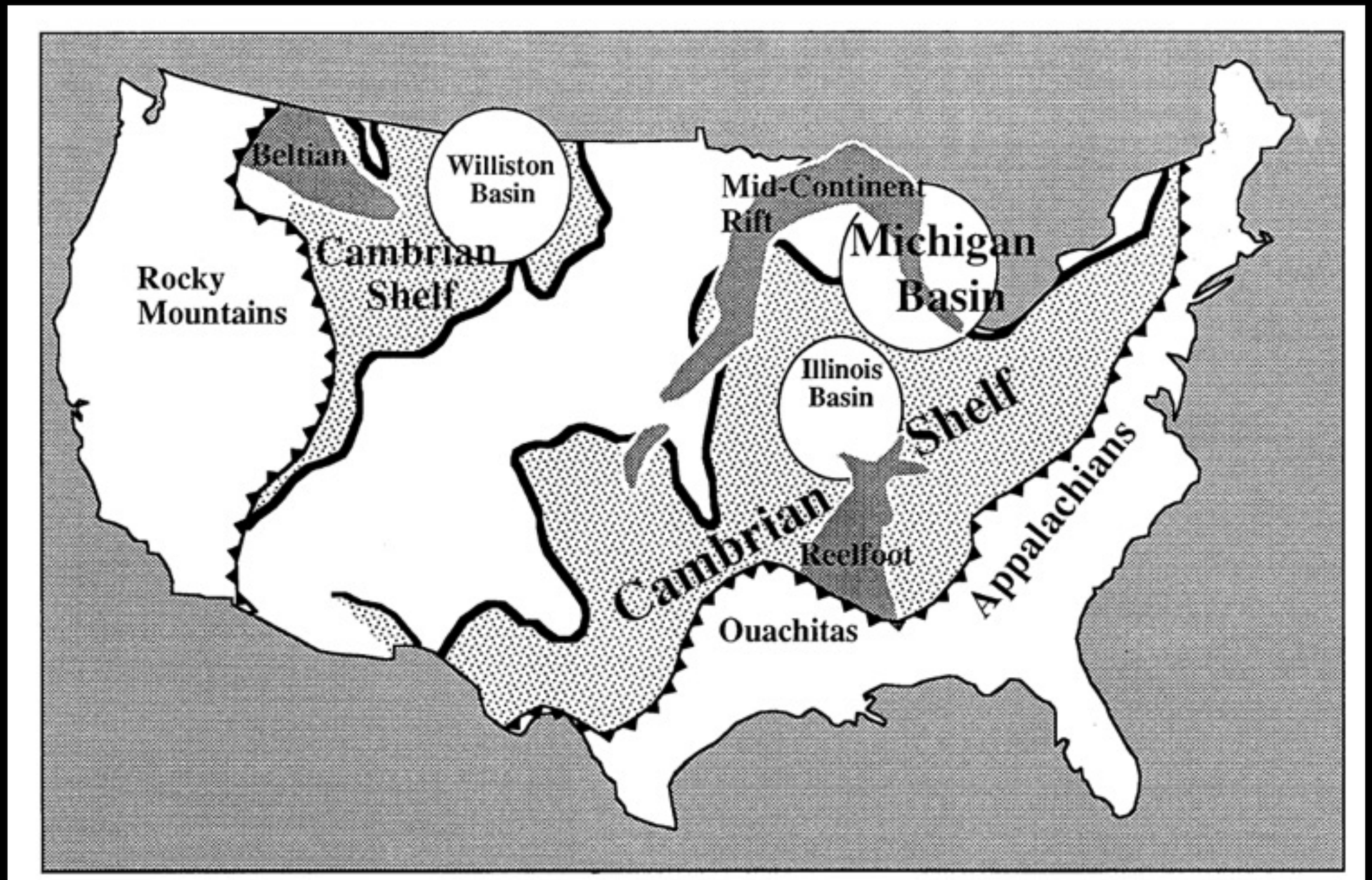

Michigan Basin

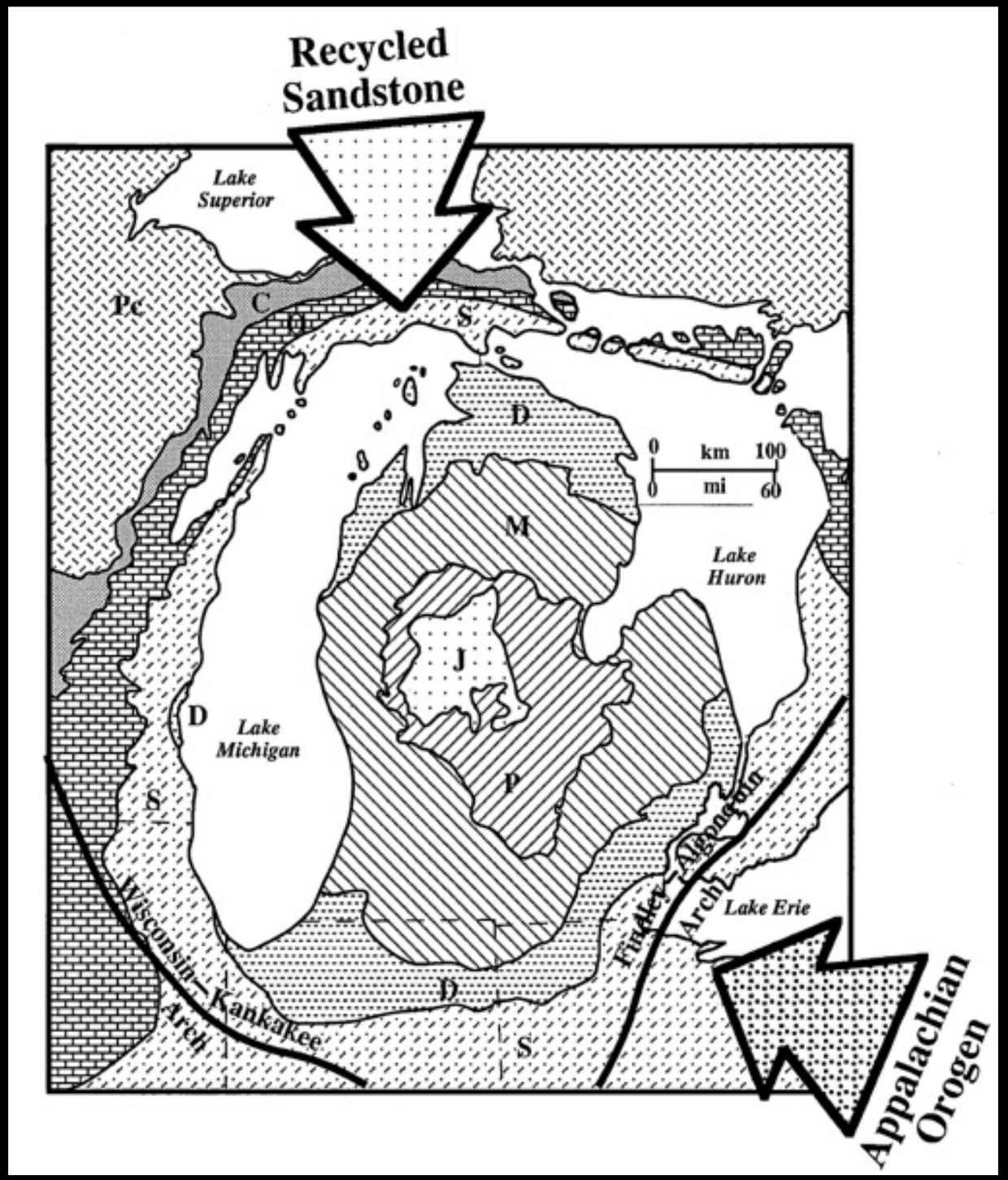

Sloss's Sequences

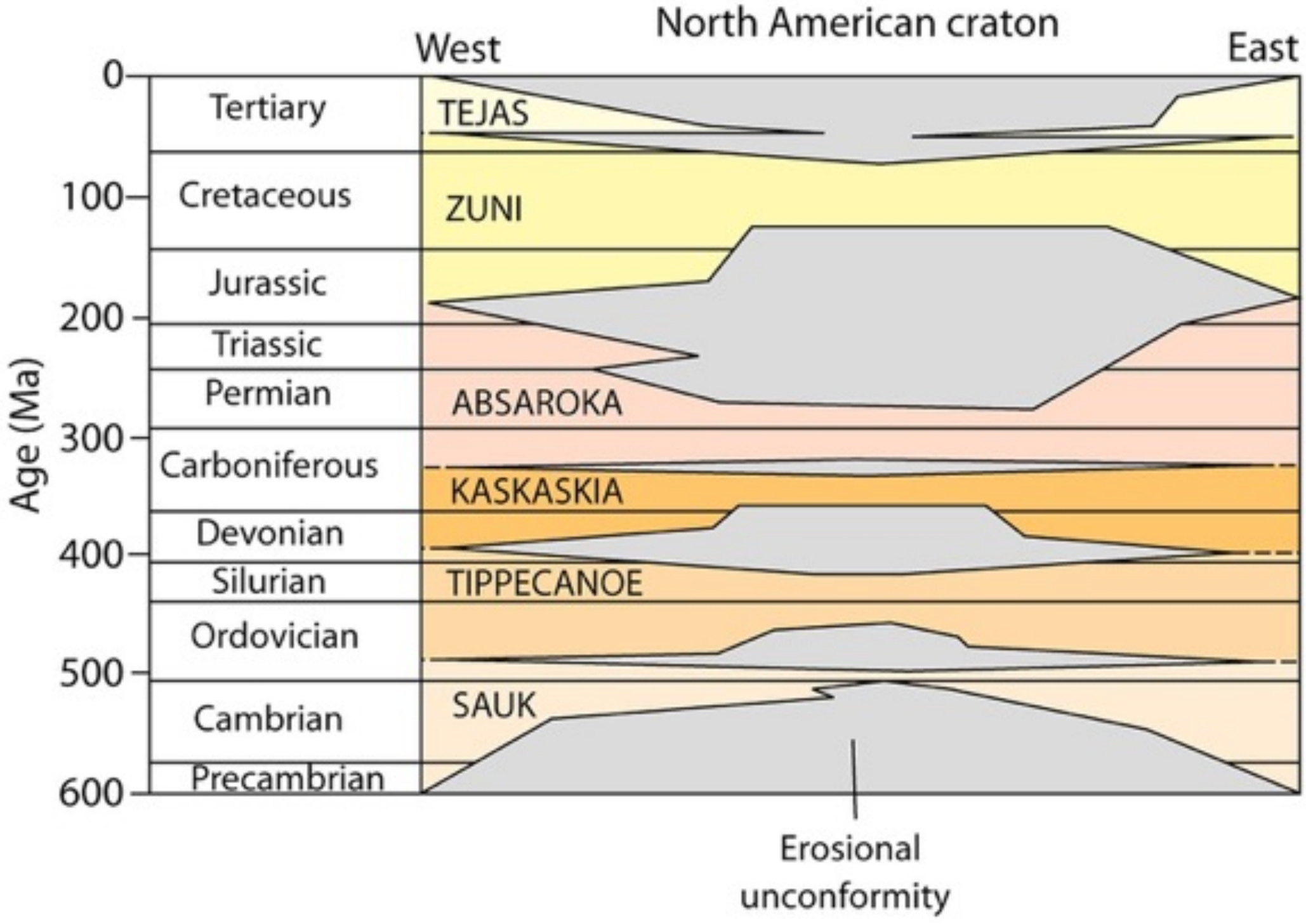

Fig. 8.6 The supersequences of the North American craton of Sloss (1963).

deepest well in the Michigan Basin

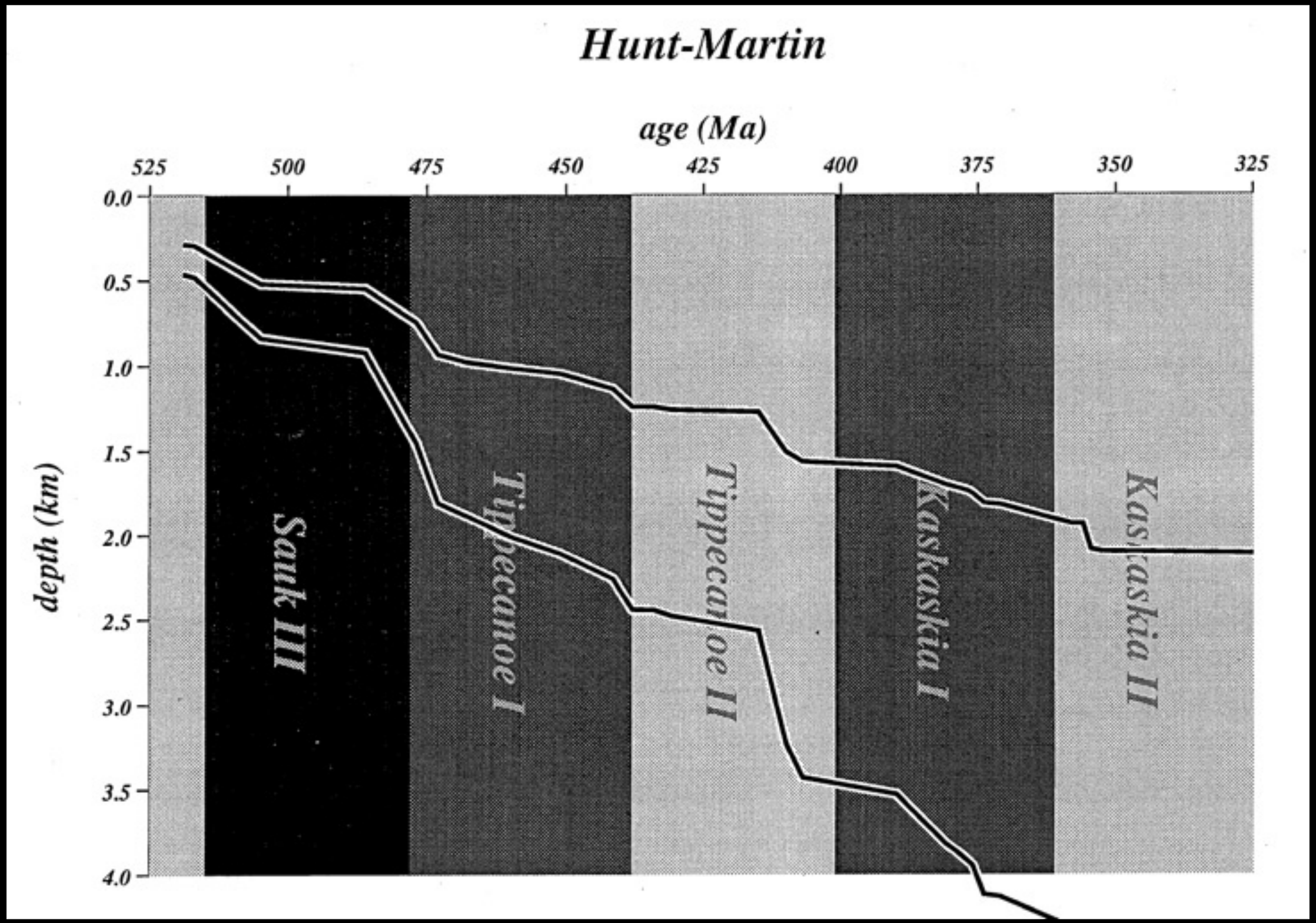

correlated subsidence events in deep wells

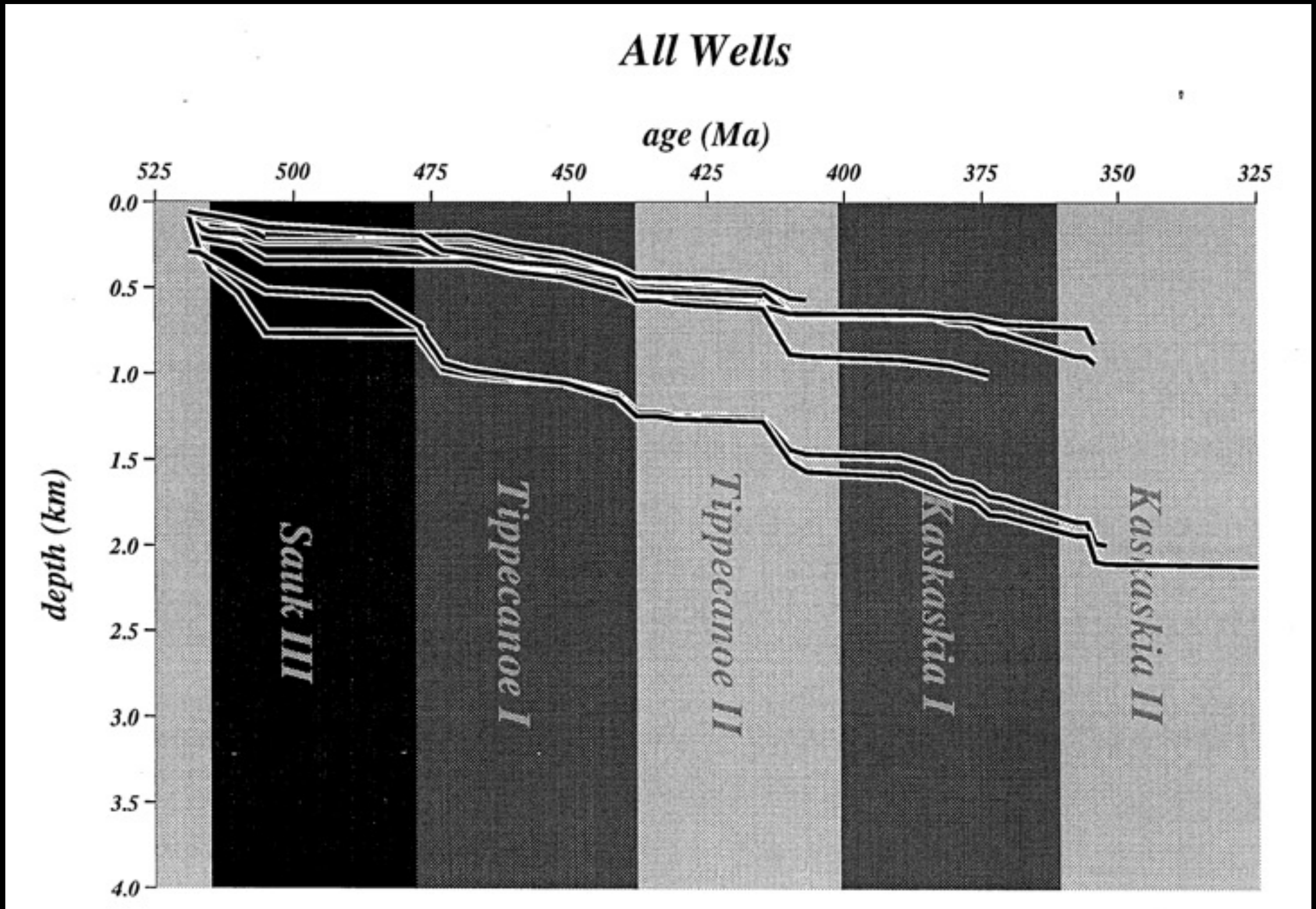

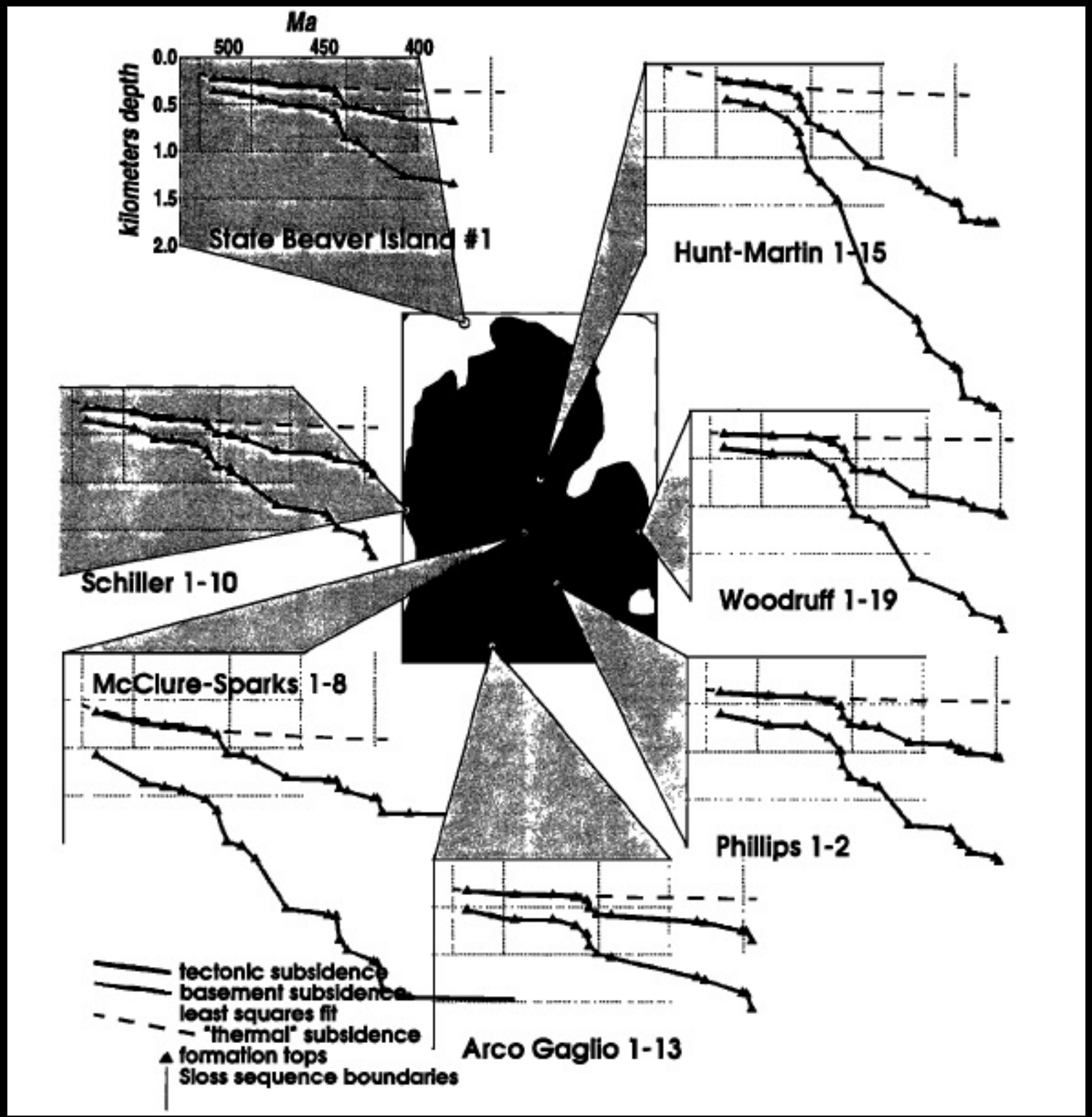
Ma
500
450
400
0.0
0.5
1.0
1.5
2.0
kilometers depth
State Beaver Island #1
Hunt-Martin 1-15
Schiller 1-10
Woodruff 1-19
McClure-Sparks 1-8
Phillips 1-2
Arco Gaglio 1-13
tectonic subsidence
basement subsidence
least squares fit
"thermal" subsidence
formation tops
Sloss sequence boundaries

well database

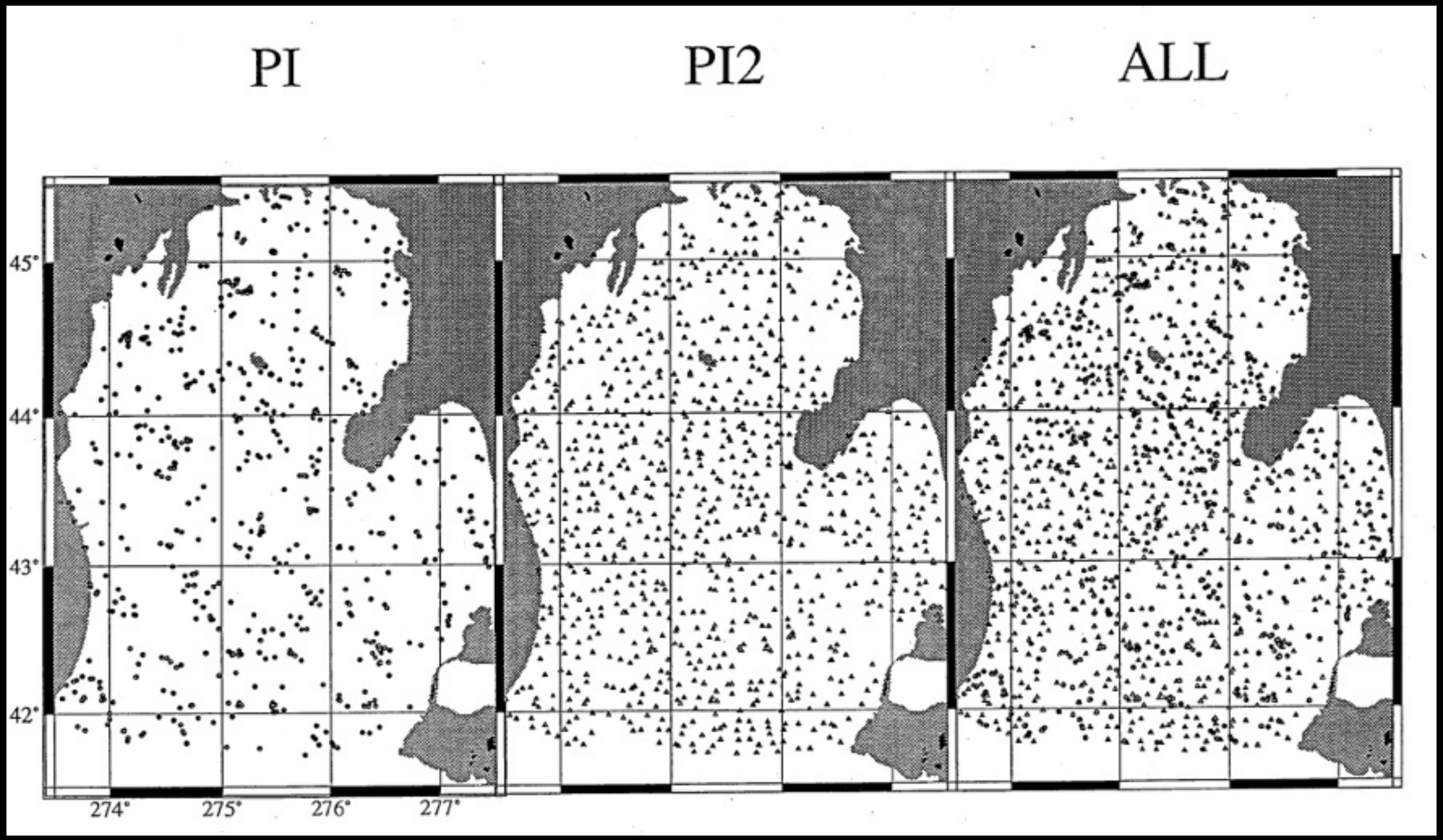

basin-centered subsidence

St Peter sandstone, Shakopee

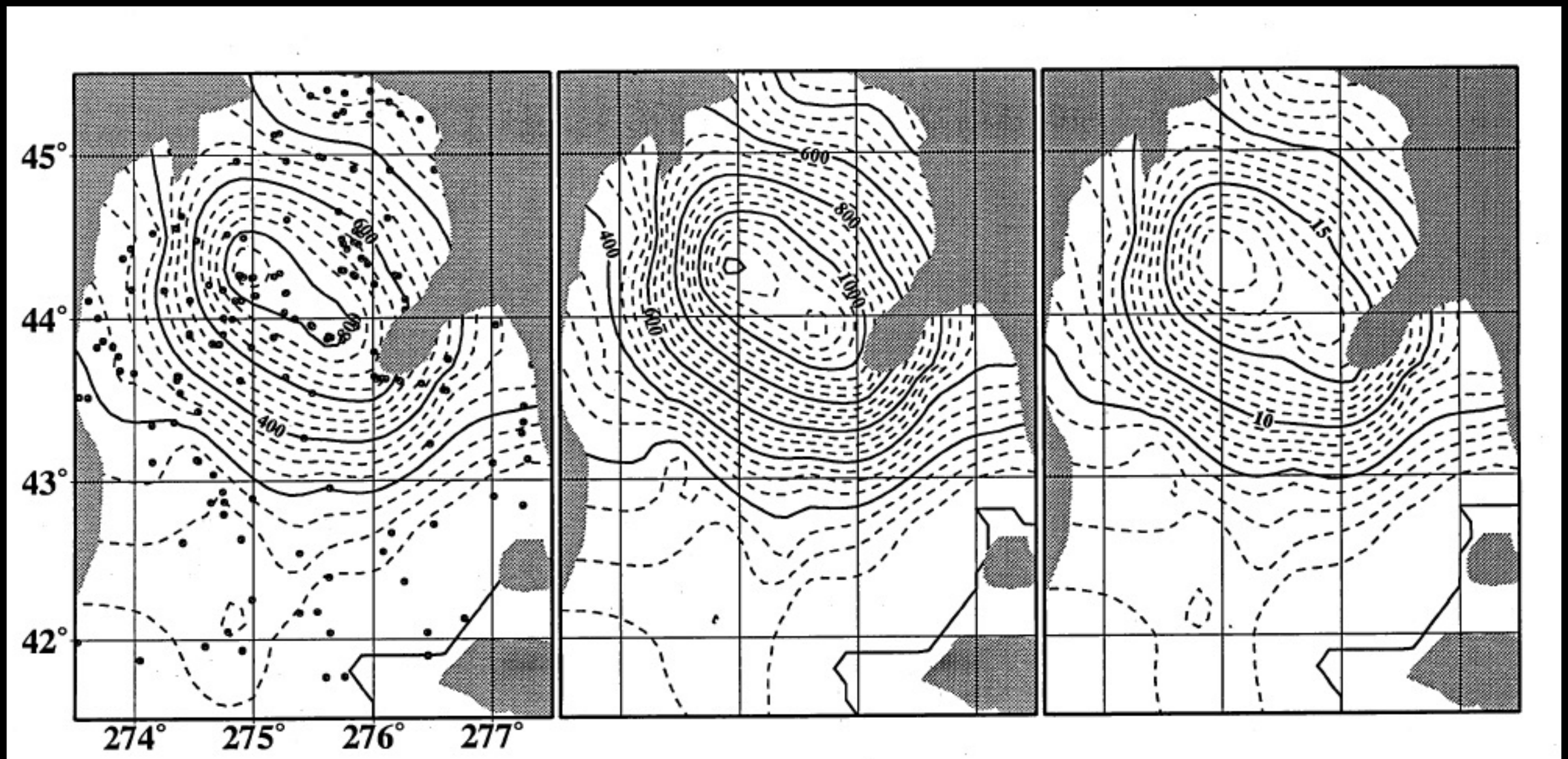

basin tilted to the east

Black River and Trenton (carbonates)

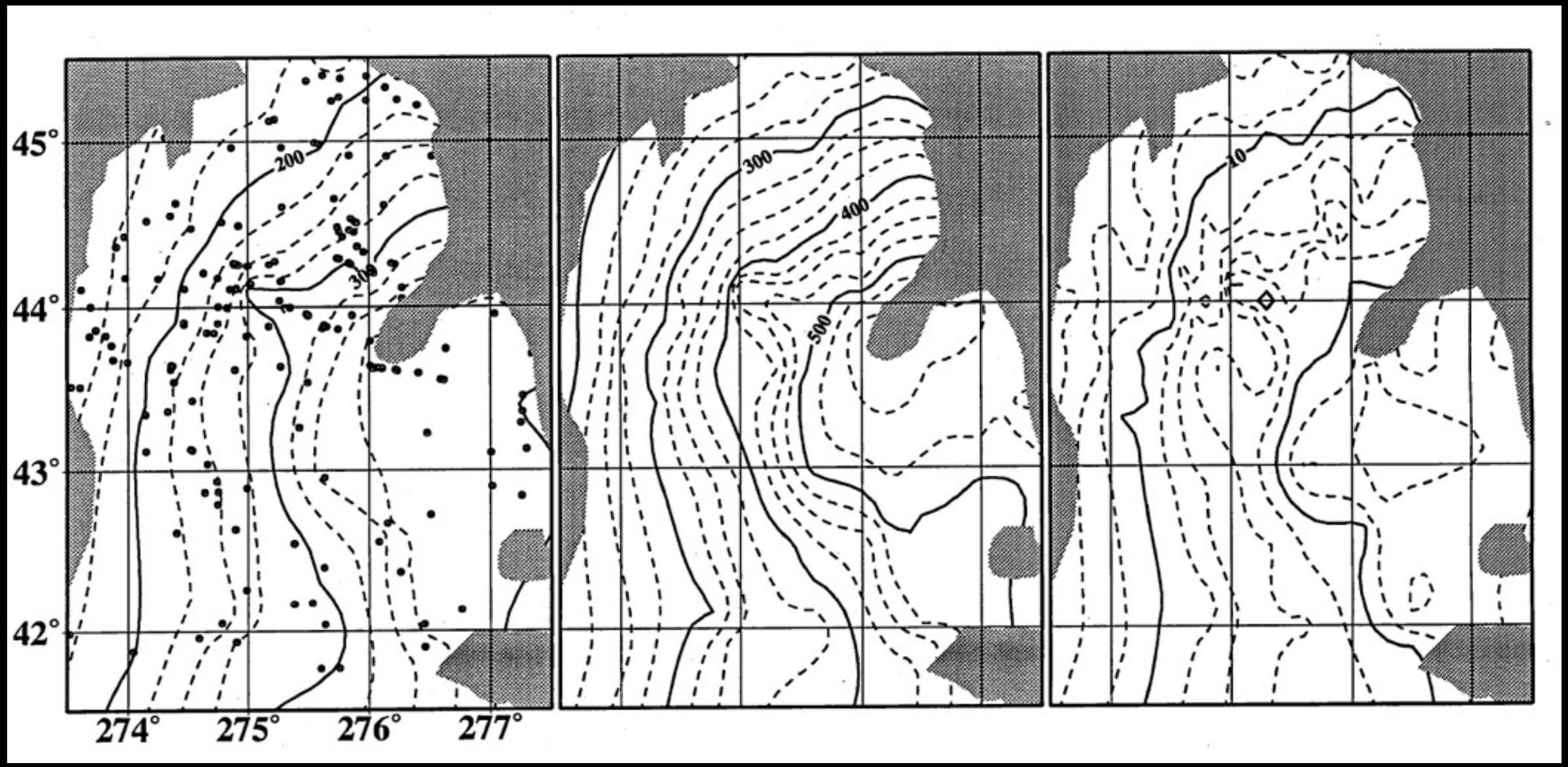

stratigraphy hung on
Trenton - Black River contact

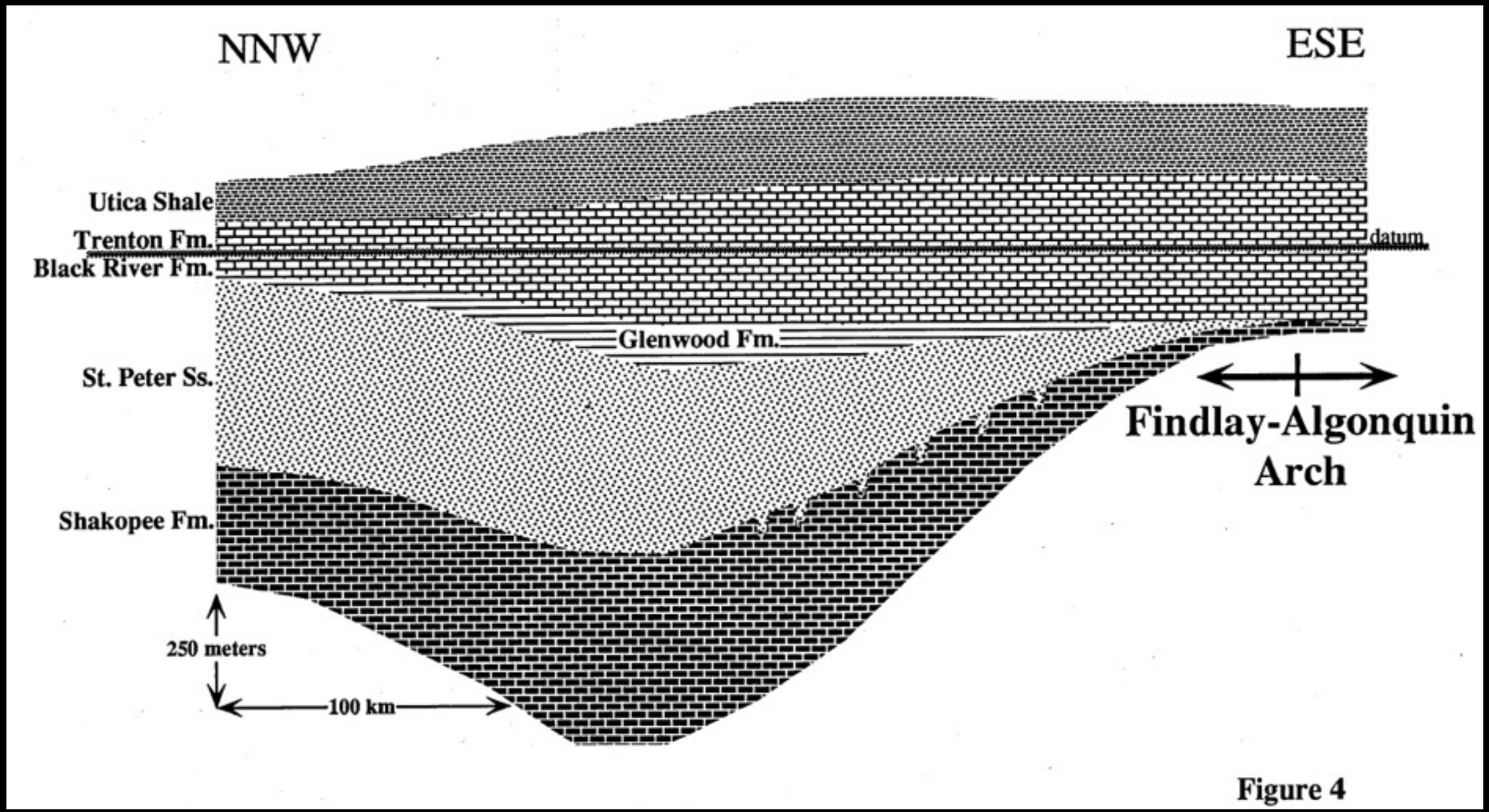

Figure 4

Ordovician Depo-centers

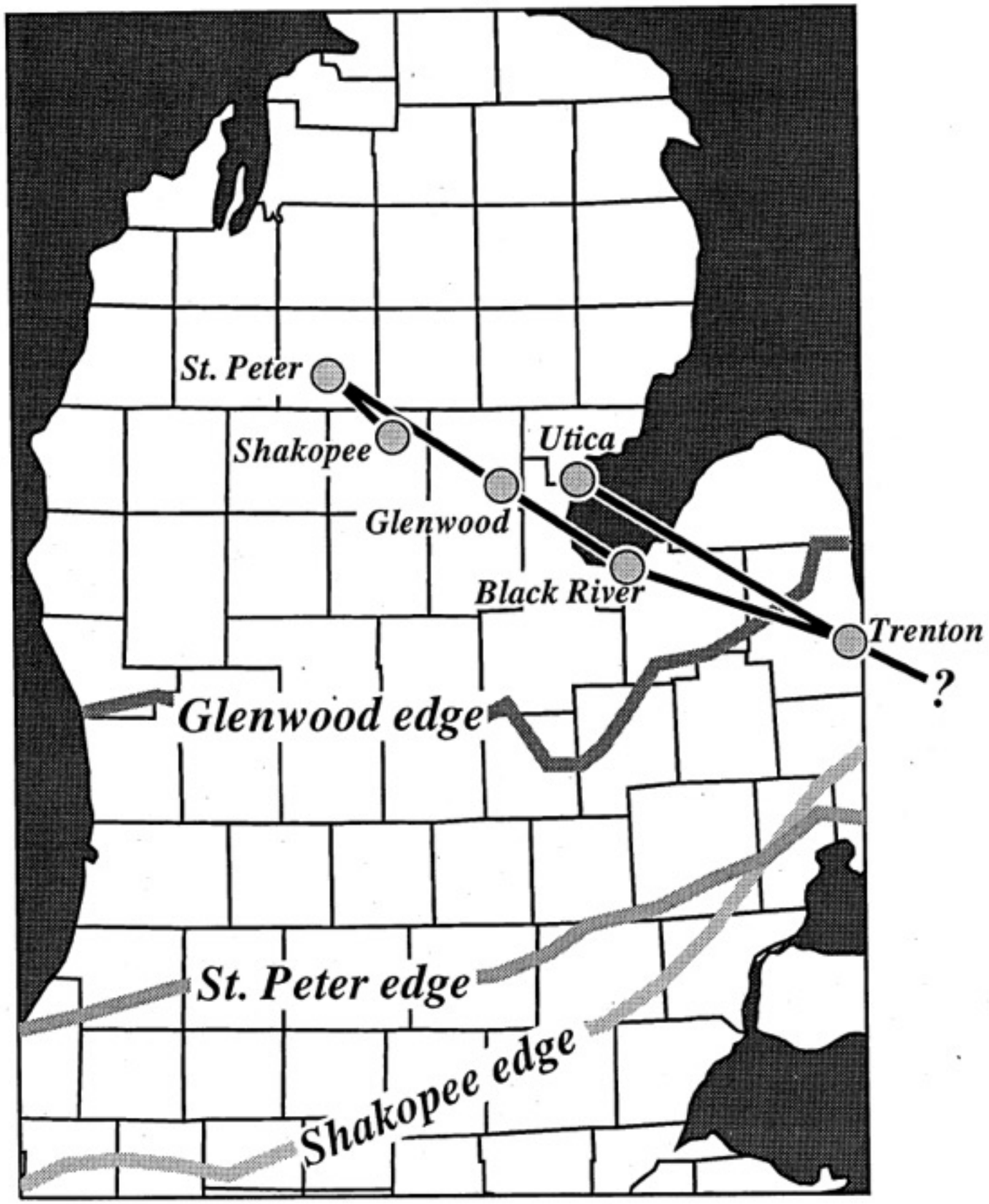

stratigraphic column

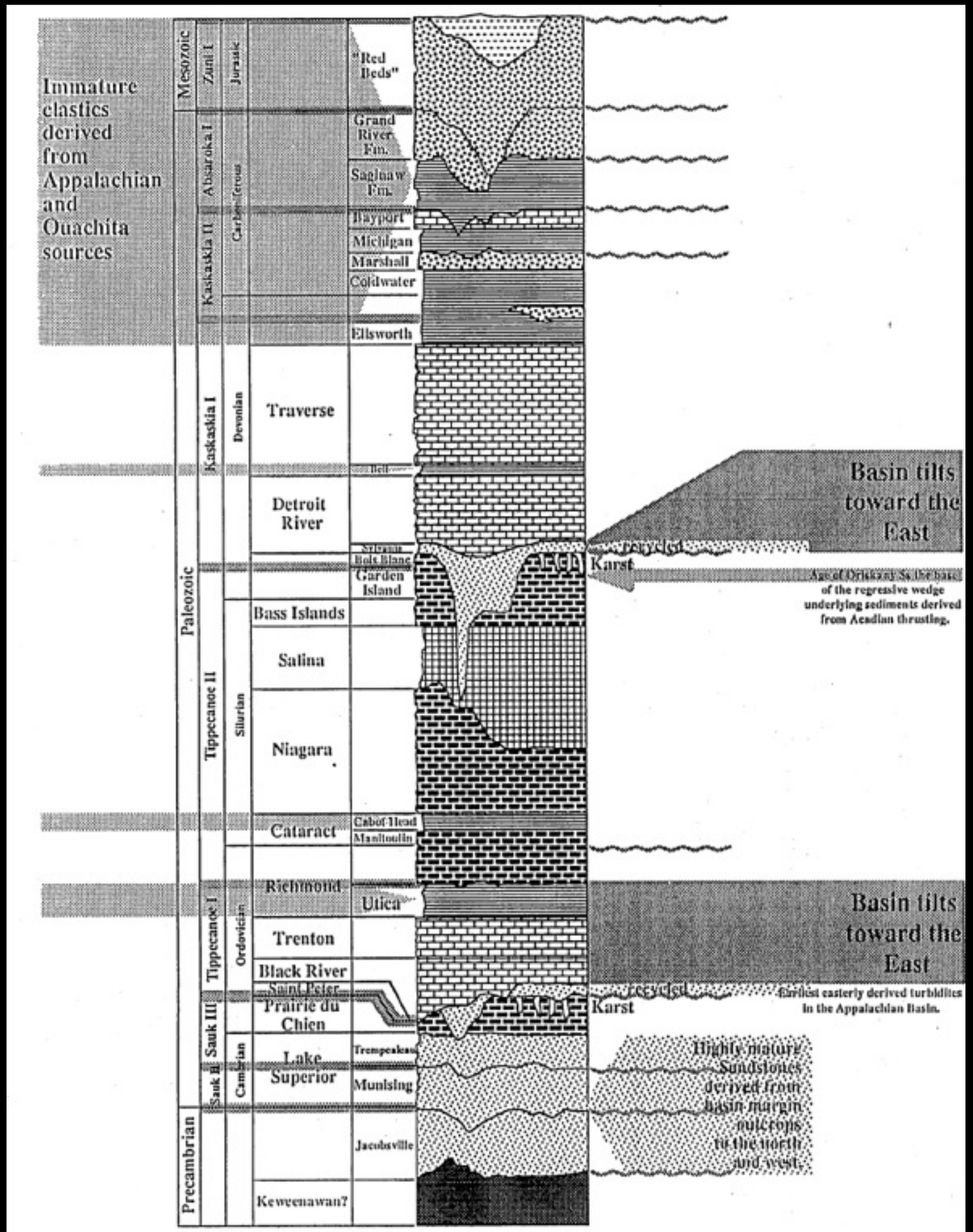

subsidence events

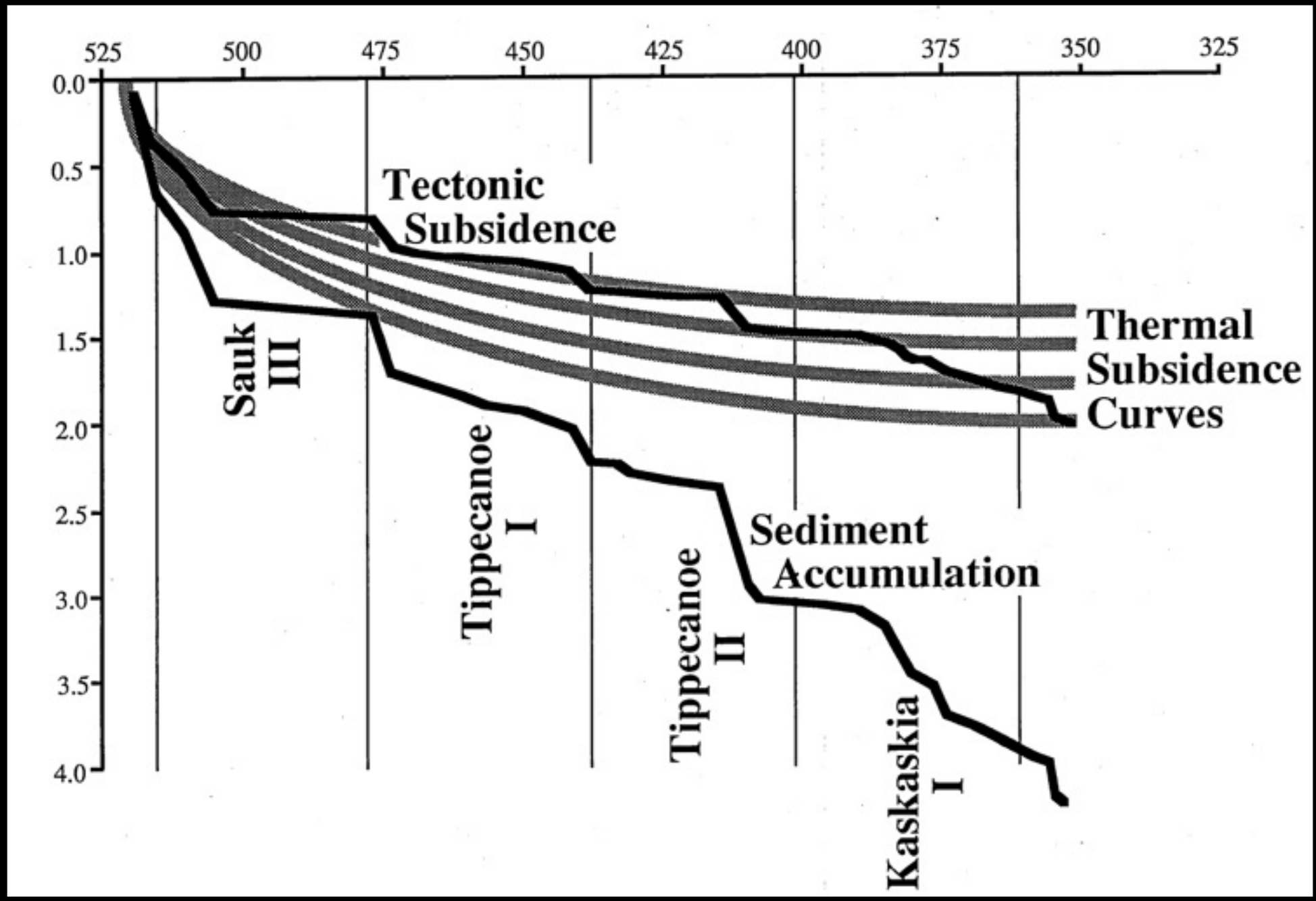

stratigraphic-tectonic evolution

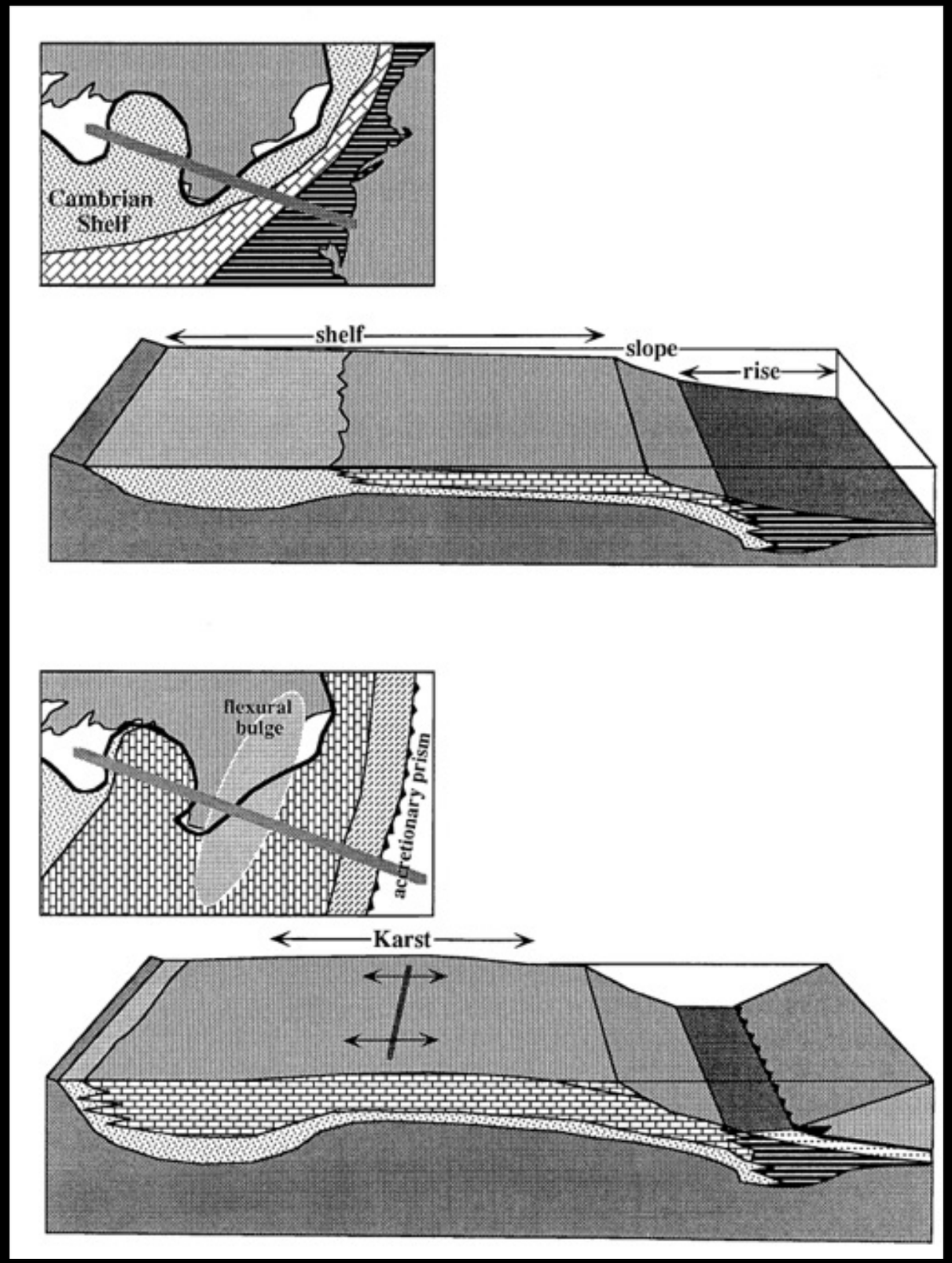

stratigraphic-tectonic evolution II

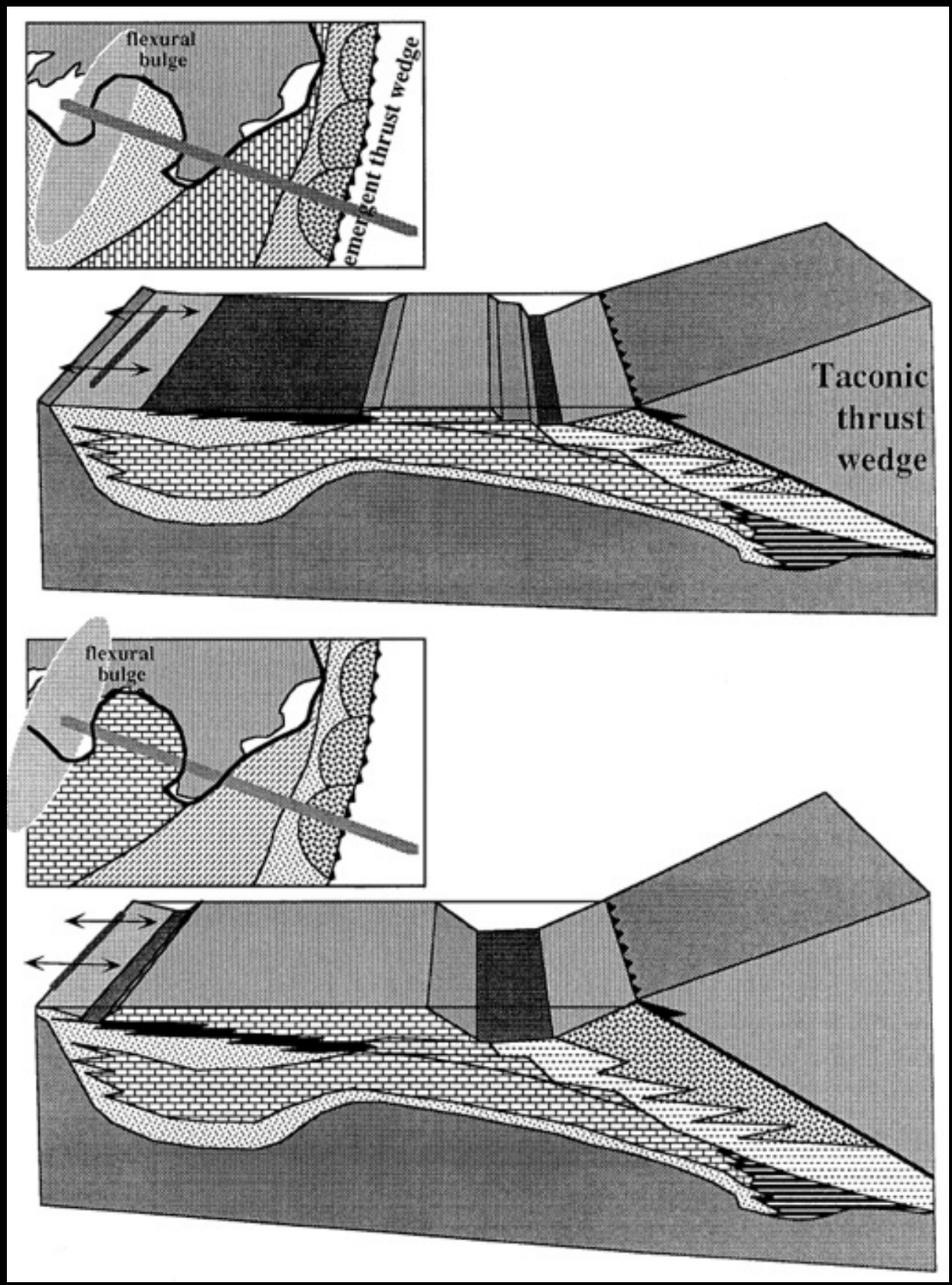

Some Arctic Ocean

International Bathymetric Chart of the Arctic Ocean IBCAO v. 3.0

Two distinct basins of different ages

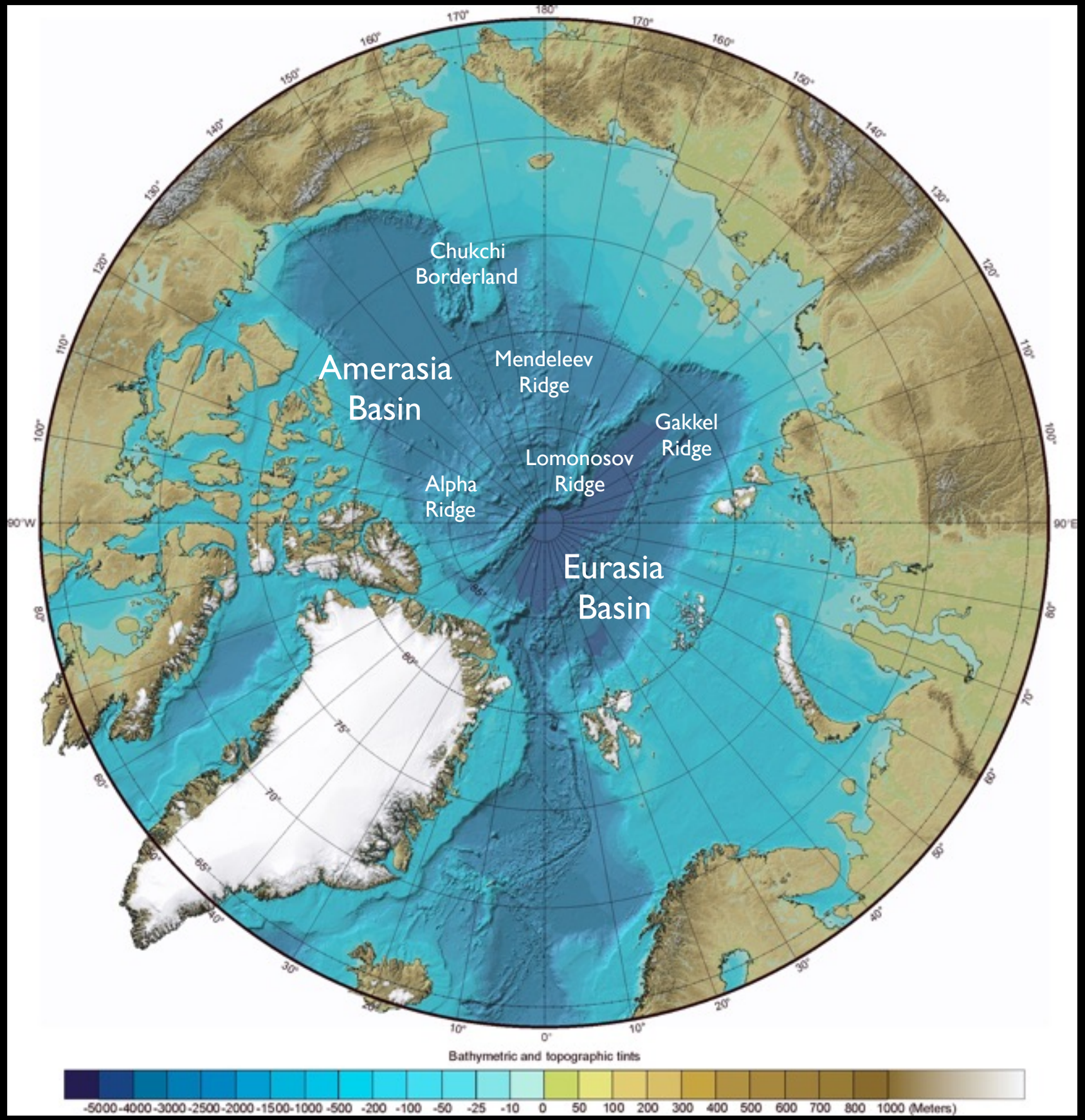

Shelf Edge-Northwind Ridge
Shelf Margin Development

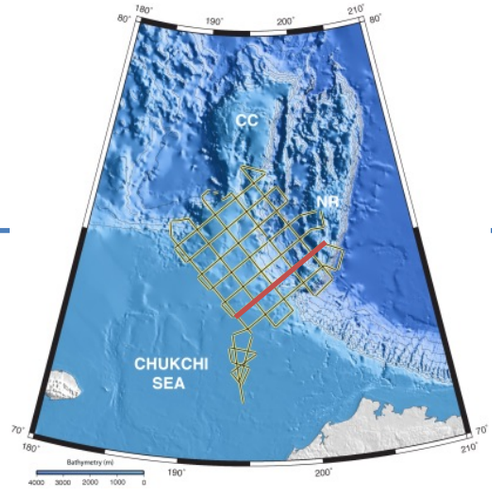

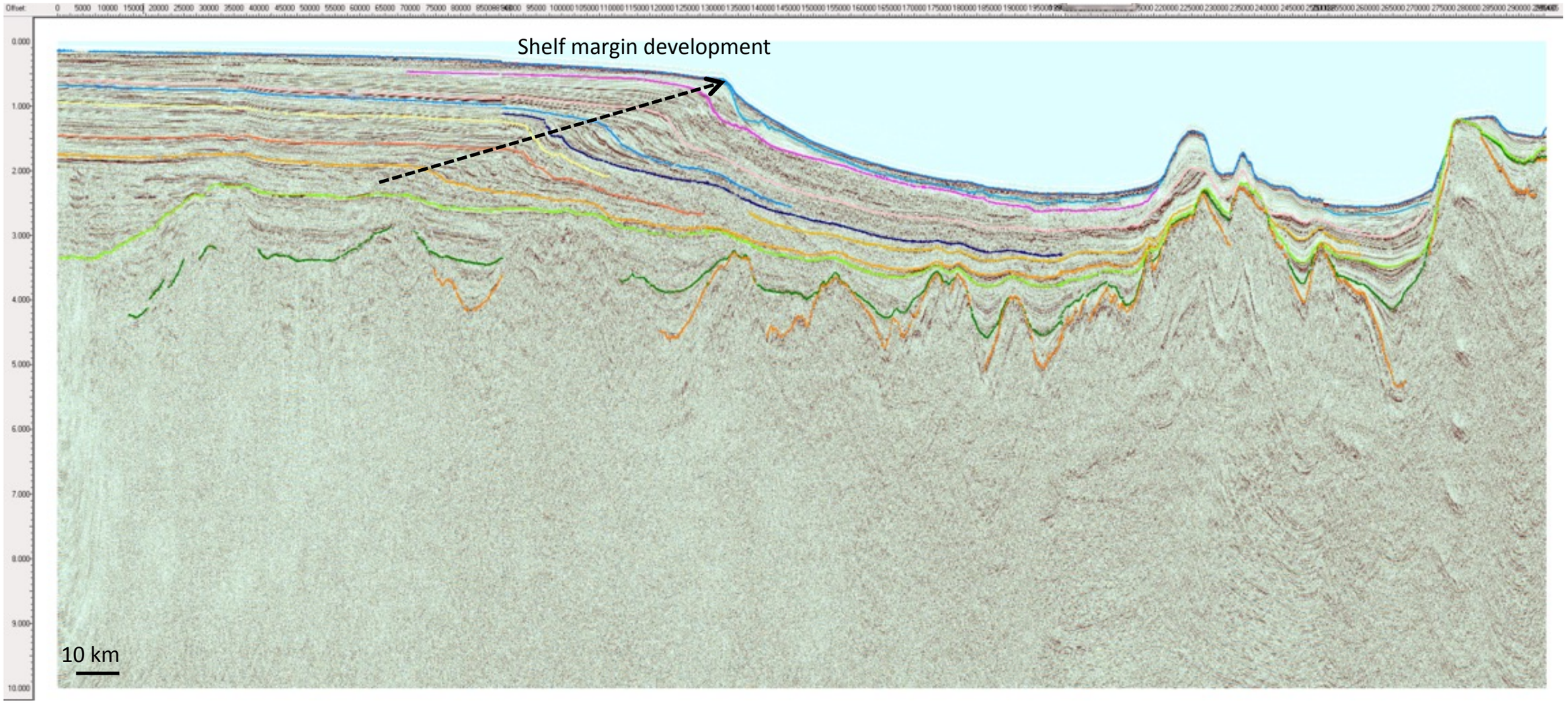

SW-NE seismic profile indicating continuity of the seismic units from the shelf edge to the deeper basin. **Light green** is the key unconformity tying the seismic units throughout the seismic grid. Arrow indicates the shelf margin development.

Western North Chukchi Basin to the Deep Basin

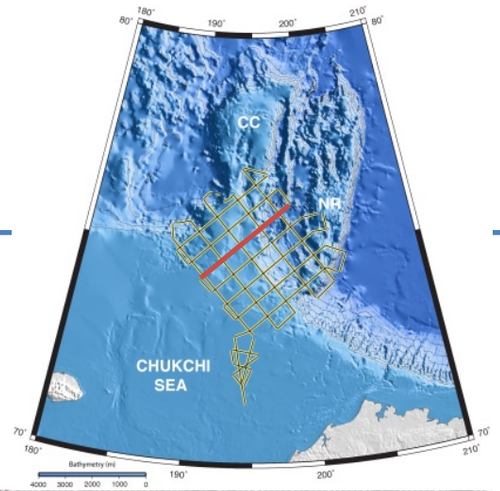

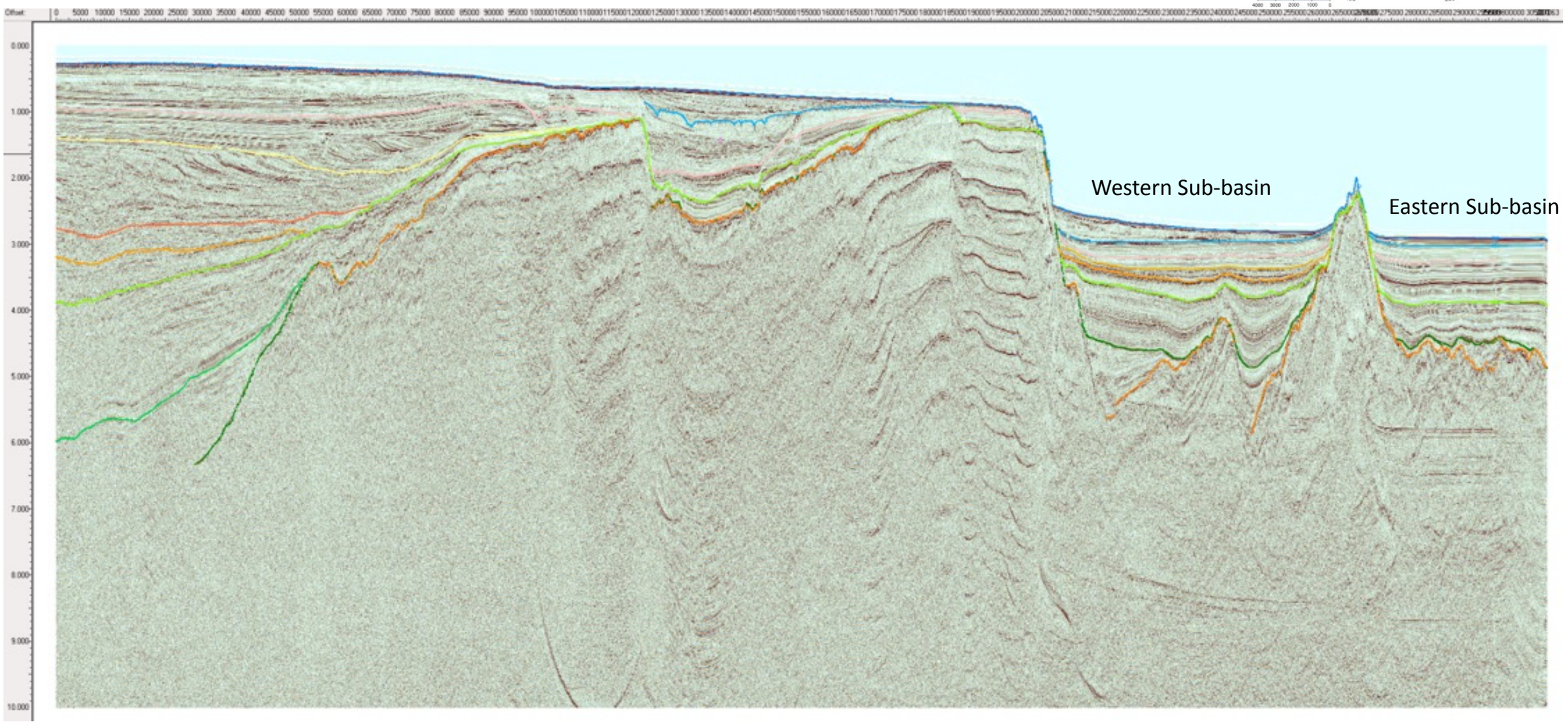

SW-NE seismic profile-5 indicates basement structure and stratigraphic differences in the Western and Eastern Sub-basins (see fanning of syn-rift strata in the Western Sub-basin).

Multi-Channel Seismic Reflection from Chukchi Borderland

SW

NE

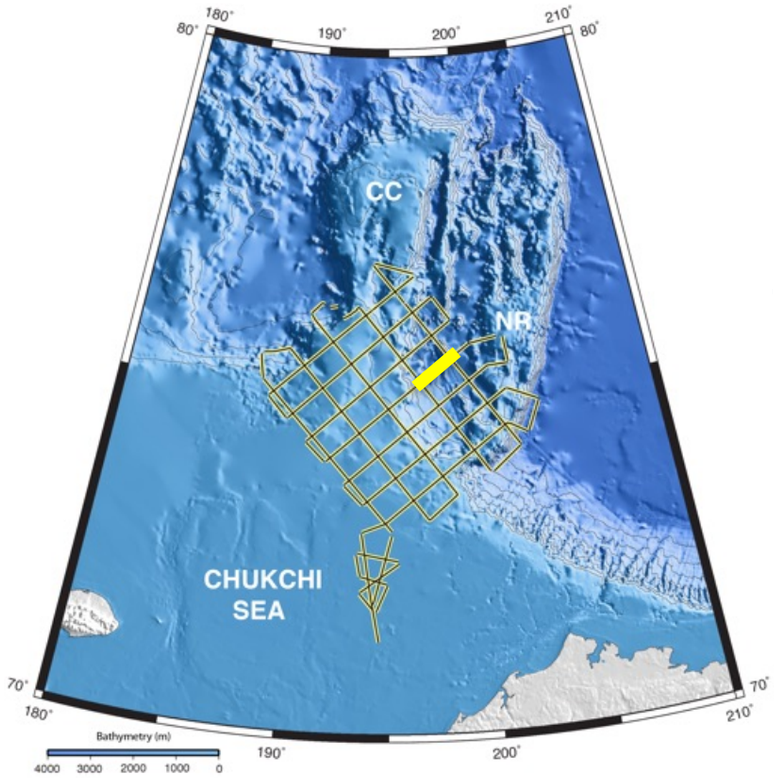

strike-slip related basins

mostly small and very complicated

basins due to strike-slip deformation

- associated with oblique faults
- most deformation is concentrated on a principal displacement zone (PDZ)
- typically segmented, small and complex
- not simply modeled for heat flow or subsidence

simple stress regime for strike-slip faults

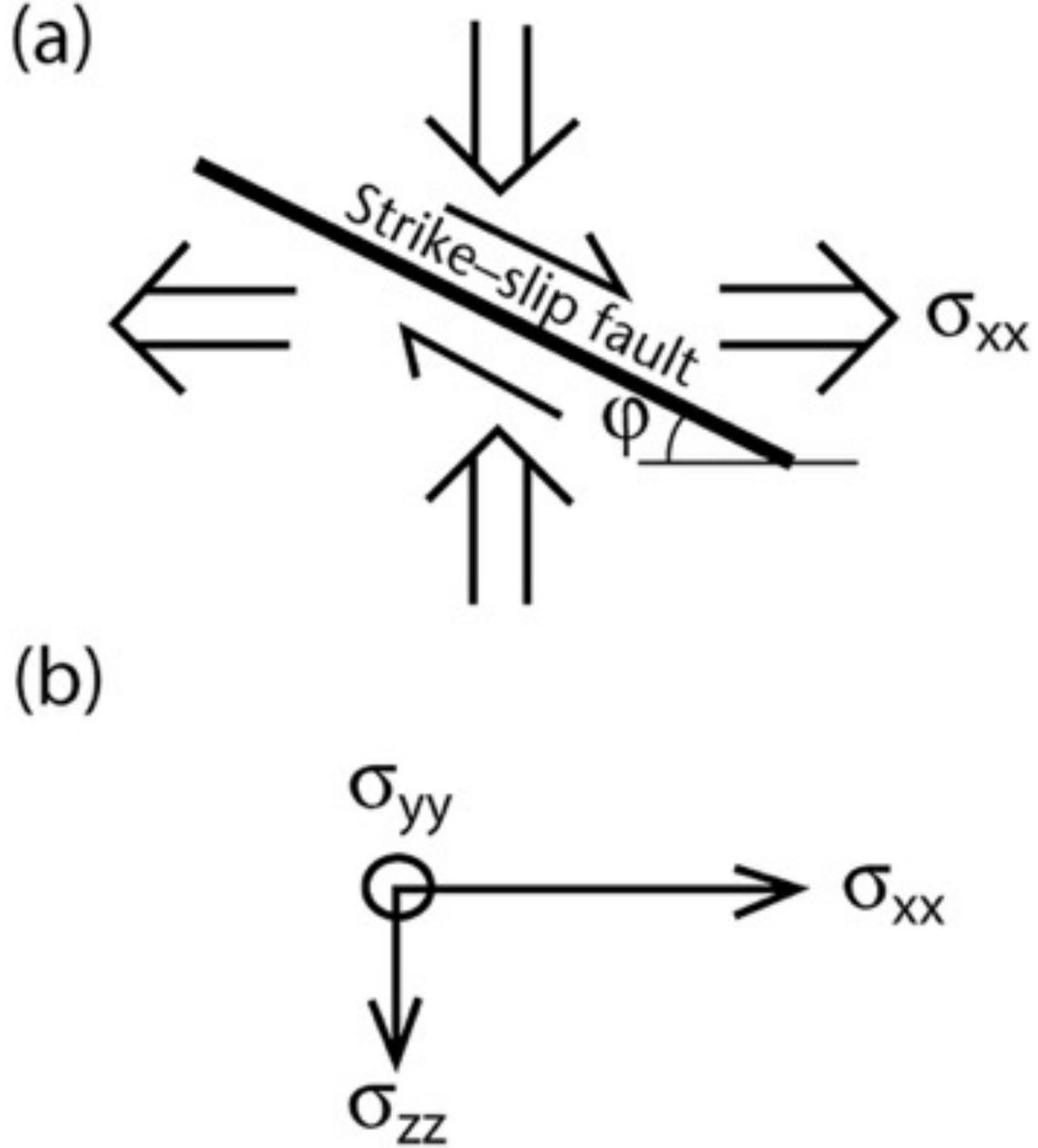

Fig. 6.1 Plane strain approximation for strike-slip faults. (a) Conjugate strike-slip faults at an angle φ to the principal stress σ_{xx}. (b) Principal stresses are related by $\sigma_{zz} > \sigma_{yy} > \sigma_{xx}$.

restraining and releasing bends

local convergence and divergence

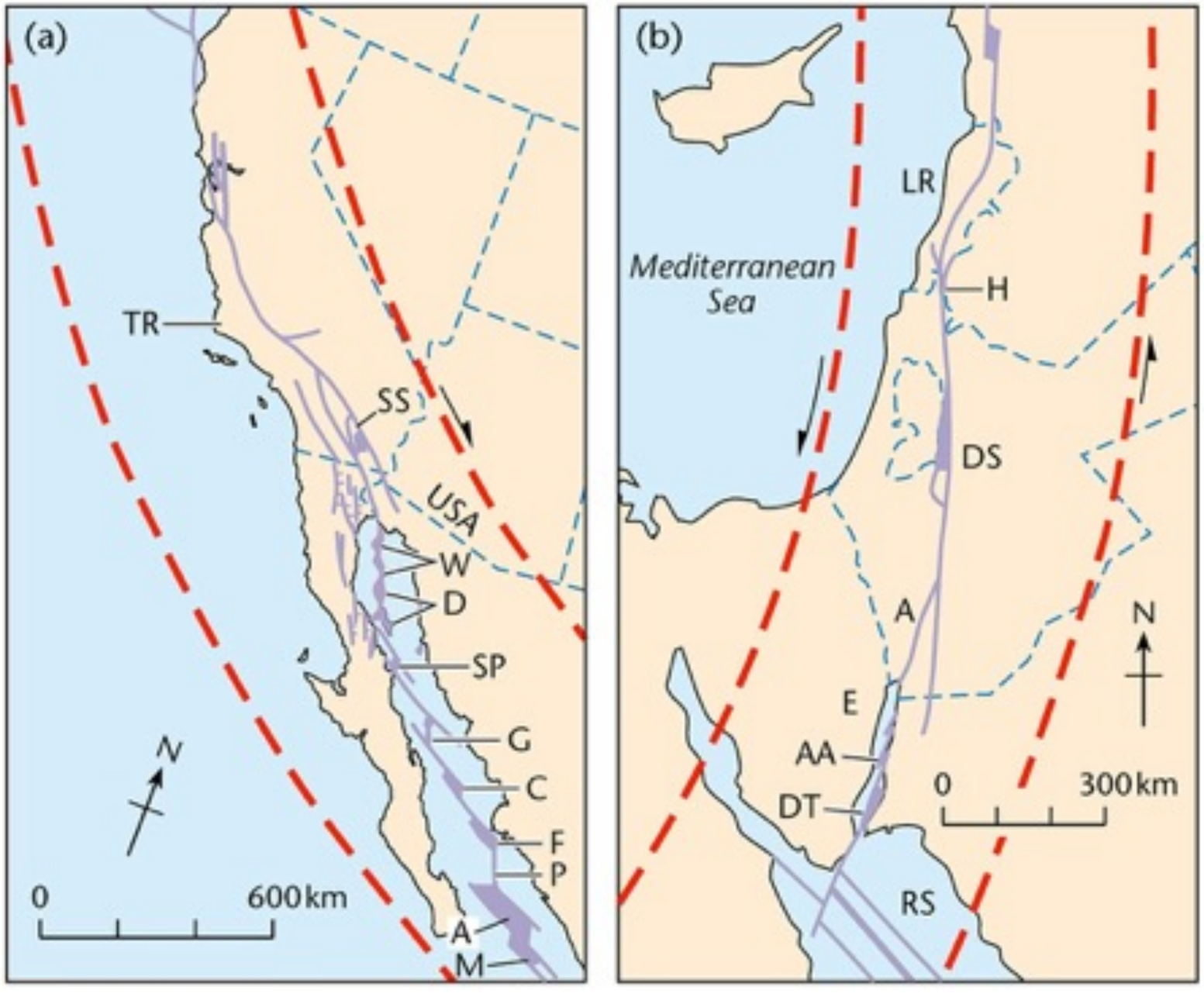

Fig. 6.3 Regions of compression and extension along strike-slip boundaries between rigid continental plates related to the orientation of the fault zone with respect to the plate slip vector. After Mann *et al.* (1983). (a) Pacific–North American plate boundary. The dashed lines are theoretical interplate slip lines from Minster *et al.* (1974). The major zone of compression is the push-up block of the Transverse Ranges where the dextral San Andreas Fault zone has a 'convergent' orientation with respect to the interplate slip line. The prominent pull-apart basins, however, are situated relatively to the south where the fault zone has a 'divergent' orientation with respect to the interplate slip line. TR, Transverse Ranges; SS, Salton Sea pull-apart at a right step between the San Andreas and Imperial faults. Pull-aparts in the Gulf of California include: W, Wagner Basin; D, Delfin Basin; SP, San Pedro Martir Basin; G, Guaymas Basin; C, Carmen Basin; F, Farallon Basin; P, Pescadero Basin complex; A, Alarcon Basin; M, Mazatlan Basin. (b) Arabia–Sinai (Levant) plate boundary zone (Garfunkel 1981; Ben-Avraham *et al.* 1979). Theoretical interplate slip lines are from Le Pichon & Francheteau (1978). The prominent area of compression is the Lebanon Ranges push-up block where the sinistral Dead Sea Fault zone is 'convergent' with respect to the interplate slip lines. Most of the pull-apart basins are in the Dead Sea and Gulf of Aqaba regions where the fault zone is locally 'divergent' with respect to the interplate slip lines. Pull-aparts include: H, Hula Basin; DS, Dead Sea Basin; A, Arava Fault trough; E, Elat Basin in the northern Gulf of Aqaba; AA, Arnona-Aragonese Basin; DT, Dakar-Tiran Basin. Dead Sea Fault Zone extends from Lebanon Ranges (LR) in the north to Red Sea (RS) in the south. © *Journal of Geology* 1983. Reproduced with the permission of University of Chicago Press Journals.

Plate boundaries prefer continents

strike-slip geomorphology

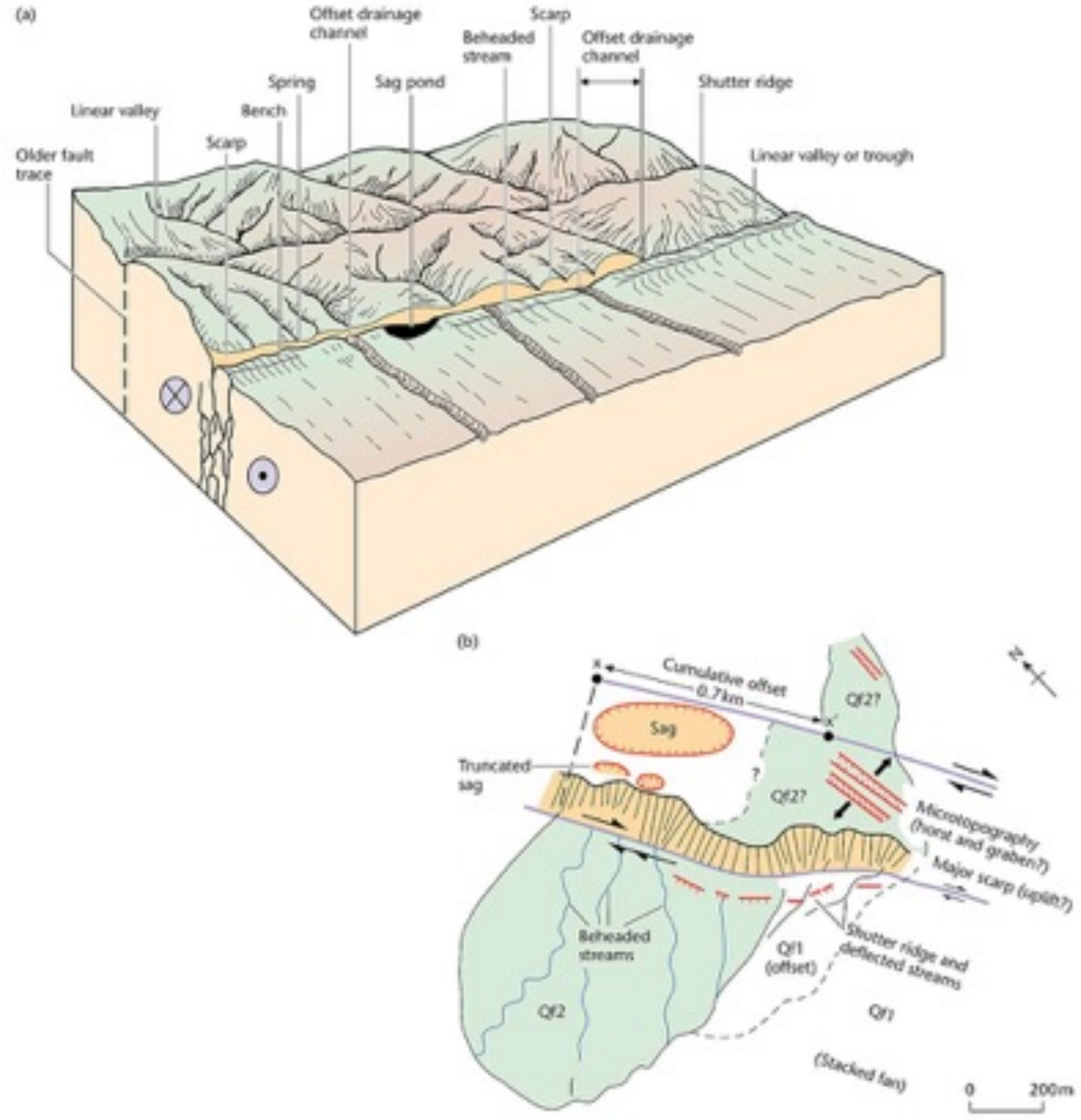

Fig. 6.8 Geomorphic features associated with strike-slip faults in the San Andreas system of California. (a) A linear trough along the fault, sag ponds, shutter ridges, offset ridges and drainages, springs, scarps and beheaded streams are typical geomorphic features indicative of strike-slip faulting. The older, abandoned fault trace displays analogous but erosionally degraded features. Modified from Wesson *et al.* (1975). (b) A large fan is offset from its catchment system, producing beheaded streams, shutter ridges and extensional fault scarps. Modified from Keller *et al.* (1982), reproduced with permission of John Wiley & Sons, Ltd.

thick and thin skinned pull aparts - mantle involvement

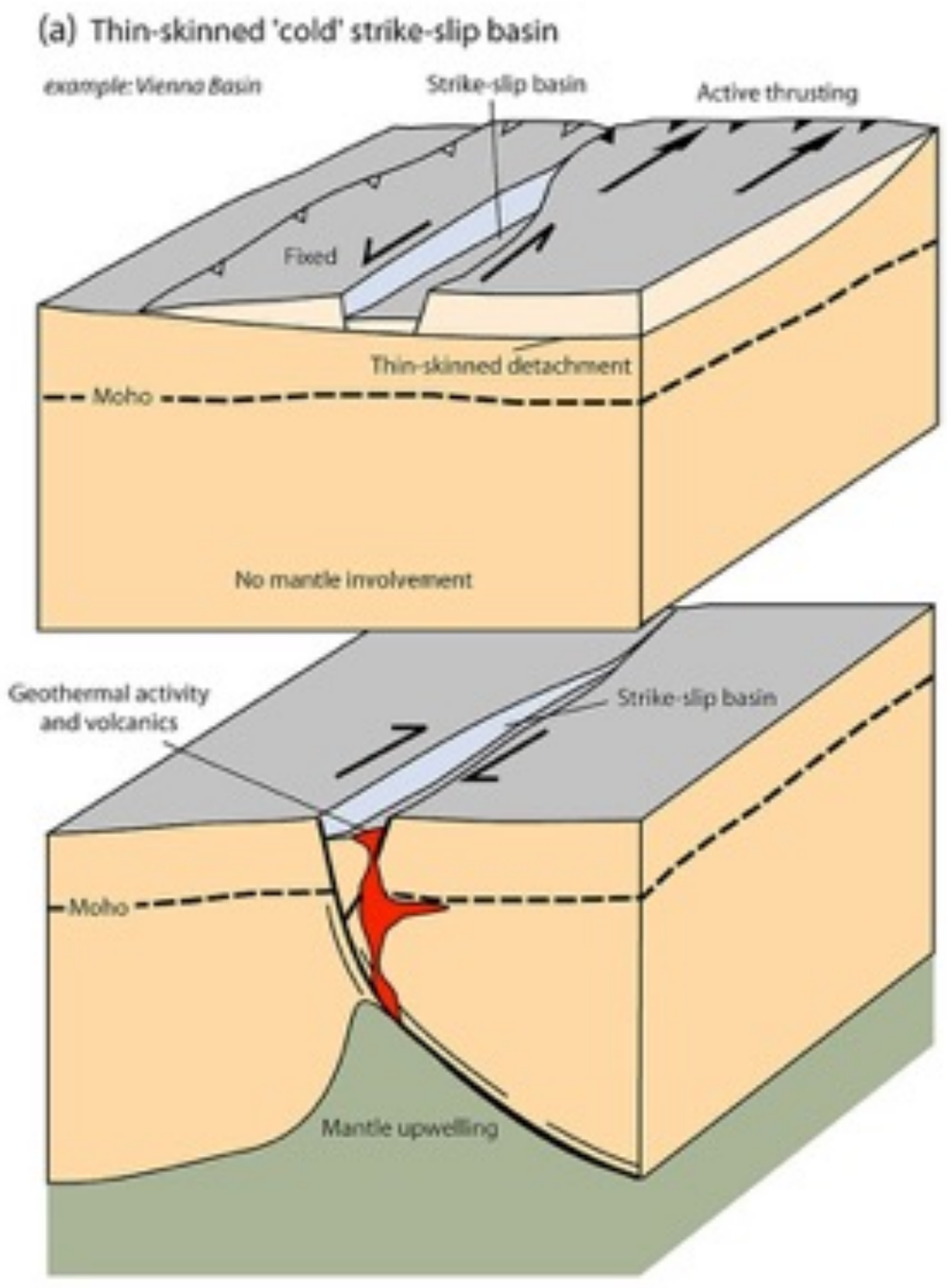

Fig. 6.9 Schematic diagram of broad classes of strike-slip basins. (a) Thin-skinned strike-slip basins, which are hypothermal. (b) Strike-slip basins with mantle involvement, which are hyperthermal.

negative flower structures

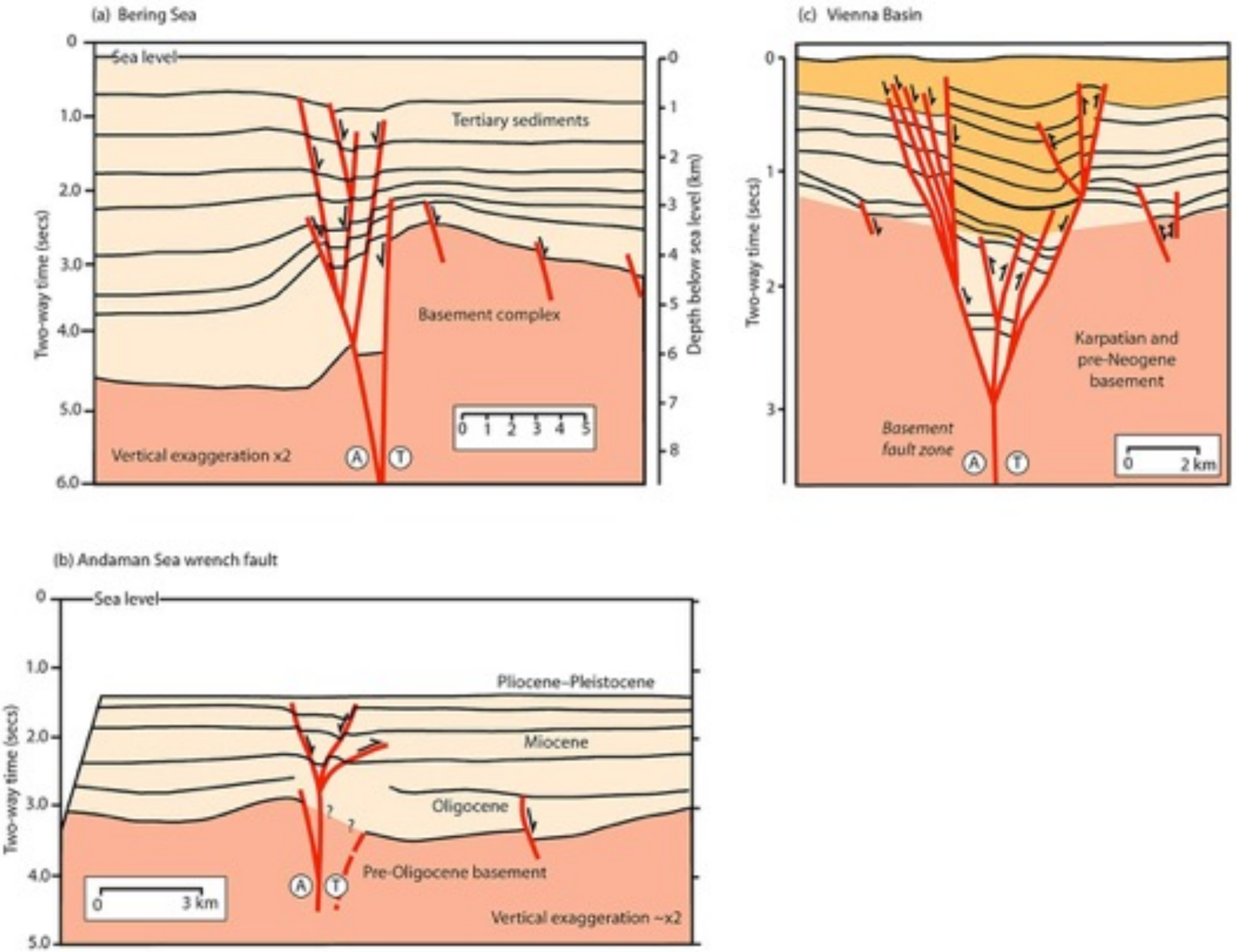

Fig. 6.11 The major characteristics in cross-sectional view of an idealised strike-slip fault. (a) Major fault zone in Bering Sea, and (b) Andaman Sea wrench fault (modified from Christie-Blick & Biddle 1985). (c) Vienna Basin, Austria, showing an asymmetric negative flower structure from seismic data, in Hinsch *et al.* (2005), reinterpreted by Wu *et al.* (2009, p. 1617, fig. 9; reprinted with permission from Elsevier). A, displacement away from reader; T, displacement towards reader.

restraining and releasing bends

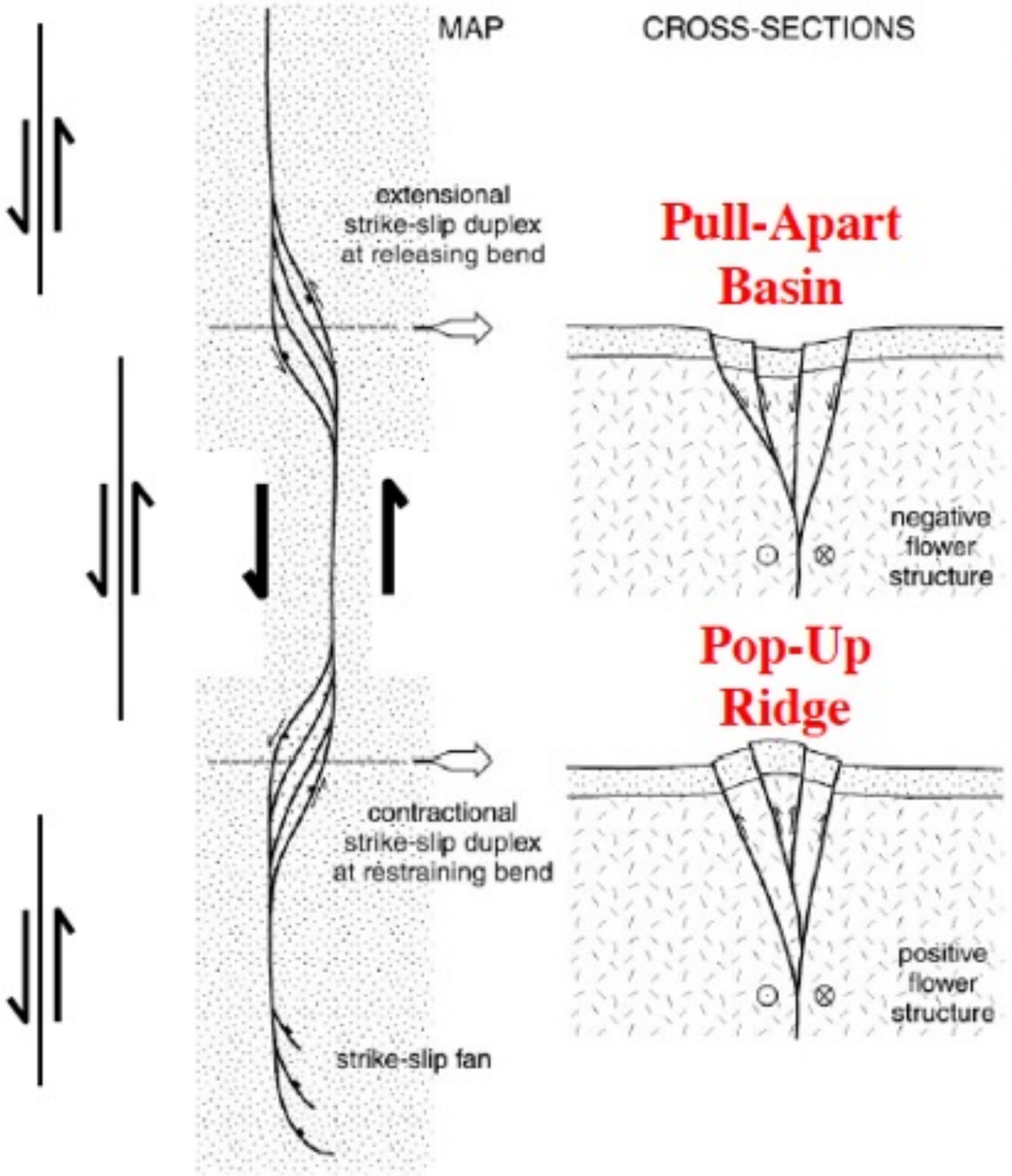

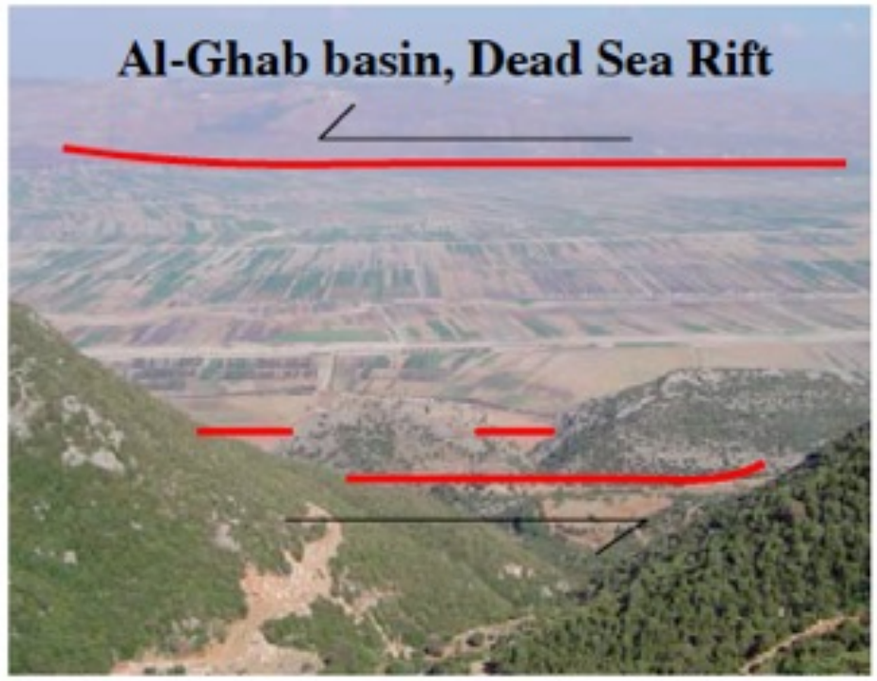

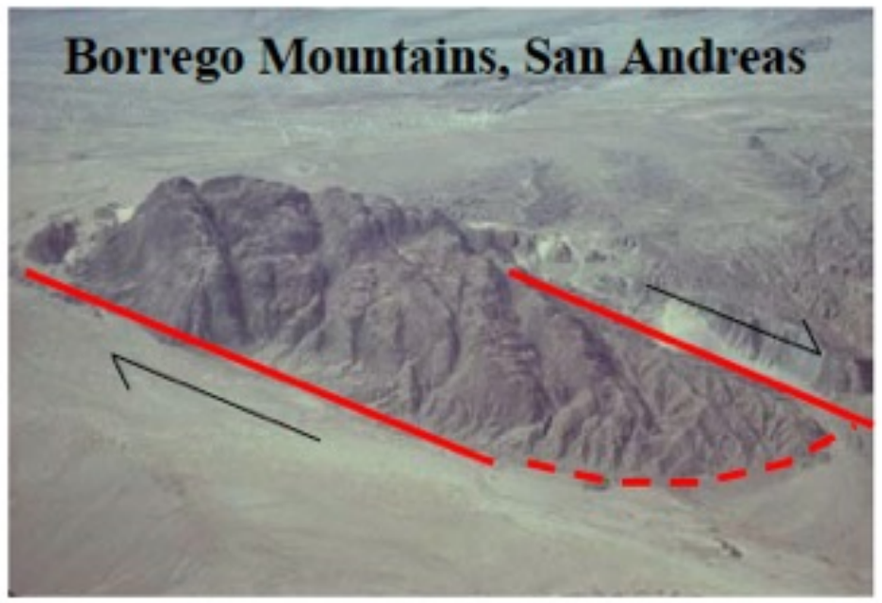

complex structures

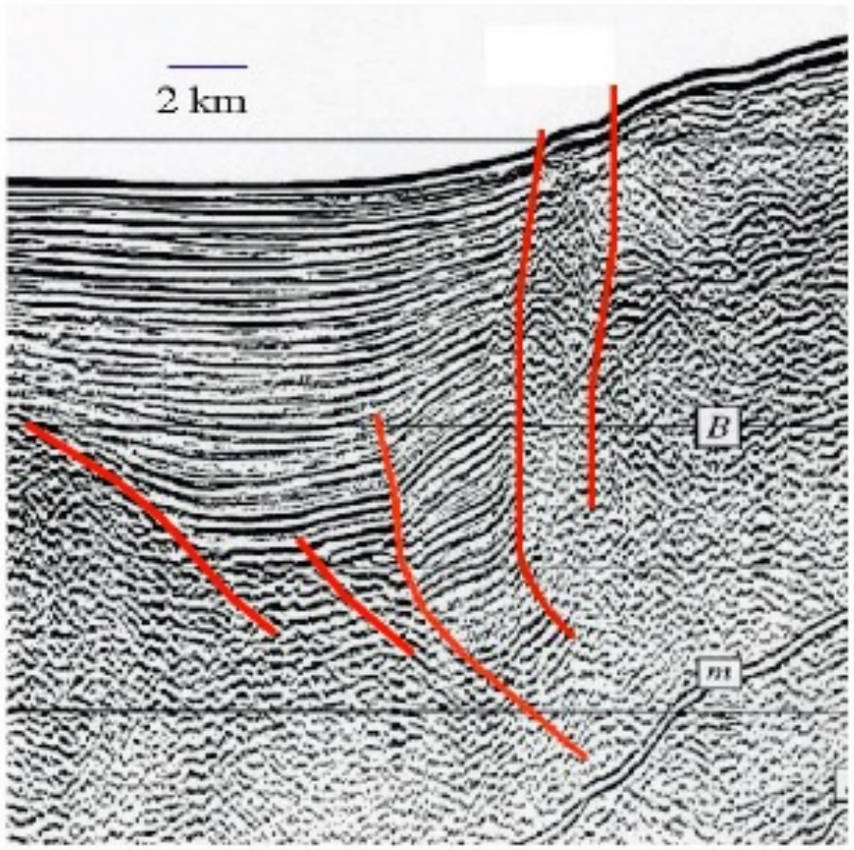

e.g. Yusuf basin - Alboran Sea

Negative flower structure

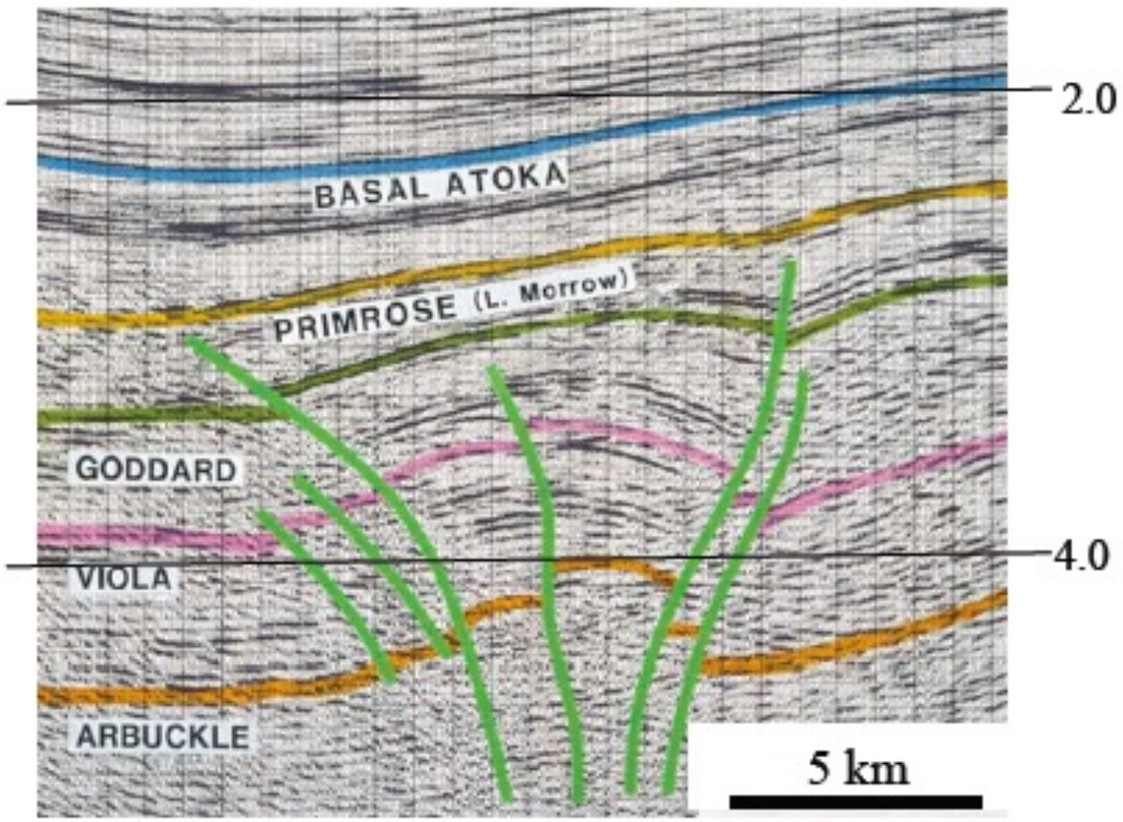

e.g. Ardmore basin - Oklahoma

Positive flower structure

varieties of pull-apart basins

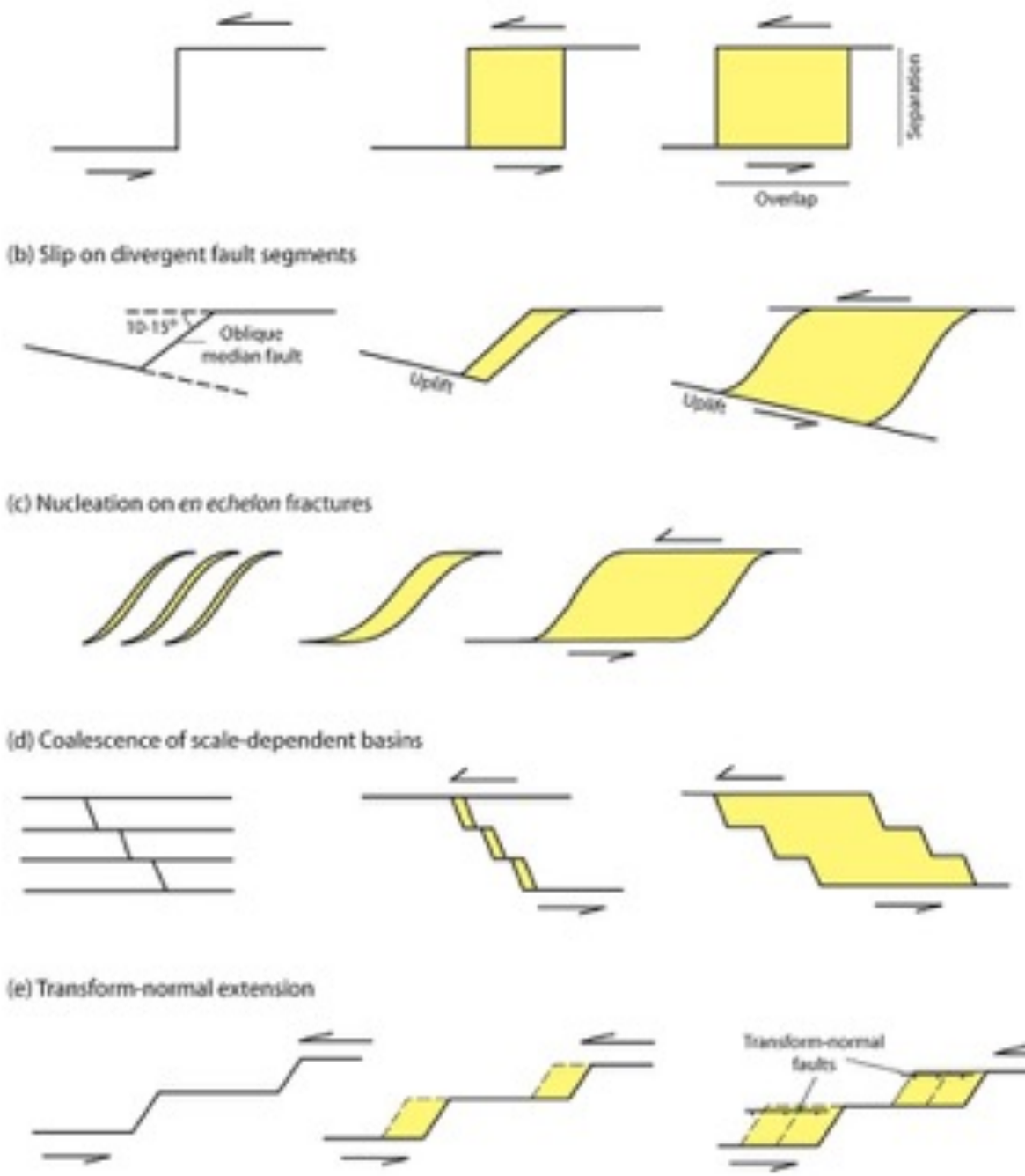

Fig. 6.19 Models of pull-apart basin development (after Mann *et al*. 1983 (reproduced with permission of University of Chicago Press) and Ben-Avraham & Zoback 1992). (a) Pull-apart opening between left-stepping and sinistral master strike-slip faults. Fault separation and basin width remain constant through time whereas fault overlap and basin length increase with the amount of strike-slip displacement. The elastic dislocation model of Rodgers (1980) applies to this kind of pull-apart mechanism. (b) Pull-apart opening across an oblique median fault and non-parallel master faults. Note that compression and uplift occur on one side of the pull-apart while an extensional 'gap' develops on the other. (c) Pull-apart formation by nucleation from extensional fractures, based on shear box experiments (Koide & Bhattacharji 1977). (d) Pull-apart formation by coalescence of small-scale similar sub-basins, as suggested by Aydin & Nur (1982). This allows the widening of pull-aparts with increased offset, in contrast to (a). (e) Pull-apart basin formation caused by simultaneous strike-slip motion on a transform fault and transform-normal extension (after Ben-Avraham & Zoback 1992). The pull-aparts are markedly asymmetric towards the transform fault.

pull apart basin on a releasing bend

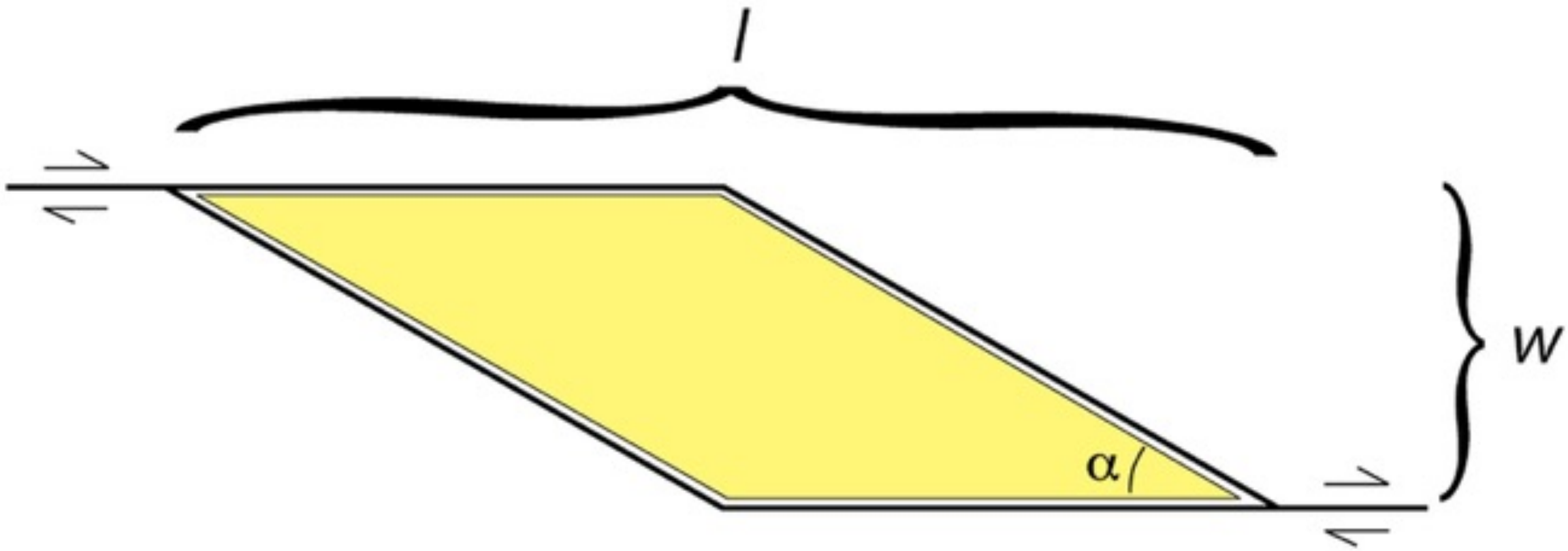

Fig. 6.17 Notation for a pull-apart basin at an overstep between two parallel strike-slip fault segments. After Gürbüz (2010).

width versus length for pull-apart basins

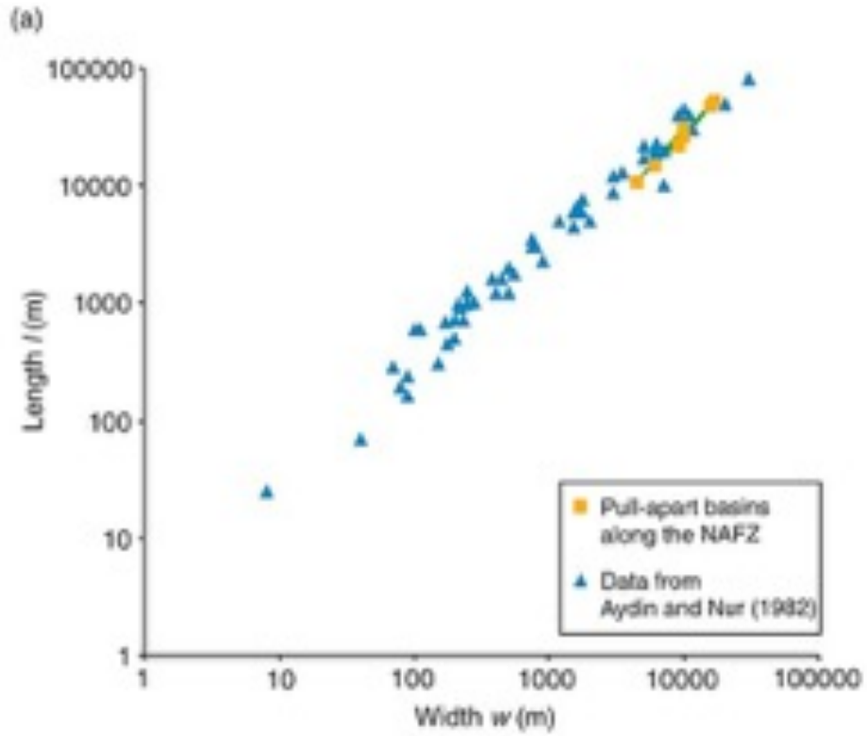

Fig. 6.18 (a) Plot of pull-apart basin width-length (displacement) relationship using the dataset of Aydin & Nur (1982) supplemented by the Turkish data of Gürbüz (2010). Turkish pull-apart basins are shown in the map in (b). MS, Marmara Sea; NAFZ, North Anatolian Fault zone; EAFZ, East Anatolian Fault zone; DSFZ, Dead Sea Fault zone; BZSZ, Bitlis–Zagros suture zone. From west to east along the NAFZ, the pull-apart basins are Tekirdag, Yenisehir, Pamukova, Bolu and Yenicaga, Tasova-Erbaa and Niksar, Susehri and Erzincan.

left lateral fault

no evidence of mantle involvement

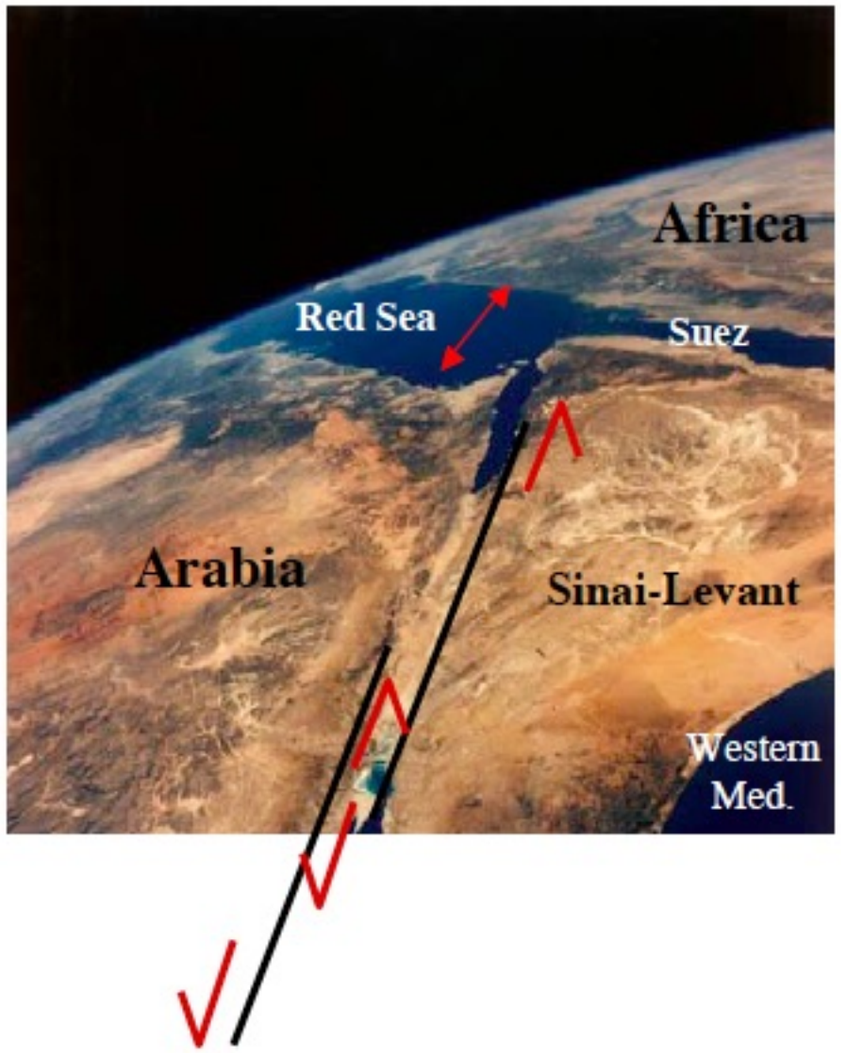

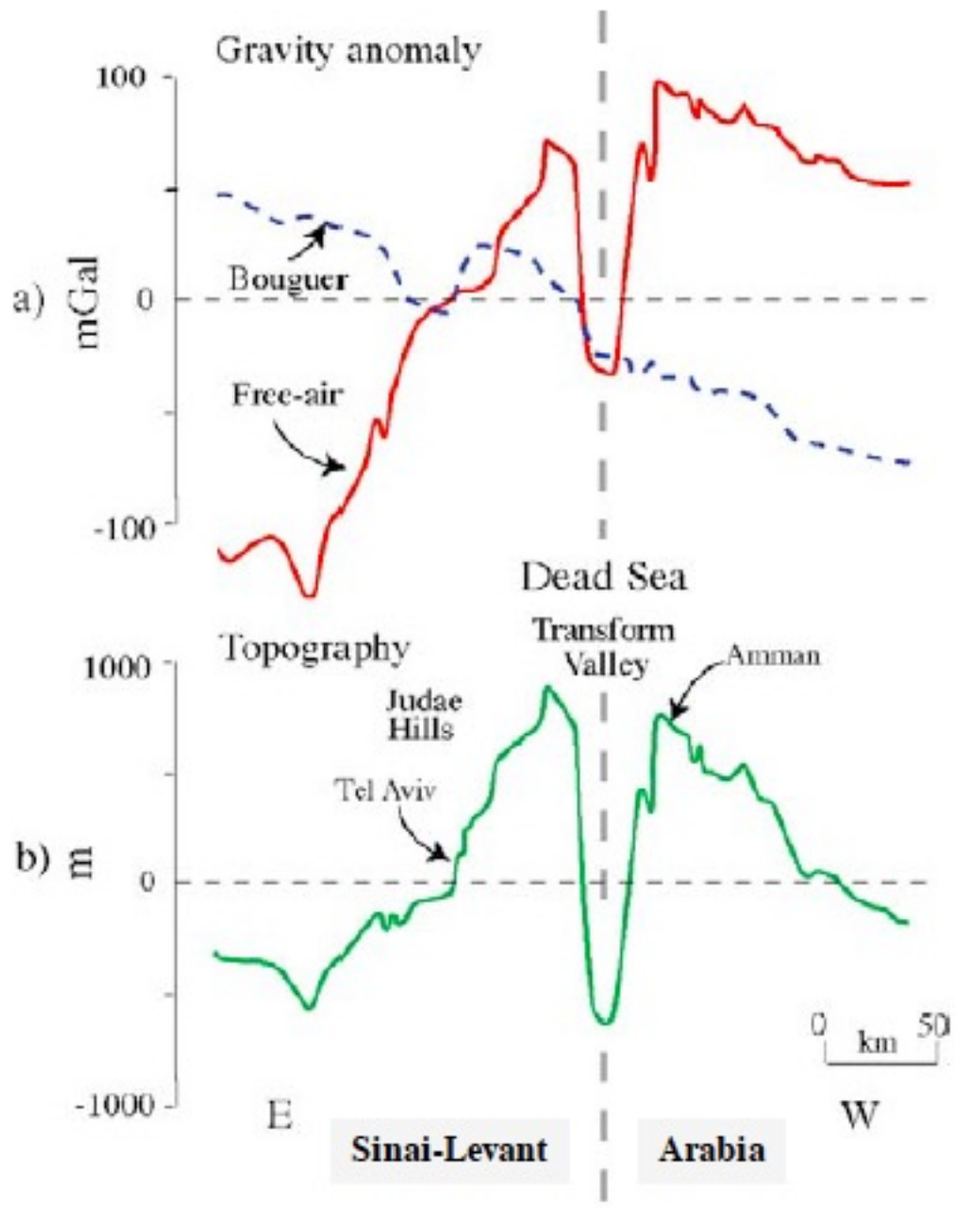

pull-apart stratigraphy

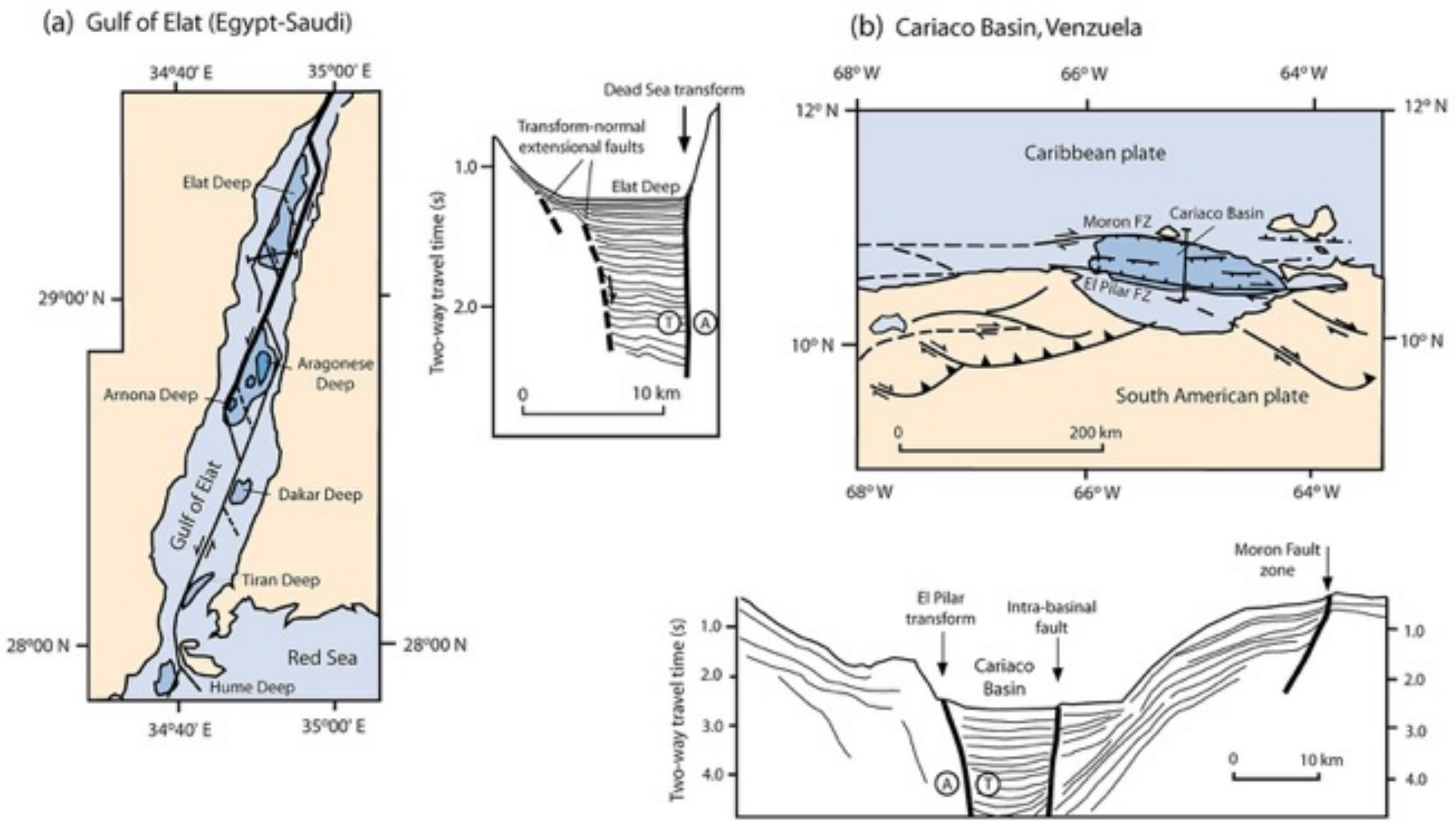

Fig. 6.20 (a) Bathymetry and structure of the Gulf of Elat showing segments of the Dead Sea Transform and location of main topographic depressions. Inset shows cross-sectional geometry across the Elat Deep derived from seismic reflection surveys. Asymmetry of the basin-fill is towards the transform fault. (b) Tectonic map and seismic profile across Cariaco Basin, northern Venezuela (Schubert 1982), showing basin asymmetry towards El Pilar Transform. A, displacement away from reader; T, displacement toward reader. Modified from Ben-Avraham and Zoback (1992).

Dead Sea basin - pull apart stratigraphy

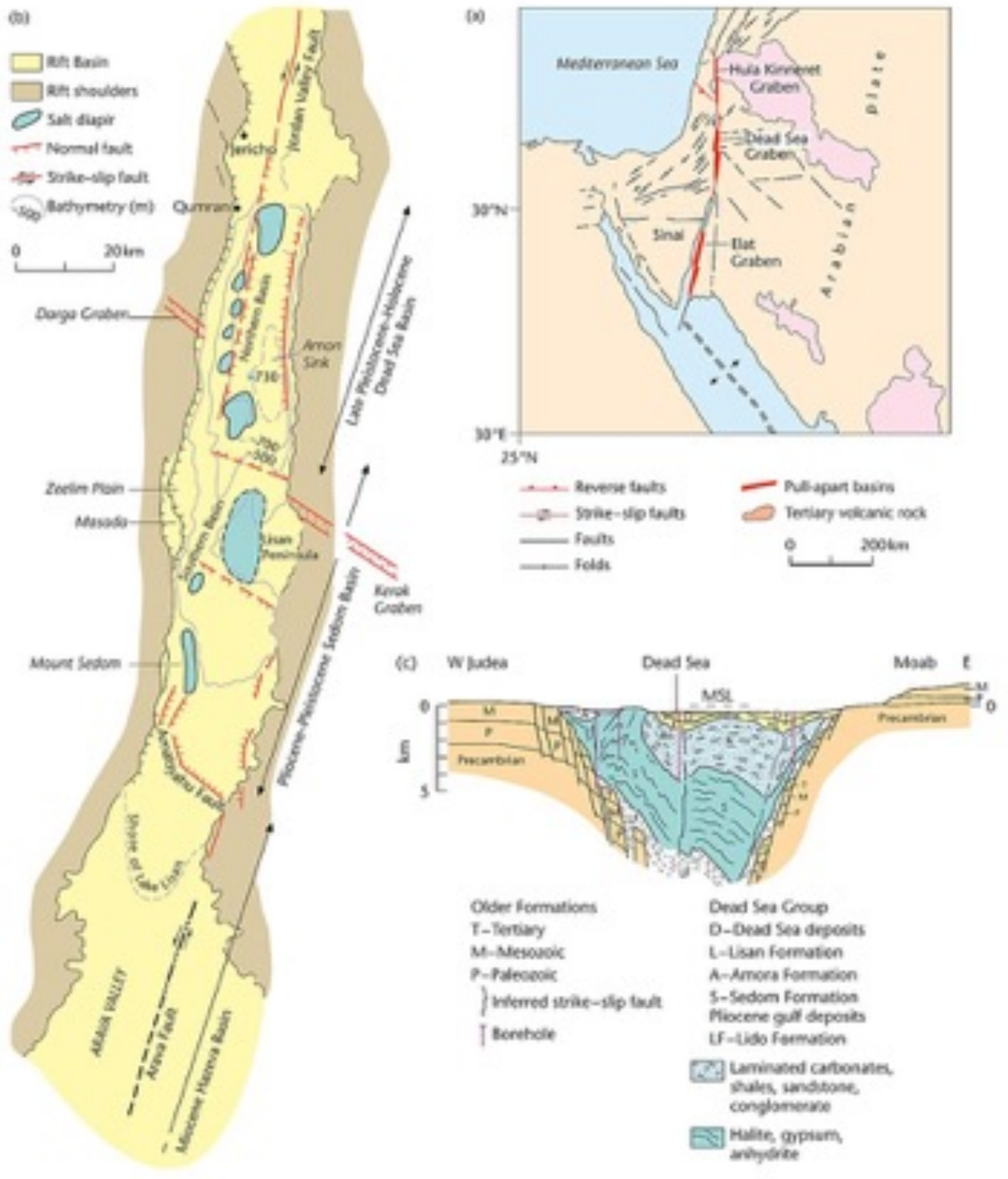

Fig. 6.29 (a) Location of Dead Sea Basin. (b) Structural interpretation, showing main faults, basins and salt diapirs (from Garfunkel *et al.* 1981). (c) Cross-section of Dead Sea Basin between Mount Sedom and Moab (from Zak & Freund 1981). MSL, Mean sea level. (b), (c) Reprinted with permission from Elsevier.

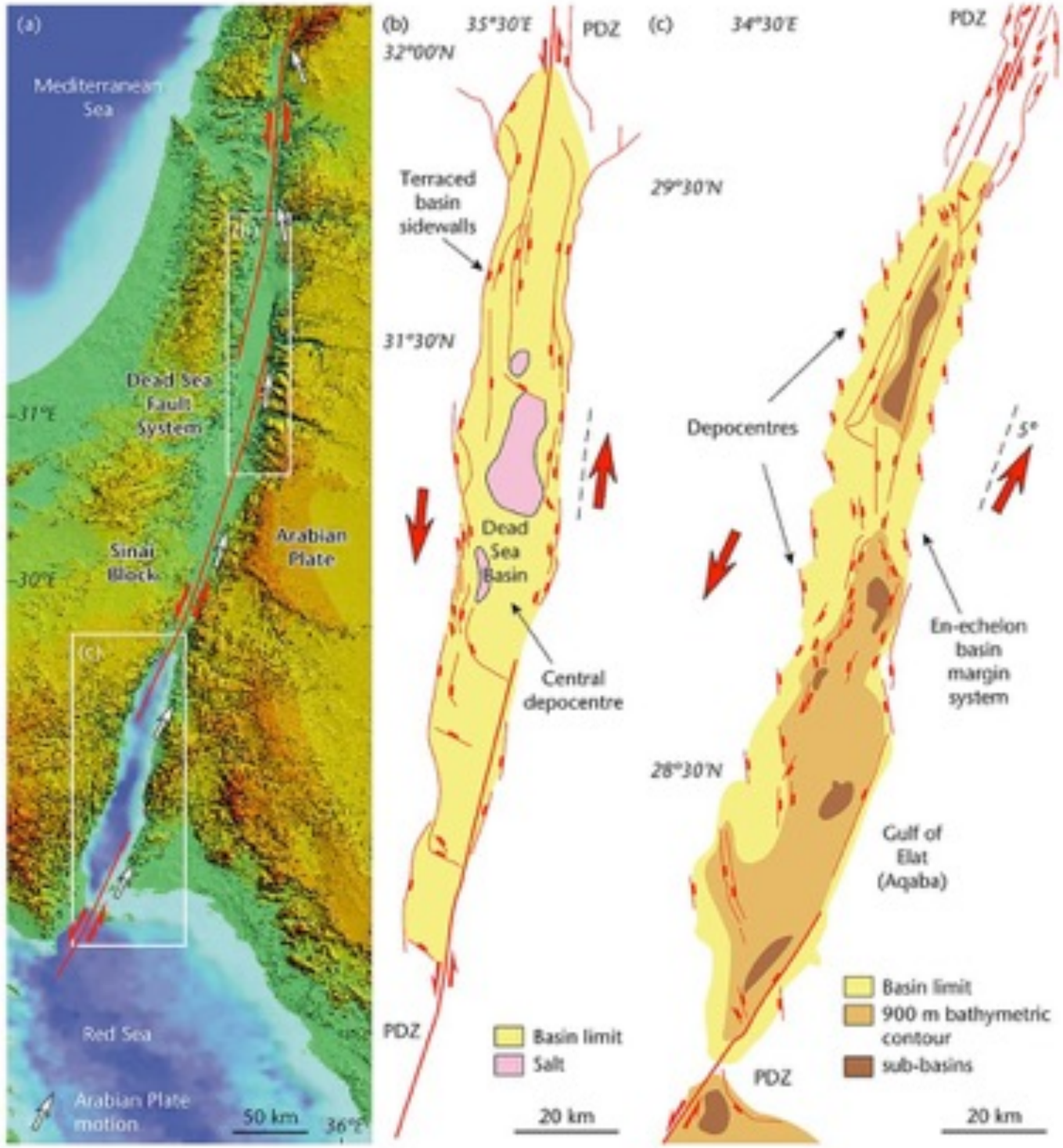

Fig. 6.35 Pull-apart basins in the Dead Sea Fault system. (a) Digital elevation model showing topography and main faults. The Dead Sea pull-apart basin in the north (b) is pure strike-slip, whereas the Gulf of Elat (Aqaba) in the south (c) is transtensional with $\alpha = 5°$ (Wu *et al.* 2009, p. 1618, fig. 10). Reprinted with permission from Elsevier.

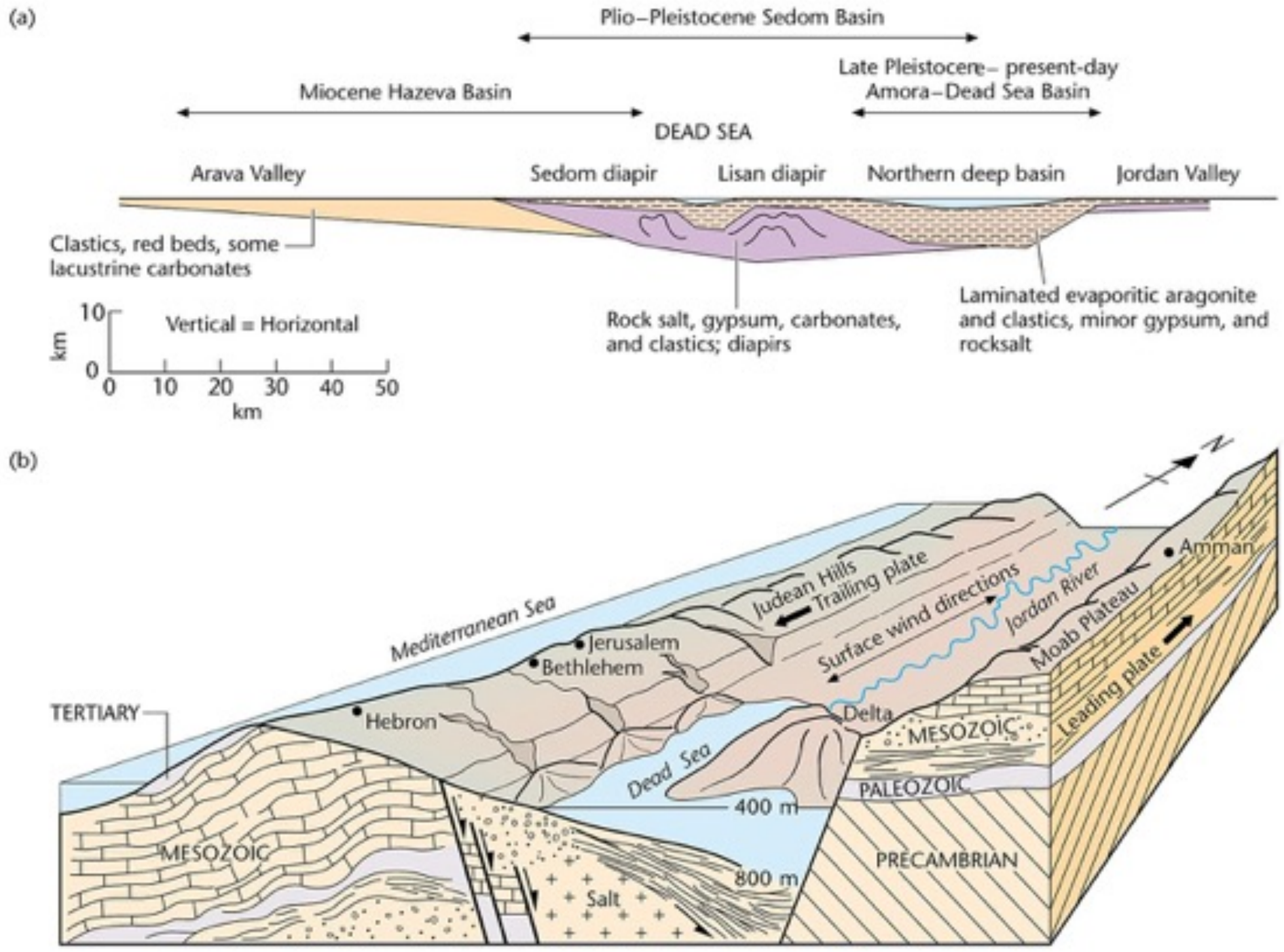

Fig. 6.39 Cross section (a) and 3-D view (b) of the Dead Sea-Arava depression. (a) The northward migration of the basin depocentres. Early Miocene (25–14 Ma) strike-slip of about 60–65 km opened up the Arava Basin, which was filled with about 2 km of red beds during a pause in the strike-slip displacement. Later movement in the last 4.5 Myr has allowed the deposition of >4 km of marine to lacustrine rock salt of the Sedom Formation, followed by 3.5 km of lacustrine evaporitic carbonates and clastics (after Zak and Freund 1981). Reproduced with permission from Elsevier. (b) Today, sediment enters the northern basin via high discharge ephemeral streams feeding fan deltas along the semi-arid western edge of the basin (Judean Hills), and the perennial, axial-flowing Jordan River. The Jordan has a drainage area in a humid region, and deposits a fine-grained delta at its mouth. Autochthonous supply to the lake is of aragonite and gypsum precipitates (Manspeizer 1985).

sequential model
of pull-apart development

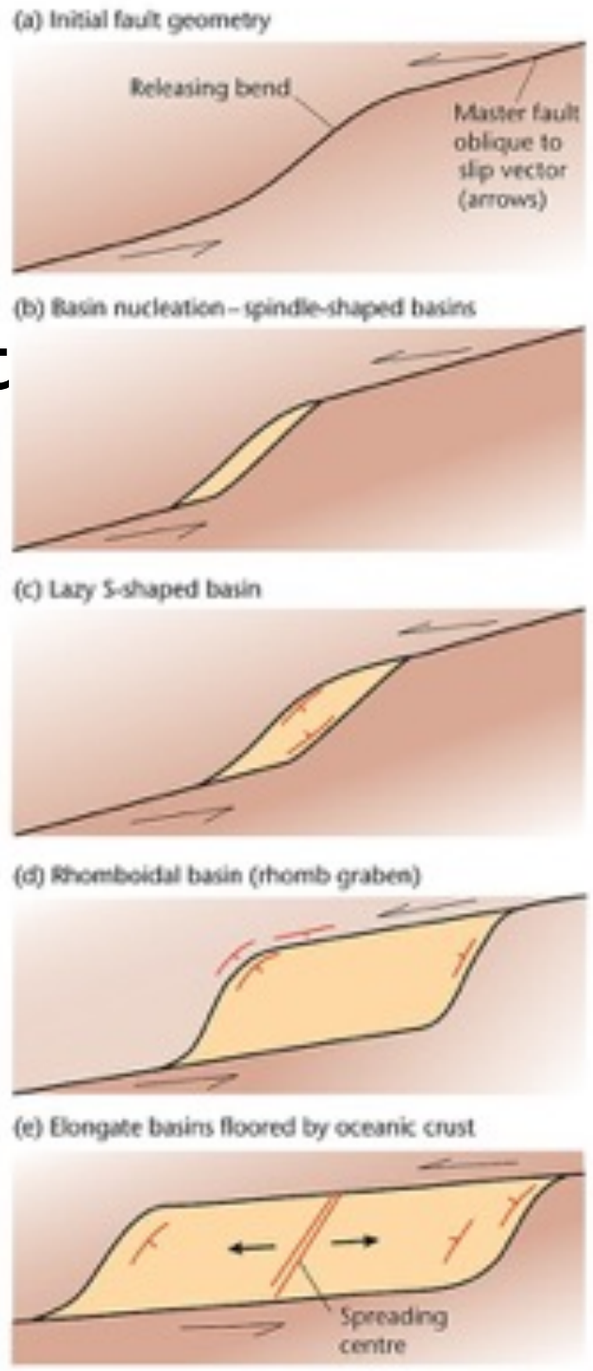

Fig. 6.21 Continuum model of pull-apart development, after Mann *et al.* (1983). (a) Pull-apart begins life on a releasing fault bend. The size of the bend controls the pull-apart basin width. (b) Spindle-shaped basin. Continued offset produces lazy S-shaped basin (c), then a rhomb-shaped basin (d), then, finally, a long, elongate trough floored with oceanic crust (e). Most pull-aparts do not reach the stage represented by (e); instead they tend to be terminated after the basin length has reached about three times the original width of the releasing bend (or fault separation). © *Journal of Geology* 1983. Reproduced with permission of University of Chicago Press Journals.

mega-scale evolution of strike-slip tectonics

the "watermelon seed"

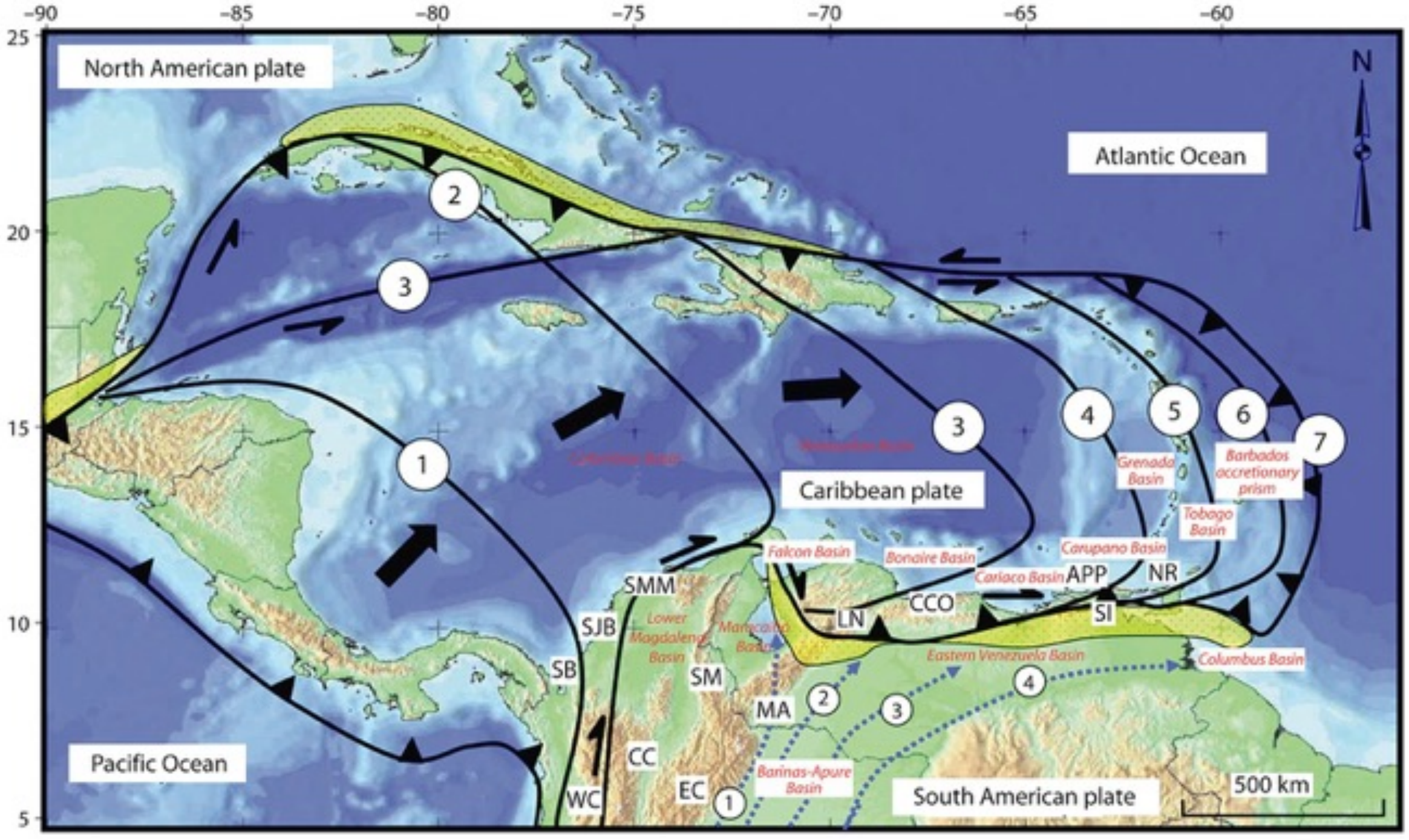

Fig. 6.22 Diachronous eastwards movement of the Caribbean plate, with numbers showing the locations of the leading edge, from Late Cretaceous (1) at 80 Ma to Recent (7) at 0 Ma, from Escalona & Mann (2011). Stippled yellow areas are foreland basins caused by diachronous oblique convergence. Dashed blue lines are the paleo-courses of the Orinoco River between Paleocene (1) at 60 Ma to Recent (4) at 0 Ma. Abbreviations: WC, Western Cordillera; CC, Central Cordillera; EC, Eastern Cordillera; SB, Sinu Belt; SJB, San Jacinto Belt; SM, Santander massif; MA, Merida Andes; LN, Lara nappes; CCO, Cordillera de la Costa; APP, Araya-Paria Peninsula; SI, Serrania del Interior; NR, Northern Range of Trinidad. Main sedimentary basins are also labelled. Reprinted with permission from Elsevier.

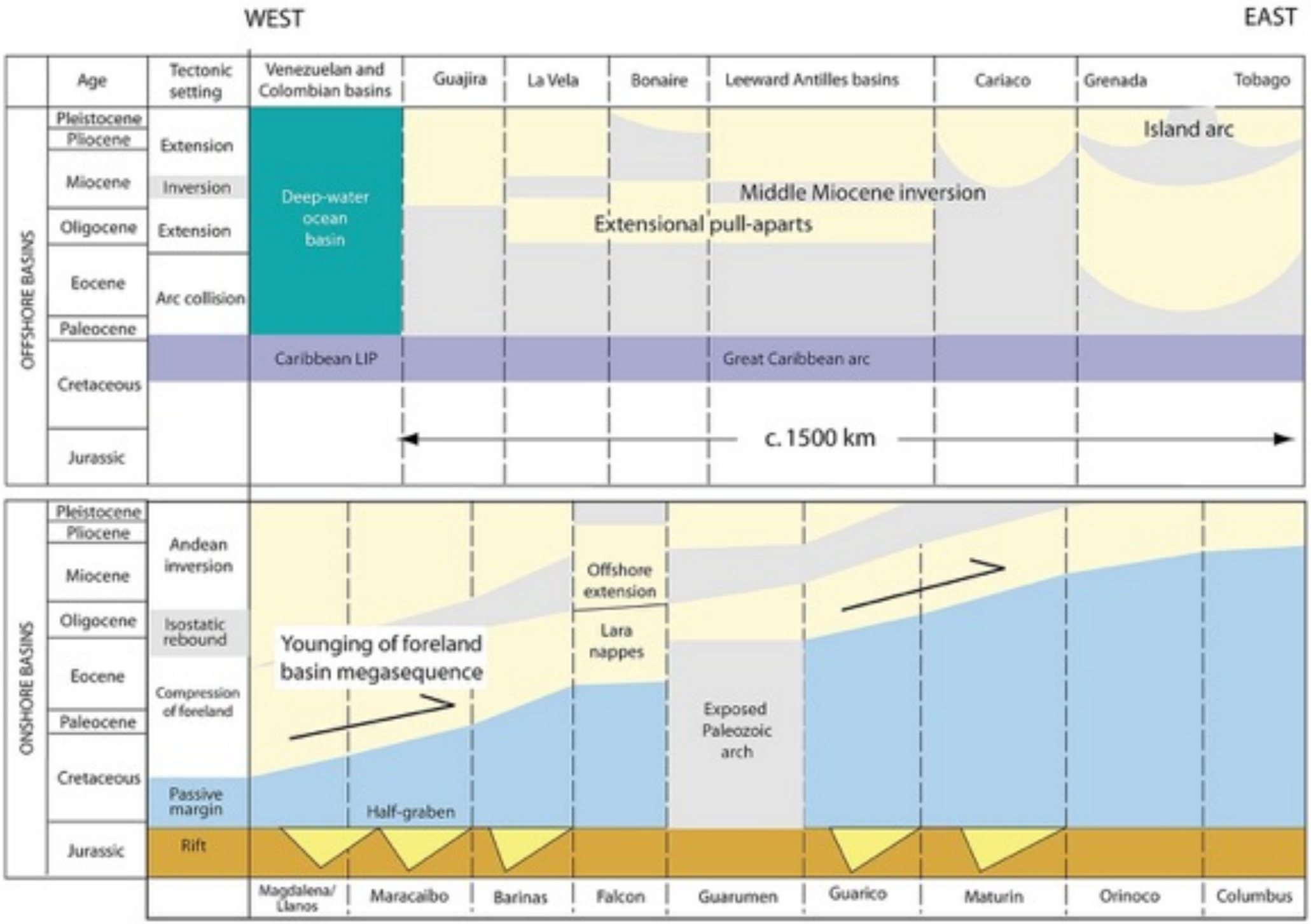

Fig. 6.24 Basin development in the offshore and onshore areas of the margin of the Caribbean and South American plates, modified from Audemard & Serrano (2001) in Escalona & Mann (2011). Grey tone indicates stratigraphic gaps. The onshore basins are dominated by the eastward migration of a wave of flexural subsidence caused by tectonic shortening along the transpressional plate margin. The offshore basins lack this flexural signature, and instead subside by local extension, commonly with a mid-Miocene phase of inversion. Reprinted with permission from Elsevier.

Ridge Basin - California

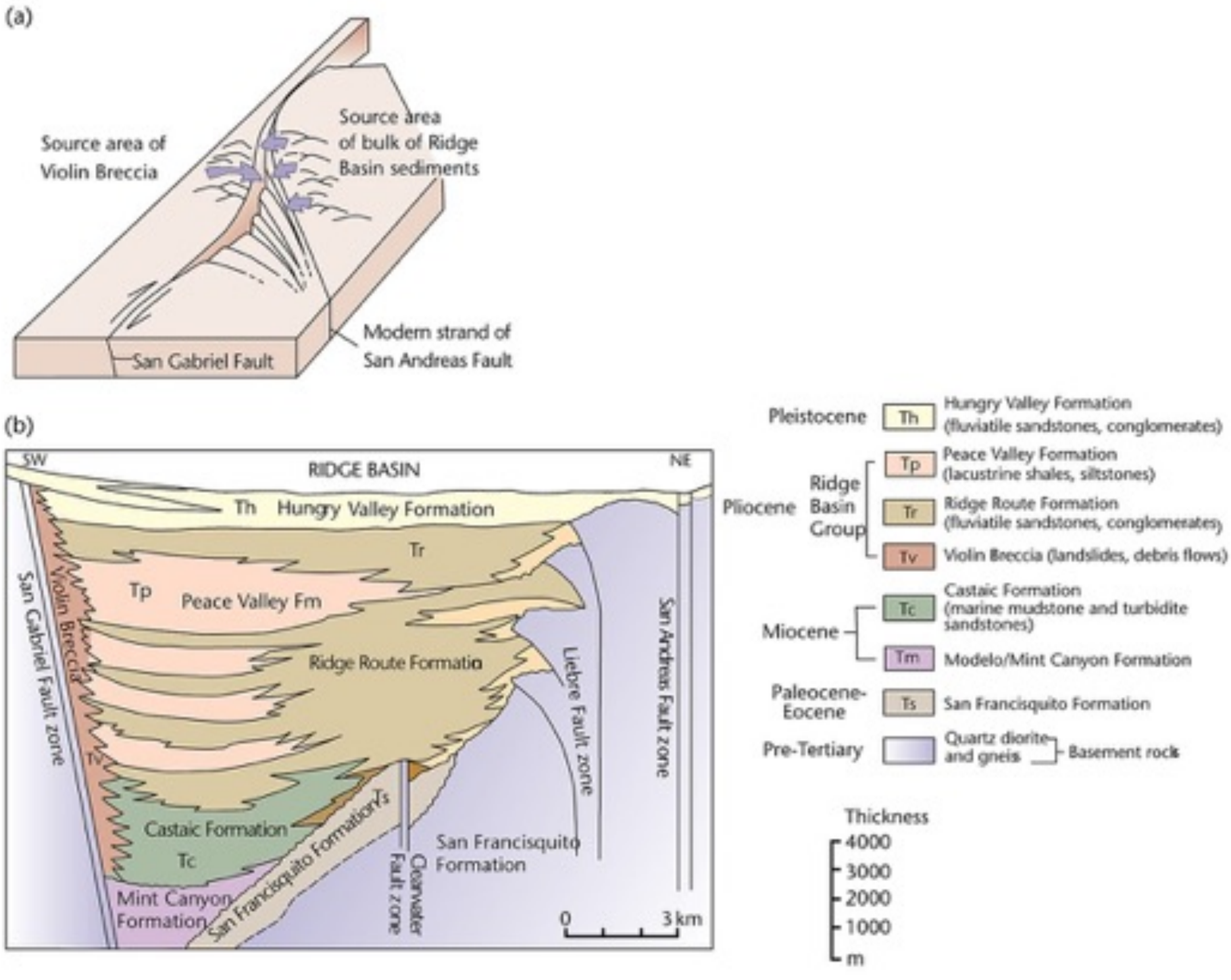

Fig. 6.37 Ridge Basin, California. (a) General tectonic and depositional setting for the Ridge Basin as a pull-apart on the releasing bend of the San Gabriel Fault (Crowell 1974b). (b) Generalised cross-section showing the sedimentary facies and principal faults. The fine-grained lacustrine depocentres (Peace Valley) and landslide/debris flow breccias (Violin Breccia) occur close to the San Gabriel Fault zone (after Link & Osborne 1978 and Crowell & Link 1982).

offshore strike-slip basins of the California Borderland

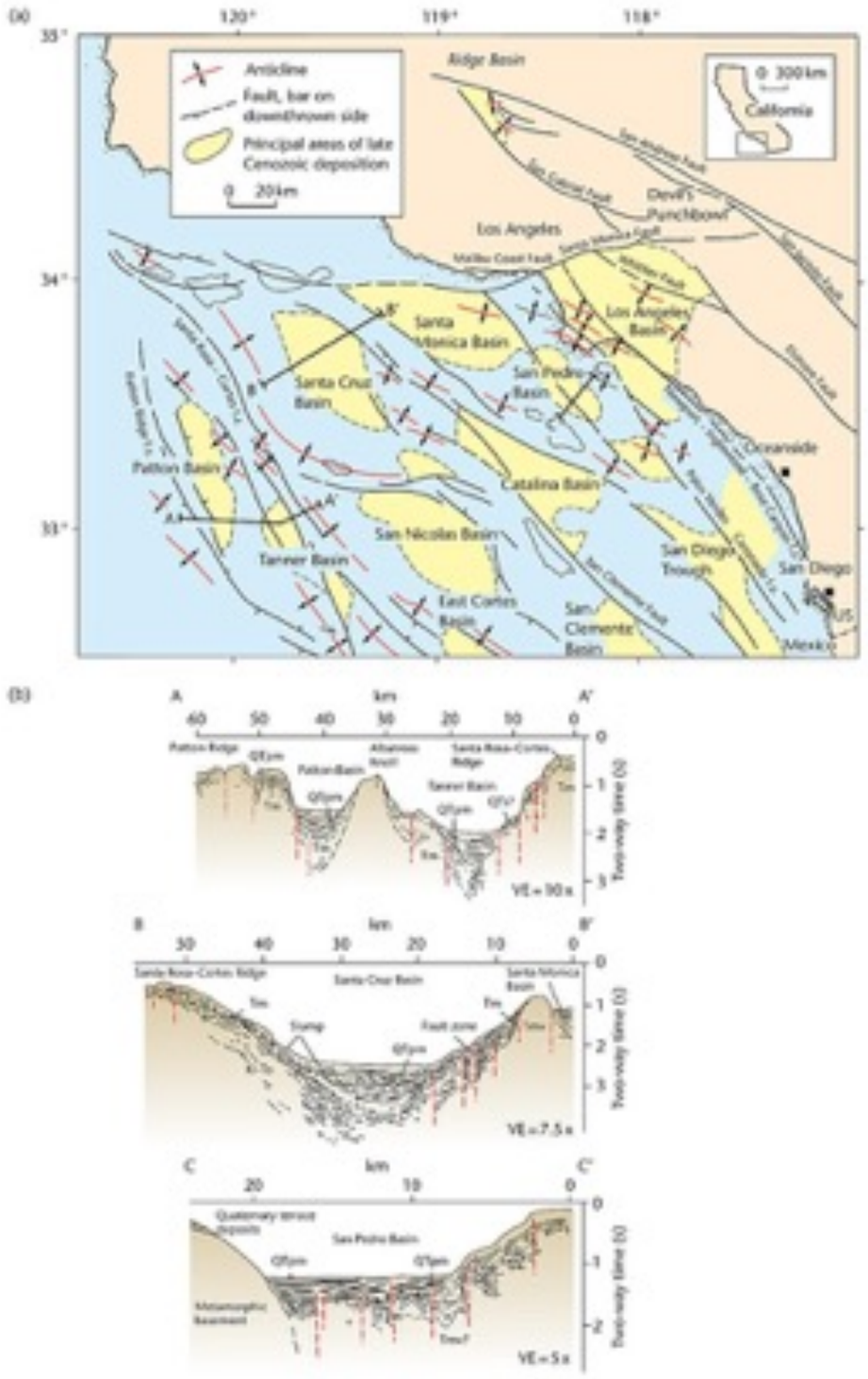

Fig. 6.38 Strike-slip basins of the California Borderland (Moore 1969; Junger 1976). (a) Map view. (b) Interpretations of seismic reflection profiles (Howell *et al.* 1980), vertical exaggeration x10. Q, Pleistocene and Holocene sediments; Tp, middle and late Pliocene sediments; Tpm, Miocene and early Pliocene sediments; Tm, early to middle Miocene sediments; Tmo, cherty, calcareous and siliceous shale of late Oligocene to middle Miocene; Tmv, Miocene volcanics; Kl-To, Late Cretaceous to Oligocene sediments. Reproduced with permission of John Wiley & Sons, Ltd.

strike-slip in convergence - escape tectonics

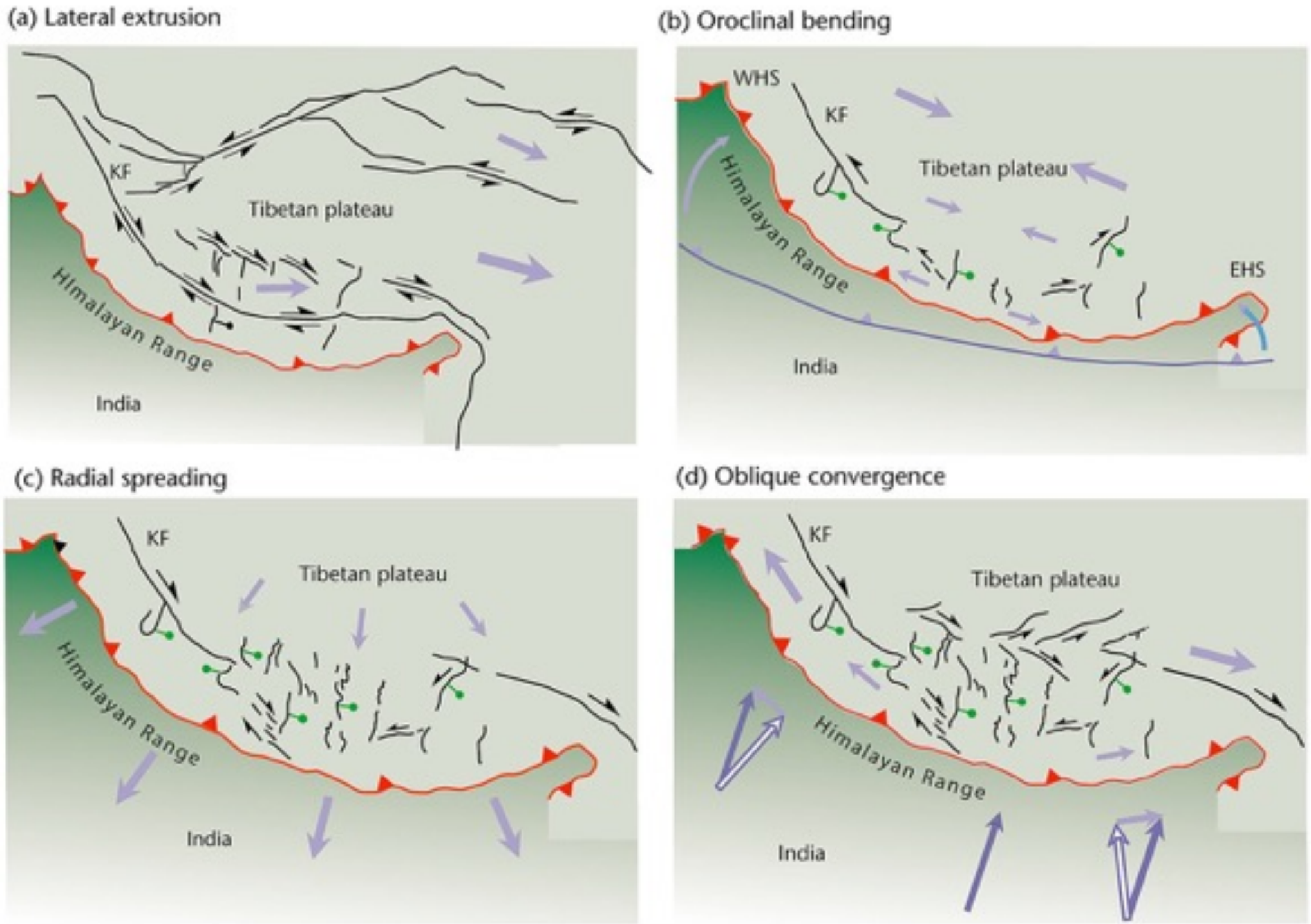

Fig. 6.26 Models for large-scale response to indentation of India in the Himalayan-Tibet region, from Styron *et al.* (2011). (a) Lateral extrusion to the east; (b) regional oroclinal bending; (c) radial spreading from Tibet; (d) oblique convergence causing northwestwards and eastwards escape. KF, Karakorum Fault; EHS, Eastern Himalayan Syntaxis.

course review

- I am in Berlin until 17 November
- Would the local people like to meet (weekly?) to discuss their data?

If you have questions about the material, you can reach me at bjcoakley@alaska.edu

Even long after this class is over

What is needed for exploration?

- Predictive models
- We are looking for small anomalies
- We have three nested theories to work with;

Plate Tectonics - explains deformation and horizontal motion at the earth's surface

Basin Formation - explains the deposition and preservation of sediments

Basin Formation

- Basin Forming Mechanism (Tectonics)

  creates “accommodation space” where sediments can accumulate

- Sediment source
- Sediment delivery system
- Influence of isostasy and compaction

  modifies and partitions “accommodation space” in space and time

More mechanisms than tests

a partial catalog of basin forming mechanisms

- crustal thinning
- lithospheric thickening
- sedimentary and volcanic loading
- tectonic supra-crustal loading
- sub-crustal loading
- mantle flow
- crustal densification

Flexure and the Lithosphere

sedimentation modifies its context

Flexure of the Lithosphere

- Flexure is isostasy applied on a strong lithosphere

  local isostasy is the zero strength case

  defines response of the earth to mass redistribution (erosion and deposition)

- Vertical forces, horizontal forces and torques applied to a continuous plate

- Bending moment is the integration of fibre stresses normal to a vertical cross section

  related to the local radius of curvature by the flexural rigidity

- We can derive a general flexural equation that defines deflection in terms of load, moment and rigidity

- We can use this equation to study geologic problems

Lithosphere defined

- The rigid, outer shell of the earth

  Can sustain differential stress

- Thermal and mechanical boundary layer

  Conductive heat flow above, convection below

- Defined by the melting point for olivine

  ~1200° C

  Underlain by the partly molten asthenosphere

How are deep earth and surface processes coupled?

A general principle

Micro relations can explain macro behavior or

the big picture is the sum of a lot of small pictures

Strength profiles - a function of temperature and composition

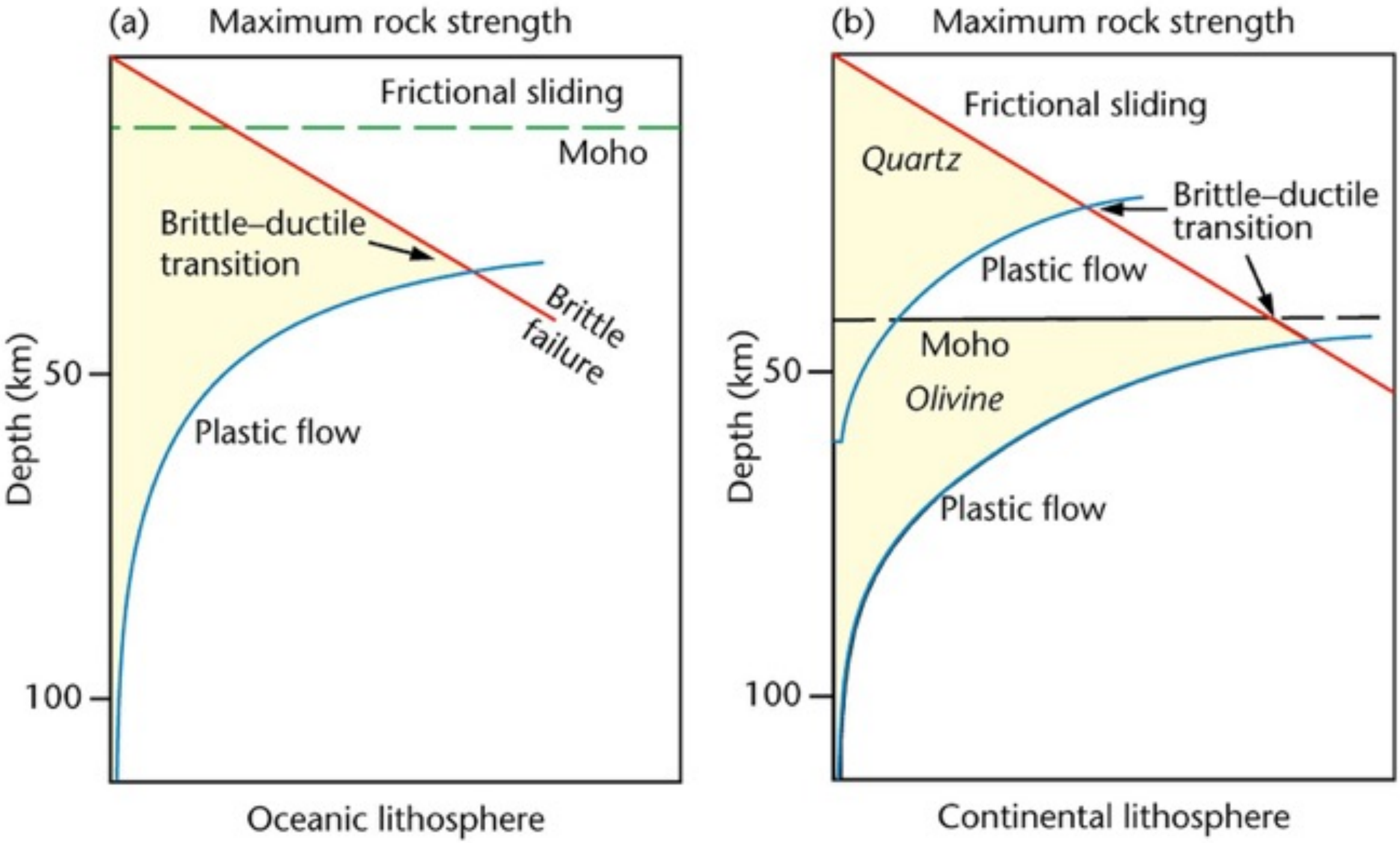

Fig. 1.9 Strength profiles of the continental and oceanic lithosphere. Strength also depends on whether the lithosphere is in tension or compression, and on the presence of volatiles such as water (Jackson 2005). The model for the continental lithosphere is called 'jelly sandwich', but an alternative view for the continental lithosphere is that the upper mantle is not strong and is aseismic, which is termed 'crème brûlée' (compare Burov & Watts 2006 and Jackson 2002).

Hawaiian bathymetry

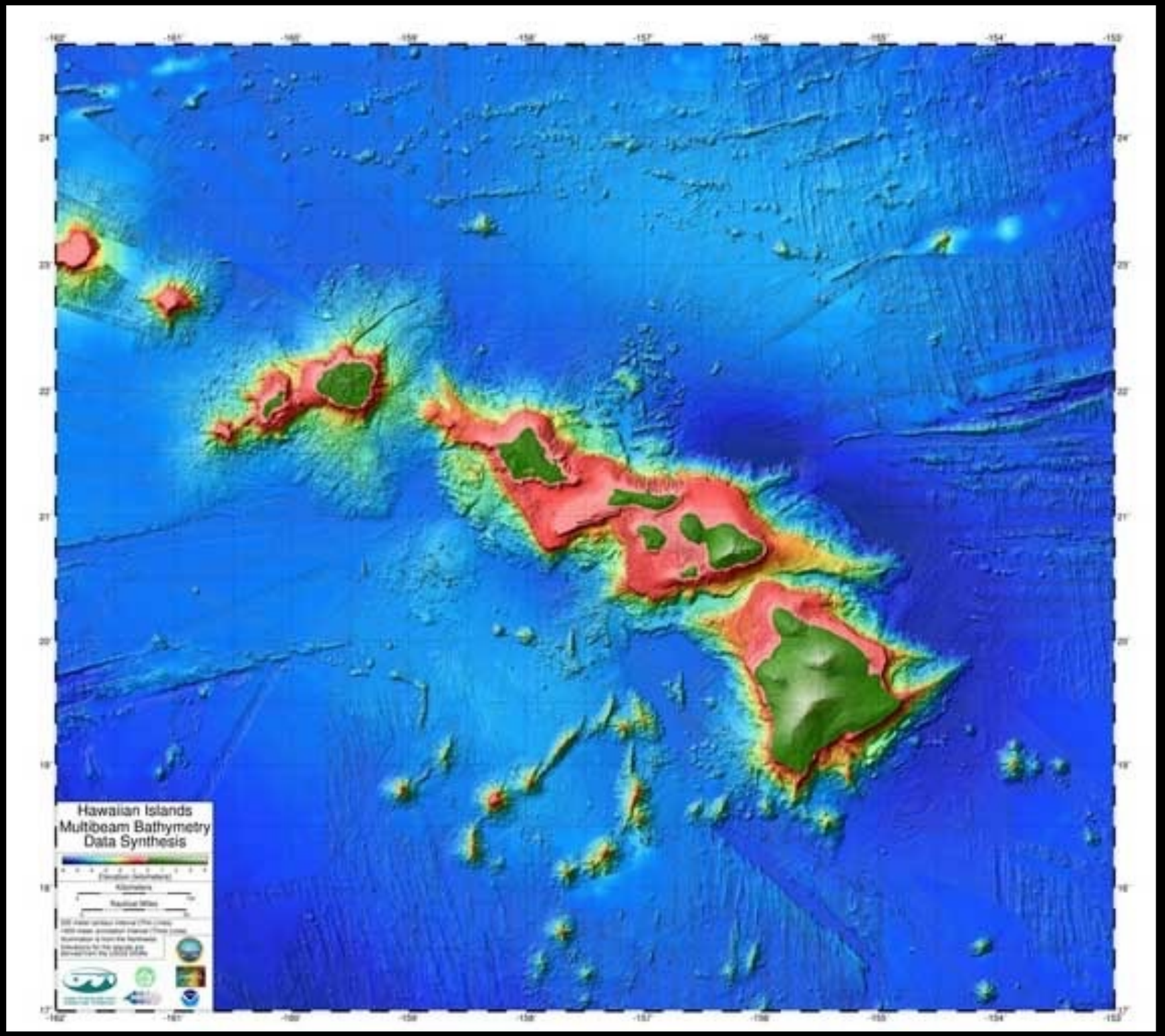

Flexure in the oceans

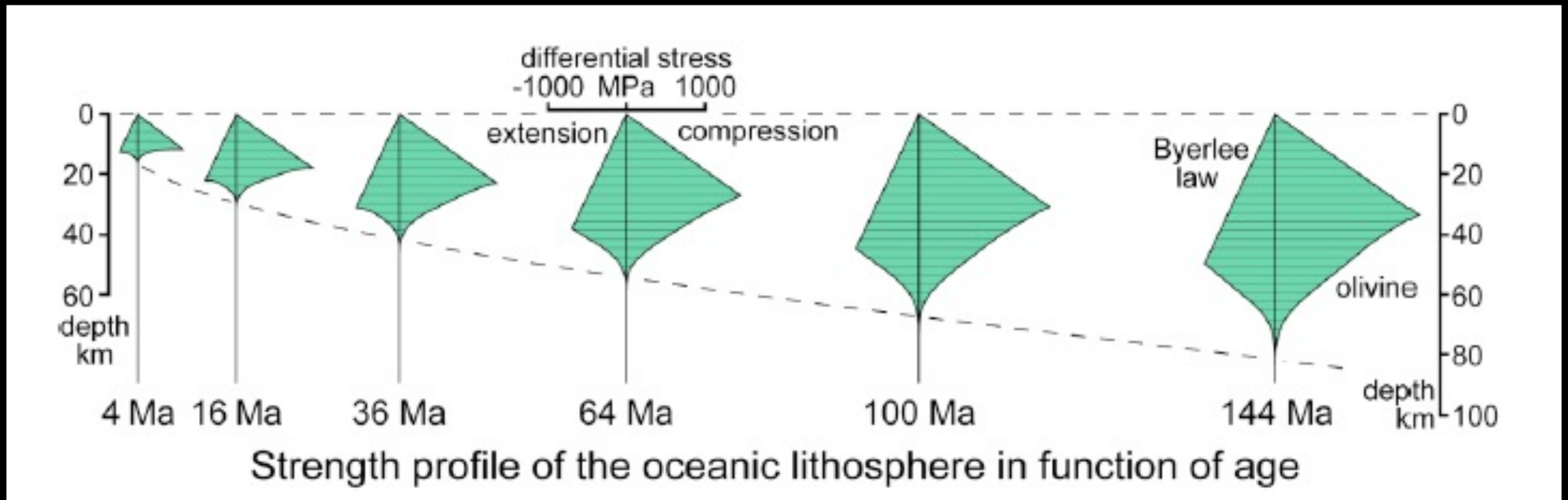

Strength profile of the oceanic lithosphere in function of age

strength increases as the lithosphere cools

Extensional Processes

stretching factor - ß
McKenzie model

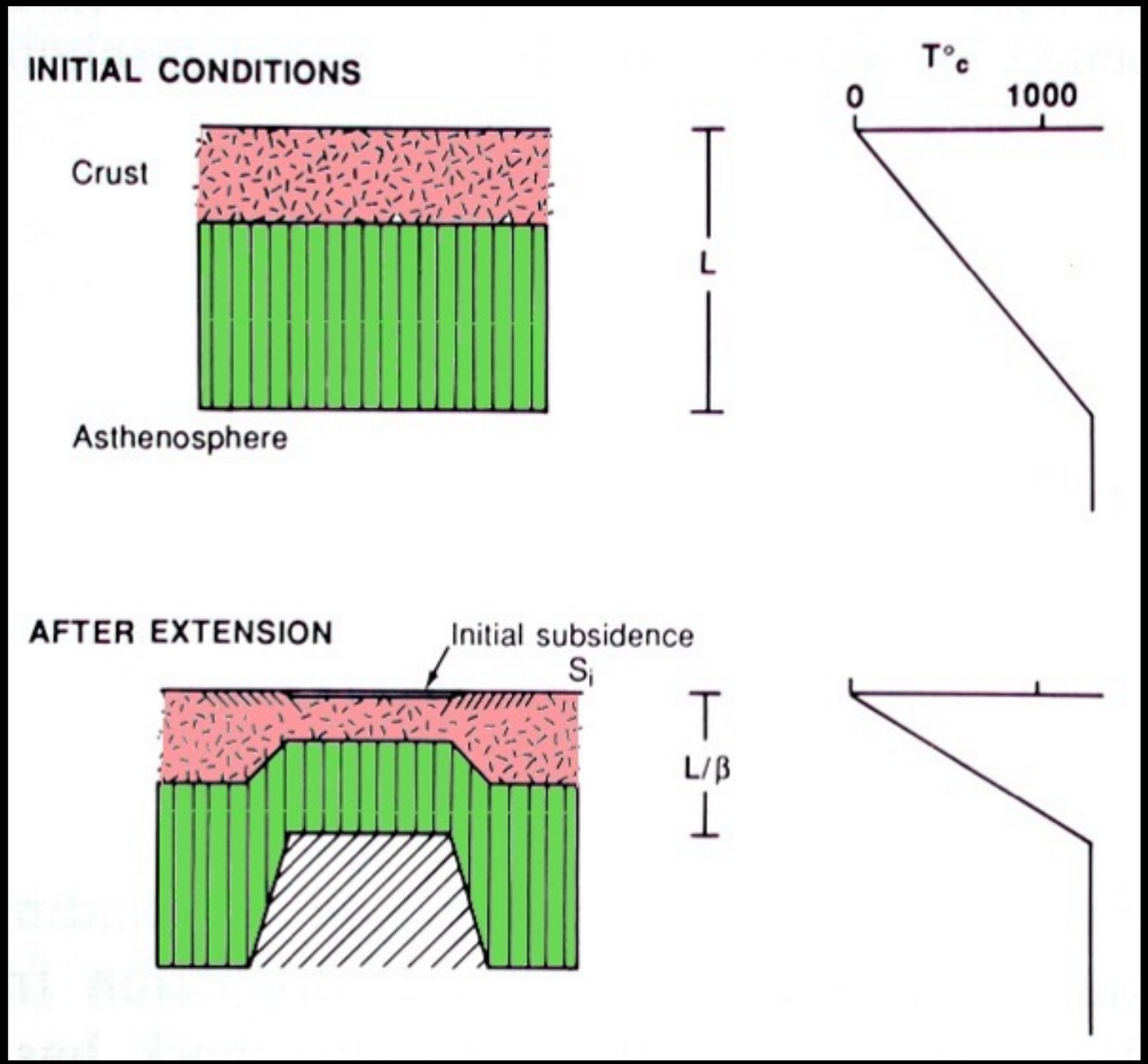

Evolution of the McKenzie model

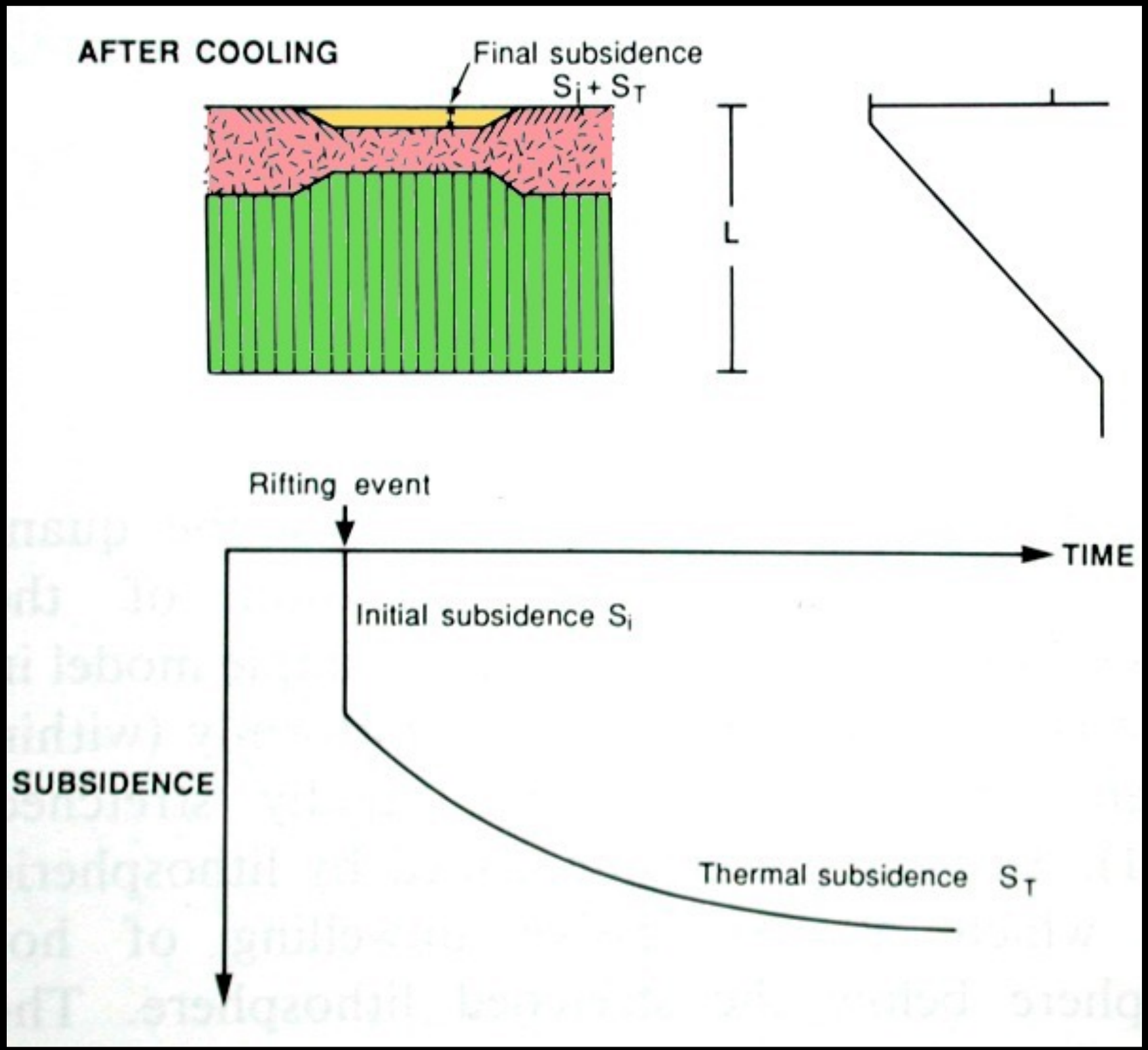

subsidence due to distributed stretching

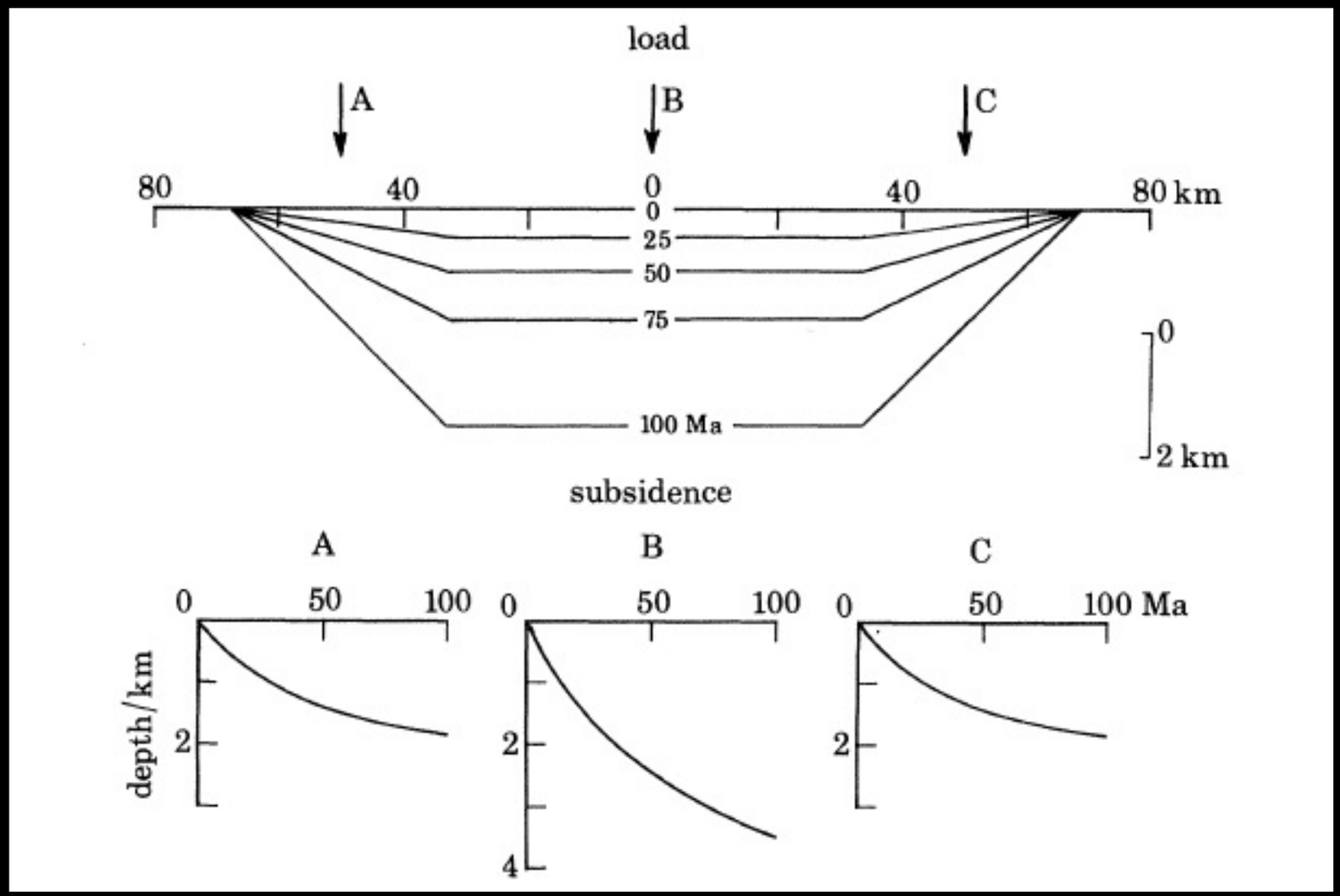

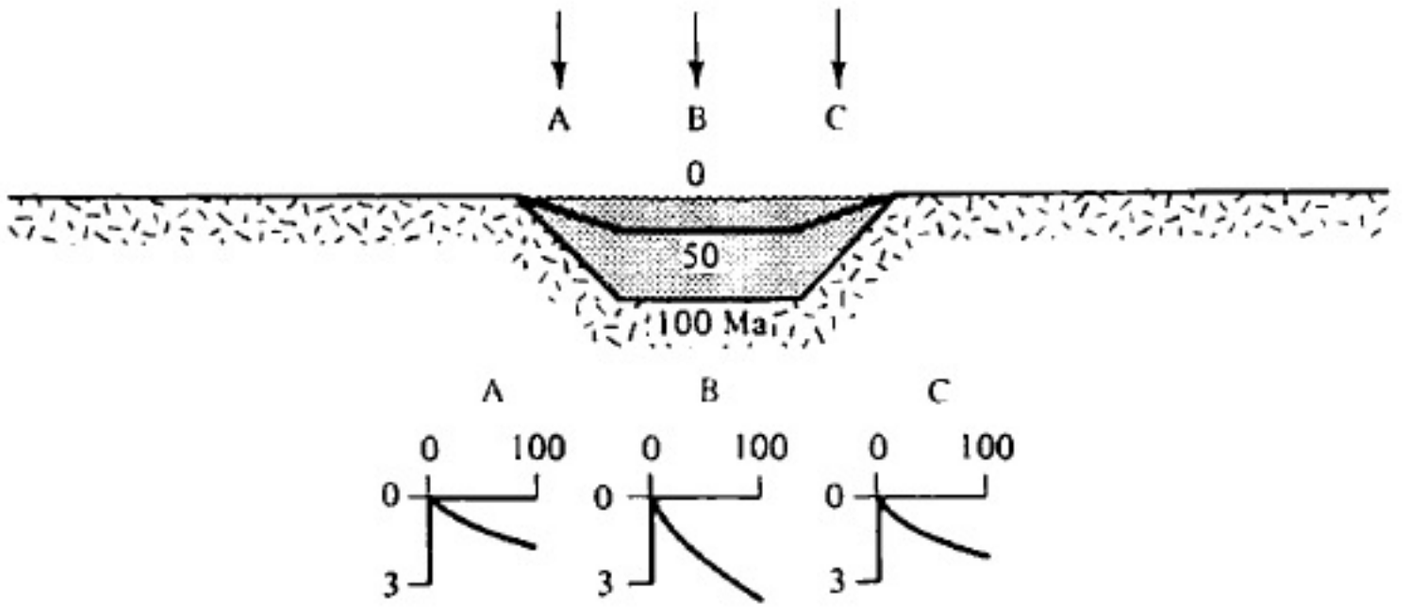

Sediment loading

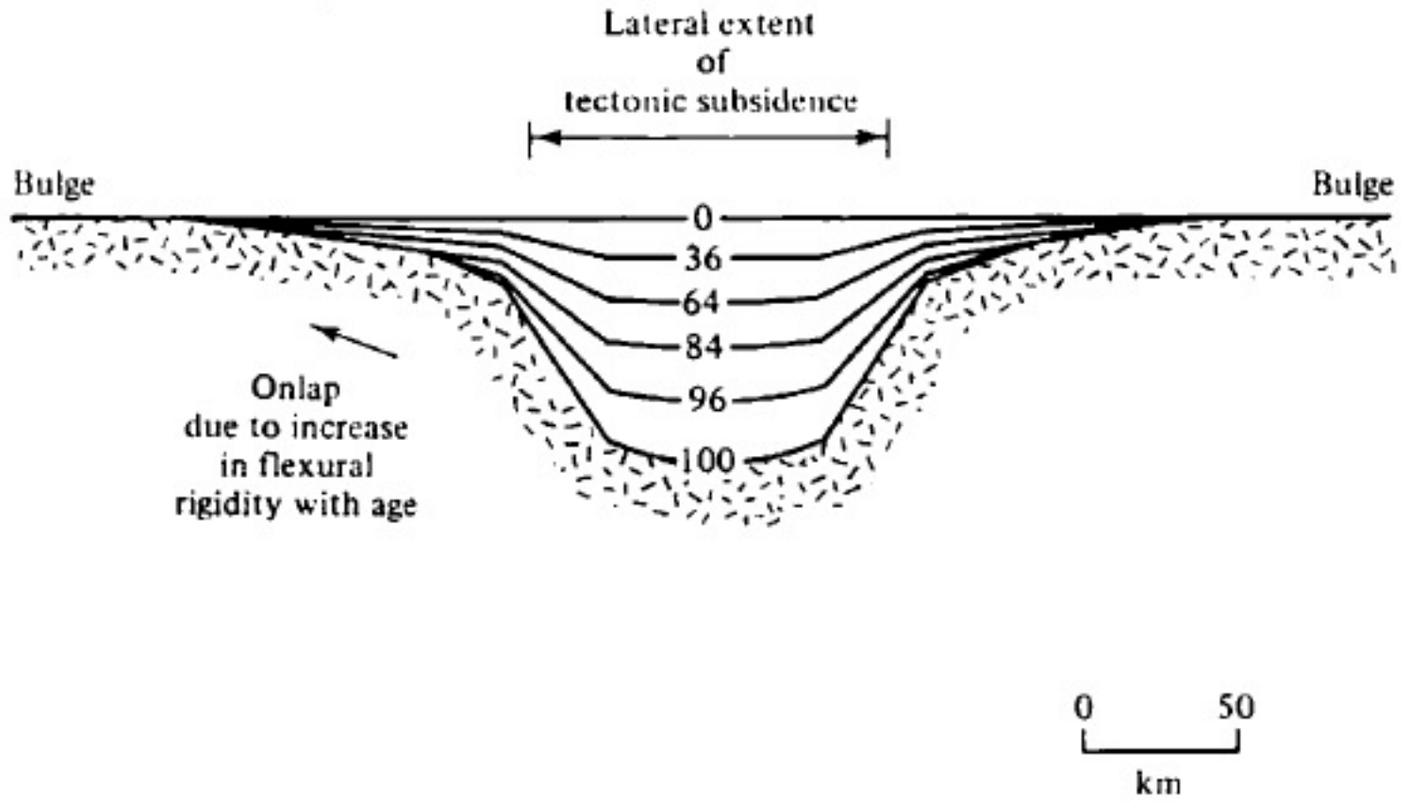

elastic and visco-elastic

Tau = 10^5 years

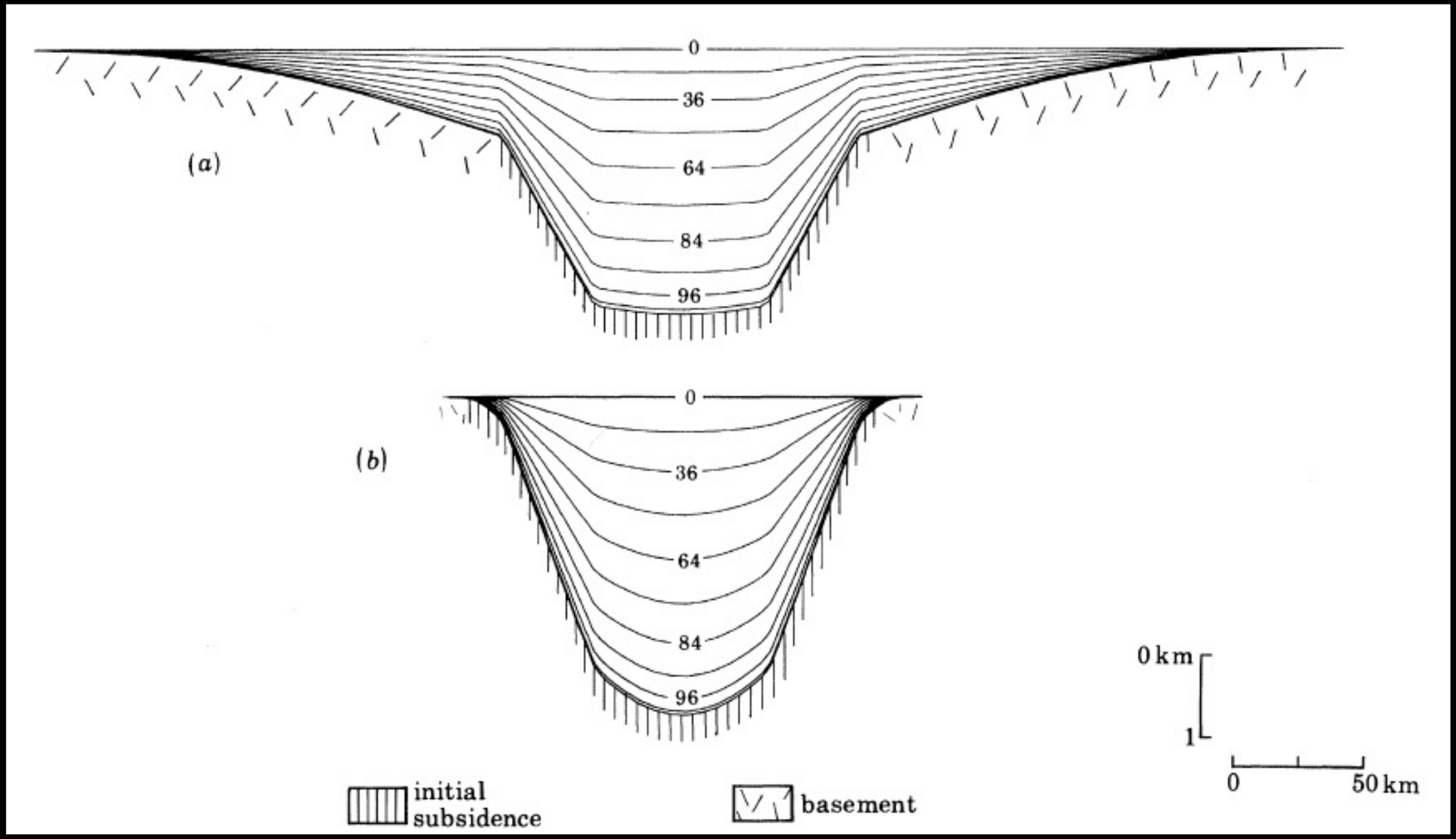

Thrust Wedges

loads for foreland basins

accretionary prism in 3-D

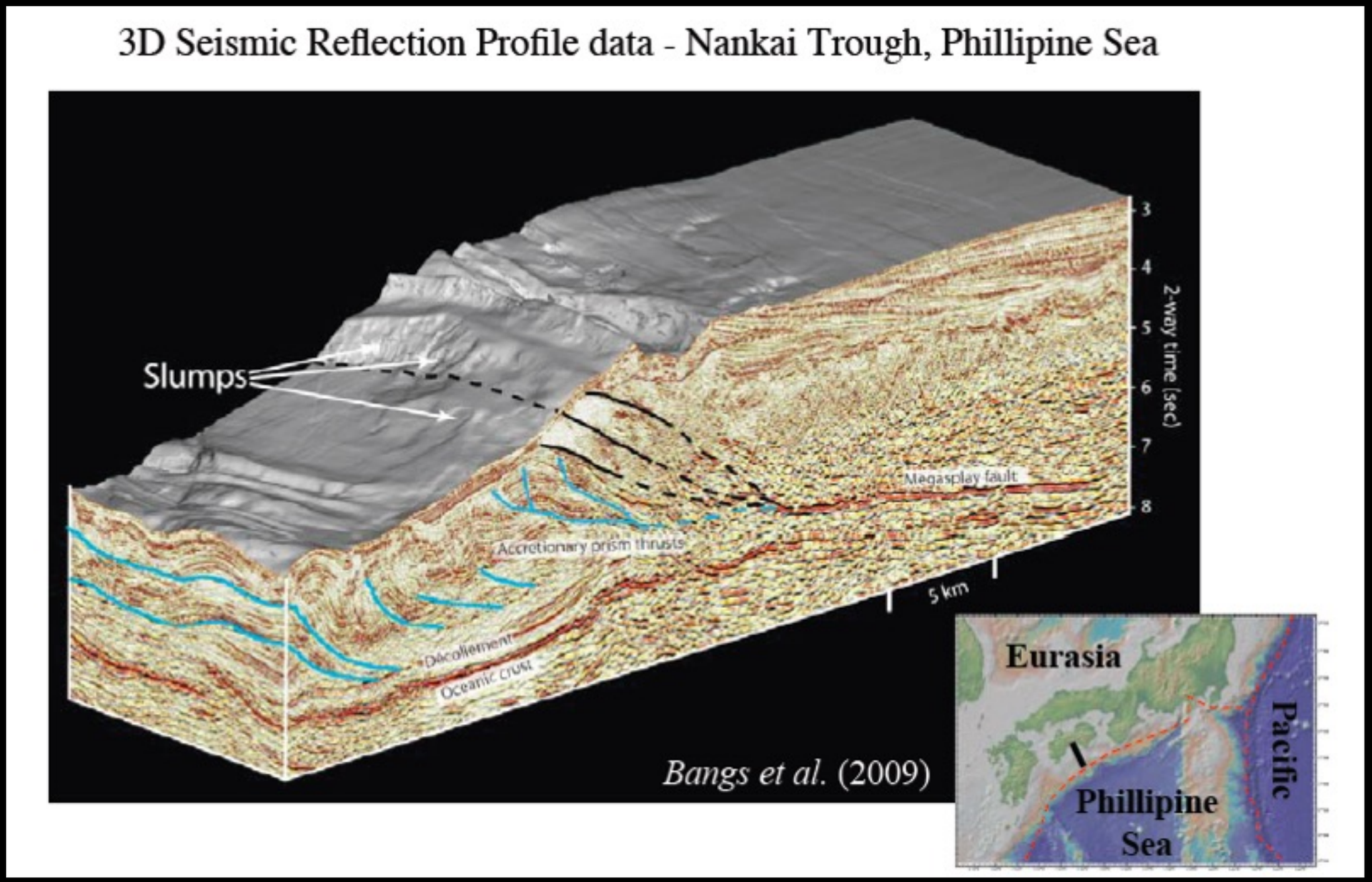

critical taper - a stressed wedge, everywhere on the verge of failure

an excellent model for accretionary prisms

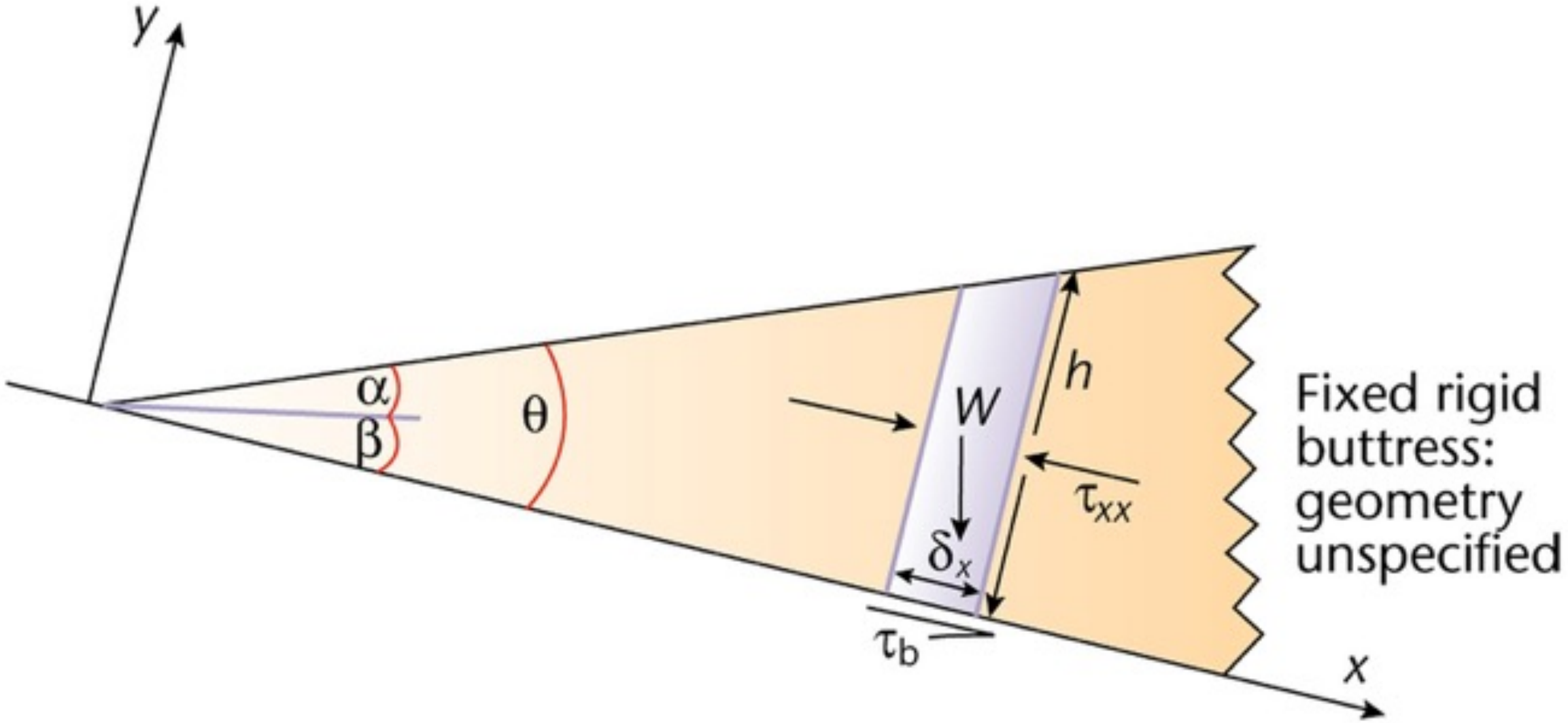

Fig. 4.23 Simplified model of an accretionary wedge (after Platt 1986). α is the surface slope, β is the basal slope and θ is the taper angle ($\alpha + \beta$). A small segment of the wedge of basal length δx and height h is subjected to a body force W, to a basal traction $\tau\delta x$, and to 'push' forces from the rear, produced by the longitudinal deviatoric stresses τ_{xx}. Frontal accretion, underplating, erosion and changes in basal shear stress (for example by changes in the rate of convergence/subduction) place the wedge out of equilibrium. The wedge responds by shortening and thickening or by collapsing by extension.

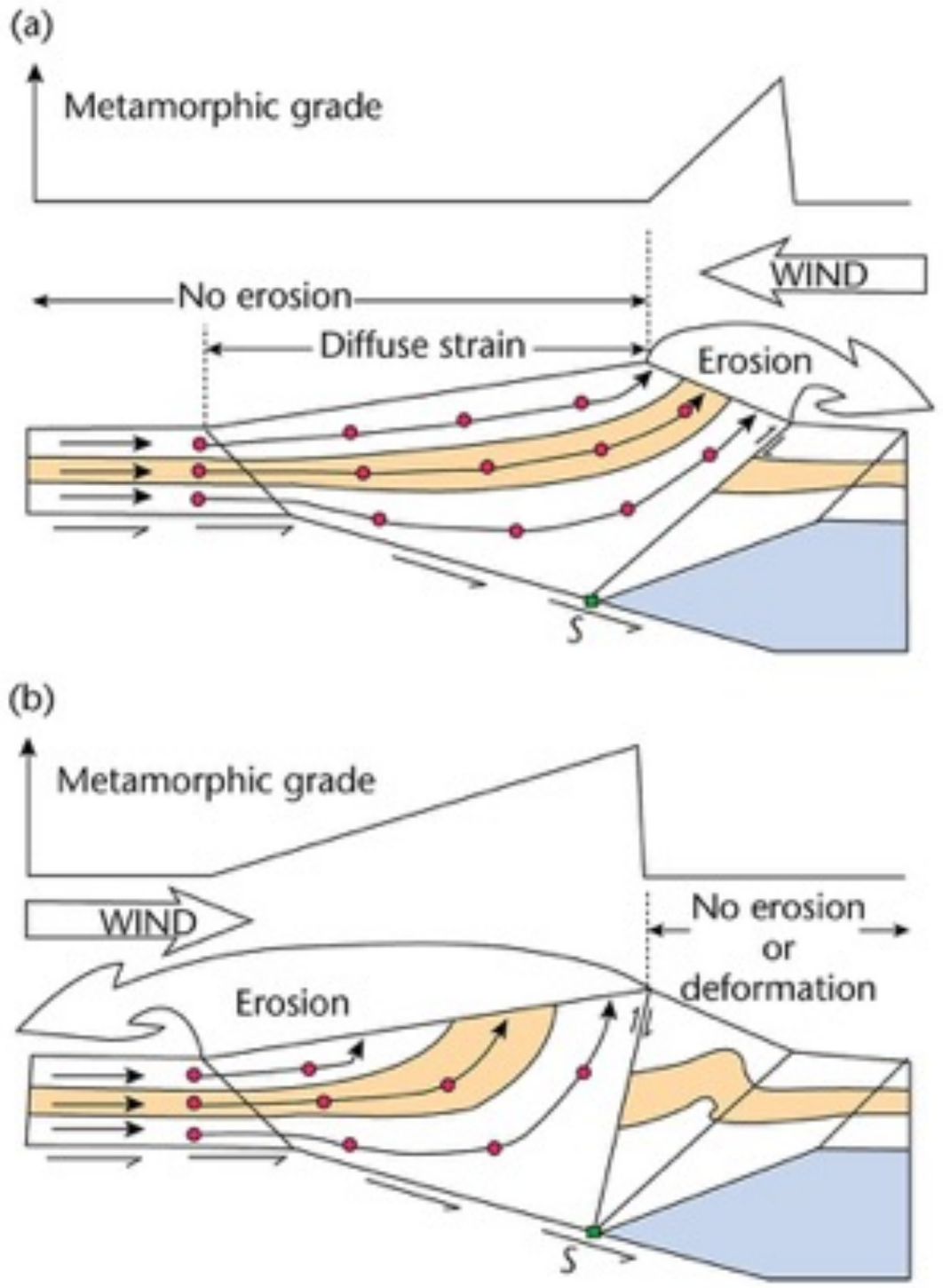

Fig. 4.28 Effects of erosion on a bivergent wedge (after Willett *et al*. 1993). Precipitation concentrated on the retro-wedge (a), and pro-wedge (b) increases erosion, causing an advection of high-grade metamorphic rocks from the middle and lower crust (and even mantle lithosphere) to the surface. Passive shaded layer shows middle crust. Lines are material trajectories, and dots show progressive equal-time positions of points originally aligned vertically.

erosion, deformation and exhumation

An assumption about tectonics

- Plate motions are the engine of earth deformation
- If plate motions are smooth and steady, then **local** tectonic reorganization is the only possible tectonic cause for basin-scale unconformities
- for a foreland basin, this requires changes in the distribution of the thrust load

Flexural Effects

North and South

Colville Trough

Barrow Arch

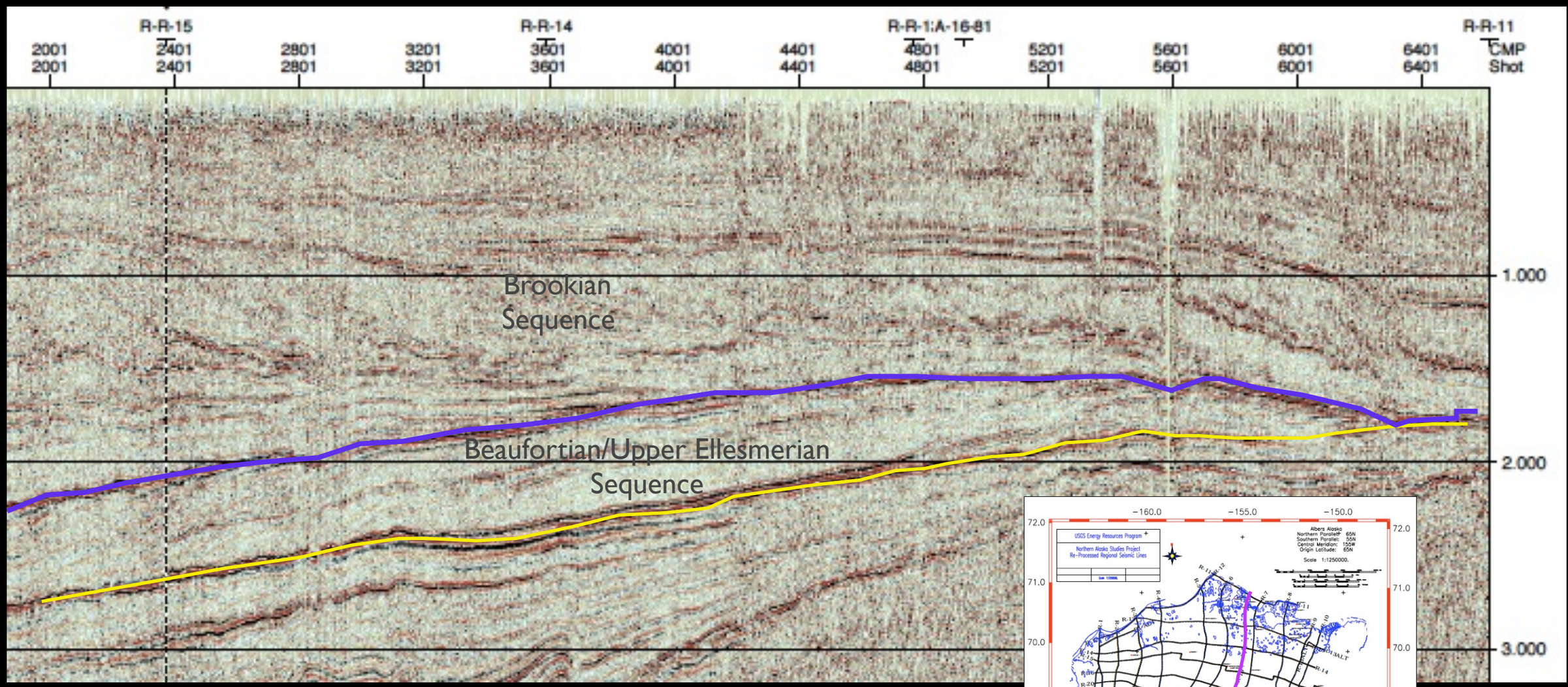

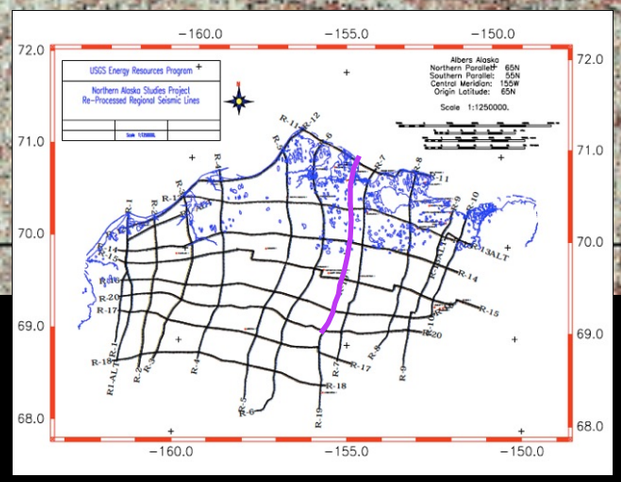

What about passive margins?

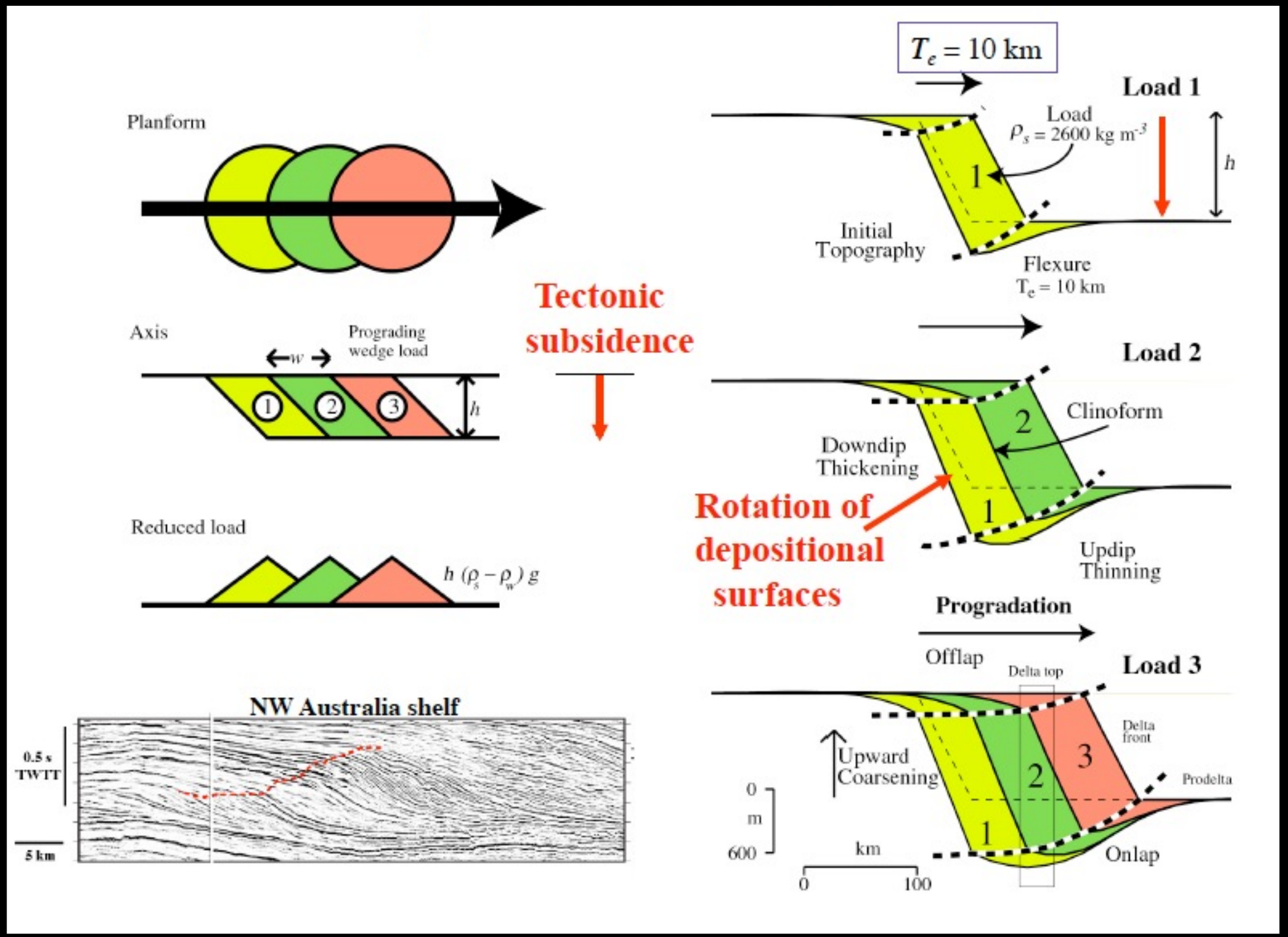

Watts 1989

in map view

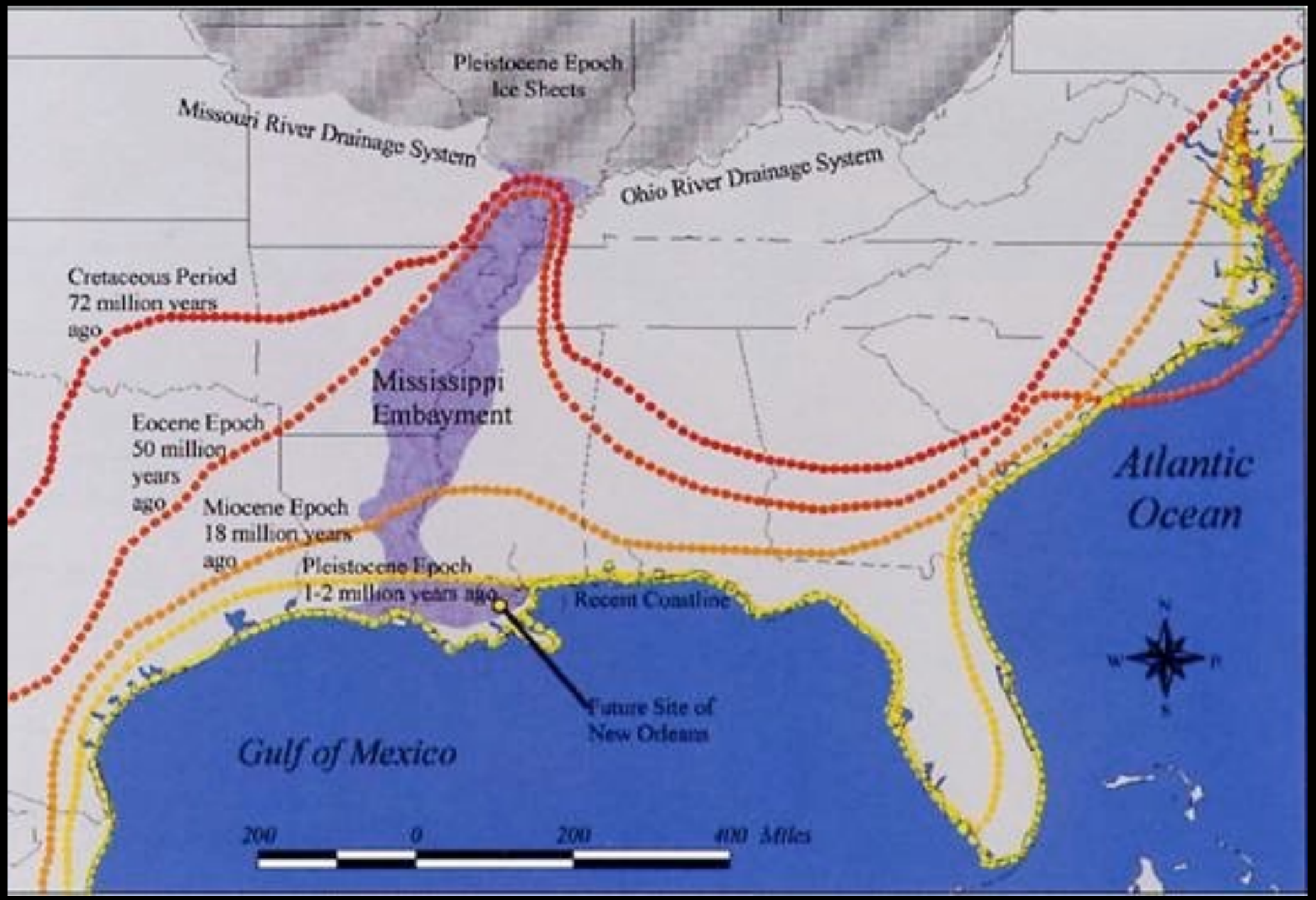
Pleistocene Epoch
Ice Sheets
Missouri River Drainage System
Ohio River Drainage System
Cretaceous Period
72 million years
ago
Mississippi
Embayment
Eocene Epoch
50 million
years
ago
Miocene Epoch
18 million years
ago
Pleistocene Epoch
1-2 million years ago
Recent Coastline
Future Site of
New Orleans
Gulf of Mexico
Atlantic
Ocean
200
0
200
400 Miles

sequence stratigraphy

resolution of seismic reflection data

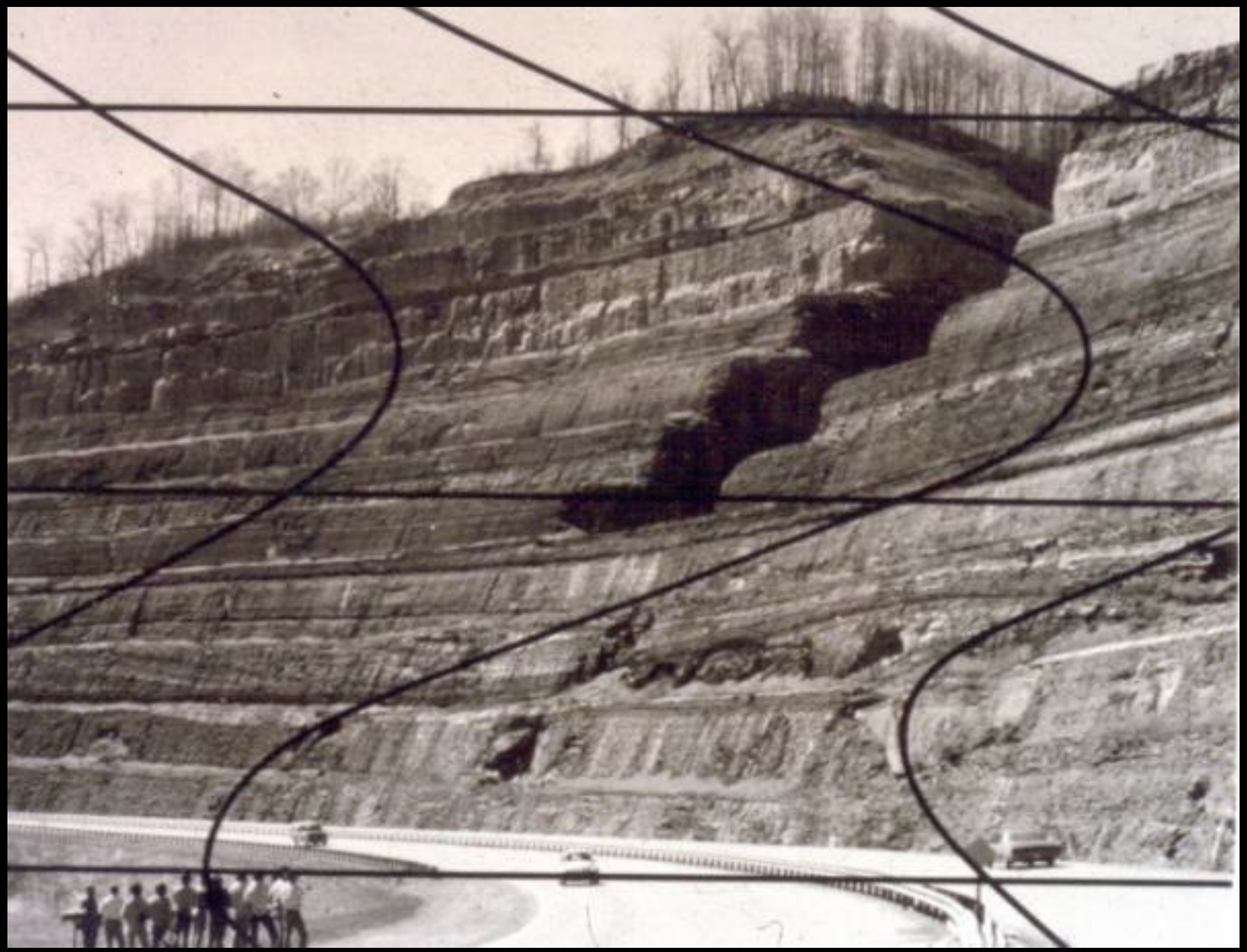

Accommodation Space

Space made available for sediment accumulation by basement subsidence and/or sea level change.

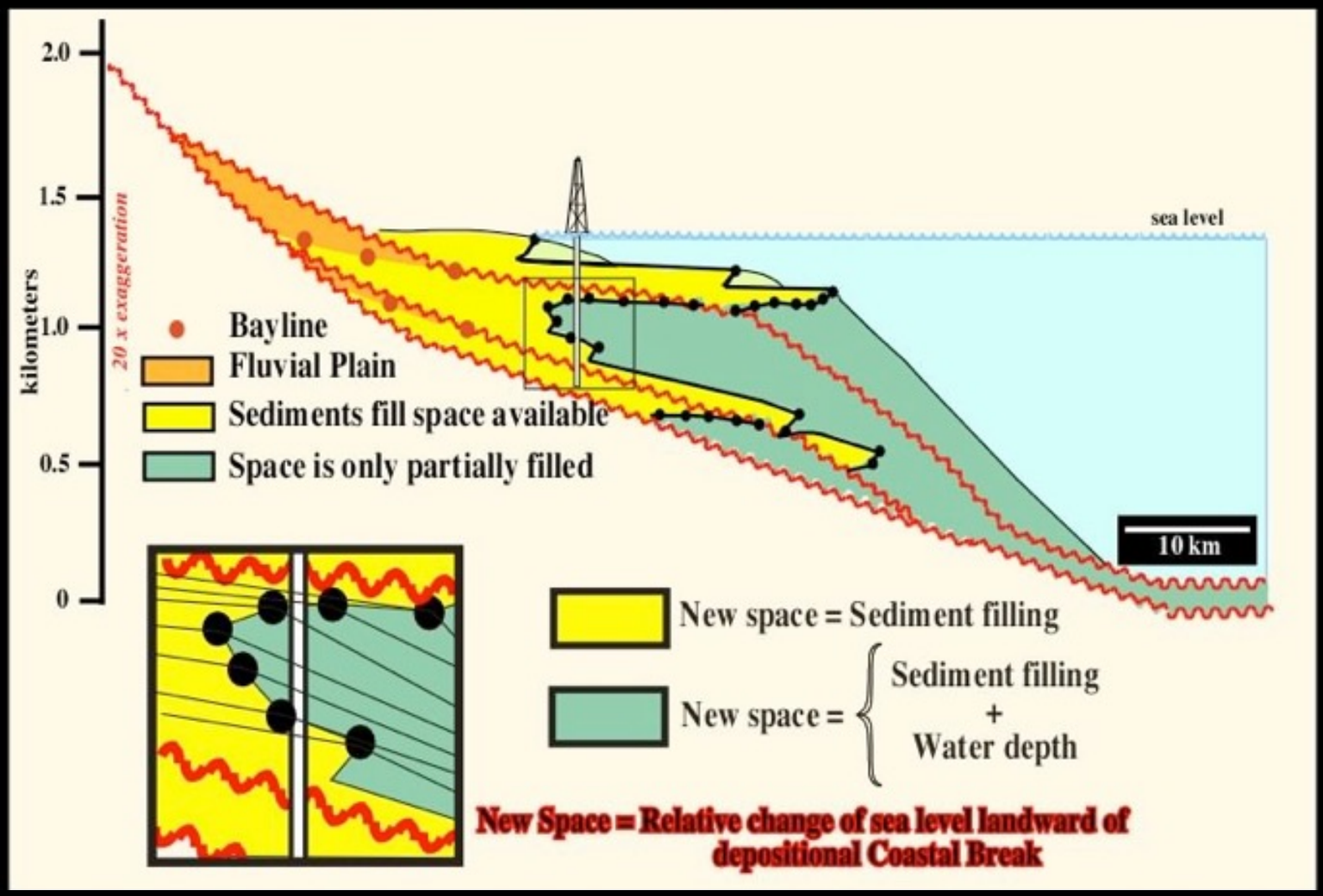

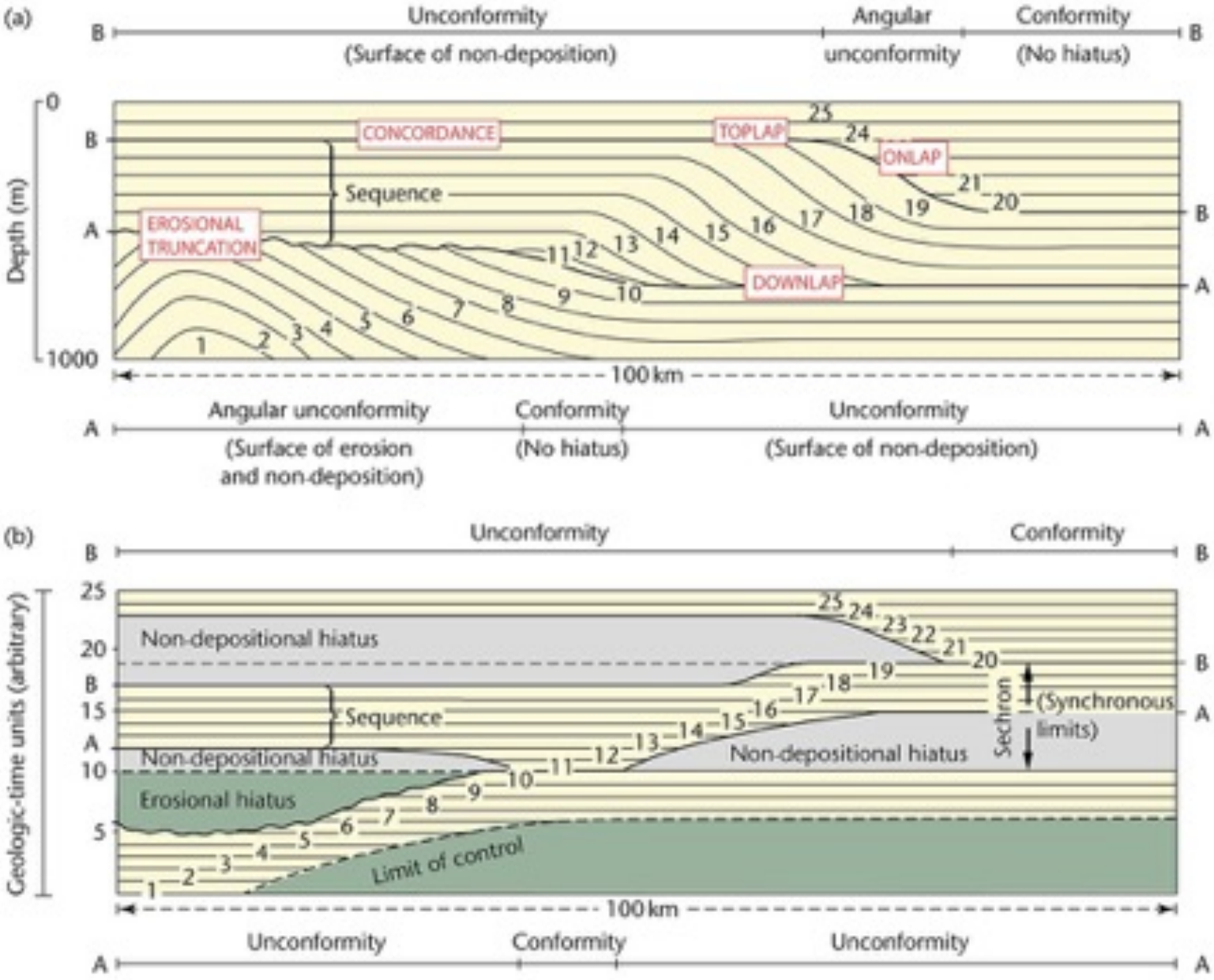

Fig. 8.7 The basic concept of the depositional sequence as outlined by Vail *et al.* (1977a). (a) Generalised stratigraphic section of a depositional sequence. A sequence boundary A changes from an angular unconformity in the left half of the diagram to a conformity in the centre and to a non-depositional unconformity on the right. The sequence boundary B passes from a non-depositional unconformity on the left to an angular unconformity in the centre and a lateral conformity on the right. Unconformities are dated at the points where they have become conformable. Units 1 to 25 represent strata deposited during successive time intervals. (b) Generalised chronostratigraphic section of the same stratigraphic sequence as in (a). The depositional sequence between surface A and B ranges in age from the beginning of chron 11 until the end of chron 19. Chronostratigraphic charts of this type are sometimes termed 'Wheeler diagrams', following Wheeler (1958). Boxes: the geometrical relationships of strata to a depositional sequence boundary or to any other surface within a depositional sequence. Relations to upper surface include (1) erosional truncation, (2) toplap (commonly non-depositional rather than erosional) and (3) concordance. Relations to lower surface include (1) onlap where the overlying strata are near-horizontal and the surface is inclined, (2) downlap where the overlying strata are inclined and (3) concordance. AAPG © 1977. Reprinted by permission of the AAPG whose permission is required for further use.

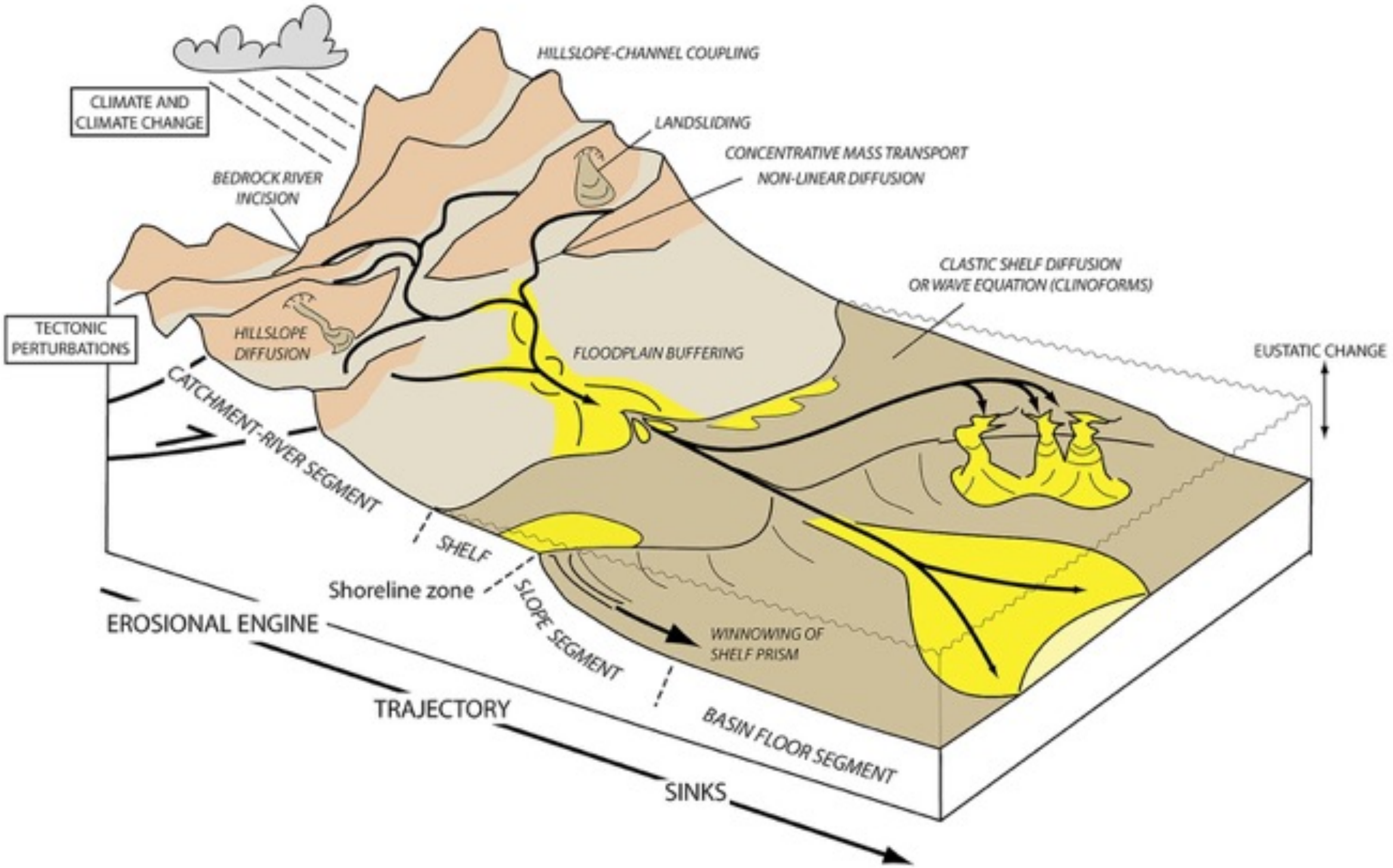

Fig. 7.1 Concept of the sediment routing system from source to sink. The sediment routing system is driven and perturbed by tectonics and climate. It comprises a number of morphodynamic, mutually coupled subsystems or segments. The erosional engine feeds sediment to a predominantly transportational system (the trajectory) and to long-term sinks. From Allen & Heller (2012, p. 113, fig 6.2), modified from Somme *et al.* (2009).

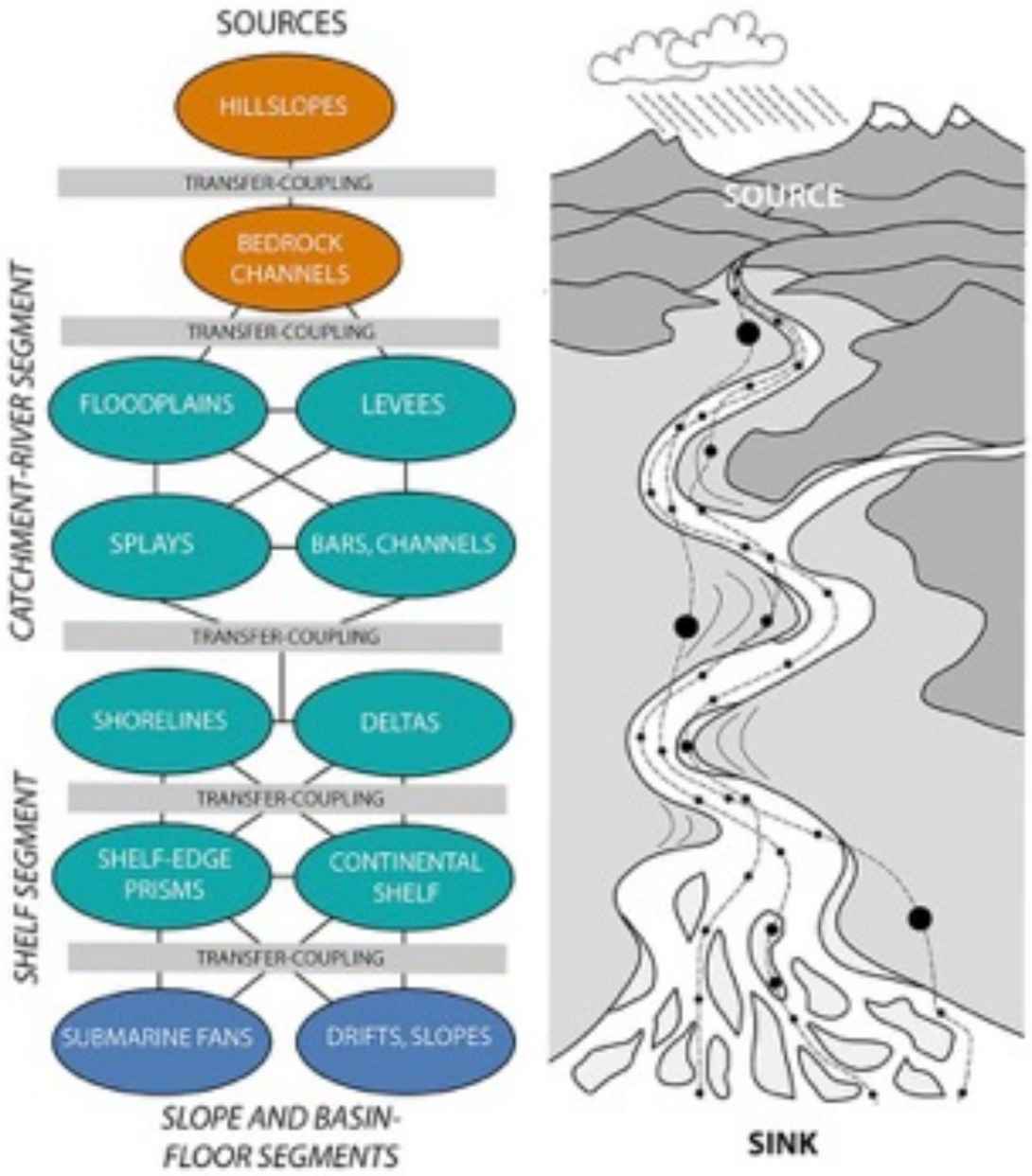

Fig. 7.2 Right: sediment is transferred from a source region to a sink along trajectories (dashed lines). Some trajectories involve short times with brief periods of storage in the sediment routing system (small circles) whereas others involve long transit times with prolonged periods of storage in transient states (large circles). Long periods of storage of sediment in transient states implies buffering of sediment supply signals. Left: sources (orange), sites of temporary storage (transient states) in green and sites of permanent storage (absorbing states) in blue. The transfer of sediment between macrogeomorphic segments may be complex and involve dynamic feedbacks. From Allen & Heller (2012, p. 112, fig 6.1).

Decompaction of stratigraphic units

- In order to decompact we need to know the variation of porosity with depth:

$$\phi = \phi_0 e^{-cy}$$

Where $\varnothing$ is the porosity at any depth y, $\varnothing_0$ is the surface porosity and *c* is the coefficient that is dependent on lithology and describes the rate at which the exponential decrease in porosity takes place with depth

Airy backstripping (i.e. local isostatic compensation)

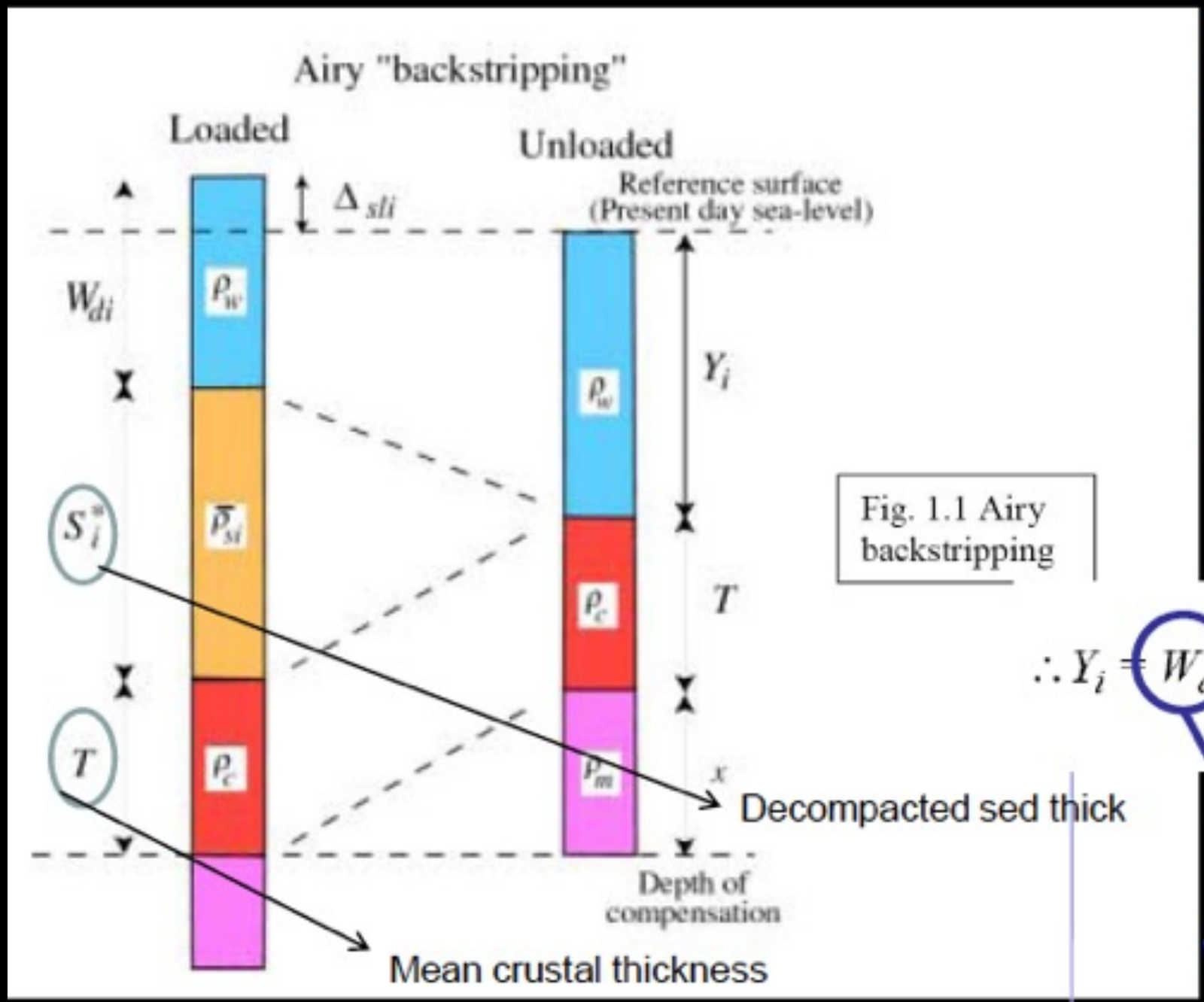

Fig. 1.1 Airy backstripping

Considering two colums of the crust and upper mantle that are in isotatic equilibrium and balancing the pressure at the base:

$\rho_w g W_{di} + \rho_{si} g Si^* + \rho_c g T =$
$Yi \rho_w g + \rho c g T + x \rho_m g$

$$\therefore Y_i = W_{di} + S_i^* \left[\frac{(\rho_m - \bar{\rho}_{si})}{(\rho_m - \rho_w)} \right] + \Delta_{sli} \frac{\rho_m}{(\rho_m - \rho_w)}$$

Water depth

sediment loading

Sea-level loading

Tectonic subsidence

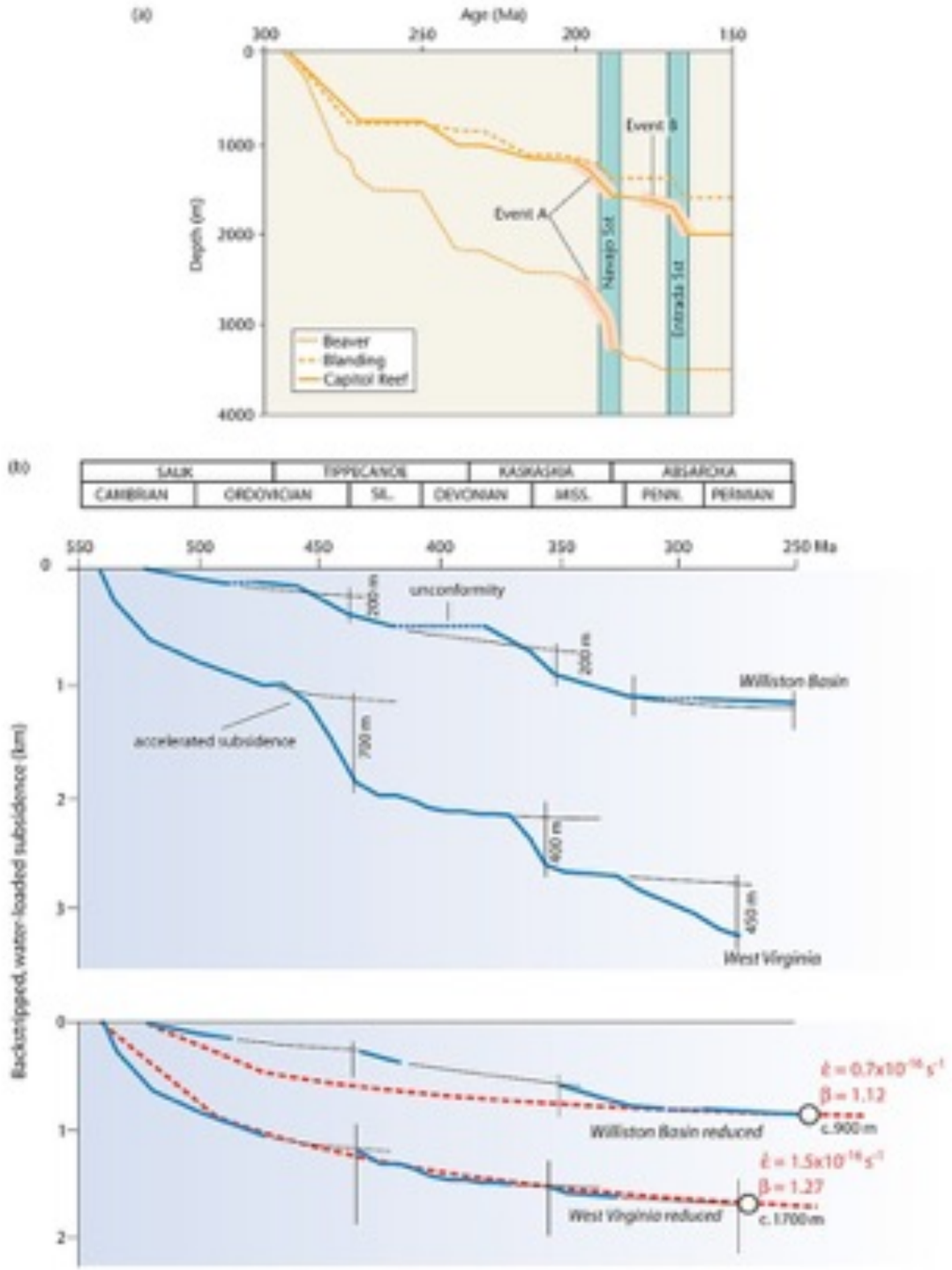

Fig. 9.18 Subsidence histories showing long-term drift superimposed by phases of accelerated subsidence and uplift. (a) Periods of convex-up accelerated subsidence ascribed to flexural subsidence in the retro-foreland of the Colorado Plateau region, western USA (Allen *et al.* 2000). (b) Residuals superimposed on long-term drift from the North American craton (Armitage & Allen 2010). Top: Total backstripped tectonic subsidence for two locations showing periods of accelerated subsidence and unconformities. Base: Same localities with residuals removed to give a long-term drift with model fits (red dashed lines) for extensional strain rates and stretch factors of $0.7 \times 10^{-16} s^{-1}$ and $\beta = 1.12$ (Williston) and $1.5 \times 10^{-16} s^{-1}$ and $\beta = 1.27$ (West Virginia) respectively.